



HAL
open science

Adaptive observer and control design of different classes of coupled partial differential equations

Mohammad Ghousein

► **To cite this version:**

Mohammad Ghousein. Adaptive observer and control design of different classes of coupled partial differential equations. Automatic Control Engineering. Université Grenoble Alpes [2020-..], 2020. English. NNT : 2020GRALT049 . tel-03139948

HAL Id: tel-03139948

<https://theses.hal.science/tel-03139948>

Submitted on 12 Feb 2021

HAL is a multi-disciplinary open access archive for the deposit and dissemination of scientific research documents, whether they are published or not. The documents may come from teaching and research institutions in France or abroad, or from public or private research centers.

L'archive ouverte pluridisciplinaire **HAL**, est destinée au dépôt et à la diffusion de documents scientifiques de niveau recherche, publiés ou non, émanant des établissements d'enseignement et de recherche français ou étrangers, des laboratoires publics ou privés.

THÈSE

Pour obtenir le grade de

DOCTEUR DE L'UNIVERSITÉ GRENOBLE ALPES

Spécialité : AUTOMATIQUE - PRODUCTIQUE

Arrêté ministériel : 25 mai 2016

Présentée par

Mohammad GHOUSEIN

Thèse dirigée par **Emmanuel WITRANT**, Université Grenoble Alpes

préparée au sein du **Laboratoire Grenoble Images Parole Signal Automatique**
dans l'**École Doctorale Electronique, Electrotechnique, Automatique, Traitement du Signal (EEATS)**

Observateurs adaptatifs et synthèse de correcteurs pour différentes couplages d'équations aux dérivées partielles

Adaptive observer and control design of different classes of coupled partial differential equations

Thèse soutenue publiquement le **5 novembre 2020**,
devant le jury composé de :

Monsieur Emmanuel WITRANT

PROFESSEUR DES UNIVERSITES, Université Grenoble Alpes,
Directeur de thèse

Monsieur Eduardo CERPA

PROFESSEUR ASSOCIE, Pontificia Universidad Católica de Chile,
Rapporteur

Monsieur Hugues MOUNIER

PROFESSEUR, Supélec, Université Paris Sud 11, Rapporteur

Monsieur Christophe PRIEUR

DIRECTEUR DE RECHERCHE, CNRS Grenoble, Président

Monsieur Liguozhang ZHANG

PROFESSEUR, Beijing University of Technology (BJUT), Examineur



Acknowledgements

In my thesis, I have experienced different types of feelings and emotions. There were moments full of joy, excitement and achievements, but also moments of depression and lack of motivation. I think this is quite normal when searching for new solutions and investigating totally new problems. Luckily, by the time I succeeded to adapt to the varying conditions with the help of my supervisor, friends and also my family.

I would like to thank my thesis supervisor Emmanuel Witrant. I thank him for his advices, and for giving me the necessary directions to advance in the thesis. Professor Emmanuel has offered me the necessary space and time to think, try new ideas and develop new theories. I gained to be autonomous under his supervision. I would like also to thank Prof. Liguozhang from Beijing University of Technology (BJUT) in Beijing, China, for the two months of collaboration. Prof. Zhang is a hard worker with a keen knowledge in the domain of traffic control. He was a great support for me during my stay in Beijing and I enjoyed doing research with him.

For my friends inside and outside the Gipsa-Lab: Ayman RAMDAN, Ali HAMDAN, Bilal TFAÏLY, Antonia YOUSSEF, Kaouther MOUSSA and Amgad MOHAMMAD, I send a big THANK YOU. They were all what I needed when I wanted to speak about my thesis. They have been always asking me about the problems that I am facing and we used to discuss and share the solutions. They were all there in the critical moments giving me the essential support.

Last but not least is my family. At this moment of truth and justice, I can say that without my family: Hassan (my father), Mona (my mother), Bilal (my brother), Amani (my oldest sister) and Ayat (my youngest sister), all what I have achieved in my professional career and in my thesis is not possible. My parents may not be able to read this paragraph, but I would like for everyone reading my thesis to know that I owe my parents what I am today and what I will be in the future. My mom has always believed in me. She gives the unconditional and endless love that have supported me in the difficult moments. She was always there regardless of all life problems. For her I say: I do not know if my life time will be sufficient to just give you in return some of all your sacrifices.

For all the people whom maybe I unintentionally forgot, thank you. For the people in Gipsa Lab, the RH services and to all the professors and friends whom I used to see them in the laboratory and in the coffee breaks, you made my thesis experience dynamic and full of social life.

Contents

Contents	v
List of Figures	ix
List of Tables	xi
0.1 Chapitre 1: Énoncé du problème et les motivations	xviii
0.2 Chapitre 2: Conception d'observateurs adaptatifs aux frontières pour les systèmes hyperboliques linéaires; Application à l'estimation dans les échangeurs de chaleur	xviii
0.3 Chapitre 3: Observateur aux frontières pour les échangeurs de chaleur diphasique	xviii
0.4 Chapitre 4: Contrôle Backstepping pour une classe de systèmes des EDPs hyperbolique-parabolique couplées	xix
0.5 Systèmes EDOs-EDPs	xix
0.6 Chapitre 6: Conclusion et perspectives	xix
1 Problem statement and motivating applications	1
1.1 CO ₂ cooling of silicon detectors at CERN	1
1.2 Problem 1: CO ₂ single phase heat exchangers	4
1.3 Problem 2: CO ₂ two phase heat exchangers	6
1.4 Problem 3: Coupled hyperbolic-parabolic PDEs	7
1.5 Problem 4: Coupled ODEs-Hyperbolic PDEs networks	9
1.6 Conclusion	13
2 Adaptive Boundary Observer Design for Hyperbolic Systems; Application to CO₂ single phase heat exchangers	15
2.1 Linearization	17
2.2 Observation problem formulation	19
2.3 Literature review	20
2.3.1 Contribution	21
2.4 Adaptive observer design	22
2.5 Swapping Design	22
2.6 Exponential stability of $Z(x, t)$	25
2.7 Boundedness of $\Lambda(x, t)$	27
2.7.1 Boundedness of $\Lambda_1(x, t)$ and $\Lambda_2(x, t)$	27

2.7.2	Boundedness of $Q(x, t)$	31
2.8	Parameter adaptation laws and exponential stability of $\tilde{\theta}(t)$	32
2.9	Exponential stability of $E(x, t)$	34
2.10	Numerical Simulation Results	35
2.10.1	Scenario 1: Stable plant	35
2.10.2	Scenario 2: Unstable plant	37
2.11	Experimental evaluation of the observer (CERN)	41
2.11.1	In-domain evaluation of the observer through simulations	44
2.11.2	Comparison with literature observers	47
2.11.3	Experimental evaluation of the observer	47
2.12	Conclusion	51
3	Boundary Observer Design for CO₂ two phase heat exchangers	55
3.1	Physical modeling of the two phase line	56
3.1.1	Flow regimes	56
3.1.2	3D Two-Fluid Model	57
3.1.3	Averaging and the 1D Two Fluid Model	58
3.1.4	Homogenous Equilibrium Model (HEM)	60
3.2	Modeling of the CO ₂ two phase heat exchanger	61
3.2.1	Equation of State (CO ₂)	63
3.3	Model Implementation	66
3.4	Boundary Observer Design	67
3.4.1	Linearization	70
3.4.2	Characteristic Form and Diagonalization	71
3.4.3	Observer Architecture	72
3.5	Numerical Evaluation of the Obsever	75
3.6	Conclusion	76
4	Backstepping control for a class of coupled hyperbolic-parabolic PDE systems	81
4.1	Literature review	82
4.1.1	Contribution	83
4.2	Backstepping Control Design	84
4.2.1	Transformation 1: Eliminate the effect of $\lambda(x)$	85
4.2.2	Transformation 2: Eliminate the effect of $\sigma(x)$ and $S(x, y)$	87
4.3	Stability of the closed loop system	94
4.4	Numerical Simulation Results	98
4.4.1	Calculation of c and $T(x, y)$	99
4.5	Conclusion	99
5	Adaptive Boundary Observer Design for coupled ODEs-Hyperbolic PDEs systems	105
5.1	Literature review	106
5.1.1	Contribution	107
5.2	Adaptive Observer Design	108

5.3	PDE-ODE Decoupling by Swapping Design	109
5.4	Exponential convergence of $\{\tilde{\xi}(x, t), \tilde{X}(t), \tilde{\theta}(t)\}$ in the L^2 sense	110
5.5	Numerical evaluation of the observer	116
5.6	Conclusion	121
6	Conclusion and Perspectives	123
	Bibliography	127

List of Figures

1.1	Cooling loop.	2
1.2	The 2PACL refrigeration method [77].	3
1.3	Concentric-tube heat exchanger in counter-current flows.	4
1.4	CO ₂ single phase heat exchanger.	4
1.5	CO ₂ two phase heat exchanger.	6
1.6	Fluid temperature vs tube temperature [77].	7
1.7	Hot line with wall thickness.	8
1.8	Schematic of the dual-loop EGR engine air-path.	11
2.1	CO ₂ single phase heat exchanger.	15
2.2	State estimation map	19
2.3	In-domain state estimations at $x = 0.25$ and $x = 0.75$	37
2.4	Parameter estimations and parameter estimation errors	38
2.5	The evolution of the L^2 norm of $\{\tilde{u}(x, t), \tilde{v}(x, t)\}$	38
2.6	In-domain state estimations at $x = 0.25$ and $x = 0.75$	39
2.7	Parameter estimations and parameter estimation errors	40
2.8	The evolution of the L^2 norm of $\{\tilde{u}(x, t), \tilde{v}(x, t)\}$	40
2.9	15kW TIF plant at CERN	41
2.10	Schematic of the TIF plant	42
2.11	Steady state error on the distributed temperature profiles for three different operating points	45
2.12	Estimated heat transfer coefficient $\hat{h}(t)$ for three different operating points	46
2.13	Comparison of the L^1 estimation error resulting from three different methods for three different operating points	48
2.14	Comparison between the reference model and experimental results	50
2.15	Comparison between the estimation laws for the hot and cold fluid temperatures.	52
2.16	Comparison between the estimation errors for the hot and cold fluid temperatures.	53
2.17	Estimated heat transfer coefficient $\hat{h}(t)$	54
3.1	CO ₂ two phase heat exchanger.	55
3.2	Vapor-liquid Flow Regimes	56
3.3	CO ₂ Pressure-Enthalpy Diagram.	63
3.4	Finite volume staggered grid	66

3.5	Steady state distributions of different thermodynamic variables.	68
3.6	The transient behavior of the output mass flow rates, pressures, temperatures and quality.	69
3.7	Boundary observer architecture.	73
3.8	Estimation of the complete thermodynamic profile (\dot{m}, P, H) at $x = 0.25$	77
3.9	Estimation of the complete thermodynamic profile (\dot{m}, P, H) at $x = 0.75$	78
3.10	Time variation of the L^2 norm of the estimation error $\varepsilon(x, t)$	79
4.1	Schematic diagram of the diffusive - advective system	81
4.2	Schematic diagram of the diffusive - advective system considered in [54]	83
4.3	Schematic diagram of the diffusive - advective system considered in [31]	83
4.4	Control design strategy	85
4.5	$M(x, y)$ kernel representation	91
4.6	The unstable system in open loop.	100
4.7	The control gain kernels.	101
4.8	The two controllers $F_1(t)$ and $F_2(t)$	101
4.9	The exponentially stable closed loop system.	102
5.1	PDE - ODE network	105
5.2	Calculated observer gain $L(t)$	118
5.3	Estimation error of the PDE state $\tilde{\xi}(x, t)$ and the ODE states $\tilde{X}(t)$ and $\tilde{\theta}(t)$	119
5.4	Lyapunov function $V(t)$	120
5.5	Estimation of the parameter state $\hat{\theta}(t)$	120

List of Tables

2.1	RSE for three different operating points	47
2.2	Heating power modulation	49
3.1	Variables definitions of the 3D Two-Fluid Model	58

Nomenclature and Acronyms

Unless it is specified, all variables are in SI Metric Units.

Variables

T	Temperature
ρ	Density
\dot{m}	Mass flow rate
v	Velocity
Q_{egr1}	Mass flow rate through the LP-EGR valve
P	Pressure
e	Internal energy
r	External heat source
τ	Stress tensor
b	Body forces
v_i	Interface velocity
σ	Surface tension
$H_{s,g}$	Algebraic value of the minimum curvature of the interface
α	Void fraction
Q_w	Heat transfer from the wall
f_w	Friction done by the wall
μ^*	Effective interface chemical potential

Constant parameters

A	Surface area
D_1	Tube diameter
C_p	Specific heat at constant pressure
L	Length of the heat exchanger
h	Heat transfer coefficient
T_{amb}	Ambient temperature
H	Specific enthalpy

Acronyms

PDE	Partial differential equation
ODE	Ordinary differential equation
EGR	Exhaust gas regulation
LHC	Large hadron collider
2PACL	Two-phase accumulator controlled loop
HP-EGR	High-pressure exhaust gas regulation
LP-EGR	Low-pressure exhaust gas regulation
VGT	Variable geometry turbine
DPF	Diesel particle filter
DOC	Diesel oxidation catalyst
0D	Zero-dimensional
1D	One-dimensional
3D	Three-dimensional
LTI	Linear time invariant
LTV	Linear time varying
LPV	Linear parameter varying
EoS	Equation of state
PLC	Programming logic controller
HEM	Homegenous equilibrium model
sat	Saturation
FVM	Finite Volume method
GES	Globally exponentially stable
SNR	Signal to noise ratio
LMI	Linear matrix inequality
BMI	Bilinear matrix inequality
UES	Uniformly exponentially stable
PIDE	Partial integro differential equation

List of Publications

Journal articles

- M.Ghousein, E.Witrant, V.Bhanot, P.Petagne. "Adaptive boundary observer design for linear hyperbolic systems; Application to estimation in heat exchangers". In: *Automatica* (2020), vol. 114 (108824), pp. 1–13.

Conference papers

- M.Ghousein, E.Witrant. "Backstepping control for a class of coupled hyperbolic-parabolic PDE systems". In: *2020 American Control Conference (ACC)*, IEEE, pp. 1600-1605, Invited session.
- M.Ghousein, E.Witrant. "Adaptive Boundary Observer Design for coupled ODEs-Hyperbolic PDEs systems". In: *21st IFACWorld Congress*, IFAC (2020), Invited session.
- M.Ghousein, E.Witrant. "A Boundary Observer for Two Phase Heat Exchangers". In: *18th European Control Conference (ECC)*. IEEE (2019), pp. 2332– 2337.

Contexte de la thèse

La thèse aborde sur l'estimation et le contrôle d'équations aux dérivées partielles couplées (EDP). La première application est dans le domaine de la cryogénie des systèmes de fluides au CERN. Une nouvelle technologie de refroidissement est maintenant développée au CERN, utilisant le CO₂ comme réfrigérant. L'objectif d'un cycle de refroidissement est de faire circuler un liquide de refroidissement froid dans les détecteurs au silicium chauds. Le cycle de refroidissement est constitué avec d'éléments appelés échangeurs de chaleur. Ces dispositifs sont utilisés pour échanger l'énergie du fluide chaud vers le fluide froid à travers une interface solide. La dynamique des échangeurs est modélisée par des variables qui évoluent non seulement dans le temps, mais aussi dans l'espace, telles que les températures, les pressions et les débits massiques. Nous abordons dans cette thèse trois problèmes de contrôle automatique liés aux échangeurs de chaleur. Le premier consiste à synthétiser un observateur adaptatif pour estimer les températures distribuées ainsi que le coefficient de transfert de chaleur d'un échangeur fonctionnant au CO₂ monophasé comme fluide de refroidissement. Le modèle mathématique est basé sur des équations hyperbolique aux dérivées partielles linéaires couplées dans le domaine. Le deuxième problème est de concevoir un observateur de frontière pour estimer les états d'un échangeur de chaleur avec des fluides qui changent de phase. Le modèle mathématique implique des équations hyperboliques non linéaires décrivant les lois d'équilibre. Le troisième problème est d'étudier l'importance de la propriété de diffusion dans les échangeurs de chaleur. Ceci implique l'étude de modèles mathématiques impliquant le couplage entre différentes classes d'EDP: hyperboliques et paraboliques. La deuxième motivation de la thèse est le système d'échappement de voiture équipé de doubles boucles EGR pour moteurs diesel (Renault). Des limites d'émission pour les moteurs diesel ont été imposées par la législation européenne pour minimiser la pollution des transports routiers, qui reste la source la plus importante de pollution de l'air urbain en Europe en ce qui concerne les NO_x (oxydes d'azote) et CO (monoxyde de carbone). Les exigences environnementales obligent les concepteurs de moteurs de voitures à développer de nouvelles technologies pour diminuer la consommation de carburant et les niveaux d'émissions tout en satisfaisant les conditions de conduite du moteur souhaitées. L'une des nouvelles configurations, qui peut fournir des conditions adéquates pour plusieurs modes de combustion, est la double régulation des gaz d'échappement (EGR) avec recirculation à la fois haute pression (HP) et basse pression (LP). Le système EGR est modélisé à l'aide d'un réseau d'EDP hyperboliques couplées à d'équations aux dérivées ordinaire (EDO) variant dans le temps. Le quatrième objectif de la thèse est de concevoir des estimateurs adaptatifs aux frontières du domaine pour ce type de systèmes.

La thèse est composée de six chapitres:

0.1 Chapitre 1: Énoncé du problème et les motivations

Nous introduisons dans ce chapitre les quatre problèmes de contrôle automatique qui sont abordés dans cette thèse. Les trois premiers sont liés aux échangeurs de chaleur avec des applications dans la cryogénie des systèmes de fluides au CERN, tandis que le quatrième est motivé par les réseaux d'écoulement des mélanges gazeux avec une application dans les moteurs de voitures diesel équipés par un système de régulation des gaz d'échappement (EGR). Le cadre mathématique implique des équations différentielles partielles de deux types: hyperboliques et paraboliques, avec un couplage possible entre les deux types et également un couplage avec des équations différentielles ordinaires (EDOs).

0.2 Chapitre 2: Conception d'observateurs adaptatifs aux frontières pour les systèmes hyperboliques linéaires; Application à l'estimation dans les échangeurs de chaleur

Dans ce chapitre, notre but est d'estimer les températures distribuées d'un échangeur de chaleur concentrique fonctionnant au CO₂ monophasés comme fluide de refroidissement. Le phénomène de transport est modélisé par un système linéaire (2×2) des équations hyperboliques aux dérivées partielles, une équation représente l'écoulement du fluide chaud vers la droite et l'autre représente l'écoulement du fluide froid vers la gauche. L'échange de l'énergie entre les deux flux se fait à travers une interface solide, ce qui induit physiquement un couplage entre les deux dynamiques. Notre objectif est d'estimer la température distribuée à partir des mesures aux extrémités des tubes. Dans ce cadre, nous proposons un observateur adaptatif aux frontières qui peuvent estimer non seulement l'état complet du système, mais aussi des paramètres inconnus dans le domaine. La conception est basée sur la transformation du système d'erreur via une transformation backstepping de dimension finie en un système filtré désiré, pour lequel des techniques standard d'observation et des lois d'adaptation peuvent être utilisées. Les résultats théoriques sont évalués par rapport aux mesures de températures prises à partir d'un cycle de refroidissement fonctionnant au CO₂ construit au CERN en Suisse.

0.3 Chapitre 3: Observateur aux frontières pour les échangeurs de chaleur diphasique

Dans ce chapitre, notre but est d'estimer les variables thermodynamiques (pressions, enthalpies, températures) et les débits massiques d'un échangeur de chaleur concentrique fonctionnant au CO₂ comme réfrigérant de refroidissement. Les phénomènes de transport sont modélisés à l'aide d'équations Navier-Stokes en 1D pour les fluides chauds et froids, où nous considérer les écoulements monophasés et biphasés. L'estimation est faite avec un observateur des EDPs qui utilise des mesures prises aux extrémités du tube pour construire les profils thermodynamiques distribuées. La convergence de cet observateur est prouvée en utilisant l'analyse de Lyapunov et les résultats théoriques sont illustrés par des simulations.

0.4 Chapitre 4: Contrôle Backstepping pour une classe de systèmes des EDPs hyperbolique-parabolique couplées

Dans ce chapitre, notre objectif est de stabiliser un système composé d'une équation de diffusion linéaire couplée à une équation de transport en utilisant des correcteurs aux frontières. Ce type des EDPs (équation aux dérivées partielles) hyperbolique-parabolique couplées s'apparaît dans de nombreux systèmes biologique, chimiques et thermiques. Les deux équations sont couplées à l'intérieur du domaine et à la frontière. L'architecture du couplage dans le domaine est considérée bi-directionnelle, c'est-à-dire un terme source d'advection induit par l'EDP de transport et un terme source intégral du type Volterra induit par l'EDP parabolique. En utilisant la méthode de Backstepping, nous dérivons deux lois de contrôle asservies et nous obtenons des conditions suffisantes pour la stabilité exponentielle du système couplé pour la norme L2. Les gains du correcteur sont calculés en résolvant des équations de kernel du types hyperboliques -paraboliques issus par les transformations de Backstepping. Les résultats théoriques sont illustrés par des simulations numériques.

0.5 Chapitre 5: Conception d'observateurs adaptatifs pour de systèmes EDOs-EDPs hyperbolique couplées

Le but de ce chapitre est l'estimation de l'état de n_ξ EDPs hyperboliques couplées à n_x équations différentielles ordinaires (EDOs) à la frontière du domaine. Le système hyperbolique est linéaire et se propage dans la direction positive de l'axe x . Le système EDO est linéaire variante dans le temps (LTV) et inclus un ensemble de n_θ paramètres constants inconnus, qui doivent être estimés simultanément avec les états des EDPs. Nous concevons un observateur d'état du type Luenberger, et notre méthode est principalement basée sur le découplage d'erreur d'estimation des EDPs de celui des EDOs via le swapping design. Ensuite, nous déduisons les gains de l'observateur grâce à l'analyse de Lyapunov du système découplé. De plus, nous obtenons des conditions suffisantes de convergence exponentielle de l'observateur adaptatif représentés par des inégalités différentielles de Lyapunov (DLIs) et nous illustrons les résultats théoriques par des simulations numériques.

0.6 Chapitre 6: Conclusion et perspectives

La thèse se termine par les conclusion générales, les orientations futurs de recherche en vue d'améliorer et de compléter les méthodes développés dans cette thèse.

Chapter 1

Problem statement and motivating applications

We introduce the four automatic control problems which are tackled in this thesis. The first three are basically related to heat exchangers with applications in the area of fluid systems-cryogenics at CERN, while the fourth one is motivated by the flow networks of gas mixtures with possible application in diesel car engines equipped with exhaust gas regulation (EGR) systems. The mathematical framework involves partial differential equations of two main types: hyperbolic and parabolic, with possible coupling between the two types and also coupling with ordinary differential equation (ODEs).

The general interest in considering this networked aspect of PDE/PDE or PDE/ODE systems is the lack of generalized control and estimation tools that can handle this type of coupling architecture. Each networked problem may require special reasoning and a specific adapted solution. For instance, when two stable PDEs of the same class or of different class are coupled together in the domain or at the boundary, the stability of the coupled system is directly affected as a result of the distributed nature of the PDEs. This leads to enormous technical complications in the control design as well as the observer design regarding the actuators positions and also the placement of the sensors. The ultimate objectives of this thesis is to provide solutions to certain control and estimation problems of systems involving PDE/PDE or PDE/ODE networks.

In the next sections, we classify these problems by considering the main motivation behind each application while defining clearly the mathematical models along with the objectives and the main concerns.

1.1 CO₂ cooling of silicon detectors at CERN

CERN, the European Organization for Nuclear Research, is one of the world's largest and most known centres for scientific research. Physicists and engineers at CERN use complex scientific instruments to study the composition of matter. The instruments are particle accelerators and detectors. Inside the accelerators, subatomic particles beams are boosted to reach the speed of light and made to collide with each other. The LHC (Large Hadron Collider) built at CERN is the world's largest particle accelerator. The beams inside the LHC collide at four locations

around the accelerator ring, corresponding to the positions of four particle detectors – ATLAS, CMS, ALICE and LHCb. These detectors are used to observe and record the collisions, they gather clues about the particles – including their speed, mass and charge – from which physicists can work out a particle’s identity. During operation time, the silicon detectors heat up, and they require efficient and sophisticated cooling to maintain their proper functionality. Cooling of the silicon detector at CERN is the main motivation of problems 1, 2 and 3 of the thesis. In what follows, we detail the cooling strategy proposed by the researchers at CERN, and we specify our main points of interest on which we define the first three objectives of the thesis. In detector applications, it is important to minimize the hardware used for cooling inside the detectors while maximizing the heat transfer from the detectors to the cooling tubes. To get a better insight, let us consider the sketch of a cooling loop depicted on Fig. 1.1.

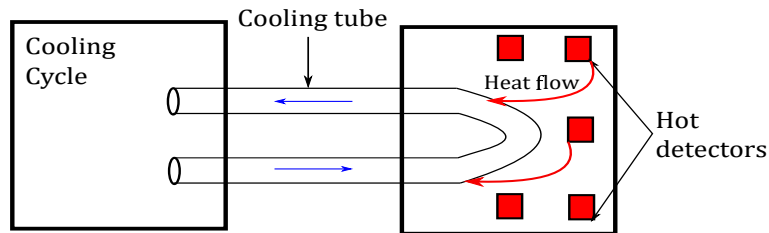


Figure 1.1: Cooling loop.

The cooling fluid propagates from the cooling cycle towards the detectors to absorb their generated heat energy. Two important specifications are required: 1) the cooling tubes should be of small diameters at the detector site, 2) the cooling tubes should absorb the maximum amount of heat from the detectors. To achieve these objectives, two questions must be answered. The first one is "what is the type and the physical state of the cooling fluid?" and second "what are the components of the cooling cycle that will pump into the detectors this suitable type of fluid". The researchers at CERN proposed answers to the questions through a number of articles [86],[78] and [77]. For detector applications, the authors in [77] show the superiority of CO_2 as an evaporative cooling fluid over fluor - carbons C_2F_6 and C_3F_8 . The results are obtained through a thermodynamic analysis which we summarize here:

- two phase (liquid +gas) cooling is more efficient than single phase (liquid or gas) cooling. The heat transfer is higher for two phase fluids.
- CO_2 has high latent heat, low viscosity and low vapor speed. A CO_2 evaporator needs the smallest diameter and it has the highest heat transfer coefficient.

Hence, the fluid circulating in the cooling tube (Fig. 1.1) is CO_2 and it is evaporating i.e. it is undergoing a phase change from liquid to gas. According to the authors in [77], to get this proper two phase flow into the cooling tube, there are two methods: one is the traditional vapor compression method and second is the two-phase accumulator controlled loop (2PACL) method with pumped liquid system. The main advantage of the 2PACL over the traditional method is that it requires no actuators or sensors in the inaccessible detector area. A schematic diagram of the 2PACL refrigeration method is shown on Fig. 1.2.

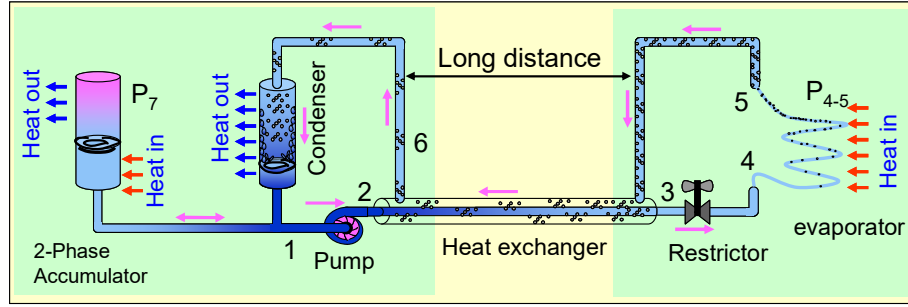


Figure 1.2: The 2PACL refrigeration method [77].

Before giving some brief details on the functioning of the 2PACL loop, it is useful to note the comparison between Fig. 1.1 and Fig. 1.2. Every component to the left of the nodes 4 and 5 on Fig. 1.2 compose the cooling cycle on Fig. 1.1. The capillary tube between the nodes 4 and 5 on Fig. 1.2 stands for the cooling tube on Fig. 1.1 and the "Heat in" on Fig. 1.2 is the heat generated by the detectors. We start the analysis of the 2PACL loop at node 1 where CO₂ is in the liquid phase. The pump increases the pressure and temperature of the fluid to have a high pressure liquid at node 2, the outlet of the pump. Heat is then added by the heat exchanger to reduce the sub-cooling (sub-cooling refers to a liquid existing at a temperature below its normal boiling point). Between nodes 3 and 4, the restrictor expands the liquid into a saturated liquid at the inlet of the evaporator. Passing through the evaporator capillary tubes, the heat generated by the detectors is absorbed by the two phase (liquid+vapor) CO₂. This leads to an increase in the vapor to liquid ratio between the nodes 4 and 5. The downstream fluid between nodes 5 and 6 is now undergoing a two phase condensation. It is exchanging energy with the cold liquid flow, which is also passing through the exchanger but in the opposite direction. We call this heat transfer configuration a two phase heat exchange. The condenser situated between the nodes 6 and 1 ensures the sub-cooling of the flow at the inlet of the pump. Finally, the accumulator helps in setting out the pressure of the entire cooling loop.

To manage energy efficiently in such a cooling cycle, each component should be precisely modeled and accurately controlled. Our main focus in the thesis is between the nodes 2 and 3, i.e. the heat exchanger line. This part of the cooling cycle is extremely important as it spreads along large distances and leads to significant delays in the refrigeration loop. In contrary to the other refrigeration components, the heat exchanger has a distributed nature where temperatures and other thermodynamic variables vary not only in time but also in space. In order not to lose the essential transients of the physical behavior of the system, the control and the estimation algorithms must handle the distributed nature of the physical variables.

Heat exchangers are devices used to exchange energy between fluids. They are key components present in any refrigeration system where they come in different construction geometries and also in different flow configurations [52]. Problems 1, 2 and 3 are concerned with heat exchangers of concentric geometrical shape and of counter-current direction for fluid propagation, as typically shown on Fig. 1.3.

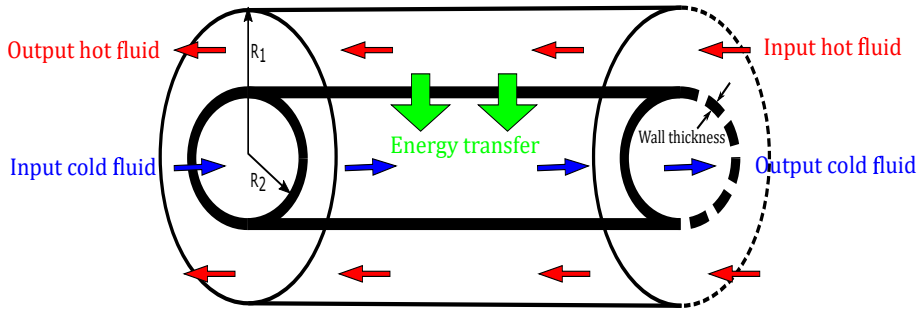


Figure 1.3: Concentric-tube heat exchanger in counter-current flows.

The exchanger in Fig. 1.3 is a schematic diagram of the heat exchanger line situated between nodes 2 and 3 in Fig. 1.2. It is a double pipe, i.e. it is composed of two concentric pipes: an inner pipe of radius R_2 and an outer pipe of radius R_1 . The flows directions are counter-current: the cold and the hot fluids propagate in the opposite directions (this is to maximize the energy transfer). The flow of energy is always from the hot refrigerant to the cold one through the wall interface. Passing through the exchanger, the hot refrigerant loses energy and becomes colder at the output while the cold refrigerant gains energy and becomes more warmer.

1.2 Problem 1: CO₂ single phase heat exchangers

We recall that the thermodynamic profile of the heat transfer line in the 2PACL loop (Fig. 1.2) is two phase for the hot fluid (liquid+vapor) while the cold fluid is single phase (liquid only). In Problem 1, we consider only liquid CO₂ flows (no phase change inside the exchanger). This means that CO₂ enters and leaves in liquid phase for both the hot and the cold lines. A cross-sectional view of the CO₂ single phase heat exchanger is given in Fig. 1.4. We will consider the two phase aspect later in Problem 2. Problem 1 is significantly less complicated than Problem 2 from a thermodynamical point of view.

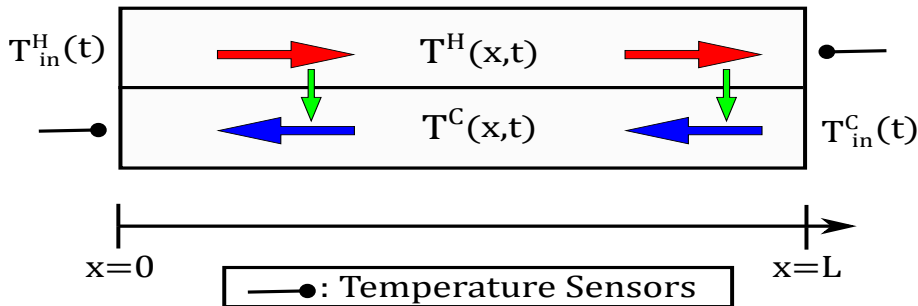


Figure 1.4: CO₂ single phase heat exchanger.

The hot CO₂ liquid propagates in the positive x-axis direction while the cold one flows in the negative direction. The flow of energy (green arrows on Fig. 1.4) is from the hot side to the cold side. The two flows are driven by two control inputs: $T_{in}^H(t)$ and $T_{in}^C(t)$. Based on a

series of assumptions which we will state in Chapter 2, the system is modeled using two infinite dimensional states: the temperature of the hot fluid $T^H(x, t)$ and the temperature of the cold fluid $T^C(x, t)$. The dynamics of the temperature distributions is described using two coupled hyperbolic PDEs of balance laws as follows, $\forall x \in [0, 1]$:

$$\partial_t T^H(x, t) + \frac{\dot{m}^H}{LA^H \rho^H} \partial_x T^H(x, t) = -\frac{h\pi D_1}{A^H \rho^H C_p^H} (T^H(x, t) - T^C(x, t)) \quad (1.1)$$

$$\partial_t T^C(x, t) - \frac{\dot{m}^C}{LA^C \rho^C} \partial_x T^C(x, t) = \frac{h\pi D_1}{A^C \rho^C C_p^C} (T^H(x, t) - T^C(x, t)) \quad (1.2)$$

where ρ^k (kg/m³) is the density, k denotes the considered fluid (H or C), \dot{m}^k (kg/s) is the mass flow rate, A^k (m²) is the tube surface area, D_1 (m) is the inner tube diameter, L (m) is the length of the exchanger, C_p^k (J/kg.K) is the specific heat at constant pressure and h (W/m².K) is the heat transfer coefficient, all considered constants. This system has two-sided boundary conditions:

$$T^H(0, t) = T_{in}^H(t) \quad T^C(1, t) = T_{in}^C(t) \quad (1.3)$$

We can now directly pose the objective of **Problem 1**:

- design an adaptive observer that can simultaneously estimate the distributed temperatures $T^H(x, t)$, $T^C(x, t)$ and the heat transfer coefficient h using only the available measurements at the boundaries $T^H(1, t)$ and $T^C(0, t)$.

Problem 1 is an estimation problem. The overall objective is to estimate the temperature distribution inside the domain using boundary measurements. However, the heat transfer coefficient h is likely to be unknown. This necessitates an adaptive estimator. Here are the main motivations in considering Problem 1:

1. Problem 1 coincides with practical demands. In practice, sensors are placed at the boundaries of the exchanger (only inputs and outputs are measured). Hence, we do not know exact temperatures inside the domain. Also, we do not know what is the value of the heat transfer coefficient h . h is responsible for the amount of energy flowing from the hot side to the cold side. Unlike all the other parameters of the exchanger, the heat transfer coefficient depends on many physical variables e.g. temperature, mass flow rates and fluids viscosity. It is usually calculated from physical correlations that lead to uncertainty on its value. Therefore, it is of great interest to also estimate h online using boundary measurements.
2. certain types of control laws (ex. Backstepping control) require to have full knowledge of the distributed temperatures all over the domain. Knowing the full temperatures with the real time estimation of h helps in efficiently controlling the refrigeration loop. This will contribute to low rates of energy consumption while maximizing the heat transfer rates.
3. continuous monitoring of the temperatures distribution in real time over long distances helps in detecting faults in case of energy leakage.

4. various physical problems can be reformulated in the context of Problem 1. For example, the linearized ARZ-model [16] for traffic has almost the same structure as the heat exchanger model (1.1)-(1.2) with density $\rho(x,t)$ and velocity $v(x,t)$ as systems states. The ARZ model has also the unknown relaxation time τ similar to h in the heat exchanger model. We also mention that other physical systems e.g. electrical power transmission lines [34] and water flow in open canals (shallow water equations [32]) and many more, include unknown in-domain parameters that are equivalent to h in the heat exchanger model.

Our proposed solution to Problem 1 is presented in Chapter 2. The theoretical results of the adaptive observer are accompanied by numerical simulations, and they are also evaluated against the temperature measurements taken from the CO₂ refrigeration apparatus at CERN.

1.3 Problem 2: CO₂ two phase heat exchangers

In this problem, we consider the two phase aspect in CO₂ heat exchangers. The heat exchange scenario occurring in the heat transfer line of the 2PACL loop is replicated for the evaporation phase. Hence, we consider a concentric tube heat exchanger where the hot flow is in the liquid phase while the cold flow is evaporating and changing its phase from liquid to vapor, as shown on the Fig. 1.5.

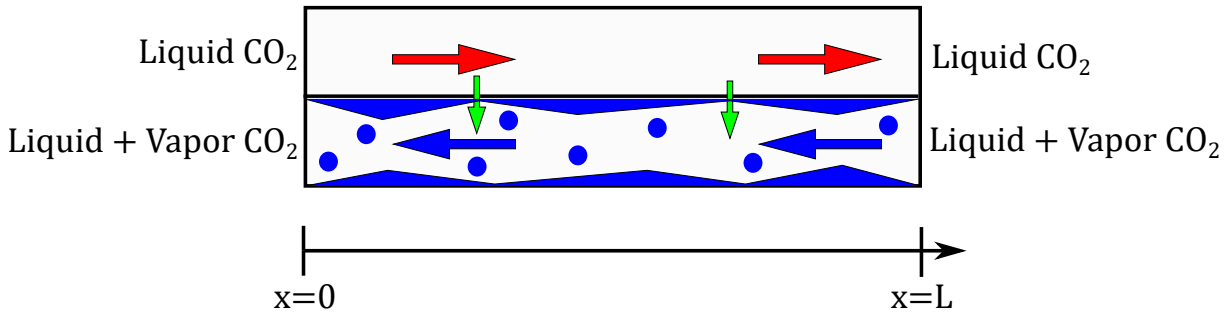


Figure 1.5: CO₂ two phase heat exchanger.

Through the wall interface, energy is transferred from the hot liquid side to the cold evaporating side. **Problem 2** has two main objectives:

- obtain a control-oriented model for the CO₂ two phase heat exchanger;
- based on the obtained model, design a boundary observer to estimate the vapor to liquid ratio of the two phase flow inside the domain, while sensing its values at the boundary.

These objectives are motivated by the following issues:

1. as we have mentioned in the 2PACL loop explanation, the two phase evaporator-tube is the key component for the developing CO₂ cooling technology at CERN;

2. the control-oriented modeling of the two phase line helps in integrating it easily inside the control system of the cooling cycle;
3. estimating the vapor to liquid ratio inside the domain allows to minimize the energy consumption used for cooling;
4. as we have already stated in Problem 1, boundary sensing is more practical than distributed sensing. Sensors are usually placed at the extremities of the tube.

Unlike the configuration of Problem 1, the two phase line in Problem 2 introduces a significant physical complication that necessitates careful modeling. Once the model is obtained, suitable boundary estimation techniques can be applied. The solution details for Problem 2 will be extensively detailed in Chapter 3.

1.4 Problem 3: Coupled hyperbolic-parabolic PDEs

It is mentioned above (see Fig. 1.3), that in heat exchangers energy flows from one fluid to the other through a wall interface. So far, in Problems 1 and 2, we have neglected the effect of the wall thickness. However, according to the authors in [77], the tube temperature and the fluids temperature may have different values depending on the flow regime, as shown on Fig. 1.6.

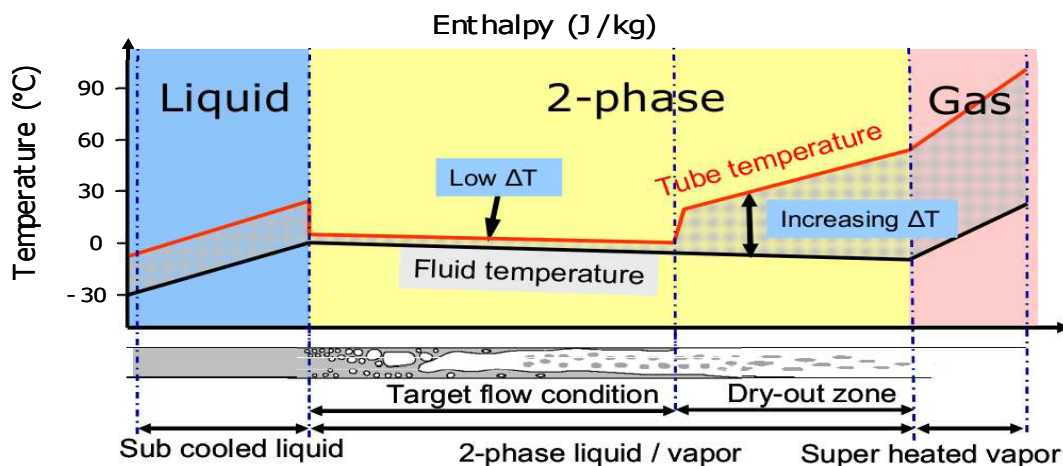


Figure 1.6: Fluid temperature vs tube temperature [77].

The lower part of the graph gives a complete scenario of what can happen in an evaporating tube. The fluid starts in the liquid region, and then begins to evaporate to enter into the two phase zone. Finally, all the liquid is evaporated and the fluid reach the gaseous state. The fluid temperature is in black while the tube temperature is in red. First, we can notice a temperature difference ΔT in the liquid region. This temperature difference decreases in the target flow condition regime to increase again significantly in the dry-out and the super heated zones. The sudden increase in ΔT is due to the fact that the remaining liquid is no longer touching the tube wall, while in the dry-out zone. A high ΔT means that the dynamics of the wall temperature

cannot be neglected any more in the modeling phase. This can introduce an interesting coupling between two different classes of systems: transport equations (the fluid) and heat equations (the wall). To help clarify the idea, we take a simple example: a tube containing hot liquid that is placed in an environment of cold temperature T_{amb} as shown in Fig. 1.7.

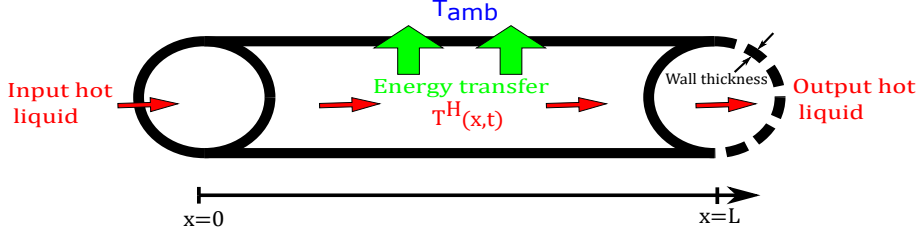


Figure 1.7: Hot line with wall thickness.

Energy is transferred from the hot flow to the wall through convection. Passing through the wall thickness, energy is conducted to reach the outer surface of the tube. We represent the two different types of physical phenomena, namely convection and conduction, using two states: $T^H(x, t)$ which is the liquid temperature and $T^w(x, t)$ which is the wall temperature. Using the principle of conservation of energy, and assuming 1D flows, the dynamics of the states are:

$$\partial_t T^w(x, t) = \epsilon(x) \partial_{xx} T^w(x, t) + h_{H,w} (T^H(x, t) - T^w(x, t)) + (T^w(x, t) - T_{amb}) \quad (1.4)$$

$$\partial_t T^H(x, t) = -\frac{\dot{m}^H}{LA^H \rho^H} \partial_x T^H(x, t) - \frac{h_{H,w} \pi D_1}{A^H \rho^H C_p^H} (T^H(x, t) - T^w(x, t)) \quad (1.5)$$

where $\epsilon(x)$ is the diffusion coefficient, $h_{H,w}$ and $h_{w,amb}$ are the heat transfer coefficients from the liquid to the wall and from the wall to the environment, respectively. The transport equation (1.5) is a hyperbolic PDE that is coupled with the heat equation (1.4) which is a parabolic PDE. The coupling is inside the domain through the linear advection terms of the heat transfer energy. Hence, if the wall thickness is not neglected, the mathematical models of the heat exchangers will certainly involve an interesting coupling between different classes of systems (hyperbolic and parabolic). The overall aim of Problem 3 is to study such kinds of systems. This helps in understanding the effect of diffusion on the transport of energy from one fluid to the other. As a result, **in Problem 3** we consider the following class of mixed hyperbolic-parabolic system evolving in $\{(t, x) \mid t \geq 0, x \in [0, 1]\}$:

$$v_t(x, t) = v_{xx}(x, t) + \lambda(x)v(x, t) + \sigma(x)u(x, t) \quad (1.6)$$

$$u_t(x, t) = u_x(x, t) + \int_0^x S(x, y)v(y, t)dy \quad (1.7)$$

$$v_x(0, t) = u(0, t) \quad (1.8)$$

$$v(1, t) = F_1(t) \quad (1.9)$$

$$u(1, t) = F_2(t) \quad (1.10)$$

where v and u are the coupled parabolic and hyperbolic states of the system, respectively. $S(x, y) \in C^\infty$ represents the coupling kernel from diffusion to transport, while $\sigma(x) \in C^1[0, 1]$

is the linear coupling from transport to diffusion. The reaction term $\lambda(x) \in C^1[0, 1]$ is considered arbitrary. The outflow of the transport equation also drives the parabolic equation at the boundary $x = 0$. Furthermore, the two coupled states are actuated using the two control laws $F_1(t)$ and $F_2(t)$ at $x = 1$. System (1.6)-(1.10) is motivated by the phenomena of extreme ultraviolet light generation (EUV) for next-generation photolithography [80]. The EUV technology involves a liquid metal droplet which is convecting through plasma. The plasma influences the droplet and diffuses it in space. The convection phenomena is modeled by the hyperbolic PDE while diffusion in space is modeled by the parabolic PDE. The main objective of **Problem 3** is:

- design two feedback control laws $F_1(t)$ and $F_2(t)$ that can ensure the exponential stability of the system (1.6)-(1.10) in the $L^2 \times H^1$ norm.

Note that equation (1.7) involves an integral coupling with diffusion, whereas (1.5) has only a linear coupling term. Thus, the two systems differ in the type of coupling between the hyperbolic and parabolic states. We will show in Chapter 4 that certain types of coupling topologies are quite hard to be tackled from a control theory point of view. System (1.4)-(1.5) is a prime example on this difficulty, and hence, we propose a solution based on the model (1.6)-(1.10).

Now, we state the main motivations in considering Problem 3:

1. system (1.6)-(1.10) is considered as an intermediate step to consider more complicated types of coupling topologies in the future works (e.g. the linear advection coupling in system (1.4)-(1.5));
2. investigating the control techniques that can work on mixed classes of hyperbolic-parabolic systems. The existence of control designs such as Backstepping transformations or simple Lyapunov functions for hyperbolic or parabolic systems is well known, but the application of these techniques on systems of mixed classes is still under research.

The solution of Problem 3 is given in Chapter 4. The theoretical results are illustrated in details and we also give some numerical simulations to demonstrate the application of the proposed method.

1.5 Problem 4: Coupled ODEs-Hyperbolic PDEs networks

Many physical processes are modeled using linear hyperbolic partial differential equations coupled with linear ordinary differential equations. The infinite state which is modeled by the PDE represents the transport in space, and its value at the boundary is usually constrained to some exterior dynamics represented by the ODEs. The mentioned coupling topology mostly appears in networks, where the edges are modeled using transport PDEs and the nodes are modeled using ODEs. Examples of such systems can be found in ventilation networks [69], road traffic [44], gas flow in pipelines [46], flow in open channels [33], exhaust gas regulation (EGR) in cars engines [27], etc. In Problem 4, we are interested more specifically in diesel car engines equipped with (EGR) systems.

Over the years, the regulation of the emissions of diesel car engines has become more strict. Emission limits for Diesel engines [61] have been imposed by the European legislation to minimize

the road transport pollution, which remains the most important source of urban air pollution in Europe with respect to NO_x (nitrogen oxides) and CO (carbon monoxide) [82]. The environmental demands force the car engine designers to develop new technologies to decrease the fuel consumption and the emission levels while satisfying the desired engine drivability conditions. Many alternative combustion modes such as homogenous charge compression ignition, low-temperature combustion, pre-mixed controlled compression ignition [4], [6] and [72] are introduced to decrease the engine emissions level. These modes require specific fueling strategies and in-cylinder conditions, thus creating a vital need for complex, reliable and accurate control system technologies. One of the new configurations, that can provide adequate conditions for multiple combustion modes is the Dual exhaust gas regulation (EGR) with both high-pressure (HP) and low-pressure (LP) recirculations [49]. A schematic diagram of a dual EGR loop is shown on Fig. 1.8.

The engine presented in Fig. 1.8 is a four cylinder (1.6 liter) diesel engine with dual-loop EGR system (HP-EGR valve and LP-EGR valve) and a variable geometry turbine (VGT). It is equipped with an exhaust treatment system: diesel particle filter (DPF) and diesel oxidation catalyst (DOC). The general idea of an EGR system is that some portion of the exhaust gas at the output of the engine are returned back to the intake manifold through the EGR valves. With the high pressure (HP-EGR), the burned gases from the exhaust manifold are reintroduced into the intake manifold. While, the burned gases in the LP-EGR are taken downstream through the post-treatment filters and then mixed with the fresh air coming from outside to be reintroduced upstream of the compressor. The mixing of the hot HP-EGR gas with the cold LP-EGR gas at the intake can be set to reach the optimal temperature inside the cylinders, which reduces the emissions of HC-CO gases.

It is difficult to achieve the adequate in-cylinder conditions due to the lack of measurements of the EGR flow rates and also the air mass fractions (mass of air/total mass).

Indeed, several control and estimation techniques [29], [45], [81], [84] are proposed to estimate the EGR rates and also to estimate and control the air-mass fractions. These schemes are built on 0D models of the engine air-path. In 0D models, the air-path is decomposed into sets of control volumes glued together with other different components such as compressors, valves, coolers, etc. The conservation laws (mass conservation, momentum conservation, energy conservation) are applied to each control volume and finally a 0D model of coupled ordinary differential equations is obtained for the whole air-path (see the manuscript [28] and references therein). One of the draw backs of 0D models is not considering the mass transport time inside the engine admission air-path. During strong engine transients, the mass transport can cause a degradation in the overall performance of the engine emissions rates. This fact is considerably persistent in the LP-EGR path where the gas travels much longer distance than the one associated with the HP-EGR path. To overcome this limitation, a delay representation is used by the authors in [23] to model the transport time while others (e.g. [27]) have used linear parameter varying (LPV)-hyperbolic systems. Let us focus on the model proposed by the authors in [27], as it is the main inspiration of Problem 4.

The authors in [27] model the air-mass transport inside the LP-EGR path. The model consists of three transport equations $\xi(x, t)$ that model the air-fraction transport inside the tubes and three ODEs $X(t)$ to model the variation of the air-fraction in the control volumes connecting

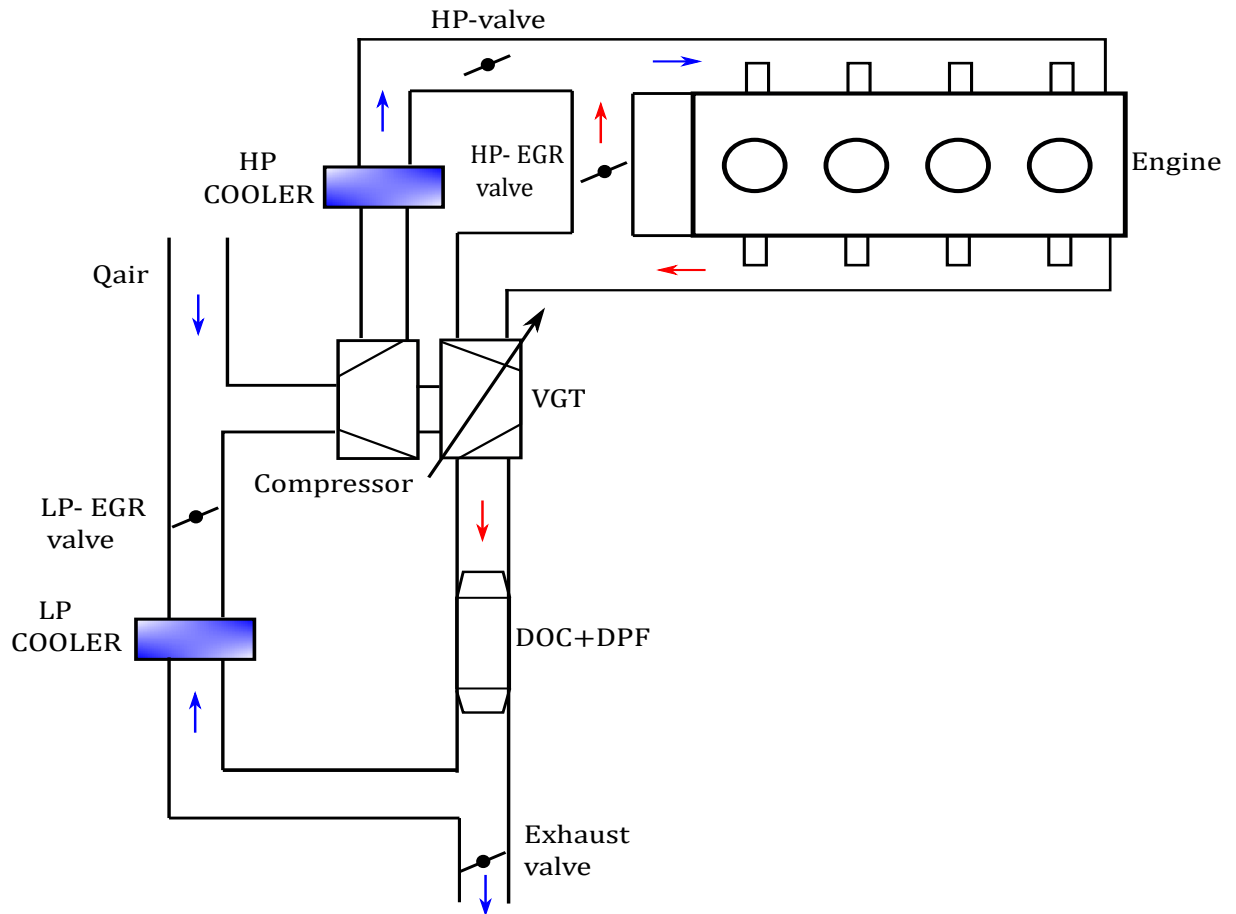


Figure 1.8: Schematic of the dual-loop EGR engine air-path.

the tubes. The overall model is as follows:

$$\partial_t \xi(x, t) + \Lambda(\phi) \partial_x \xi(x, t) = 0 \quad (1.11)$$

$$\xi(0, t) = X(t) \quad (1.12)$$

$$\dot{X}(t) = A(\phi)X(t) + B(\phi)\xi(1, t) + \psi(\phi)Q_{egr1} + Q_{air} \quad (1.13)$$

where ϕ is the set of varying parameters of known bounds and Q_{egr1} is the control variable through the LP-EGR valve. It is not our aim to explain in details the modeling procedure of the LP-EGR path (see [27] for more details). However, the model general structure is of great importance for the continuity of the explanation. Model (1.11)-(1.13) is a set of hyperbolic PDEs coupled with a parameter-varying set of ODEs at the boundary $x = 0$. The problem considered in [27] is to synthesize a control law Q_{egr1} in order to drive the states $\xi(x, t)$ and $X(t)$ to a desired steady state using the measurements of $\xi(1, t)$. In Problem 4, we consider nearly the dual problem. It is an estimation problem. Let us introduce the system considered in Problem 4. We consider the following class of cascade ODEs-hyperbolic PDEs systems evolving in $\Omega = [0, 1] \times [0, +\infty)$:

$$\partial_t \xi(x, t) + \Lambda^+ \partial_x \xi(x, t) = F\xi(x, t) \quad (1.14)$$

$$\xi(0, t) = C(t)X(t) + D(t)u(t) + \psi_1(t)\theta \quad (1.15)$$

$$\dot{X}(t) = A(t)X(t) + B(t)u(t) + \psi_2(t)\theta \quad (1.16)$$

where $\xi(x, t) : \Omega \mapsto \mathbb{R}^{n_\xi}$ is the PDE state vector, $X(t) : [0, +\infty) \mapsto \mathbb{R}^{n_x}$ is the ODE state vector, $\theta \in \mathbb{R}^{n_\theta}$ is the vector of the unknown parameters, $u(t) : [0, +\infty) \mapsto \mathbb{R}^{n_u}$ is a known input vector that possibly depends on $\xi(1, t)$ and $\Lambda^+ \in D_+^{n_\xi}$ is the matrix of the constant transport speeds:

$$\Lambda^+ = \begin{bmatrix} \lambda_1 & & 0 \\ & \ddots & \\ 0 & & \lambda_{n_\xi} \end{bmatrix} \quad \text{with } 0 < \lambda_1 < \dots < \lambda_{n_\xi} \quad (1.17)$$

$F \in \mathbb{R}^{n_\xi \times n_\xi}$. We assume that all the time-dependent matrices: $A(t) \in \mathbb{R}^{n_x \times n_x}$, $B(t) \in \mathbb{R}^{n_x \times n_u}$, $C(t) \in \mathbb{R}^{n_\xi \times n_x}$, $D(t) \in \mathbb{R}^{n_\xi \times n_u}$, $\psi_1(t) \in \mathbb{R}^{n_\xi \times n_\theta}$ and $\psi_2(t) \in \mathbb{R}^{n_x \times n_\theta}$ are bounded and piece-wise continuous in time.

The main objective of Problem 4 is:

- design an adaptive observer that can estimate $\xi(x, t)$, $X(t)$ and θ simultaneously assuming that the measurement available is $y(t) = M\xi(1, t)$ where $M \in \mathbb{R}^{n_y \times n_\xi}$ is the output matrix.

The main motivations in considering Problem 4 are:

1. in case of a slowly-varying LP-EGR mass flow rate, i.e $\dot{Q}_{egr1} = 0$, the adaptive observer of problem 4 can be extended to give estimations of the air-fractions and the LP-EGR mass flow rate Q_{egr1} using end tubes sensing $\xi(1, t)$. This is obvious from the close structure of the two models (1.11)-(1.13) and (1.14)-(1.16) while considering $\theta \equiv Q_{egr1}$.

2. system (1.14)-(1.16) can be considered an extension to the LTV case since it has an LTV boundary conditions and also LTV ODEs. This is more general than the LPV case. The transport speeds in system (1.14)-(1.16) can be time-varying, as we will show in Chapter 5.
3. although we focus on the EGR exhaust system as the principal application, the main theoretical results extend to large amount of industrial applications of significant importance such as hydraulic networks [39], road traffic networks [47], gas flow in pipelines [7], etc.

The solution of Problem 4 is given in Chapter 5. The theoretical results of the adaptive estimator are illustrated by numerical examples.

1.6 Conclusion

In this chapter, we show the four different automatic control problems that are solved in this thesis. We directly state the problems with the main motivations. In the mathematical framework, the problems involves coupled hyperbolic-hyperbolic PDE systems (Problems 1 and 2). In Problem 3, we investigate a different type of couplings which is hyperbolic-parabolic PDEs. The network aspect is investigated in Problem 4 with a different coupling topology, which is hyperbolic PDEs coupled with ODEs. Problems 1, 2 and 4 are boundary estimation problems with unknown parameters present in the domain and at the boundary, while Problem 4 is a boundary control problem for different kinds of PDEs.

In the next chapters, we start by detailing the solutions of the problems. In each chapter, we give the literature review related to each problem while clearly stating our contributions and the added value for each of our methods. The mathematical derivations with the proofs are discussed in details and finally numerical and experimental tests (when available) are offered to evaluate the results.

Chapter 2

Adaptive Boundary Observer Design for Hyperbolic Systems; Application to CO₂ single phase heat exchangers

We consider the concentric tubes heat exchanger schematically depicted in Fig. 2.1. This exchanger is a counter-flows heat exchanger, in which hot and cold fluids flow in opposite directions to maximize the heat transfer. Both the hot and the cold fluids enter in liquid phase and leave in liquid phase (no change of phase inside the exchange). The flow of heat from the hot side to the cold side is done through the wall interface.

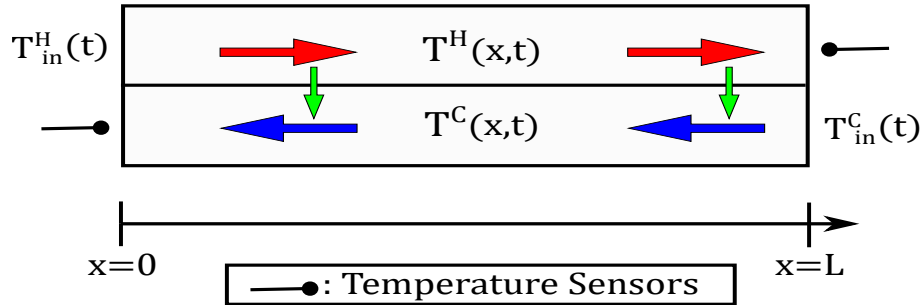


Figure 2.1: CO₂ single phase heat exchanger.

The mathematical model of the exchanger is derived based on the following assumptions:

- the flow is 1-D unidirectional (the hot fluid flows in the positive x direction);
- the kinetic and potential energies of the flows entering and leaving the tubes are neglected;
- the wall thickness is neglected (no wall dynamics) and the heat transfer coefficient h is uniform and quasi-steady i.e. using the classical "random walk" model, $\dot{h} = 0 + e(t)$ where $e(t)$ is a white noise;

- the flow is considered incompressible; i.e. no significant change in density and equivalently in mass flow rate with time and along the length of the exchanger (only energy conservation equations are considered);
- in our working range of pressures and temperatures, we can assume a linear relation between enthalpy and temperature as follows:

$$H^H = C_P^H T^H, \quad H^C = C_P^C T^C \quad (2.1)$$

where H^k (J/kg) is the specific enthalpy, k denotes the considered fluid (H or C), C_p^k (J/kg.K) is the specific heat at constant pressure and T^k (K) is the temperature.

Under these assumptions, the 1D flow transport can be described by a set of first order hyperbolic partial differential equations of balance laws (see e.g. [83]) as follows, $\forall x \in [0, 1]$:

$$\partial_t T^H(x, t) + \frac{\dot{m}^H}{L A^H \rho^H} \partial_x T^H(x, t) = -\frac{h \pi D_1}{A^H \rho^H C_p^H} (T^H(x, t) - T^C(x, t)) \quad (2.2)$$

$$\partial_t T^C(x, t) - \frac{\dot{m}^C}{L A^C \rho^C} \partial_x T^H(x, t) = \frac{h \pi D_1}{A^C \rho^C C_p^C} (T^H(x, t) - T^C(x, t)) \quad (2.3)$$

where ρ^k (kg/m³) is the density, \dot{m}^k (kg/s) is the mass flow rate, A^k (m²) is the tube surface area, D_1 (m) is the inner tube diameter, L (m) is the length of the exchanger, C_p^k (J/kg.K) is the specific heat at constant pressure and h (W/m².K) is the heat transfer coefficient, all considered constants. This system has two-sided boundary conditions:

$$T^H(0, t) = T_{in}^H(t) \quad T^C(1, t) = T_{in}^C(t) \quad (2.4)$$

and initial conditions (assumed to be in $L^2[0, 1]$):

$$T^H(x, 0) = T_0^H(x), \quad T^C(x, 0) = T_0^C(x) \quad (2.5)$$

The objective is to design an adaptive observer that can simultaneously estimate the distributed temperatures $T^H(x, t)$, $T^C(x, t)$ and the heat transfer coefficient h using only the available measurements at the boundary $T^H(1, t)$ and $T^C(0, t)$.

The classical approach used for solving control and estimation problems for hyperbolic partial differential equations is to discretize the PDEs and then apply classical control methods designed for finite dimensional systems. However, key information on the system transient behavior is lost, and the observability and controllability of the system will depend on the chosen space-discretization method. This leads to the idea of extending finite dimensional control theory to the infinite case. Hence, the PDE architecture is conserved and the goal is to design an observer that can estimate the infinite dimensional states.

The main difficulty induced by the dynamics (2.2)-(2.5) is that it involves a bilinear parametric nonlinearity i.e. the unknown parameter h multiplies the unknown states $T^H(x, t)$ and $T^C(x, t)$. In fact, if h is known, Problem 1 is already solved in the literature and it has two categories of

solutions: 1) is the work done by the authors in [85] via a PDE observer of Lunberguer type that uses dissipative boundary conditions (standard static boundary output feedback) to stabilize the estimation error. And 2) the backstepping observer design in [14] (among others for instance [76]). The main idea of the backstepping method is to introduce an invertible Volterra transformation that maps the original system into a target system with the desired stability properties, for which static boundary controls and observer gains are synthesized to ensure the system convergence to a desired set in finite time. However, to the best of our knowledge, if h is unknown and in the infinite dimensional framework, Problem 1 has not been yet addressed in the literature.

2.1 Linearization

We decrease the level of complexity by augmenting the vector of states of the system from $\{T^H, T^C\}$ to $\{T^H, T^C, h\}$ with $\dot{h} = 0$. The augmented system is then linearized around the nominal system $\{T_N^H, T_N^C, h^N\}$ given by:

$$\partial_t T_N^H(x, t) + \frac{\dot{m}^H}{LA^H \rho^H} \partial_x T_N^H(x, t) = -\frac{h^N \pi D_1}{A^H \rho^H C_P^H} (T_N^H(x, t) - T_N^C(x, t)) \quad (2.6)$$

$$\partial_t T_N^C(x, t) - \frac{\dot{m}^C}{LAC \rho^C} \partial_x T_N^C(x, t) = \frac{h^N \pi D_1}{AC \rho^C C_P^C} (T_N^H(x, t) - T_N^C(x, t)) \quad (2.7)$$

with boundary conditions:

$$T_N^H(0, t) = T_{in}^H(t), \quad T_N^C(1, t) = T_{in}^C(t) \quad (2.8)$$

and initial conditions (assumed to be in $L^2[0, 1]$):

$$T_N^H(x, 0) = T_{N0}^H(x), \quad T_N^C(x, 0) = T_{N0}^C(x) \quad (2.9)$$

such that:

$$\begin{cases} T^H(x, t) &= T_N^H(x, t) + \Delta T^H(x, t), \\ T^C(x, t) &= T_N^C(x, t) + \Delta T^C(x, t), \\ h &= h^N + \Delta h, \end{cases} \quad (2.10)$$

where $\Delta T^H(x, t)$, $\Delta T^C(x, t)$ and Δh are perturbations around the nominal states. Using a Taylor expansion of order 1, one can obtain the dynamics of the perturbed states:

$$\begin{aligned} \partial_t \Delta T^H(x, t) + c_1 \partial_x \Delta T^H(x, t) &= -K_1^N (\Delta T^H(x, t) - \Delta T^C(x, t)) \\ &\quad + \Delta h \frac{\pi D_1}{A^H \rho^H C_P^H} (-T_N^H(x, t) + T_N^C(x, t)) \end{aligned} \quad (2.11)$$

$$\begin{aligned} \partial_t \Delta T^C(x, t) - c_2 \partial_x \Delta T^C(x, t) &= K_2^N (\Delta T^H(x, t) - \Delta T^C(x, t)) \\ &\quad + \Delta h \frac{\pi D_1}{AC \rho^C C_P^C} (T_N^H(x, t) - T_N^C(x, t)) \end{aligned} \quad (2.12)$$

where $c_1 = \frac{\dot{m}^H}{LA^H \rho^H}$, $c_2 = \frac{\dot{m}^C}{LA^C \rho^C}$, $K_1^N = \frac{h^N \pi D_1}{A^H \rho^H C_P^H}$ and $K_2^N = \frac{h^N \pi D_1}{A^C \rho^C C_P^C}$. The boundary conditions of the perturbed system are:

$$\Delta T^H(0, t) = 0, \quad \Delta T^C(1, t) = 0 \quad (2.13)$$

The initial conditions $\Delta T_0^H(x)$ and $\Delta T_0^C(x)$ are assumed to be in $L^2[0, 1]$. Using a simple exponential transformation: $\Delta T_1^H(x, t) = e^{\frac{K_1^N}{c_1} x} \Delta T^H(x, t)$ and $\Delta T_1^C(x, t) = e^{-\frac{K_2^N}{c_2} x} \Delta T^C(x, t)$, we can eliminate the homogeneous terms in (2.11)-(2.12) to get:

$$\begin{aligned} \partial_t \Delta T_1^H(x, t) + c_1 \partial_x \Delta T_1^H(x, t) &= K_1^N e^{(\frac{K_1^N}{c_1} + \frac{K_2^N}{c_2})x} \Delta T_1^C(x, t) \\ &+ \Delta h \frac{\pi D_1 e^{-\frac{K_1^N}{c_1} x}}{A^H \rho^H C_P^H} (-T_N^H(x, t) + T_N^C(x, t)) \end{aligned} \quad (2.14)$$

$$\begin{aligned} \partial_t \Delta T_1^C(x, t) - c_2 \partial_x \Delta T_1^C(x, t) &= K_2^N e^{-(\frac{K_1^N}{c_1} + \frac{K_2^N}{c_2})x} \Delta T_1^H(x, t) \\ &+ \Delta h \frac{\pi D_1 e^{\frac{K_2^N}{c_2} x}}{A^C \rho^C C_P^C} (T_N^H(x, t) - T_N^C(x, t)) \end{aligned} \quad (2.15)$$

and the boundary conditions remains the same

$$\Delta T_1^H(0, t) = 0, \quad \Delta T_1^C(1, t) = 0 \quad (2.16)$$

The initial conditions $\Delta T_{0,1}^H(x)$ and $\Delta T_{0,1}^C(x)$ are assumed to be in $L^2[0, 1]$. System (2.14)-(2.16) has boundary measurements as:

$$\begin{aligned} y_1^H(t) &= e^{\frac{K_1^N}{c_1}} \Delta T^H(1, t) = e^{\frac{K_1^N}{c_1}} (T^H(1, t) - T_N^H(1, t)) \\ y_2^C(t) &= \Delta T^C(0, t) = T^C(0, t) - T_N^C(0, t) \end{aligned} \quad (2.17)$$

In practice and especially in heat exchanger networks, it is common to have a prior knowledge of the plant; e.g. ranges of pressures, ranges of temperatures, fluid speeds etc. This practical understanding of the system can help in deriving inaccurate estimates of the systems parameters, e.g. use correlations from the physics to calculate an estimate for the heat transfer coefficient as in [43]. These estimates are considered as the nominal values for the exchanger parameters (c_1 , c_2 , K_1^N and K_2^N) and they are used in constructing the nominal model (2.6)-(2.9). Hence, synthesizing an adaptive observer for $\{\Delta T_1^H(x, t), \Delta T_1^C(x, t), \Delta h\}$ will lead to an approximate estimate for $\{T^H(x, t), T^C(x, t), h\}$ according to the map depicted in Fig. 2.2. Therefore, by knowing the operating point of the system and by measuring input/output temperatures, one can use our adaptive observer scheme to have an online estimation of the distributed states $T^H(x, t)$, $T^C(x, t)$ and also to recover the deviation of the heat transfer coefficient h from the correlation-based nominal value h^N . Now, we focus on the adaptive observer design for system (2.14)-(2.17). In fact, the structure of the equations (2.14)-(2.17) inspires us to pose the estimation problem on a more general class of systems.

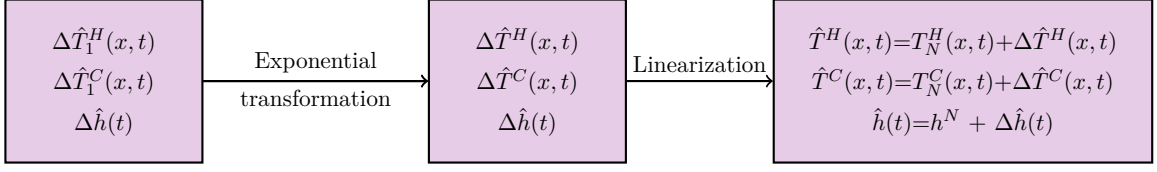


Figure 2.2: State estimation map

2.2 Observation problem formulation

We consider the following class of linear hyperbolic systems evolving in $\{(t, x) \mid t \geq 0, x \in [0, 1]\}$:

$$\partial_t u(x, t) + c_1 \partial_x u(x, t) = \sigma_1(x)v(x, t) + \theta_1 \phi_1(x, t) \quad (2.18)$$

$$\partial_t v(x, t) - c_2 \partial_x v(x, t) = \sigma_2(x)u(x, t) + \theta_2 \phi_2(x, t) \quad (2.19)$$

$$u(0, t) = qv(0, t) + U(t), \quad v(1, t) = V(t) \quad (2.20)$$

where u and v are the system states, $[u, v]^T : [0, 1] \times [0, +\infty) \rightarrow \mathbb{R}^2$. $c_1 > 0$ and $c_2 > 0$ are the transport speeds, and σ_1, σ_2 are assumed to be $C^0([0, 1]; \mathbb{R})$ known functions. Furthermore, ϕ_1 and ϕ_2 are also bounded known functions of class $C^1([0, 1] \times [0, +\infty); \mathbb{R})$, and q, θ_1 and θ_2 are unknown real scalar parameters. The initial conditions, denoted u_0 and v_0 , are assumed to belong to $L^2([0, 1])$. $U(t)$ and $V(t)$ are considered as known boundary inputs. Our goal is to estimate the state of the system (2.18)-(2.20) and the unknown parameters q, θ_1 and θ_2 , assuming that the following measurements are available:

$$y_1(t) = u(1, t), \quad y_2(t) = v(0, t) \quad (2.21)$$

Remark 2.2.1. *It is clear that the exact congruence of system (2.18)-(2.21) with system (2.14)-(2.17) is achieved for: $u(x, t) \equiv \Delta T_1^H(x, t)$, $v(x, t) \equiv \Delta T_1^C(x, t)$, $\sigma_1(x) \equiv K_1^N e^{(\frac{K_1^N}{c_1} + \frac{K_2^N}{c_2})x}$, $\sigma_2(x) \equiv K_2^N e^{-(\frac{K_1^N}{c_1} + \frac{K_2^N}{c_2})x}$, $\phi_1(x, t) \equiv \frac{\pi D_1 e^{-\frac{K_1^N}{c_1} x}}{A^H \rho^H C^H} (-T_N^H + T_N^C)$, $\phi_2(x, t) \equiv \frac{\pi D_1 e^{\frac{K_2^N}{c_2} x}}{A^C \rho^C C^C} (T_N^H - T_N^C)$, $\theta_1 \equiv \theta_2 \equiv \Delta h$ and $q \equiv U(t) \equiv V(t) \equiv 0$.*

Remark 2.2.2. *While the method extends to spatially varying transport speeds $c_1(x)$ and $c_2(x)$, we consider here constant transport speeds for the sake of technical simplicity.*

System (2.18)-(2.20) is a 2×2 linear hyperbolic system. It is coupled inside the domain and at the boundary. The system is two-sided actuated, and unknown parameters are present inside the domain and at the boundary. The objective is to design an adaptive observer to estimate the system states and the parameters. The literature review on control and estimation for hyperbolic systems is as follows.

2.3 Literature review

Hyperbolic systems and more specifically linear and quasi-linear hyperbolic systems are well studied by the control community. These systems can model many physical processes, like road traffic [44], gas flow in pipelines [46], flow of fluids in open channels [32], transmission lines [34], multiphase flow [35], etc.. The early results on stability and controllability of such systems can be dated back to the 70s [68], [71]. During that period, the stability issue was tackled by computing the explicit solution of the equations along the characteristic curves in the framework of the C^1 norm. Afterwards, using Lyapunov-based functions, dissipative boundary conditions (standard static boundary output feedback) are designed to guarantee exponential stability in the L^2 , C^1 and H^2 norms [83, 26, 17]. One drawback of using this kind of boundary conditions to stabilize the system is that it imposes some restrictions on the magnitude of the coupling between the system states. However, this limitation can be overcome by the use of the so-called backstepping-method. In [76], the authors solve the problem of one-sided boundary stabilization (actuation only at one boundary) of a two by two quasilinear first-order hyperbolic system in finite time. The approach is then generalized by the authors in [50] to a general system of heterodirectional coupled hyperbolic equations. The backstepping method is also used for two-sided boundary control (actuation on both boundaries) of heterodirectional hyperbolic systems. The authors in [14] derive control laws using a Fredholm transformation (unlike Volterra transformation, Fredholm transformation is not always invertible) that also ensures convergence in finite time. However, all the results mentioned so far do not allow unknown in-domain parameters or unknown boundary parameters to be present. In order to address this problem, we consider adaptive boundary control for hyperbolic systems. The first results on adaptive control for hyperbolic PDEs were obtained by the authors in [20], where a general first-order hyperbolic partial integro-differential equation (PIDE) with one rightward convecting PDE is adaptively stabilized by boundary sensing only. This result is extended by the authors in [8] to 2 by 2 hyperbolic partial differential equations with unknown transport speeds, unknown couplings and also unknown boundary parameters.

Infinite dimensional boundary observers are less investigated in the literature. The problem with systems that have distributed parameters is that it is most of the time impossible to take measurements at every point in space. It is more natural for the sensors to be located at the boundaries of the domain, which led to the idea of boundary observers. Boundary control design is achieved using boundary observers based on two methods: Lyapunov and backstepping-based methods. Concerning Lyapunov methods, the authors in [25] design a boundary observer for n rightward hyperbolic transport equations. The observer uses measurements taken from the right boundary to correct the estimation error on the left one. This result is extended by the authors in [85] to one rightward and one leftward transport equation for the plate heat exchanger. Nevertheless, both methods assume perfect knowledge of the model parameters. Backstepping-based boundary observers are also well established in the literature. In fact, static control design using backstepping requires a full knowledge of the distributed states. A collocated boundary observer is thus synthesized to fulfill this requirement (see previously mentioned results such as [76], [50], [14]). These designs also assume a perfect knowledge of the system. In many practical cases,

some model parameters are unknown, which motivates the need for adaptive estimators. The objective of an adaptive boundary observer is to simultaneously construct the system's distributed states and the unknown parameters from only boundary sensing. The problem of adaptive boundary estimation was first addressed by the authors in [74] for parabolic PDEs using backstepping techniques. Such method is applied to hyperbolic systems in [37], where the authors design an adaptive observer for first-order hyperbolic systems with uncertain additive boundary parameters (the adaptive laws for these parameters are derived using Lyapunov analysis). This result is extended by the authors in [21] to unknown additive and multiplicative parameters in the boundary. We can also mention the results on disturbance rejection for hyperbolic systems (see e.g. [2], [3]), which can be interpreted as results on adaptive observers for hyperbolic PDEs. As a different approach, swapping design is also used in the derivation of adaptive observers. This method relies on using K-filters to derive static relationships between the system states and the unknown parameters: this relationship is used to build Lyapunov-based adaptive laws to estimate the unknown parameters (see [55] and [53] for ODEs and [74] for PDEs). In the work of the authors in [12], [13], and [11] swapping design is used to estimate unknown boundary parameters for some classes of hyperbolic systems. However, few results exist in the literature on in-domain parameter estimation. The works [20] and [8] on adaptive control include in-domain parameter estimations based on swapping design methods. In these works, an adaptive observer is designed for systems in the "canonical observable form" to serve as an intermediate step in deriving the control law. However, the convergence of the in-domain parameters to their true value is not guaranteed by the designs [20] and [8] as the objective is to adaptively control the system and not to estimate the parameters.

2.3.1 Contribution

In Problem 1, we consider the problem of estimating the distributed states of a 2×2 hyperbolic system, two-sided actuated with unknown in-domain and boundary parameters. The motivation behind considering such system is the application to heat exchanger networks. To the best of our knowledge, this type of estimation problem is not addressed yet in the literature. We propose an adaptive boundary observer that can estimate not only the full state of the system, but also unknown-in-domain and boundary parameters. We have used the swapping design method to write the estimation error system as a linear combination of the parameters estimation errors. This leads to the decoupling of the PDE estimation errors from the ODE estimation errors. As a consequence, standard backstepping observer techniques and adaptation laws are used.

From the practical aspect, we contribute to an adaptive design that gives online estimates for the heat transfer coefficient and for the distributed temperatures from only boundary sensing. Furthermore, we validate our adaptive design against the experimental data taken from a CO₂ refrigeration apparatus built at CERN, and we also show its advantages over the pre-existing observer designs that assume perfect knowledge of the model parameters (the dissipative Luneberger observer [85] and two sided backstepping observer [14]).

The work presented in this chapter is published in:

M.Ghousein, E.Witrant, V.Bhanot, P.Petagne."Adaptive boundary observer design for linear

hyperbolic systems; Application to estimation in heat exchangers". In: *Automatica* (2020), vol. 114 (108824), pp. 1–13.

2.4 Adaptive observer design

We introduce the following adaptive observer design:

$$\partial_t \hat{u}(x, t) + c_1 \partial_x \hat{u}(x, t) = \sigma_1(x) \hat{v}(x, t) + \hat{\theta}_1(t) \phi_1(x, t) - p_1(x) (\hat{u}(1, t) - y_1(t)) + m_1(x, t) \quad (2.22)$$

$$\partial_t \hat{v}(x, t) - c_2 \partial_x \hat{v}(x, t) = \sigma_2(x) \hat{u}(x, t) + \hat{\theta}_2(t) \phi_2(x, t) - p_2(x) (\hat{u}(1, t) - y_1(t)) + m_2(x, t) \quad (2.23)$$

$$\hat{u}(0, t) = \omega (\hat{v}(0, t) - y_2(t)) + \hat{q}(t) v(0, t) + U(t) \quad (2.24)$$

$$\hat{v}(1, t) = V(t) \quad (2.25)$$

where $p_1(x)$ and $p_2(x)$ are the observer gains, ω is a non-zero real parameter that can be chosen arbitrarily, and $m_1(x, t)$ and $m_2(x, t)$ are additional feedback gains to be determined later. The observer initial conditions are denoted by \hat{u}_0 and \hat{v}_0 , and are assumed to belong to $L^2[0, 1]$. The estimates are denoted by hat, and we define the error variables $\tilde{u}(x, t) = u(x, t) - \hat{u}(x, t)$, $\tilde{v}(x, t) = v(x, t) - \hat{v}(x, t)$, $\tilde{q}(t) = q - \hat{q}(t)$, $\tilde{\theta}_1(t) = \theta_1 - \hat{\theta}_1(t)$, $\tilde{\theta}_2(t) = \theta_2 - \hat{\theta}_2(t)$.

Forming the error system by subtracting (2.18)-(2.20) from (2.22)-(2.25) we have:

$$\partial_t \tilde{u}(x, t) + c_1 \partial_x \tilde{u}(x, t) = \sigma_1(x) \tilde{v}(x, t) + \tilde{\theta}_1(t) \phi_1(x, t) - p_1(x) \tilde{u}(1, t) - m_1(x, t) \quad (2.26)$$

$$\partial_t \tilde{v}(x, t) - c_2 \partial_x \tilde{v}(x, t) = \sigma_2(x) \tilde{u}(x, t) + \tilde{\theta}_2(t) \phi_2(x, t) - p_2(x) \tilde{u}(1, t) - m_2(x, t) \quad (2.27)$$

$$\tilde{u}(0, t) = \omega \tilde{v}(0, t) + \tilde{q}(t) v(0, t), \quad \tilde{v}(1, t) = 0 \quad (2.28)$$

The observer designed in (2.22)-(2.25) is a PDE observer of Luenberger-type, which is a copy of the system with output injection terms $(y_1(t), y_2(t))$ added in the domain and at the left boundary. The problem is then to find the observer gains $p_1(x)$ and $p_2(x)$, and the proper parameter update laws in order to guarantee the exponential convergence of the error system (2.26)-(2.28) to zero.

2.5 Swapping Design

In this section, we derive a static relationship which connects the estimation error on the states with the estimation error on the parameters. This relationship will then be used to derive the parameters adaption laws. By writing the error system (2.26)-(2.28) using swapping filters we have:

$$z_1(x, t) = \tilde{u}(x, t) - \lambda_{11}(x, t) \tilde{\theta}_1(t) - \lambda_{12}(x, t) \tilde{\theta}_2(t) - Q_1(x, t) \tilde{q}(t) \quad (2.29)$$

$$z_2(x, t) = \tilde{v}(x, t) - \lambda_{21}(x, t) \tilde{\theta}_1(t) - \lambda_{22}(x, t) \tilde{\theta}_2(t) - Q_2(x, t) \tilde{q}(t) \quad (2.30)$$

We can write (2.29)-(2.30) in the compact form:

$$Z(x, t) = E(x, t) - \Lambda(x, t)\tilde{\theta}(t) \quad (2.31)$$

where:

$$Z(x, t) = \begin{pmatrix} z_1(x, t) \\ z_2(x, t) \end{pmatrix}, \quad E(x, t) = \begin{pmatrix} \tilde{u}(x, t) \\ \tilde{v}(x, t) \end{pmatrix}, \quad \tilde{\theta}(t) = \begin{pmatrix} \tilde{\theta}_1(t) \\ \tilde{\theta}_2(t) \\ \tilde{q}(t) \end{pmatrix},$$

$$\Lambda(x, t) = \begin{bmatrix} \lambda_{11}(x, t) & \lambda_{12}(x, t) & Q_1(x, t) \\ \lambda_{21}(x, t) & \lambda_{22}(x, t) & Q_2(x, t) \end{bmatrix}$$

The swapping filters $\lambda_{ij}(x, t) : [0, 1] \times [0, +\infty) \rightarrow \mathbb{R}$, ($1 \leq i \leq 2$, $1 \leq j \leq 2$) and $Q_i(x, t) : [0, 1] \times [0, +\infty) \rightarrow \mathbb{R}$ are to be defined later. Differentiating (2.29) with respect to time and substituting with (2.30) we get:

$$\begin{aligned} \partial_t z_1(x, t) = & -c_1 \partial_x \tilde{u}(x, t) + \sigma_1(x) \tilde{v}(x, t) + \tilde{\theta}_1(t) \phi_1(x, t) - p_1(x) \tilde{u}(1, t) - m_1(x, t) - \partial_t \lambda_{11}(x, t) \tilde{\theta}_1(t) \\ & - \lambda_{11}(x, t) \dot{\tilde{\theta}}_1(t) - \partial_t \lambda_{12}(x, t) \tilde{\theta}_2(t) - \lambda_{12}(x, t) \dot{\tilde{\theta}}_2(t) - \partial_t Q_1(x, t) \tilde{q}(t) - Q_1(x, t) \dot{\tilde{q}}(t) \end{aligned} \quad (2.32)$$

In order to keep (2.32) linear in $\tilde{\theta}_1(t)$, $\tilde{\theta}_2(t)$ and $\tilde{q}(t)$, we choose the following feedback law $m_1(x, t)$:

$$m_1(x, t) = -\lambda_{11}(x, t) \dot{\tilde{\theta}}_1(t) - \lambda_{12}(x, t) \dot{\tilde{\theta}}_2(t) - Q_1(x, t) \dot{\tilde{q}}(t) \quad (2.33)$$

Now, differentiate (2.29) with respect to space, substitute in (2.32) with (2.30) to obtain:

$$\begin{aligned} \partial_t z_1(x, t) + c_1 \partial_x z_1(x, t) = & \sigma_1(x) z_2(x, t) - p_1(x) z_1(1, t) \\ & + \tilde{\theta}_1 (- \partial_t \lambda_{11}(x, t) - c_1 \partial_x \lambda_{11}(x, t) + \sigma_1(x) \lambda_{21}(x, t) - p_1(x) \lambda_{11}(1, t) + \phi_1(x, t)) \\ & + \tilde{\theta}_2 (- \partial_t \lambda_{12}(x, t) - c_1 \partial_x \lambda_{12}(x, t) + \sigma_1(x) \lambda_{22}(x, t) - p_1(x) \lambda_{12}(1, t)) \\ & + \tilde{q}(t) (- \partial_t Q_1(x, t) - c_1 \partial_x Q_1(x, t) + \sigma_1(x) Q_2(x, t) - p_1(x) Q_1(1, t)) \end{aligned} \quad (2.34)$$

Similarly, deriving (2.30) with respect to time and following the same procedure, one gets for the feedback law $m_2(x, t)$:

$$m_2(x, t) = -\lambda_{21}(x, t) \dot{\tilde{\theta}}_1(t) - \lambda_{22}(x, t) \dot{\tilde{\theta}}_2(t) - Q_2(x, t) \dot{\tilde{q}}(t) \quad (2.35)$$

and the following dynamics:

$$\begin{aligned} \partial_t z_2(x, t) - c_2 \partial_x z_2(x, t) = & \sigma_2(x) z_1(x, t) - p_2(x) z_1(1, t) \\ & + \tilde{\theta}_1 (- \partial_t \lambda_{21}(x, t) + c_2 \partial_x \lambda_{21}(x, t) + \sigma_2(x) \lambda_{11}(x, t) - p_2(x) \lambda_{11}(1, t)) \\ & + \tilde{\theta}_2 (- \partial_t \lambda_{22}(x, t) + c_2 \partial_x \lambda_{22}(x, t) + \sigma_2(x) \lambda_{12}(x, t) - p_2(x) \lambda_{12}(1, t) + \phi_2(x, t)) \\ & + \tilde{q}(t) (- \partial_t Q_2(x, t) + c_2 \partial_x Q_2(x, t) + \sigma_2(x) Q_1(x, t) - p_2(x) Q_1(1, t)) \end{aligned} \quad (2.36)$$

Equations (2.34) and (2.36) suggest the following dynamics of the swapping filters:

$$\begin{cases} \partial_t \lambda_{11}(x, t) + c_1 \partial_x \lambda_{11}(x, t) &= \sigma_1(x) \lambda_{21}(x, t) - p_1(x) \lambda_{11}(1, t) + \phi_1(x, t) \\ \partial_t \lambda_{21}(x, t) - c_2 \partial_x \lambda_{21}(x, t) &= \sigma_2(x) \lambda_{11}(x, t) - p_2(x) \lambda_{11}(1, t) \end{cases} \quad (2.37)$$

$$\begin{cases} \partial_t \lambda_{12}(x, t) + c_1 \partial_x \lambda_{12}(x, t) &= \sigma_1(x) \lambda_{22}(x, t) - p_1(x) \lambda_{12}(1, t) \\ \partial_t \lambda_{22}(x, t) - c_2 \partial_x \lambda_{22}(x, t) &= \sigma_2(x) \lambda_{12}(x, t) - p_2(x) \lambda_{12}(1, t) + \phi_2(x, t) \end{cases} \quad (2.38)$$

$$\begin{cases} \partial_t Q_1(x, t) + c_1 \partial_x Q_1(x, t) &= \sigma_1(x) Q_2(x, t) - p_1(x) Q_1(1, t) \\ \partial_t Q_2(x, t) - c_2 \partial_x Q_2(x, t) &= \sigma_2(x) Q_1(x, t) - p_2(x) Q_1(1, t) \end{cases} \quad (2.39)$$

and we impose the following boundary conditions:

$$\lambda_{11}(0, t) = \omega \lambda_{21}(0, t), \quad \lambda_{21}(1, t) = 0 \quad (2.40)$$

$$\lambda_{12}(0, t) = \omega \lambda_{22}(0, t), \quad \lambda_{22}(1, t) = 0 \quad (2.41)$$

$$Q_1(0, t) = w Q_2(0, t) + v(0, t), \quad Q_2(1, t) = 0 \quad (2.42)$$

with zero distributed initial conditions $\Lambda(x, 0) = 0$. It is important to notice that the systems (2.37)-(2.40), (2.38)-(2.41) and (2.39)-(2.42) are independent from each other. Hence, we can denote by:

$$\Lambda_1(x, t) = \begin{pmatrix} \lambda_{11}(x, t) \\ \lambda_{21}(x, t) \end{pmatrix}, \quad \Lambda_2(x, t) = \begin{pmatrix} \lambda_{12}(x, t) \\ \lambda_{22}(x, t) \end{pmatrix}, \quad Q(x, t) = \begin{pmatrix} Q_1(x, t) \\ Q_2(x, t) \end{pmatrix} \quad (2.43)$$

three separate subsystems of $\Lambda(x, t)$. Doing so, and substituting equations (2.37)-(2.39) in (2.34) and (2.36), the dynamics of the transformed state $Z(x, t)$ becomes

$$\partial_t z_1(x, t) + c_1 \partial_x z_1(x, t) = \sigma_1(x) z_2(x, t) - p_1(x) z_1(1, t) \quad (2.44)$$

$$\partial_t z_2(x, t) - c_2 \partial_x z_2(x, t) = \sigma_2(x) z_1(x, t) - p_2(x) z_1(1, t) \quad (2.45)$$

Also, using the boundary conditions given in (2.40)-(2.42), we can then derive the boundary conditions of $Z(x, t)$ using transformation (2.31) as:

$$z_1(0, t) = w z_2(0, t), \quad z_2(1, t) = 0 \quad (2.46)$$

In view of the transformation (2.31), the state estimation error $E(x, t)$ splits into two parts. The first component is the observation error represented by $Z(x, t)$, which is totally decoupled from the parameters estimation errors $\tilde{\theta}(t)$ and always present whether we have parameters to estimate or not. The second component is the parameter-induced error represented by $\Lambda(x, t) \tilde{\theta}(t)$, which is proportional to the parameters mismatch. It is important to mention that the idea of state parametrization was first introduced by the authors in [53] for ODEs. To sum up, the problem of the exponential stability of the error system (2.26)-(2.28) is equivalent to address three problems: the exponential stability of $Z(x, t)$, the exponential stability of $\tilde{\theta}(t)$ and the boundedness of $\Lambda(x, t)$.

2.6 Exponential stability of $Z(x, t)$

We start our analysis by considering the $Z(x, t)$ system (2.44)-(2.46). Our goal is to select the observer gains $p_1(x)$ and $p_2(x)$ such that the equilibrium $z_1 \equiv z_2 \equiv 0$ is exponentially stable in the L^2 sense. In fact, equation (2.31) allows a straightforward application of the results in [76] (Section 4). The authors use a Volterra-backstepping transformation of the second kind to map the system (2.44)-(2.46) into an exponentially stable target system. We present here the transformation for the sake of completeness:

$$Z(x, t) = \tilde{\gamma}(x, t) - \int_x^1 P(x, \xi) \tilde{\gamma}(\xi, t) d\xi \quad (2.47)$$

$$P(x, \xi) = \begin{pmatrix} P^{11}(x, \xi) & P^{12}(x, \xi) \\ P^{21}(x, \xi) & P^{22}(x, \xi) \end{pmatrix}, \quad (2.48)$$

$$\tilde{\gamma}(x, t) = \begin{pmatrix} \tilde{\alpha}(x, t) \\ \tilde{\beta}(x, t) \end{pmatrix}$$

The transformation evolves in the triangular domain $\Omega = \{(x, \xi), 0 \leq x \leq \xi \leq 1\}$, and maps the $Z(x, t)$ system (2.44)-(2.46) into the target system $\tilde{\gamma}(x, t)$ given by:

$$\partial_t \alpha(x, t) + c_1 \partial_x \alpha(x, t) = 0 \quad (2.49)$$

$$\partial_t \beta(x, t) - c_2 \partial_x \beta(x, t) = 0 \quad (2.50)$$

$$\alpha(0, t) = \omega \beta(0, t), \quad \beta(1, t) = 0 \quad (2.51)$$

To achieve this transformation, the kernel equations must satisfy the following equations:

$$c_1 P_x^{11}(x, \xi) + c_1 P_\xi^{11}(x, \xi) = \sigma_1(x) P^{21}(x, \xi) \quad (2.52)$$

$$c_1 P_x^{12}(x, \xi) - c_2 P_\xi^{12}(x, \xi) = \sigma_1(x) P^{22}(x, \xi) \quad (2.53)$$

$$c_2 P_x^{21}(x, \xi) - c_1 P_\xi^{21}(x, \xi) = -\sigma_2(x) P^{11}(x, \xi) \quad (2.54)$$

$$c_2 P_x^{22}(x, \xi) + c_2 P_\xi^{22}(x, \xi) = -\sigma_2(x) P^{12}(x, \xi) \quad (2.55)$$

with boundary conditions:

$$P^{11}(0, \xi) = \omega P^{21}(0, \xi), \quad P^{12}(x, x) = \frac{\sigma_1(x)}{c_1 + c_2} \quad (2.56)$$

$$P^{21}(x, x) = -\frac{\sigma_2(x)}{c_1 + c_2}, \quad P^{22}(0, \xi) = \frac{1}{\omega} P^{12}(0, \xi) \quad (2.57)$$

The observer gains $p_1(x)$ and $p_2(x)$ serve as additional conditions on the output injection kernels as:

$$p_1(x) = -c_1 P^{11}(x, 1), \quad p_2(x) = -c_1 P^{21}(x, 1) \quad (2.58)$$

It has been shown in [76] that the kernel equations (2.52)-(2.57) have a unique solution in $C^2(\Omega)$ and are invertible. The inverse transformation is denoted by $R(x, \xi)$ and is given by:

$$\tilde{\gamma}(x, t) = Z(x, t) + \int_x^1 R(x, \xi)Z(\xi, t)d\xi \quad (2.59)$$

$$R(x, \xi) = \begin{pmatrix} R^{11}(x, \xi) & R^{12}(x, \xi) \\ R^{21}(x, \xi) & R^{22}(x, \xi) \end{pmatrix}, \quad (2.60)$$

with the following kernel equations:

$$c_1 R_x^{11}(x, \xi) + c_1 R_\xi^{11}(x, \xi) = -\sigma_2(\xi)R^{12}(x, \xi) \quad (2.61)$$

$$c_1 R_x^{12}(x, \xi) - c_2 R_\xi^{12}(x, \xi) = -\sigma_1(\xi)R^{11}(x, \xi) \quad (2.62)$$

$$c_2 R_x^{21}(x, \xi) - c_1 R_\xi^{21}(x, \xi) = \sigma_2(\xi)R^{22}(x, \xi) \quad (2.63)$$

$$c_2 R_x^{22}(x, \xi) + c_2 R_\xi^{22}(x, \xi) = \sigma_1(\xi)R^{21}(x, \xi) \quad (2.64)$$

with boundary conditions:

$$R^{11}(0, \xi) = \omega R^{21}(0, \xi), \quad R^{12}(x, x) = \frac{\sigma_1(x)}{c_1 + c_2} \quad (2.65)$$

$$R^{21}(x, x) = -\frac{\sigma_2(x)}{c_1 + c_2}, \quad R^{22}(0, \xi) = \frac{1}{\omega}R^{12}(0, \xi) \quad (2.66)$$

The derivation methodology of the kernel equations will be clarified in the next sections. We orient the interested readers to [76] and [50] for further information on the kernel equations developments, and proofs of the existence and uniqueness of solutions.

Remark 2.6.1. *Using the direct and the inverse transformation (2.47)-(2.59), one can drive the following relation between the direct kernel $P(x, \xi)$ and the inverse kernel $R(x, \xi)$ such that*

$$P(x, \xi) = R(x, \xi) - \int_x^\xi R(x, y)P(y, \xi)d\xi \quad (2.67)$$

Using a quadratic Lyapunov function and the method of characteristics, one can easily show that $\tilde{\gamma}(x, t)$ is L^2 stable and that $\alpha \equiv \beta \equiv 0$ is reached in finite time for all $0 \leq x \leq 1$. Referring back to (2.47) and (2.59), the stability properties of the $\tilde{\gamma}(x, t)$ and $Z(x, t)$ are equivalent. The following Theorem (which is Theorem 2 in [76]) states the stability results for the $Z(x, t)$ system.

Theorem 2.6.1 ([76]). *Consider the system (2.44)-(2.45) with boundary conditions (2.46), initial conditions $z_1^0(x), z_2^0(x)$ in $L^2[0, 1]$ and with observer gains (2.58). The equilibrium $z_1 \equiv z_2 \equiv 0$ is exponentially stable in the L^2 sense, and the equilibrium is reached in finite time $t_F = \frac{1}{c_1} + \frac{1}{c_2}$.*

2.7 Boundedness of $\Lambda(x, t)$

In this section, we prove the boundedness of the swapping filters $\Lambda(x, t)$. This is necessary, as introduced in Section 2.5 and shown in Section 2.9, to conclude on the exponential stability of $E(x, t)$.

$\Lambda(x, t)$ is split into three subsystems: $\Lambda_1(x, t)$, $\Lambda_2(x, t)$ and $Q(x, t)$. Looking into the dynamics of the swapping filters (2.37)-(2.42), one can realize that $\Lambda_1(x, t)$ and $\Lambda_2(x, t)$ are symmetric by their source terms ($\phi_1(x, t)$ and $\phi_2(x, t)$) whereas $Q(x, t)$ is different by its measurement signal $v(0, t)$ acting on the left boundary. As a result, we divide the boundedness analysis into two parts: first the boundedness of $\{\Lambda_1(x, t), \Lambda_2(x, t)\}$ and second is the boundedness of $Q(x, t)$.

2.7.1 Boundedness of $\Lambda_1(x, t)$ and $\Lambda_2(x, t)$

The results are inferred from the following theorem.

Theorem 2.7.1. *Consider the two subsystems $\Lambda_1(x, t)$ and $\Lambda_2(x, t)$ with zero initial conditions $\Lambda_1(x, 0) \equiv \Lambda_2(x, 0) \equiv 0$, the observer gains (2.58), and with ϕ_1 and ϕ_2 two bounded functions of class $C^1([0, 1] \times [0, +\infty); \mathbb{R})$. Then we have that $\|\Lambda_1(\cdot, t)\|_{L^2[0,1]}$ and $\|\Lambda_2(\cdot, t)\|_{L^2[0,1]}$ are bounded.*

Proof. First, consider $\Lambda_1(x, t)$. We begin by decoupling the system through the following backstepping transformation:

$$a(x, t) = \lambda_{11}(x, t) + \int_x^1 (R^{11}(x, \xi)\lambda_{11}(\xi, t) + R^{12}(x, \xi)\lambda_{21}(\xi, t))d\xi \quad (2.68)$$

$$b(x, t) = \lambda_{21}(x, t) + \int_x^1 (R^{21}(x, \xi)\lambda_{11}(\xi, t) + R^{22}(x, \xi)\lambda_{21}(\xi, t))d\xi \quad (2.69)$$

where $\Delta(x, t) = \begin{pmatrix} a(x, t) \\ b(x, t) \end{pmatrix}$ is the state of the transformed dynamics. Differentiating (2.68) with respect to time and substituting in (2.37), we get

$$\begin{aligned} \partial_t a(x, t) &= -c_1 \partial_x \lambda_{11}(x, t) + \sigma_1(x) \lambda_{21}(x, t) - p_1(x) \lambda_{11}(1, t) + \phi_1(x, t) \\ &+ \int_x^1 \left(-c_1 R^{11}(x, \xi) \partial_\xi \lambda_{11}(\xi, t) + \sigma_1(\xi) R^{11}(x, \xi) \lambda_{21}(\xi, t) - p_1(\xi) R^{11}(x, \xi) \lambda_{11}(1, t) \right. \\ &+ \phi_1(\xi, t) R^{11}(x, \xi) + c_2 R^{12}(x, \xi) \partial_\xi \lambda_{21}(x, \xi) + \sigma_2(\xi) R^{12}(x, \xi) \lambda_{11}(\xi, t) \\ &\left. - p_2(\xi) R^{12}(x, \xi) \lambda_{11}(1, t) \right) d\xi \end{aligned} \quad (2.70)$$

Integrating (2.70) by parts, and substituting by the boundary conditions (2.40) to get

$$\begin{aligned}
\partial_t a(x, t) &= -c_1 \partial_x \lambda_{11}(x, t) + \sigma_1(x) \lambda_{21}(x, t) - p_1(x) \lambda_{11}(1, t) + \phi_1(x, t) - c_1 R^{11}(x, 1) \lambda_{11}(1, t) \\
&+ c_1 R^{11}(x, x) \lambda_{11}(x, t) - c_2 R^{12}(x, x) \lambda_{21}(x, t) \\
&+ \int_x^1 \left(c_1 R_\xi^{11}(x, \xi) \lambda_{11}(\xi, t) + \sigma_1(\xi) R^{11}(x, \xi) \lambda_{21}(\xi, t) - p_1(\xi) R^{11}(x, \xi) \lambda_{11}(1, t) \right. \\
&+ \phi_1(\xi, t) R^{11}(x, \xi) - c_2 R_\xi^{12}(x, \xi) \lambda_{21}(x, \xi) + \sigma_2(\xi) R^{12}(x, \xi) \lambda_{11}(\xi, t) \\
&\left. - p_2(\xi) R^{12}(x, \xi) \lambda_{11}(1, t) \right) d\xi
\end{aligned} \tag{2.71}$$

Now, differentiate (2.68) with respect to space to compute

$$\begin{aligned}
c_1 \partial_x a(x, t) &= c_1 \partial_x \lambda_{11}(x, t) - c_1 R^{11}(x, x) \lambda_{11}(x, t) - c_1 R^{12}(x, x) \lambda_{21}(x, t) \\
&+ \int_x^1 \left(c_1 R_x^{11}(x, \xi) \lambda_{11}(\xi, t) + c_1 R_x^{12}(x, \xi) \lambda_{21}(\xi, t) \right) d\xi
\end{aligned} \tag{2.72}$$

By adding equations (2.71) and (2.72), we obtain

$$\begin{aligned}
\partial_t a(x, t) + c_1 \partial_x a(x, t) &= \phi_1(x, t) + \int_x^1 R^{11}(x, \xi) \phi_1(\xi, t) d\xi \\
&+ (\sigma_1(x) - (c_1 + c_2) R^{12}(x, x)) \lambda_{21}(x, t) \\
&- (p_1(x) + c_1 R^{11}(x, 1) + \int_x^1 (p_1(\xi) R^{11}(x, \xi) + p_2(\xi) R^{12}(x, \xi)) d\xi) \lambda_{11}(1, t) \\
&+ \int_x^1 (c_1 R_x^{11}(x, \xi) + c_1 R_\xi^{11}(x, \xi) + \sigma_2(\xi) R^{12}(x, \xi)) \lambda_{11}(\xi, t) d\xi \\
&+ \int_x^1 (c_1 R_x^{12}(x, \xi) - c_2 R_\xi^{12}(x, \xi) + \sigma_1(\xi) R^{11}(x, \xi)) \lambda_{21}(\xi, t) d\xi
\end{aligned} \tag{2.73}$$

Hence, using equations (2.61)-(2.62)-(2.65) and the direct-inverse relation (2.67), we get the following dynamics for $a(x, t)$

$$\partial_t a(x, t) + c_1 \partial_x a(x, t) = f_1(x, t) \tag{2.74}$$

where $f_1(x, t) = \phi_1(x, t) + \int_x^1 R^{11}(x, \xi) \phi_1(\xi, t) d\xi$. Now, differentiate (2.69) in time, substitute in (2.37) then integrate by parts and substitute the boundary conditions (2.40) to get

$$\begin{aligned}
\partial_t b(x, t) &= c_2 \partial_x \lambda_{21}(x, t) + \sigma_2(x) \lambda_{11}(x, t) - p_2(x) \lambda_{11}(1, t) - c_1 R^{21}(x, 1) \lambda_{11}(1, t) \\
&+ c_1 R^{21}(x, x) \lambda_{11}(x, t) - c_2 R^{22}(x, x) \lambda_{21}(x, t) \\
&+ \int_x^1 \left(c_1 R_\xi^{21}(x, \xi) \lambda_{11}(\xi, t) + \sigma_1(\xi) R^{21}(x, \xi) \lambda_{21}(\xi, t) - p_1(\xi) R^{21}(x, \xi) \lambda_{11}(1, t) \right. \\
&+ \phi_1(\xi, t) R^{21}(x, \xi) - c_2 R_\xi^{22}(x, \xi) \lambda_{21}(x, \xi) + \sigma_2(\xi) R^{22}(x, \xi) \lambda_{11}(\xi, t) \\
&\left. - p_2(\xi) R^{22}(x, \xi) \lambda_{11}(1, t) \right) d\xi
\end{aligned} \tag{2.75}$$

We differentiate (2.69) in space to compute

$$\begin{aligned} c_2 \partial_x b(x, t) &= c_2 \partial_x \lambda_{21}(x, t) - c_2 R^{21}(x, x) \lambda_{11}(x, t) - c_2 R^{22}(x, x) \lambda_{21}(x, t) \\ &\quad + \int_x^1 \left(c_2 R_x^{21}(x, \xi) \lambda_{11}(\xi, t) + c_2 R_x^{22}(x, \xi) \lambda_{21}(\xi, t) \right) d\xi \end{aligned} \quad (2.76)$$

By subtracting (2.76) from (2.75) we obtain

$$\begin{aligned} \partial_t b(x, t) - c_2 \partial_x b(x, t) &= \int_x^1 R^{21}(x, \xi) \phi_1(\xi, t) d\xi \\ &\quad + (\sigma_2(x) + (c_1 + c_2) R^{21}(x, x)) \lambda_{21}(x, t) \\ &\quad + (-p_2(x) - c_1 R^{21}(x, 1) - \int_x^1 (p_1(\xi) R^{21}(x, \xi) + p_2(\xi) R^{22}(x, \xi)) d\xi) \lambda_{11}(1, t) \\ &\quad + \int_x^1 (c_1 R_\xi^{21}(x, \xi) - c_2 R_x^{21}(x, \xi) + \sigma_2(\xi) R^{22}(x, \xi)) \lambda_{11}(\xi, t) d\xi \\ &\quad + \int_x^1 (-c_2 R_x^{22}(x, \xi) - c_2 R_\xi^{22}(x, \xi) + \sigma_1(\xi) R^{21}(x, \xi)) \lambda_{21}(\xi, t) d\xi \end{aligned} \quad (2.77)$$

Then using (2.63)-(2.64)-(2.66) and the direct-inverse relation (2.67), we get the following dynamics for $b(x, t)$

$$\partial_t b(x, t) - c_2 \partial_x b(x, t) = f_2(x, t) \quad (2.78)$$

where $f_2(x, t) = \int_x^1 R^{21}(x, \xi) \phi_1(\xi, t) d\xi$. The boundary conditions for the $\Delta(x, t)$ system are derived using (2.68)-(2.69), (2.65)-(2.66) and (2.40), and we sum up the complete dynamics in the following system of equations

$$\partial_t a(x, t) + c_1 \partial_x a(x, t) = f_1(x, t) \quad (2.79)$$

$$\partial_t b(x, t) - c_2 \partial_x b(x, t) = f_2(x, t) \quad (2.80)$$

$$a(0, t) = \omega b(0, t), \quad b(1, t) = 0 \quad (2.81)$$

with zero initial conditions $a(x, 0) = b(x, 0) = 0$. Now, we start the boundedness analysis of $\Delta(x, t)$. By the invertability of the Volterra backstepping transformation (2.68)-(2.69), all the derived boundedness properties for $\Delta(x, t)$ are equivalently applied to $\Lambda_1(x, t)$.

We define the L^2 norm of a two state vector $\Delta(x, t)$ to be

$$\|\Delta(\cdot, t)\|_{L^2[0,1]} = \sqrt{\int_0^1 a^2(x, t) + b^2(x, t) dx} \quad (2.82)$$

The objective is to find a positive constant G such that $\|\Delta(\cdot, t)\|_{L^2[0,1]} \leq G$ for all $t > 0$. To do so, we consider the following Lyapunov function:

$$V_1(t) = \frac{1}{2} \int_0^1 \frac{q_1}{c_1} e^{-\mu x} a^2(x, t) + \frac{q_2}{c_2} e^{\mu x} b^2(x, t) dx \quad (2.83)$$

where q_1 , q_2 and μ are positive constants. Taking the time derivative of (2.83) we get:

$$\dot{V}_1(t) = \int_0^1 \frac{q_1}{c_1} e^{-\mu x} a(x, t) \partial_t a(x, t) + \frac{q_2}{c_2} e^{\mu x} b(x, t) \partial_t b(x, t) dx \quad (2.84)$$

Using (2.79)-(2.81) and integrating by parts, one has:

$$\begin{aligned} \dot{V}_1(t) = & -\frac{1}{2} q_1 e^{-\mu} a^2(1, t) + \frac{1}{2} (q_1 q^2 - q_2) b^2(0, t) - \frac{\mu}{2} \int_0^1 q_1 e^{-\mu x} a^2(x, t) + q_2 e^{\mu x} b^2(x, t) dx \\ & + \int_0^1 \frac{q_1}{c_1} e^{-\mu x} f_1(x, t) a(x, t) + \frac{q_2}{c_2} e^{\mu x} f_2(x, t) b(x, t) dx \end{aligned} \quad (2.85)$$

Applying Young's inequality to the last term of (2.85), we have, for all $k_1 > 0, k_2 > 0$, that:

$$\begin{aligned} \dot{V}_1(t) \leq & -\frac{1}{2} q_1 e^{-\mu} a^2(1, t) + \frac{1}{2} (q_1 q^2 - p_2) b^2(0, t) + \left(-\frac{\mu}{2} + \frac{k_1}{2c_1}\right) \int_0^1 q_1 e^{-\mu x} a^2(x, t) dx \\ & + \left(-\frac{\mu}{2} + \frac{k_2}{2c_2}\right) \int_0^1 q_2 e^{\mu x} b^2(x, t) dx + \frac{1}{2k_1} \int_0^1 \frac{q_1}{c_1} e^{-\mu x} f_1^2(x, t) dx \\ & + \frac{1}{2k_2} \int_0^1 \frac{q_2}{c_2} e^{\mu x} f_2^2(x, t) dx \end{aligned} \quad (2.86)$$

We can choose $\mu = 1$, and q_1 and q_2 such that:

$$q_1 q^2 - q_2 \leq 0 \quad (2.87)$$

Let $\Gamma \in]0, \min\{c_1, c_2}\rangle$, $k_1 \in]0, c_1 - \Gamma]$ and $k_2 \in]0, c_2 - \Gamma]$, then we have

$$\begin{aligned} \dot{V}_1(t) \leq & -\Gamma V_1(t) + \frac{1}{2k_1} \int_0^1 \frac{q_1}{c_1} e^{-x} f_1^2(x, t) dx + \frac{1}{2k_2} \int_0^1 \frac{q_2}{c_2} e^x f_2^2(x, t) dx \\ \leq & -\Gamma V_1(t) + \underbrace{\frac{q_1}{2k_1 c_1} F_1^2 + \frac{q_2 e}{2k_2 c_2} F_2^2}_H \end{aligned} \quad (2.88)$$

where F_1 and F_2 are the upper bounds on $f_1(x, t)$ and $f_2(x, t)$ respectively i.e. $|f_1(x, t)| \leq F_1$ and $|f_2(x, t)| \leq F_2$ for all $(t, x) \in \{(t, x) \mid t \geq 0, x \in [0, 1]\}$. Using (2.88), we can deduce the following bound on $V_1(t)$:

$$V_1(t) \leq e^{-\Gamma t} V_1(0) + \frac{H}{\Gamma} (1 - e^{-\Gamma t}) \quad (2.89)$$

We start all the filters from zero initial conditions. Hence, $V_1(0) = 0$ and therefore $V_1(t) \leq \frac{H}{\Gamma}$ for all $t \geq 0$. It follows that $V_1(t)$ is bounded, as a direct consequence of the boundedness of $f_1(x, t)$ and $f_2(x, t)$. Since $V_1(t)$ serves as the weighted L^2 norm of the $\Delta(x, t)$ system, then there exist $G > 0$ such that $\|\Delta(\cdot, t)\|_{L^2[0,1]} \leq G$ for all $t > 0$. Now by the invertability of the transformation $R(x, \xi)$, we can deduce that $\|\Lambda_1(\cdot, t)\|_{L^2[0,1]}$ is bounded and the proof is complete. \square

Remark 2.7.1. *The boundedness of $\|\Lambda_2(\cdot, t)\|_{L^2[0,1]}$ is done in exactly the same way, since the two systems $\Lambda_1(x, t)$ and $\Lambda_2(x, t)$ are symmetric.*

2.7.2 Boundedness of $Q(x, t)$

The boundedness of $Q(x, t)$ in the L^2 norms is done in a similar way to the boundedness of $\Lambda_1(x, t)$. However, $Q(x, t)$ involves a plant measurement signal $v(0, t)$ at the left boundary. In order to prove the boundedness of the filter $Q(x, t)$, it is necessary to take the following assumption on the plant (2.18)-(2.20).

Assumption 2.7.1. *Assume that the plant (u, v) is bounded i.e. we assume that there exist two positive constants $M_u > 0$ and $M_v > 0$ such that $|u(x, t)| \leq M_u$ and $|v(x, t)| \leq M_v$ for all $x \in [0, 1]$ and $t \geq 0$.*

Remark 2.7.2. *Assumption 2.7.1 is only necessary for the estimation of the boundary parameter q . If the value of q is known, the boundedness of the plant is no more needed. The estimation of the parameters θ_1 and θ_2 is independent from the status of the plant (u, v) .*

The boundedness results of $Q(x, t)$ are inferred from the following theorem.

Theorem 2.7.2. *Consider the $Q(x, t)$ system (2.39)-(2.42) with zero initial conditions $Q(x, 0) \equiv 0$ and the observer gains (2.58). If assumption 2.7.1 holds, then we have that $\|Q(\cdot, t)\|_{L^2[0,1]}$ is bounded.*

Proof. As we did in section 2.7.1, the idea is first to decouple the two states $Q_1(x, t)$ and $Q_2(x, t)$. Following the same procedure of section 2.7.1, it is easy to check that the same transformation $R(x, \xi)$ defined by equations (2.61)-(2.66) maps $Q(x, t)$ to the following target system:

$$W(x, t) = Q(x, t) + \int_x^1 R(x, \xi)Q(\xi, t)d\xi \quad (2.90)$$

$$W(x, t) = \begin{pmatrix} w_1(x, t) \\ w_2(x, t) \end{pmatrix} \quad (2.91)$$

where the dynamics of $W(x, t)$ are given by:

$$\partial_t w_1(x, t) + c_1 \partial_x w_1(x, t) = 0 \quad (2.92)$$

$$\partial_t w_2(x, t) - c_2 \partial_x w_2(x, t) = 0 \quad (2.93)$$

$$w_1(0, t) = \omega w_2(0, t) + v(0, t), \quad w_2(1, t) = 0 \quad (2.94)$$

Since we choose a zero initial conditions for the filters, then the trivial solution for the transport equation $w_2(x, t)$ is zero for all times. As a result, we are left with the transport equation $w_1(x, t)$:

$$\partial_t w_1(x, t) + c_1 \partial_x w_1(x, t) = 0, \quad w_1(0, t) = v(0, t) \quad (2.95)$$

Now, we show the L^2 boundedness of $W(x, t)$ by considering the following Lyapunov function:

$$V_2(t) = \frac{1}{2} \int_0^1 e^{-x} w_1^2(x, t) \quad (2.96)$$

Differentiating (2.96) in time, substituting by (2.95) then integrate by parts to get:

$$\begin{aligned}\dot{V}_2(t) &= -\frac{c_1}{2e}w^2(1,t) + \frac{c_1}{2}w^2(0,t) - c_1V_2(t) \\ &\leq -c_1V_2(t) + \frac{c_1}{2}v^2(0,t) \\ &\leq -c_1V_2(t) + \frac{c_1}{2}M_v^2\end{aligned}\tag{2.97}$$

It follows from (2.97) that $V_2(t)$ is bounded, as a direct consequence of the boundedness of the plant (u, v) by assumption 2.7.1. Since $V_2(t)$ serves as the weighted L^2 norm of the $W(x, t)$ system and since the transformation $R(x, \xi)$ is invertible, we can deduce that $\|Q(\cdot, t)\|_{L^2[0,1]}$ is bounded and the proof is complete. \square

2.8 Parameter adaptation laws and exponential stability of $\tilde{\theta}(t)$

The authors in [51] synthesize adaptation laws for static regressors equations of this general form:

$$y(t) = \phi^T(t)\theta\tag{2.98}$$

where y is the vector of outputs, ϕ is the regressor and θ is the vector of unknown parameters. The core of the designs is based on minimizing cost functions of the squared estimation errors. Then, sufficient conditions for the exponential convergence of the estimates are given using Lyapunov analysis considering persistent excitation assumptions. In this section, we adapt the analysis of [51] to synthesize an adaptive law for our problem and prove that $\hat{\theta}(t) \rightarrow \theta$ exponentially fast.

In view of the available measurements given in (2.21), equations (2.29) and (2.30) are evaluated at $x = 1$ and $x = 0$, respectively, and we have that:

$$Z_p(t) = E_p(t) - \Lambda_p(t)\tilde{\theta}(t)\tag{2.99}$$

where:

$$Z_p(t) = \begin{pmatrix} z_1(1, t) \\ z_2(0, t) \end{pmatrix}, E_p(t) = \begin{pmatrix} \tilde{u}(1, t) \\ \tilde{v}(0, t) \end{pmatrix}, \Lambda_p(t) = \begin{bmatrix} \lambda_{11}(1, t) & \lambda_{12}(1, t) & Q_1(1, t) \\ \lambda_{21}(0, t) & \lambda_{22}(0, t) & Q_2(0, t) \end{bmatrix}$$

$Z_p(t)$ is the output of the PDE estimation error. We have shown in Theorem 2.6.1 that after a delay time $t_F = \frac{1}{c_1} + \frac{1}{c_2}$, $Z(x, t)$ reaches its zero equilibrium point, and hence, $Z_p(t)$ becomes equal to zero. Therefore, after t_F , the regressor equations (2.99) and (2.98) become equivalent and this suggests the following normalized parameter adaptation law (continuous-time recursive least squares estimator with a forgetting factor):

$$\dot{\hat{\theta}}(t) = s(t) \frac{P(t)\Lambda_p^T(t)}{1 + \|\Lambda_p^T(t)\Lambda_p(t)\|^2} E_p(t),\tag{2.100}$$

$$\dot{P}(t) = s(t) \left[\beta P(t) - \frac{P(t)\Lambda_p^T(t)\Lambda_p(t)P(t)}{1 + \|\Lambda_p^T(t)\Lambda_p(t)\|^2} \right],\tag{2.101}$$

$$s(t) = \begin{cases} 1 & \text{if } t > t_F \\ 0 & \text{else} \end{cases}\tag{2.102}$$

where $\hat{\theta}(t)$ is the estimated value of θ , $P(t) \in \mathbb{R}^{3 \times 3}$, and $\beta > 0$ is the forgetting factor. The initial conditions $\hat{\theta}(0) = \hat{\theta}_0$, and $P(0) = P_0 = P_0^T > 0$ are chosen arbitrarily. The introduction of the $s(t)$ signal in the adaptation laws means that the estimation of the parameters will only begin after the maximum time for transport t_F is passed. In other words, the signal $s(t)$ removes the effect of the initial conditions of both the filters $\Lambda(x, t)$ and the observer $\{\hat{u}(x, t), \hat{v}(x, t)\}$ on the overall adaptive scheme.

To prove that $\hat{\theta}(t) \rightarrow \theta$ exponentially fast, we assume the following:

Assumption 2.8.1. *We assume that $\Lambda_p(t)$ is persistently exciting i.e. for all $t \geq 0$ there exist positive constants T_0, c_0 and c_1 so that:*

$$c_0 I \leq \frac{1}{T_0} \int_t^{t+T_0} \Lambda_p^T(\tau) \Lambda_p(\tau) d\tau \leq c_1 I \quad (2.103)$$

where $I \in \mathbb{R}^{3 \times 3}$ denotes the identity matrix.

The convergence of the estimate $\hat{\theta}(t)$ is then given by the following Theorem.

Theorem 2.8.1. *Consider the system (2.100)-(2.102) with initial conditions given by $\hat{\theta}_0$ and P_0 . If $\Lambda_p(t), \dot{\Lambda}_p(t)$ are bounded and if (2.103) holds, then $\hat{\theta}(t) \rightarrow \theta$ exponentially fast.*

Proof. First, we compute the dynamics of the estimation error on $\tilde{\theta}(t)$ using (2.99) and (2.100) as:

$$\begin{aligned} \dot{\tilde{\theta}}(t) &= -\dot{\hat{\theta}}(t) = -s(t) \frac{P(t) \Lambda_p^T(t)}{1 + \|\Lambda_p^T(t) \Lambda_p(t)\|^2} E_p(t) \\ &= -s(t) \frac{P(t) \Lambda_p^T(t)}{1 + \|\Lambda_p^T(t) \Lambda_p(t)\|^2} Z_p(t) - s(t) \frac{P(t) \Lambda_p^T(t) \Lambda_p(t)}{1 + \|\Lambda_p^T(t) \Lambda_p(t)\|^2} \tilde{\theta}(t) \end{aligned} \quad (2.104)$$

it is also easy to check that (2.101) is equivalent to

$$\frac{d}{dt}(P^{-1})(t) = s(t) \left[-\beta P^{-1}(t) + \frac{\Lambda_p^T(t) \Lambda_p(t)}{1 + \|\Lambda_p^T(t) \Lambda_p(t)\|^2} \right] \quad (2.105)$$

where $P^{-1}(t) \in \mathbb{R}^{3 \times 3}$ is the inverse matrix of $P(t)$. It can be shown (see e.g. [51]) that if $\Lambda_p(t), \dot{\Lambda}_p(t)$ are bounded and under Assumption 2.8.1, $P^{-1}(t)$ is positive definite and bounded for all $t \geq 0$. Now, we can define the following Lyapunov function:

$$V(t) = \frac{1}{2} \tilde{\theta}^T(t) P^{-1}(t) \tilde{\theta}(t) \quad (2.106)$$

Taking the time derivative of (2.106) we obtain:

$$\dot{V}(t) = \frac{1}{2} \tilde{\theta}^T(t) \frac{d}{dt}(P^{-1})(t) \tilde{\theta}(t) + \tilde{\theta}^T P^{-1}(t) \dot{\tilde{\theta}}(t) \quad (2.107)$$

Using (2.104)-(2.105), one gets from (2.106) that:

$$\dot{V}(t) = -s(t) \frac{\tilde{\theta}^T(t) \Lambda_p^T(t)}{1 + \|\Lambda_p^T(t) \Lambda_p(t)\|^2} Z_p(t) - \frac{\beta}{2} s(t) \tilde{\theta}^T(t) P^{-1}(t) \tilde{\theta}(t) - \frac{1}{2} s(t) \frac{\tilde{\theta}^T(t) \Lambda_p^T(t) \Lambda_p(t) \tilde{\theta}(t)}{1 + \|\Lambda_p^T(t) \Lambda_p(t)\|^2} \quad (2.108)$$

If $t < t_F$, by (2.102) we have $\dot{V}(t) = 0$: the Lyapunov function is non-increasing. When t become greater than t_F ($s(t) = 1$), we have by Theorem 2.6.1 that $Z_p \equiv 0$, then (2.108) becomes

$$\dot{V}(t) = -\beta V(t) - \frac{1}{2} \frac{\tilde{\theta}^T(t) \Lambda_p^T(t) \Lambda_p(t) \tilde{\theta}(t)}{1 + \|\Lambda_p^T(t) \Lambda_p(t)\|^2} \leq -\beta V(t) \quad (2.109)$$

since the matrix $\Lambda_p^T(t) \Lambda_p(t)$ is positive semi-definite. As a result, for all $t \geq t_F$, there exists $K > 0$ such that $V(t) \leq K e^{-\beta t} V(0)$ and $\tilde{\theta}(t)$ is thus exponentially decaying to zero with a rate β : $\tilde{\theta}(t) \rightarrow \theta$ exponentially fast and the proof is complete. \square

2.9 Exponential stability of $E(x, t)$

In this section we prove the exponential stability of the error system $E(x, t)$, referring to the results in sections 2.6, 2.7 and 2.8.

Theorem 2.9.1. *Consider the error system (2.26)-(2.27) with boundary conditions (2.28) and initial conditions \tilde{u}_0, \tilde{v}_0 in $L^2[0, 1]$, with observer gains $p_1(x)$ and $p_2(x)$ given in (2.58) and with feedback gains $m_1(x, t)$ and $m_2(x, t)$ given in (2.33) and (2.35). Under Theorems 2.6.1-2.8.1 the error system is exponentially stable in the L^2 sense.*

Proof. Using (2.31), one gets the following:

$$\|E(\cdot, t)\|_{L^2[0,1]} \leq \|Z(\cdot, t)\|_{L^2[0,1]} + \|\Lambda(\cdot, t) \tilde{\theta}(t)\|_{L^2[0,1]} \quad (2.110)$$

By definition:

$$\begin{aligned} \|\Lambda(\cdot, t) \tilde{\theta}(t)\|_{L^2[0,1]}^2 &= \int_0^1 (\lambda_{11}(x, t) \tilde{\theta}_1(t) + \lambda_{12}(x, t) \tilde{\theta}_2(t) + Q_1(x, t) \tilde{q}(t))^2 dx \\ &+ \int_0^1 (\lambda_{21}(x, t) \tilde{\theta}_1(t) + \lambda_{22}(x, t) \tilde{\theta}_2(t) + Q_2(x, t) \tilde{q}(t))^2 dx \end{aligned} \quad (2.111)$$

After expanding the squared parentheses in (2.111) and using basic identity inequalities we get:

$$\|\Lambda(\cdot, t) \tilde{\theta}(t)\|_{L^2[0,1]}^2 \leq 3\tilde{\theta}_1^2 \|\Lambda_1(\cdot, t)\|_{L^2[0,1]}^2 + 3\tilde{\theta}_2^2 \|\Lambda_2(\cdot, t)\|_{L^2[0,1]}^2 + 3\tilde{q}^2 \|Q(\cdot, t)\|_{L^2[0,1]}^2 \quad (2.112)$$

Then by theorems 2.7.1-2.7.2, there exist 3 positive constants M_1, M_2 and M_3 such that:

$$\begin{aligned} \|\Lambda(\cdot, t) \tilde{\theta}(t)\|_{L^2[0,1]}^2 &\leq 3M_1 \tilde{\theta}_1^2(t) + 3M_2 \tilde{\theta}_2^2(t) + 3M_3 \tilde{q}^2(t) \\ &\leq M \|\tilde{\theta}(t)\|_2^2 \end{aligned} \quad (2.113)$$

where $M = 3 \max\{M_1, M_2, M_3\}$. Considering (2.110) along with (2.113) we have:

$$\|E(\cdot, t)\|_{L^2[0,1]} \leq \|Z(\cdot, t)\|_{L^2[0,1]} + \sqrt{M} \|\tilde{\theta}(t)\|_2 \quad (2.114)$$

Since $\|Z(\cdot, t)\|_{L^2[0,1]}$ and $\|\tilde{\theta}(t)\|_2$ are exponentially decaying (referring to Theorem 2.6.1 and Theorem 2.8.1, respectively), then so is $\|E(\cdot, t)\|_{L^2[0,1]}$. \square

2.10 Numerical Simulation Results

The effectiveness of the adaptive estimator (2.22)-(2.25), whose convergence is ensured by the theoretical results derived in Theorems 2.6.1-2.8.1, is evaluated on two separate scenarios: 1) on a stable plant and 2) on an unstable plant. As mentioned in Remark 2.7.2, that in case there is no boundary parameter q to be estimated, it is not necessary for the plant to be stable in order to estimate the unstable distributed states $\{u(x, t), v(x, t)\}$ and the other parameters θ_1 and θ_2 . Therefore, we show the convergence aspects on the following plant models.

2.10.1 Scenario 1: Stable plant

Consider the following plant toy example evolving in $\{(t, x) \mid t \geq 0, x \in [0, 1]\}$:

$$\partial_t u(x, t) + \frac{1}{15} \partial_x u(x, t) = 0.01v(x, t) + \theta_1 \cos(x) \quad (2.115)$$

$$\partial_t v(x, t) - \frac{1}{5} \partial_x v(x, t) = -0.01u(x, t) + \theta_2 \sin(x) \quad (2.116)$$

$$u(0, t) = qv(0, t) + \sin(t), \quad v(1, t) = \sin(0.25t) \quad (2.117)$$

with $\theta_1 = 1$, $\theta_2 = 2$ and $q = 0.5$. The plant (2.115)-(2.117) is open-loop stable due to the chosen small coupling values $\sigma_1(x) = 0.01$, $\sigma_2(x) = -0.01$ and also $q = 0.5 < 1$. The outputs of the plant i.e. $y_1(t) = u(1, t)$ and $y_2(t) = v(0, t)$ are fed back to the adaptive estimator (Section 2.4) as follows:

$$\partial_t \hat{u}(x, t) + \frac{1}{15} \partial_x \hat{u}(x, t) = 0.01\hat{v}(x, t) + \hat{\theta}_1(t) \cos(x) - p_1(x)(\hat{u}(1, t) - y_1(t)) + m_1(x, t) \quad (2.118)$$

$$\partial_t \hat{v}(x, t) - \frac{1}{5} \partial_x \hat{v}(x, t) = -0.01\hat{u}(x, t) + \hat{\theta}_2(t) \sin(x) - p_2(x)(\hat{v}(0, t) - y_2(t)) + m_2(x, t) \quad (2.119)$$

$$\hat{u}(0, t) = \omega(\hat{v}(0, t) - y_2(t)) + \hat{q}(t)v(0, t) + \sin(t), \quad \hat{v}(1, t) = \sin(0.25t) \quad (2.120)$$

where $m_1(x, t)$ and $m_2(x, t)$ are calculated using (2.33)-(2.35), the filters are computed using (2.37)-(2.39) and the parameter estimates are updated using (2.100)-(2.102). Four variables are still to be evaluated in order to simulate (2.118)-(2.120) which are: the weight w , the forgetting factor β and the observer gains $p_1(x)$ and $p_2(x)$. The level of confidence in the measurement $y_2(t)$ represented by w is set to 1 ($w = 1$). β is related to the speed of convergence of the algorithm and it is set to $\beta = 0.01$. The calculation of $p_1(x)$ and $p_2(x)$ is done using (2.58). This necessitates solving offline the $P(x, \xi)$ kernel equations (2.52)-(2.57). The kernel $P(x, \xi)$ is solved using successive approximations [50]. The main idea of this method is to write the set of PDEs (2.52)-(2.57) in the integral form using the method of characteristics. Afterwards, the integral equations are solved using recursion up to an order of accuracy defined by the user. We give here a brief explanation of the method.

Let us consider the kernel equations (2.52)-(2.53) with boundary conditions (2.56) of $P^{11}(x, \xi)$ and $P^{21}(x, \xi)$ (The two other kernels $P^{12}(x, \xi)$ and $P^{22}(x, \xi)$ are completely similar). Using the

method of characteristics on the domain Ω , we can write (2.52)-(2.53)-(2.56) in the integral form as follows:

$$P^{21}(x, \xi) = -\frac{\sigma_2\left(\frac{xc_1+\xi c_2}{c_1+c_2}\right)}{c_1+c_2} + \int_{\frac{x-\xi}{c_1+c_2}}^0 \left(\sigma_2(x-c_2s)P^{11}(x-c_2s, \xi+c_2s) \right) ds \quad (2.121)$$

$$\begin{aligned} P^{11}(x, \xi) &= \omega P^{21}(0, \xi-x) + \int_0^{\frac{x}{c_1}} \sigma_1(x-c_1s)P^{21}(x-c_1s, \xi-c_1s)ds \\ &= \omega \left[-\frac{\sigma_2\left(\frac{(\xi-x)c_2}{c_1+c_2}\right)}{c_1+c_2} + \int_{\frac{x-\xi}{c_1+c_2}}^0 \left(\sigma_2(-c_2s)P^{11}(-c_2s, \xi-x+c_2s) \right) ds \right] \\ &\quad + \int_0^{\frac{x}{c_1}} \sigma_1(x-c_1s)P^{21}(x-c_1s, \xi-c_1s)ds \end{aligned} \quad (2.122)$$

System (2.121)-(2.122) can then be written in the following compact form:

$$H(x, \xi) = H_0(x, \xi) + F[H](x, \xi) \quad (2.123)$$

where:

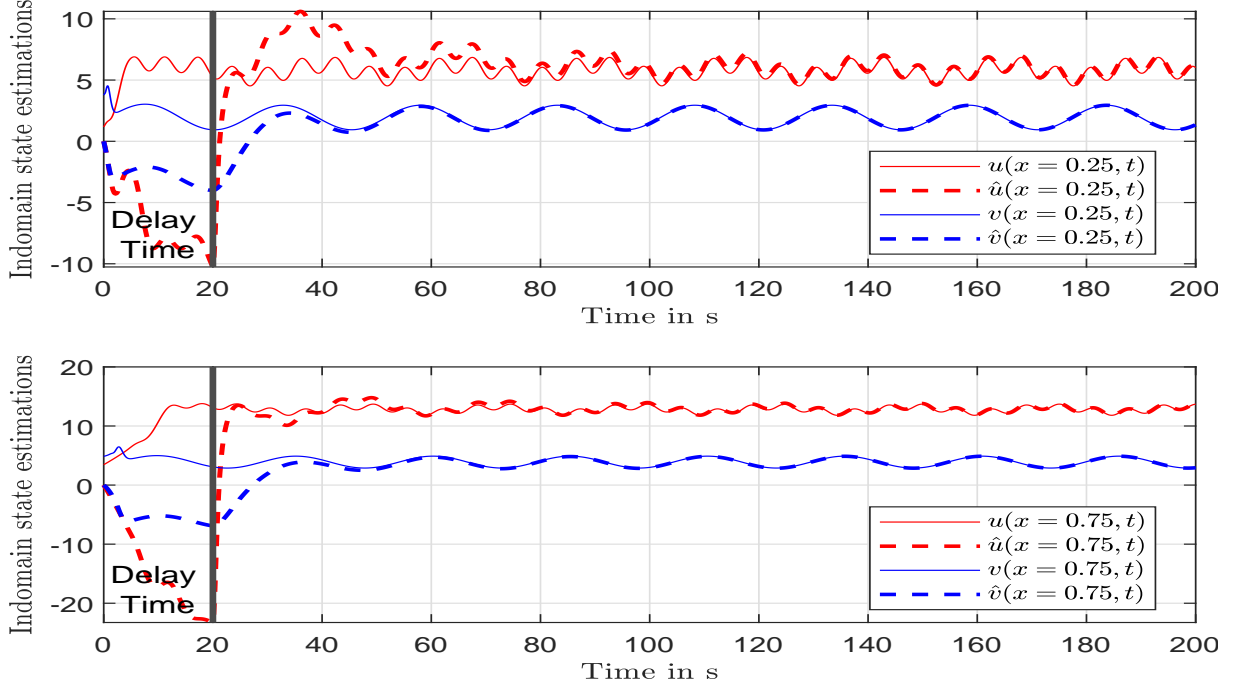
$$\begin{aligned} H(x, \xi) &= \begin{pmatrix} P^{11}(x, \xi) \\ P^{21}(x, \xi) \end{pmatrix}, \quad H_0(x, \xi) = \begin{pmatrix} -\omega \frac{\sigma_2\left(\frac{(\xi-x)c_2}{c_1+c_2}\right)}{c_1+c_2} \\ \sigma_2\left(\frac{xc_1+\xi c_2}{c_1+c_2}\right) \end{pmatrix} \\ F[H](x, \xi) &= \begin{bmatrix} \omega \int_{\frac{x-\xi}{c_1+c_2}}^0 \left(\sigma_2(-c_2s)P^{11}(-c_2s, \xi-x+c_2s) \right) ds + \int_0^{\frac{x}{c_1}} \sigma_1(x-c_1s)P^{21}(x-c_1s, \xi-c_1s)ds \\ \int_{\frac{x-\xi}{c_1+c_2}}^0 \left(\sigma_2(x-c_2s)P^{11}(x-c_2s, \xi+c_2s) \right) ds \end{bmatrix} \end{aligned}$$

Given (2.123), we now use successive approximations i.e.

$$H^n(x, \xi) = H_0(x, \xi) + F[H^{n-1}](x, \xi) \quad (2.124)$$

with $H^0(x, \xi) = H_0(x, t)$. We discretize the 2D domain Ω in rectangles, approximate the integrals in $F[H](x, \xi)$ using left Riemann sum for integrals and we simulate (2.124) for n iterations such that $|\Delta H^n(x, \xi) = H^n(x, \xi) - H^{n-1}(x, \xi)| < \epsilon$ where ϵ is the degree of accuracy defined by the user and it is very small. The sequence $\Delta H^n(x, \xi)$ is guaranteed to converge since the system has a unique solution in $C^2(\Omega)$ (see [50] for further details).

As all the observer parameters are set, we implement the plant (2.115)-(2.117) and the adaptive observer (2.118)-(2.120) in Matlab 2018. We have used second order finite difference schemes to approximate the first order derivative in space (∂_x) and the fixed step ODE3 solver in Matlab to approximate the time derivatives. The plant is started at $\{u_0(x)=5\sin(x), v_0(x)=5\cos(x)\}$, while the adaptive observer begins with $\{\hat{u}_0(x)=0, \hat{v}_0(x)=0, \hat{\theta}_1(0)=5, \hat{\theta}_2(0)=-3, \hat{q}(0)=4\}$. Fig.

Figure 2.3: In-domain state estimations at $x = 0.25$ and $x = 0.75$

2.3 shows the estimation of the states inside the domain at $x = 0.25$ and $x = 0.75$. These two in-domain points are chosen just as an example to show the effectiveness of the adaptive observer to estimate the in-domain states using only boundary sensing. The observer starts to converge after the maximum delay time of transport $t_f = 15 + 5 = 20s$ is passed. The quality of the parameter estimations is shown on Fig. 2.4. Before t_f the estimations remain at the constant initial values, but after that time, the algorithm starts to converge to the true parameter values as predicted by the theoretical results in Theorem 2.7.2. Fig. 2.5 shows the convergence of $\{\tilde{u}(x,t), \tilde{v}(x,t)\}$ in the L^2 norm. Since the estimation of the parameters is not updated before t_f , the L^2 norm increases from its initial value in the interval of time $[0, t_f]$. However, after t_f , the parameters update algorithm starts and the L^2 norm begins to decrease towards zero.

2.10.2 Scenario 2: Unstable plant

In this scenario, we consider an unstable plant evolving in $\{(t, x) \mid t \geq 0, x \in [0, 1]\}$:

$$\partial_t u(x, t) + \partial_x u(x, t) = 2.5v(x, t) + \theta_1 \cos(x) \quad (2.125)$$

$$\partial_t v(x, t) - 2\partial_x v(x, t) = 2u(x, t) + \theta_2 \sin(x) \quad (2.126)$$

$$u(0, t) = \sin(t), \quad v(1, t) = \sin(0.25t) \quad (2.127)$$

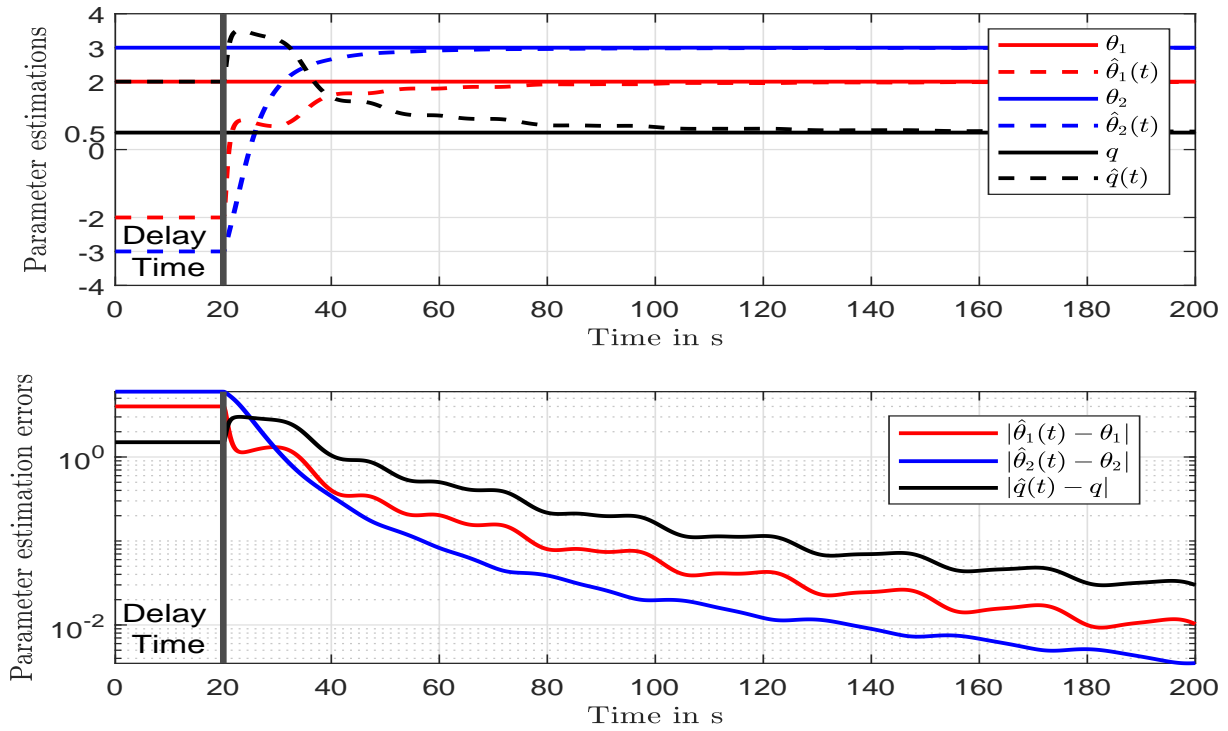
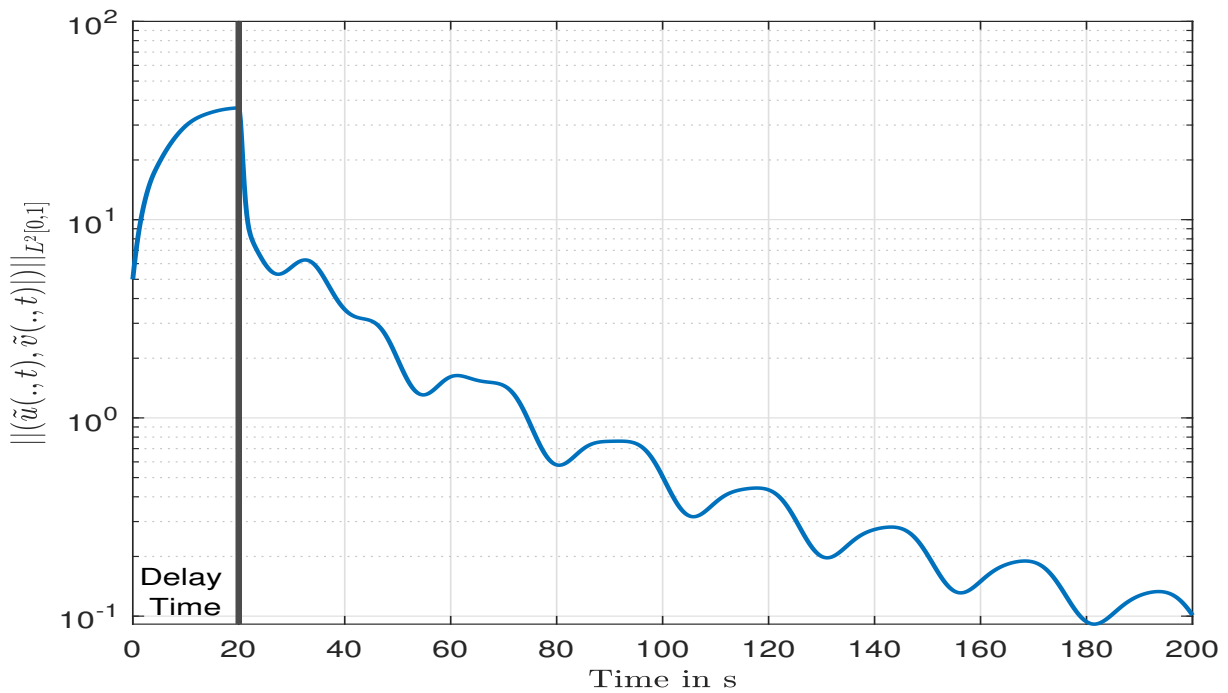
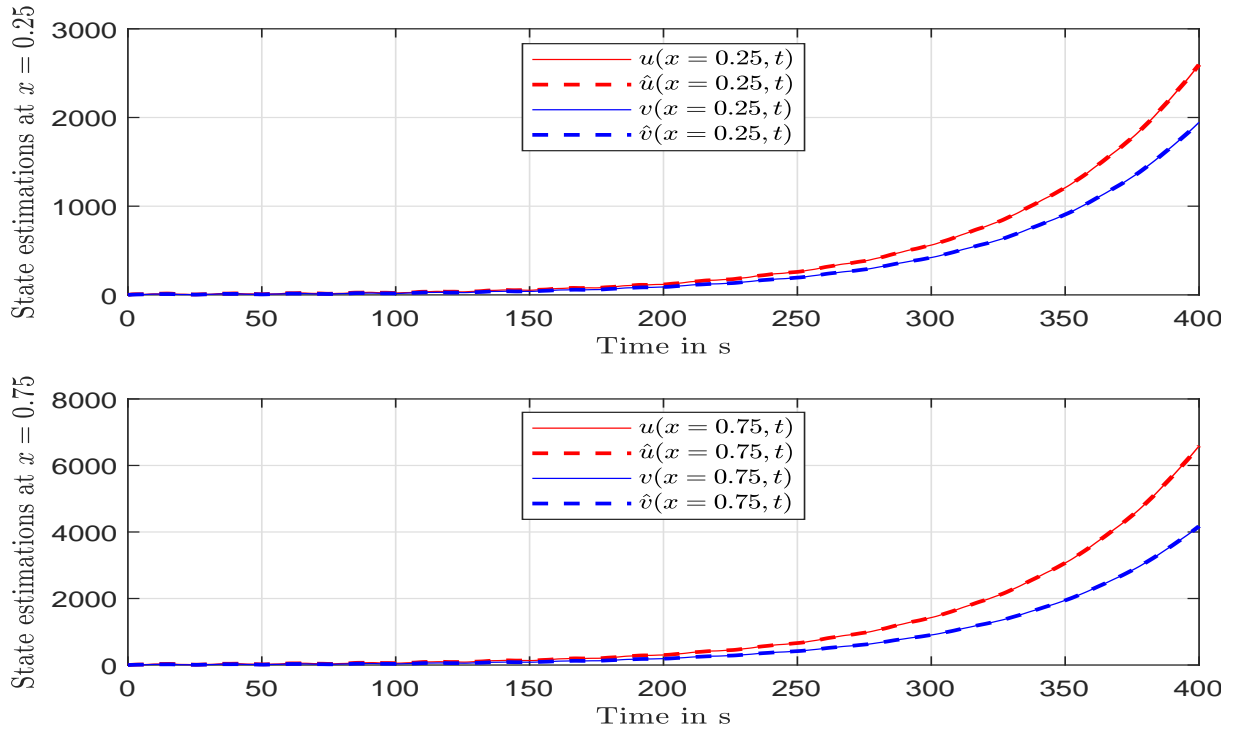


Figure 2.4: Parameter estimations and parameter estimation errors

Figure 2.5: The evolution of the L^2 norm of $\{ \tilde{u}(x,t), \tilde{v}(x,t) \}$

Figure 2.6: In-domain state estimations at $x = 0.25$ and $x = 0.75$

with $\theta_1 = 1$ and $\theta_2 = 2$. The system is unstable because of the large magnitude of the coupling ($\sigma_1(x) = 2.5$ and $\sigma_2(x) = 2$) between the two dynamics $u(x, t)$ and $v(x, t)$. No unknown boundary coupling q is involved in the system. As we mentioned in Remark 2.7.2, the estimation of boundary parameters of this type $qv(0, t)$ at the boundary is limited to bounded dynamics. The main objective of Scenario 2 is to show that it is possible to estimate the states and the parameters θ_1 and θ_2 for a plant that is diverging.

The simulation methodology is exactly the same as in Scenario 1, but it is important to pay attention to remove the filter $Q(x, t)$ from the set of filters as no boundary elements are present. The initial conditions of the plant and the observer are: $\{u_0(x)=5\sin(x), v_0(x)=5\cos(x)\}$, while for the adaptive observer, $\{\hat{u}_0(x)=0, \hat{v}_0(x)=0, \hat{\theta}_1(0)=5, \hat{\theta}_2(0)=4\}$. The results are shown on Figures 2.6-2.8. The delay time $t_f = 1 + \frac{1}{2} = 1.5s$ is small compared to the order of magnitude of the system simulation time and it is not showing on the figures. In all cases, we can observe the convergence of the in-domain states as well as the parameters to their true values. Although the plant is unbounded, the L^2 norm of the error states start to converge to zero after the sharp increase in its magnitude in the interval of time $[0, 1.5s]$. The results in both scenarios 1 and 2 shows that the stability of the estimation errors is guaranteed by the observer gains $p_1(x)$ and $p_2(x)$ while the convergence of the parameters is related to the persistency in the parameter excitations through the plant inputs $U(t) = \sin(t)$ and $V(t) = \sin(0.25t)$ and the bounded functions $\phi_1(x, t) = \cos(x)$ and $\phi_2(x, t) = \sin(x)$.

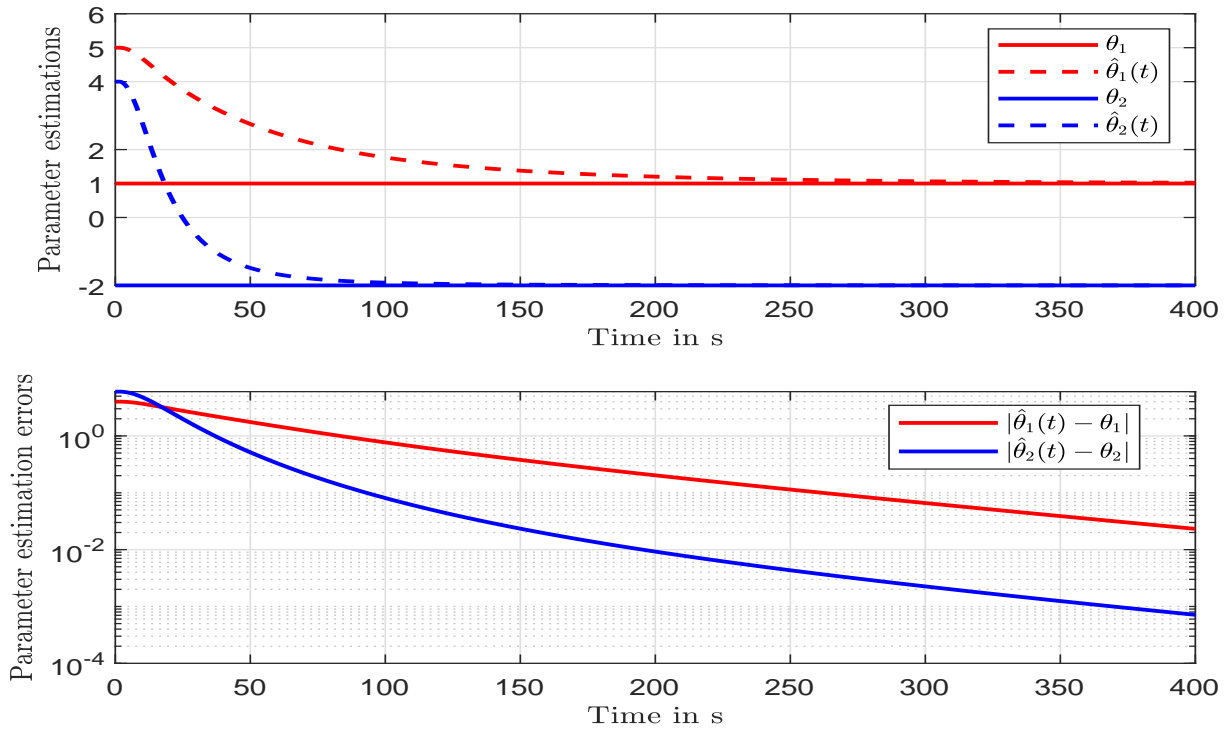


Figure 2.7: Parameter estimations and parameter estimation errors

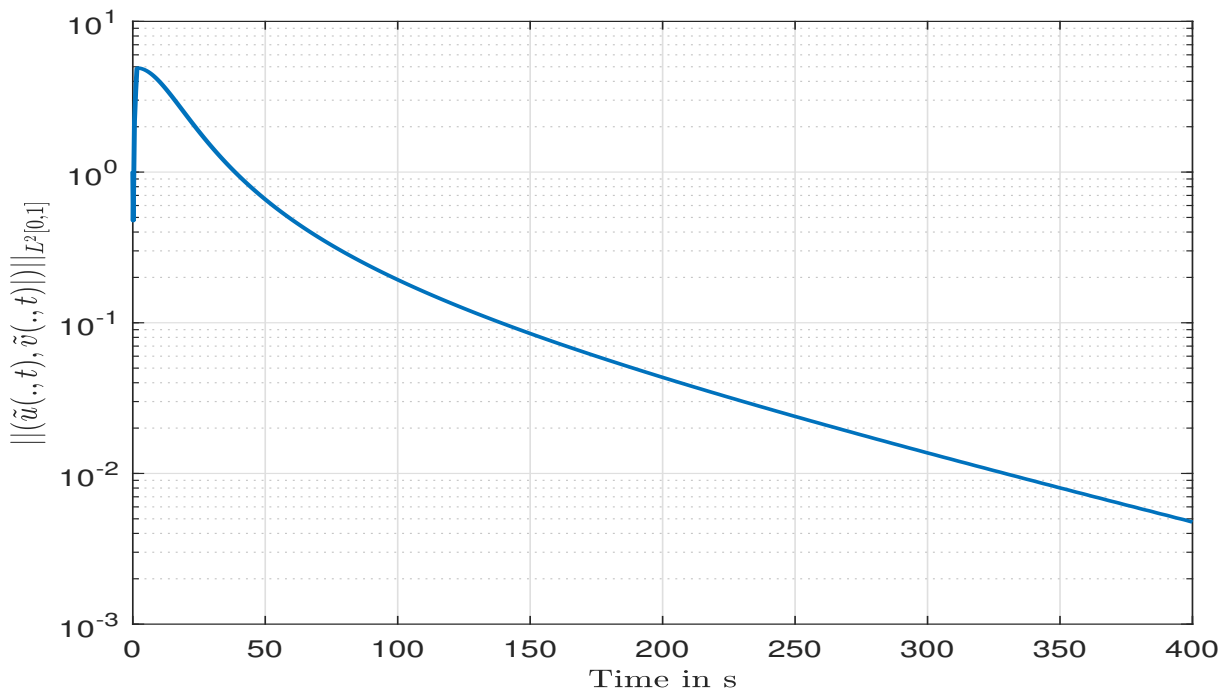
Figure 2.8: The evolution of the L^2 norm of $\{\tilde{u}(x, t), \tilde{v}(x, t)\}$



Figure 2.9: 15kW TIF plant at CERN

2.11 Experimental evaluation of the observer (CERN)

We evaluate our observer on the TIF plant, a 15kW cooling system built at CERN to run educative experiments for developing and improving CO₂ cooling technology [65]. This refrigeration system is shown on Fig. 2.9 and schematically depicted in Fig. 2.10. It consists of a circulation system where the cold CO₂ refrigerant is pumped by the pump (LP3004) to the transfer lines (two concentric cylindrical tubes in vacuum isolation) and then heated by means of two heaters (EH7027 and EH7028) to provide the hot CO₂ refrigerant. Both hot and cold refrigerants exchange heat through the transfer lines, and finally the hot fluid is cooled down by the chiller (HX3082) to be pumped again into the cold line. The accumulator is used to set a desired output pressure at the hot side. We focus on the transfer line, as this part is particularly complex to model and necessitates an advanced observation scheme for distributed systems. The plant is equipped with four temperature sensors placed at the extremities of the tubes (shown in Fig. 2.10), which measure the input and output temperatures on both hot and cold sides. The control input is through the two heaters (EH7027 and EH7028), where we can vary the temperature of the hot input by adding and removing heat and thus create some transients in the system.

We recall that the overall objective of the theoretical study presented in Sections 2.2 - 2.10 is to synthesize an adaptive observer to estimate the temperature states $\{T^H(x, t), T^C(x, t)\}$ simultaneously with the heat transfer coefficient h of a single phase heat exchanger tube carrying CO₂ as its working refrigerant (see Fig. 2.1) and the transfer line on Fig. 2.10. The system is modeled

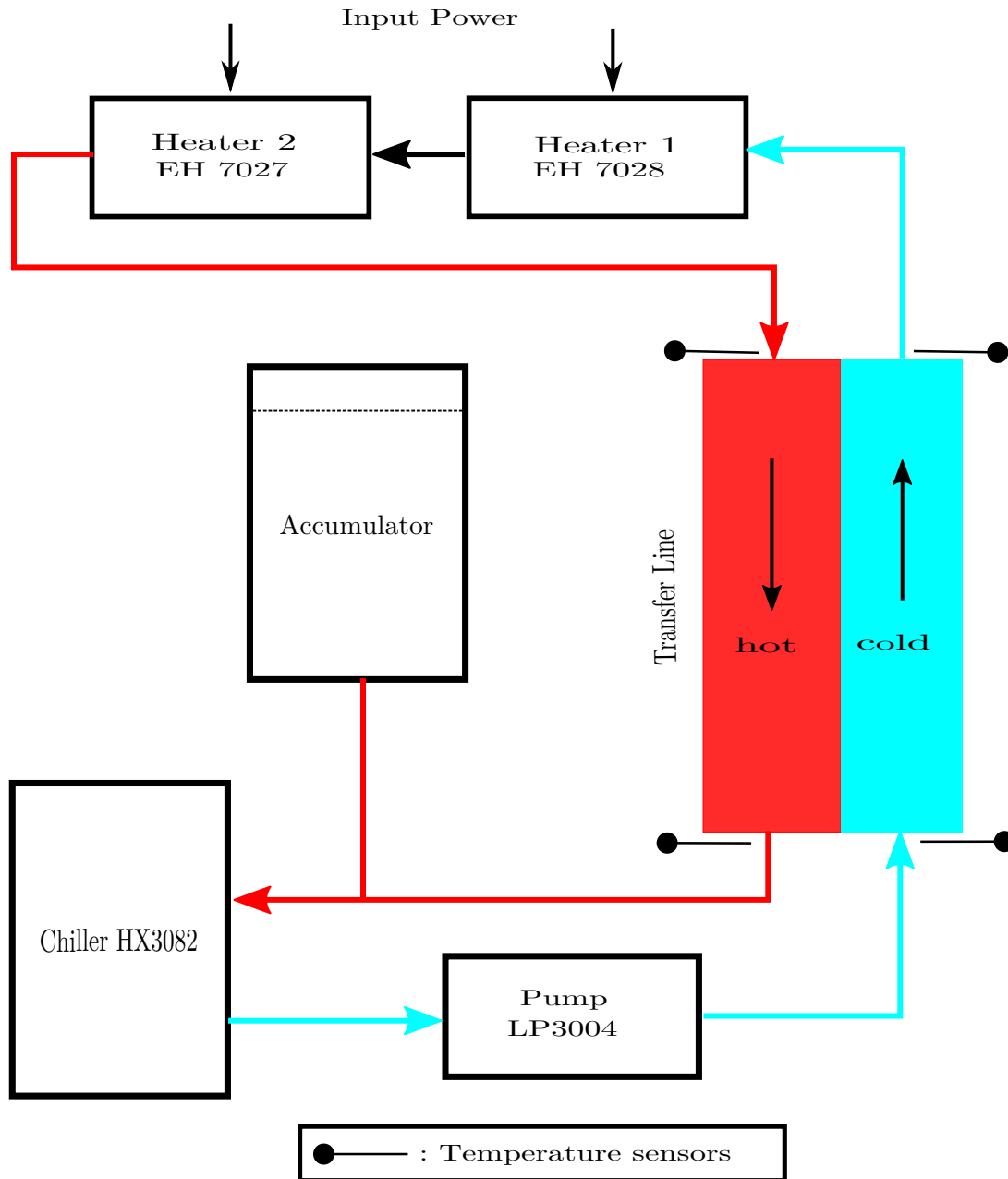


Figure 2.10: Schematic of the TIF plant

by two hetero-directional transport equations (2.2)-(2.5). One key idea of our solution to the problem is to augment the vector of states from $\{T^H(x, t), T^C(x, t)\}$ to $\{T^H(x, t), T^C(x, t), h\}$, and then do a linearization around the nominal model $\{T_N^H(x, t), T_N^C(x, t), h^N\}$ presented in equations (2.6)-(2.9). The obtained dynamics of the perturbed states $\{\Delta T^H(x, t), \Delta T^C(x, t), \Delta h\}$ are transformed by an exponential transformation to $\{\Delta T_1^H(x, t), \Delta T_1^C(x, t), \Delta h\}$ given in equations (2.14)-(2.16) with the measurements $y_1^H(t)$ and $y_2^C(t)$ in (2.17). We have mentioned in Remark 2.2.1 that synthesizing an observer for $\{\Delta T_1^H(x, t), \Delta T_1^C(x, t), \Delta h\}$ is just a special case in the more general observation problem considered in Section 2.2. Since only the estimation of the heat transfer coefficient is considered in the evaluation process, the over-parameterization in system (2.18)-(2.20) is removed by letting $\theta_1 = \theta_2 = \Delta h$, and as a consequence, the number of necessary swapping filters drops from four to only two. More precisely, the adaptive observer for $\{\Delta T_1^H(x, t), \Delta T_1^C(x, t), \Delta h\}$ is:

$$\begin{aligned} \partial_t \widehat{\Delta T}_1^H(x, t) + c_1 \partial_x \widehat{\Delta T}_1^H(x, t) &= K_1^N e^{(\frac{K_1^N}{c_1} + \frac{K_2^N}{c_2})x} \widehat{\Delta T}_1^C(x, t) - p_1(x) (\widehat{\Delta T}_1^H(1, t) \\ &\quad - y_1^H(t)) + \widehat{\Delta h}(t) \frac{\pi D_1 e^{-\frac{K_1^N}{c_1}x}}{A^H \rho^H C_P^H} (-T_N^H(x, t) + T_N^C(x, t)) + m_1(x, t) \end{aligned} \quad (2.128)$$

$$\begin{aligned} \partial_t \widehat{\Delta T}_1^C(x, t) - c_2 \partial_x \widehat{\Delta T}_1^C(x, t) &= K_2^N e^{-(\frac{K_1^N}{c_1} + \frac{K_2^N}{c_2})x} \widehat{\Delta T}_1^H(x, t) - p_2(x) (\widehat{\Delta T}_1^C(1, t) \\ &\quad - y_1^H(t)) + \widehat{\Delta h}(t) \frac{\pi D_1 e^{\frac{K_2^N}{c_2}x}}{A^C \rho^C C_P^C} (T_N^H(x, t) - T_N^C(x, t)) + m_2(x, t) \end{aligned} \quad (2.129)$$

$$\widehat{\Delta T}_1^H(0, t) = \omega (\widehat{\Delta T}_1^C(0, t) - y_2^C(t)), \quad \widehat{\Delta T}_1^C(1, t) = 0 \quad (2.130)$$

The swapping filters are

$$\begin{aligned} \partial_t \lambda_1(x, t) + c_1 \partial_x \lambda_1(x, t) &= K_1^N e^{(\frac{K_1^N}{c_1} + \frac{K_2^N}{c_2})x} \lambda_2(x, t) - p_1(x) \lambda_1(1, t) \\ &\quad + \frac{\pi D_1 e^{-\frac{K_1^N}{c_1}x}}{A^H \rho^H C_P^H} (-T_N^H(x, t) + T_N^C(x, t)) \end{aligned} \quad (2.131)$$

$$\begin{aligned} \partial_t \lambda_2(x, t) - c_2 \partial_x \lambda_2(x, t) &= K_2^N e^{-(\frac{K_1^N}{c_1} + \frac{K_2^N}{c_2})x} \lambda_1(x, t) - p_2(x) \lambda_2(1, t) \\ &\quad + \frac{\pi D_1 e^{\frac{K_2^N}{c_2}x}}{A^C \rho^C C_P^C} (T_N^H(x, t) - T_N^C(x, t)) \end{aligned} \quad (2.132)$$

$$\lambda_1(0, t) = \omega \lambda_2(0, t), \quad \lambda_2(1, t) = 0 \quad (2.133)$$

with $m_1(x, t) = \lambda_1(x, t) \dot{\hat{\theta}}(t)$ and $m_2(x, t) = \lambda_2(x, t) \dot{\hat{\theta}}(t)$. $\hat{\theta}(t)$ is calculated using the adaptive law (2.100)-(2.102) but with $\Lambda_p(t) = [\lambda_1(1, t), \lambda_2(0, t)]$. Furthermore, there is no change in

the calculation of $p_1(x)$ and $p_2(x)$ as equation (2.58) is used. Once the estimates $(\hat{\Delta T}_1^H(x, t), \hat{\Delta T}_1^C(x, t), \hat{\Delta h}(t))$ are obtained, one can use the linearization map in Section 2.1 to get the estimates of $\{\hat{T}^H(x, t), \hat{T}^C(x, t), \hat{h}(t)\}$ at each point in time.

2.11.1 In-domain evaluation of the observer through simulations

As shown in Fig. 2.10, temperatures can only be measured at the extremities of the tubes using four input/output temperature sensors. Hence, we can't validate experimentally the distributed state estimation because we can't take measurements from inside the domain. However, we evaluate the estimation of temperatures inside the domain through numerical simulations. In this section, we also discuss the effect of linearization done in Section 2.1.

First of all, assume that the model (2.2)-(2.5) represents the real dynamics of the exchanger under study. We have built our own simulator to simulate (2.2)-(2.5). The simulator implements a finite difference scheme of second order accuracy for the space derivatives, and ode15s (Matlab) for the time derivatives. Since the observer is not built directly on system (2.2)-(2.5) but on the linearized version (2.14)-(2.16), we expect the quality of the estimation to be better when the nominal model (2.6)-(2.9) is chosen close to the real system. The simulations are done in the following order:

1. Simulate system (2.2)-(2.5) with real measured inputs (see Section 2.11.3) and assume that the real heat transfer coefficient is $h_{real} = 290$. We then consider the obtained temperatures $T_{real}^H(x, t)$ and $T_{real}^C(x, t)$ as the real distributed temperatures of exchanger.
2. Use $T_{real}^H(1, t)$ and $T_{real}^C(0, t)$ as the real boundary measurements
3. Simulate the observer scheme starting with nominal heat transfer coefficient $h_1^N = 180$, $h_2^N = 230$ and $h_3^N = 250$.
4. Compute the estimation $\hat{T}(x, t) = T^N(x, t) + \Delta\hat{T}(x, t)$ and the estimation error $E(x, t) = |T_{real}(x, t) - \hat{T}(x, t)|$ on both hot and cold sides.

In order to choose different operating points, we vary the nominal heat transfer coefficients; e.g. $h_1^N = 180$ corresponds to a far operating point (since $h_{real} = 290$) and so on. The results of the steady state estimation errors are shown in Fig. 2.11. A first important remark is that the estimation error inside the domain is greater than that at the boundaries for all the operating points. A glimpse on the observer design can actually give us the reason. Considering the linear case, the adaptation law uses only boundary outputs to estimate the parameters. If the outputs are informative enough, the estimated values of the parameters will converge to the real ones when the outputs agree. Since the observer is of Luenberger type and its stability is guaranteed by the observer gains $p_1(x)$ and $p_2(x)$, the in-domain estimates should also converge. When considering the real system, the adaptation law ensures the convergence of the boundary outputs, but this does not necessarily imply an in-domain convergence since the observer is built on the linearized version of the system and not on the real plant. We can see from Fig. 2.11 that as the nominal model approaches the real model (i.e. h^N approaches h_{real}), the estimation error in the domain is decreased. By looking into the order of error magnitude, we

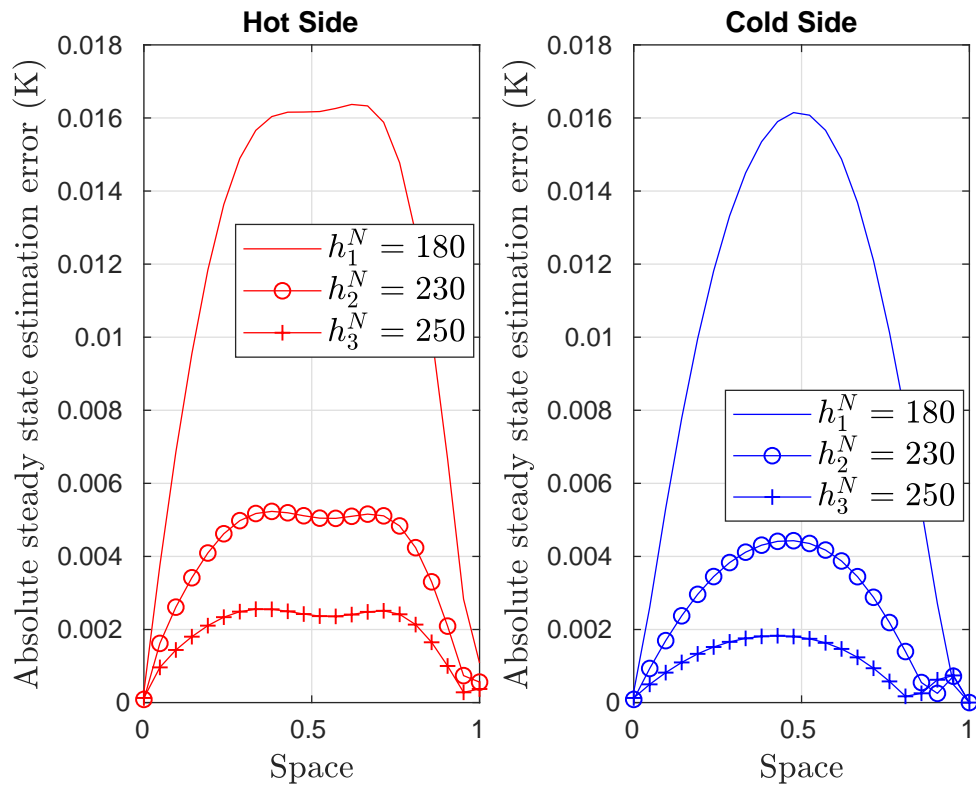


Figure 2.11: Steady state error on the distributed temperature profiles for three different operating points

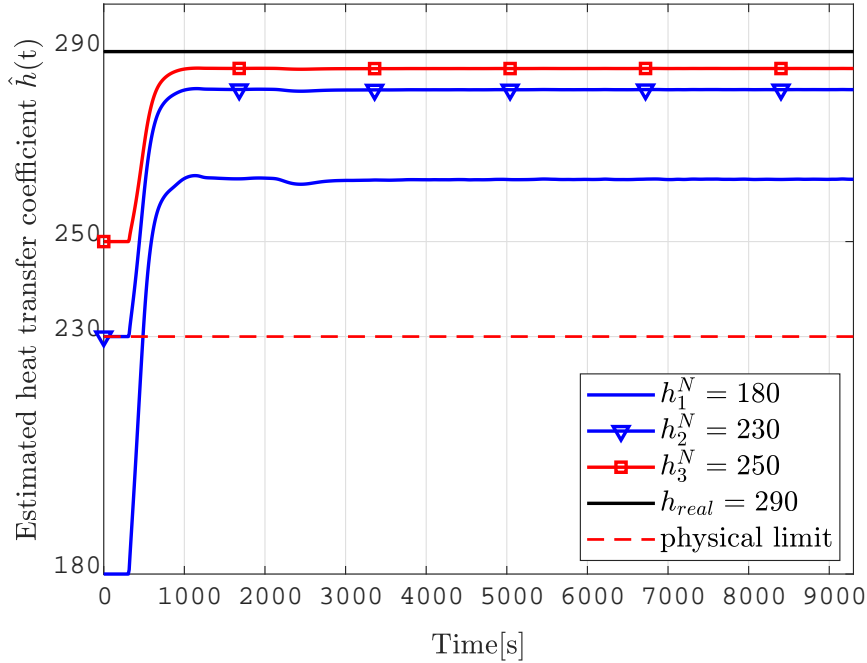


Figure 2.12: Estimated heat transfer coefficient $\hat{h}(t)$ for three different operating points

find that the maximum absolute estimation error on both sides is less than 0.018 K in the whole domain. This is significantly a negligible in-domain estimation error. We can then reasonably deduce that the effect of linearization is almost negligible and does not affect the quality of the in-domain estimation. The reason is mainly because the bilinear parameter nonlinearity ($K_1(T^H(x, t) - T^C(x, t))$) encountered in the plant is not a strong nonlinearity.

We now show the time series of the heat transfer coefficient on Fig. 2.12. We can see that the estimations from the three different nominal operating points stabilize at steady states that do not correspond to $h_{real} = 290$. The reason is clearly the linearization, since when the nominal operating point is chosen close to the system's real operating point, the estimation is improved. This is more significant if we compute the relative steady state error: $RSE(\%) = \frac{|h_{real} - \hat{h}_{steady}|}{h_{real}} * 100$ for each operating point. The RSE decreases when h^N approaches h_{real} as shown in Table 2.1 and its magnitude is less than 10% even for a very far operating point (i.e. $h^N = 180$). It is also important to mention that there is always a physical limit on the chosen values of the operating point h^N (see Fig. 2.12). This limit is calculated using thermodynamical correlations [43]. For the exchanger under study, the minimal calculated physical limit is $h^N = 230$, and we can notice on Table 2.1 that the corresponding RSE is less than 3%. This is considered very small, and we can conclude that in the physical working ranges of the exchanger, the effect of linearization on the estimation of the heat transfer coefficient is reasonably small.

Operating point	RSE (%)
$h_1^N = 180$	9.31
$h_2^N = 230$	2.79
$h_3^N = 250$	1.24

Table 2.1: RSE for three different operating points

2.11.2 Comparison with literature observers

Previously, several boundary observer designs for hyperbolic systems relying on an exact knowledge of the parameters of the system have been designed. We intend to show the importance of the adaptive design in the case where the nominal parameters differ from the real ones as this is the main problem that we faced while designing an observer for our experiment. To compare our results we choose two designs already present in the literature: the Lyapunov-based observer proposed in [85] and the two-sided backstepping observer from [14].

We simulate the observers proposed in [85] and [14] at the three different operating points ($h_1^N = 180$, $h_2^N = 230$, and $h_3^N = 250$), following exactly the procedure explained in Section 4.3 (steps 1 to 3). We recall that the observer designs in [85] and [14] are built directly using the nominal parameters of the system. The main objective of the comparison is to check if the parameter adaptation improves the accuracy of the temperature estimates.

We simulate the three observers with real measured inputs (see Section 4.4) starting with the same initial conditions. We have calculated the L^1 norm of the estimation error on both hot and cold sides for the three different operating points:

$$\|\epsilon^K(t)\|_{L^1[0,1]} = \int_0^1 |T_{real}^K(x,t) - \hat{T}^K(x,t)| dx \quad (2.134)$$

The results are shown on Fig. 2.13. We can observe that in all the plots the estimation error using the adaptive design is always less than that resulting from the observers in [85] and [14]. The adaptive observer significantly ameliorates the estimation in transient states and contributes to nearly 1K temperature improvement at steady states. These estimation enhancements provided by the parameter adaptation are very important to the designers of the CO₂ cooling technology at CERN, since they work with highly accurate temperature sensors.

2.11.3 Experimental evaluation of the observer

Once the system has reached a steady state and liquid CO₂ starts circulating in all parts of the TIF plant, the experiment is done by modulating the input heating power by several increases and decreases at different instants in time as shown in Table 2.2, thus inducing system transients and exciting the system frequencies. Keeping in mind that we have only one parameter to estimate, which is the heat transfer coefficient, the input in Table 2.2 is considered sufficiently persistently exciting. The temperature is measured by the four sensors schematically depicted on Fig. 2.10. They are PT100 RTD sensors. In particular, they are "in-flow" sensors, i.e., they are mounted inside the tube to measure the temperature of the refrigerant itself, instead of

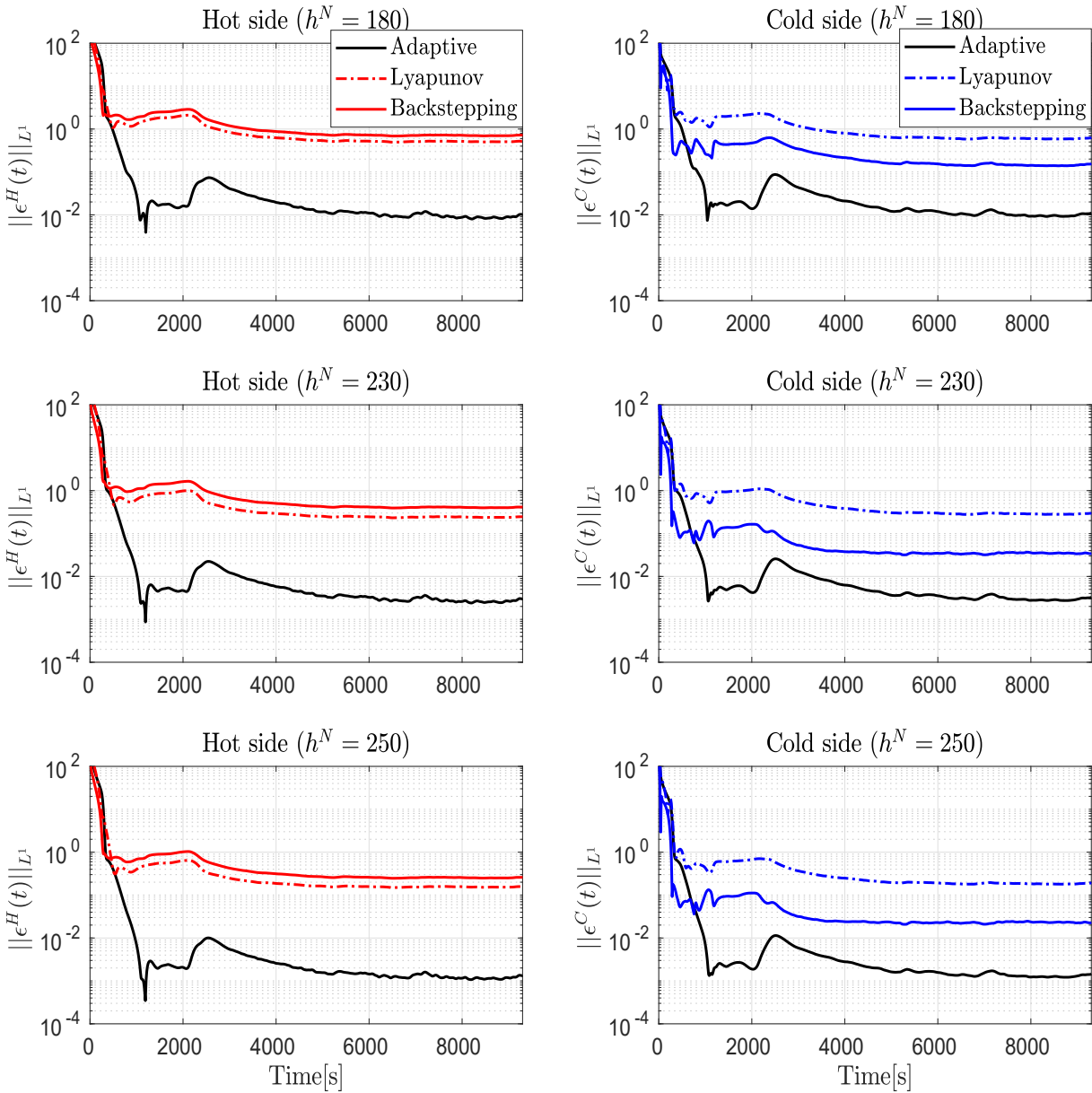


Figure 2.13: Comparison of the L^1 estimation error resulting from three different methods for three different operating points

Variation	Time(s)
increase	0(s)
decrease	479(s)
increase	800(s)
increase	1391(s)
decrease	2050(s)

Table 2.2: Heating power modulation

being glued to the top of the tube. These PT100s output a resistance to a "Conditioner", which is an object that converts the resistance signal into a 4-20 mA input for the PLC. The PLC then has a range that determines what the minimum (4mA) and maximum (20mA) values for that particular sensor are, and uses this to convert the 4-20 mA signal into a degree Celsius (C) value. On the computer, we have a SCADA system called WinCCOA, which exchanges signals from the PLC and displays it for the user. From the WinCCOA interface, we are able to export the data to a CSV file. We import the data into Matlab where we make all the analysis. The observer schemes are not implemented directly on the real plant. The experimental evaluation of the observers is done in Matlab using the real data collected in the CSV files.

The TIF plant is 17.665 m long ($L = 17.665$ m) with cross-sectional areas $A^H = 7.6306 \times 10^{-4}$ m², $A^C = 1.131 \times 10^{-4}$ m². During this experiment, the exchanger is operating in the liquid phase and in the following working ranges: pressure between [5 MPa, 6 MPa], temperatures between [253 K, 288 K] and mass flow rates close to 0.047 Kg/s. With these given information, one can use the equation of state (EoS) for CO₂ [18] with the correlation in [43] to calculate the nominal values for the exchanger parameters. We found: $c_1 = 0.0237$ s⁻¹, $c_2 = 0.0037$ s⁻¹, $K_1^N = 0.0051$ s⁻¹ and $K_2^N = 0.0351$ s⁻¹. The computed nominal heat transfer coefficient is $h^N = 230$ W/m².K. Afterwards, the nominal model (2.6)-(2.9) is simulated with the measured inputs. By comparing the temperature outputs of the nominal model $T_N^H(1, t)$ and $T_N^C(0, t)$ and the experimental measures on Fig. 2.14, one can notice that the nominal model captures the main dynamics of the real system. However, the temperatures predicted by the model involve a temperature shift and this shift changes with time. We know from the physics that the heat transfer coefficient is the parameter responsible for this shift in temperature magnitudes, since it affects the amount of energy transferred from the hot side to the cold side. One can then draw two conclusions: first the linear system (2.1)-(2.5) represents a good physical model for the exchanger, second the real heat transfer coefficient is time-varying. In fact, the dynamics of h are very complex since h can vary with the variation of many physical quantities and especially temperature. In our adaptive design, we have assumed that h is quasi-steady (see the modeling assumptions list). Doing so, we intend to use the parameter adaptation algorithm to recover the values of the heat transfer coefficient in the intervals where we have slow variations in temperature (as we will show later in the analysis).

As the nominal operating point is settled, we can proceed to the estimation part. Since we can't take measurements from inside the domain, we evaluate our theoretical results against the output sensor measurements. We start all observers with the same initial condition. Fig. 2.15 show the temperatures estimated by the three observers along with the experimental measurements. One

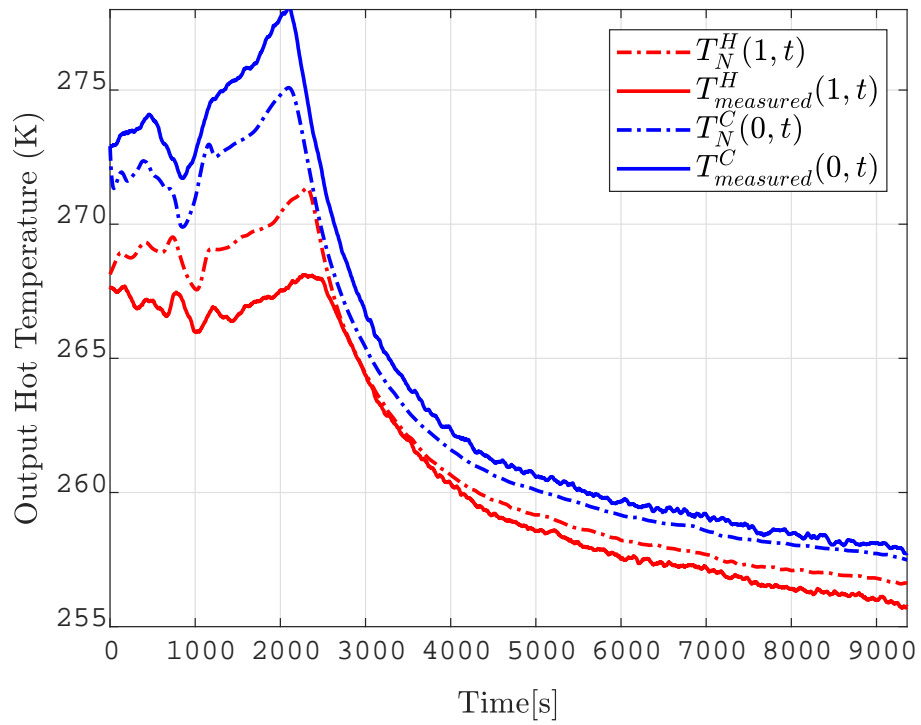


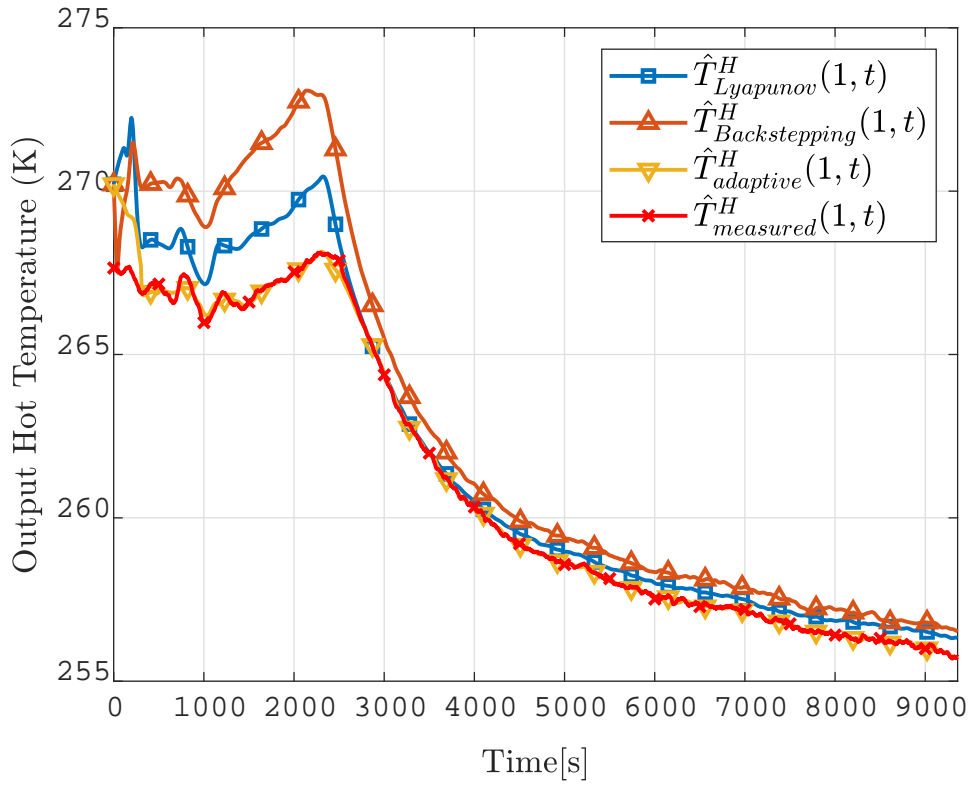
Figure 2.14: Comparison between the reference model and experimental results

can notice that the quality of the estimation is better using our proposed adaptive estimator during both transient and steady states. The estimation error magnitude on both hot and cold sides is presented on Fig. 2.16. Note that the error is decreased by nearly 5K during the transient phase and 1K in the steady state, using the adaptive estimator. The estimations using the two other designs (Lyapunov and two-sided backstepping observers) are comparable and with an accuracy limited by their assumption of a perfect knowledge of the system's parameters. Considering a negligible contribution of the linearization error as illustrated in Section 2.11.1, we can conclude that the adaptive observer can estimate the distributed state with enough degree of accuracy.

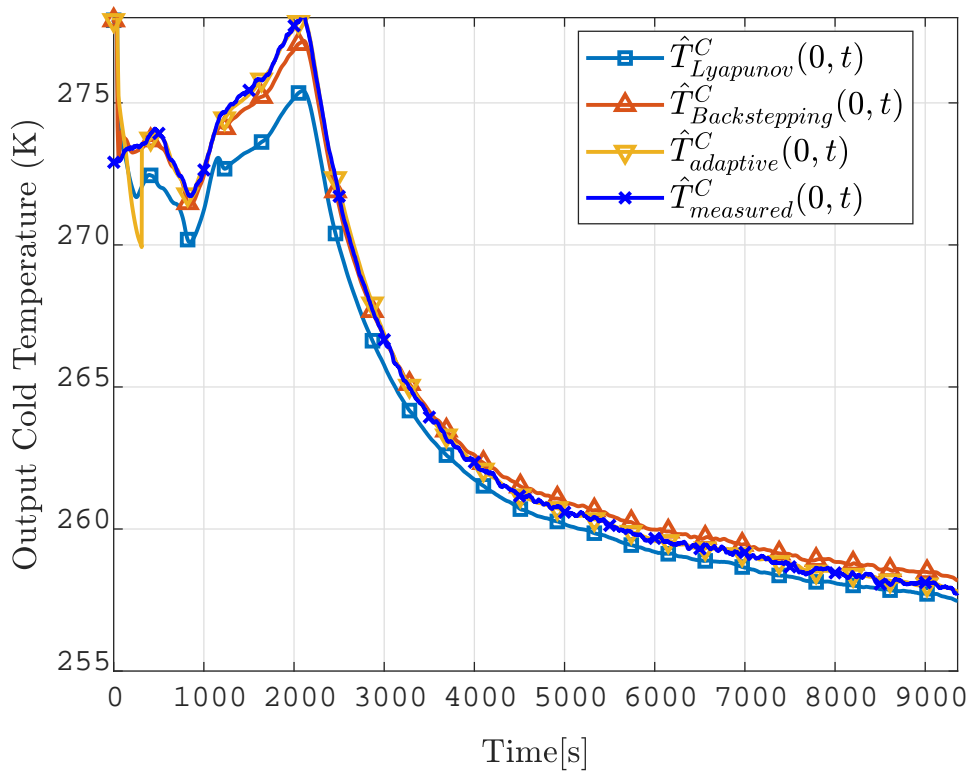
The estimation of the heat transfer coefficient is shown on Fig. 2.17: the estimation starts at the nominal value $h^N = 230$ and then after the time $t_F = \frac{1}{c_1} + \frac{1}{c_2} = 310.54$ s the adaptation law starts functioning. Since we have implicitly assumed that h is quasi-steady, we expect the estimated heat transfer coefficient to converge to different steady states at different intervals of time. We can infer from Fig. 2.17 approximately three different values of the heat transfer coefficient in three different time intervals: $h \approx 312$ for $t \in [310, 1235]$ s, $h \approx 325$ for $t \in [1625, 2530]$ s and $h \approx 295$ for $t \in [3550, 8400]$ s.

2.12 Conclusion

We have developed an adaptive observer that estimates unknown parameters inside the domain for 2-by-2 first-order 1-D hyperbolic PDEs. The observer is based on a swapping design, which allows us to write the estimation error on the states as a static linear combination of the estimation error on the parameters. Standard backstepping and parameter estimation techniques can then be used. We thus proved boundedness of regressors filters and obtained sufficient conditions to ensure the exponential convergence of the estimation errors. The designed observer uses only boundary sensing, and allows one to estimate the full distributed states. We have shown through numerical simulations the effectiveness of the observer in estimating the states of stable and unstable plants as well as the boundary and in-domain parameters. Our method is evaluated experimentally on the TIF refrigeration system at CERN, and our results show that the adaptive observer captures the main dynamics of the real system. For future works, it would be interesting to consider the bilinear parameterization directly in (2.1)-(2.5), i.e. to estimate h and $T^H(x, t)$, $T^C(x, t)$ directly without passing through the linearization step, using boundary sensing only. We discuss here some insights on this future extension of the method. The difficulty of Problem 1 is that the heat transfer coefficient h , which is unknown, multiplies the temperature $T(x, t)$ which is also unknown. One idea is to transform the system to the "canonical observable form" similar to the works done in [20] and [8]. In this specific form, the transformed parameters multiply the system measurements. The authors in [20] and [8] focus on adaptive control for hyperbolic PDEs. Hence, extensive studies must be conducted to prove the convergence of the parameters to their true values as well as proving the invertability of the parameters transformations (this part is not necessary in adaptive control, since the overall goal is to stabilize the system in presence of uncertainties and not to estimate the parameters).

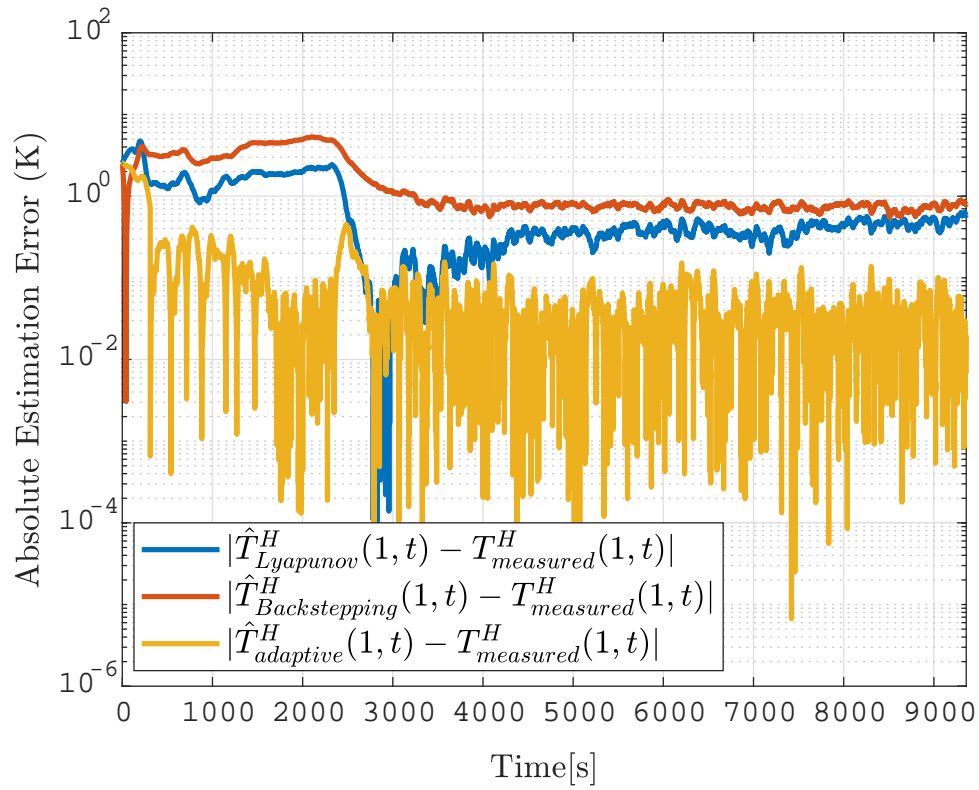


(a) Hot fluid temperature.

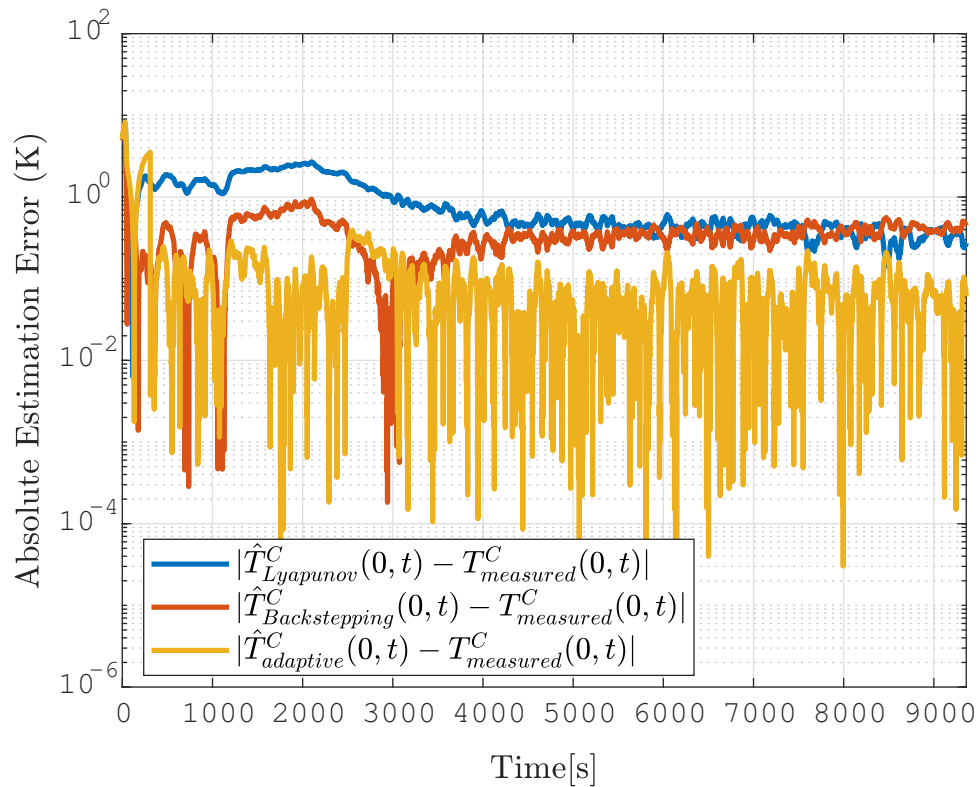


(b) Cold fluid temperature.

Figure 2.15: Comparison between the estimation laws for the hot and cold fluid temperatures.



(a) Output hot estimation errors.



(b) Output cold estimation errors.

Figure 2.16: Comparison between the estimation errors for the hot and cold fluid temperatures.

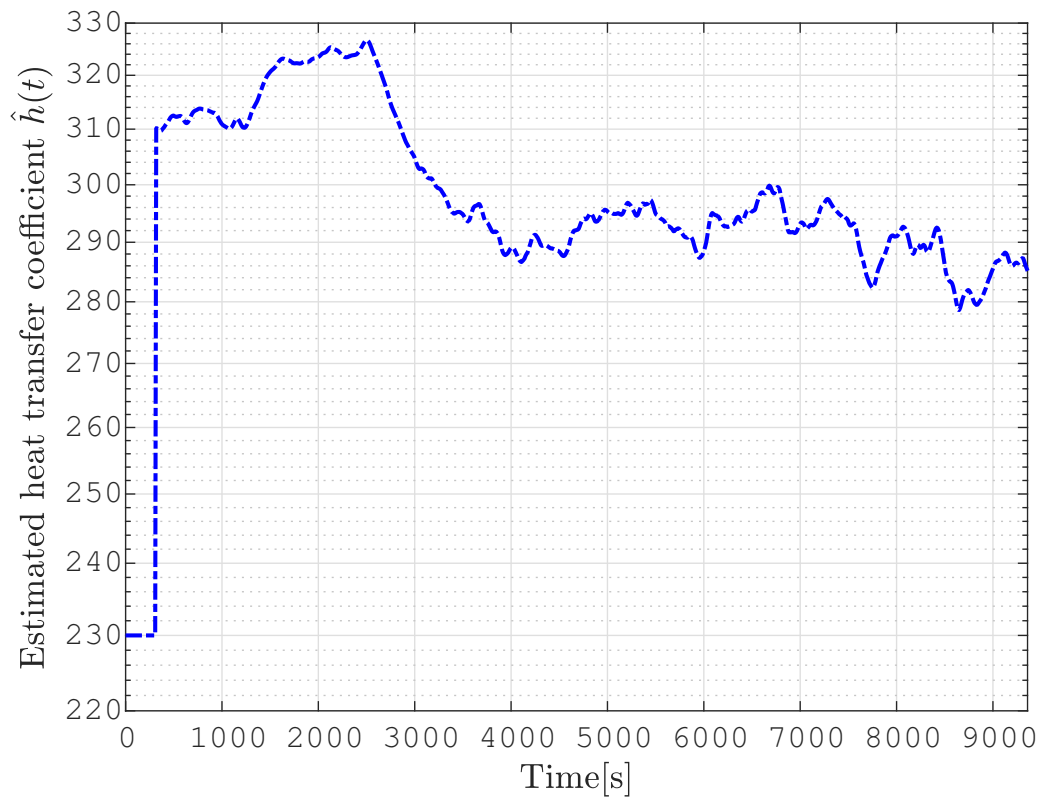


Figure 2.17: Estimated heat transfer coefficient $\hat{h}(t)$

Chapter 3

Boundary Observer Design for CO₂ two phase heat exchangers

In the previous chapter, we have considered the problem of estimating the temperatures and the heat transfer coefficient in single phase heat exchangers. The thermodynamic state of the circulating CO₂ fluids was only liquid. As a result, the system is modeled using a set of 2-by-2 linear hyperbolic PDE that describes the evolution of temperature along the length of the exchanger. In this chapter, the modeling complexity is significantly increased by introducing the two- phase aspect to one of the exchanger lines, as shown in Fig. 3.1.

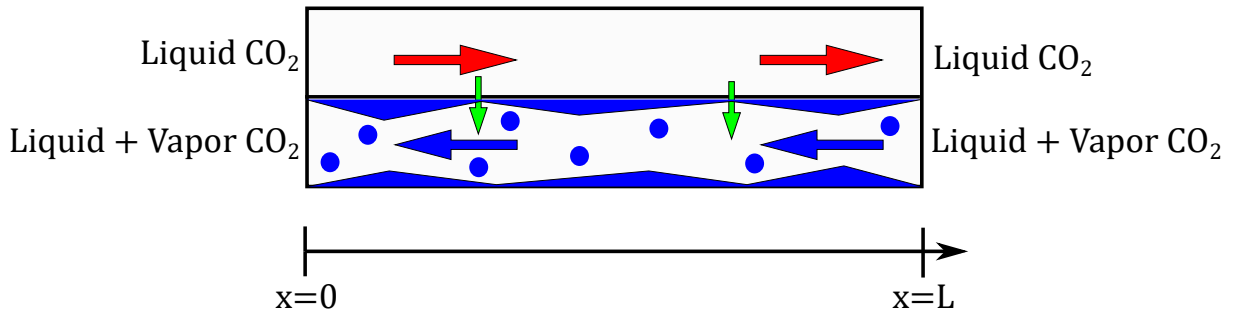


Figure 3.1: CO₂ two phase heat exchanger.

The cold line is gaining energy from the hot liquid line, and is evaporating. That leads to the presence of liquid and vapor at the same time inside the cold tube. Hence, more dynamics are needed to describe this two phase evolution in space and time. We recall that the objectives of Problem 2 are:

1. obtain a control-oriented model for the two phase exchanger
2. use boundary sensing to estimate the liquid to vapor ratio inside the domain.

The next sections are divided in two main parts: 1) is the physical modeling of the two phase line. This will allow us to deduce a control-oriented model for the two phase exchanger. And 2),

the observer architecture that will use the obtained model to estimate some thermodynamical variables of interest (e.g. the liquid to vapor ratio).

3.1 Physical modeling of the two phase line

3.1.1 Flow regimes

When liquid and vapor flow at a certain velocity inside a horizontal tube, different geometrical shapes of the phase-changing flow emerge and occupy the area. These flow configurations are called flow regimes. For instance, consider a typical example of what can happen inside a tube in which fluids are undergoing a phase change, as depicted in Fig. 3.2.

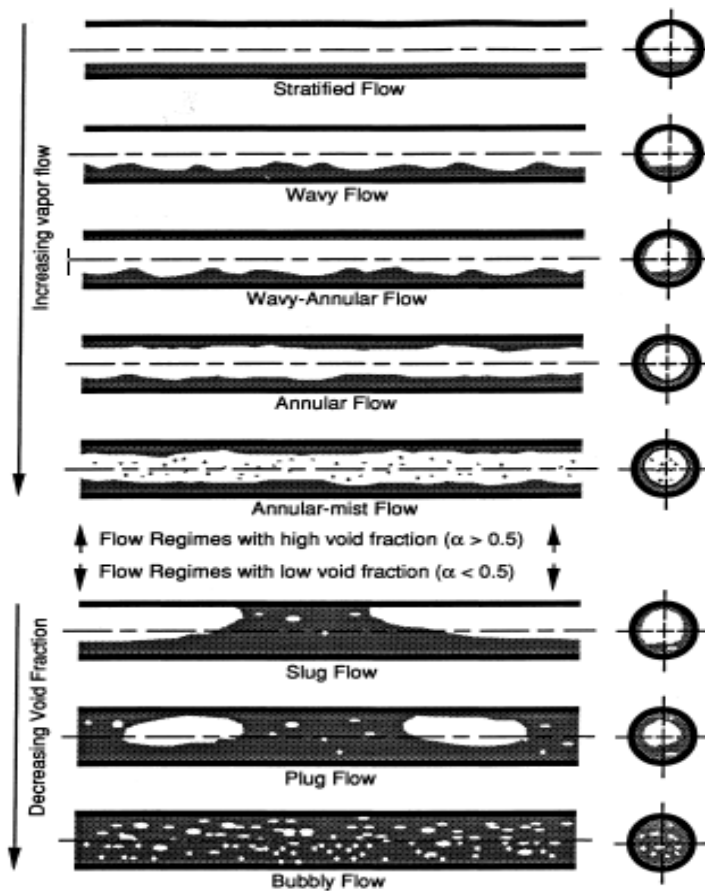


Figure 3.2: Vapor-liquid flow regimes [38]

Different flow regimes can be divided into two groups: (a) those in which vapor flows as a continuous stream, and (b) those in which vapor segments are separated from each other by liquid. The time-averaged fraction of the tube that is occupied by vapor is the void fraction α . From experiments it is observed that vapor flows continuously for $\alpha > 0.5$. At high void fraction

and low vapor flow rate, the liquid is smooth and stratified. As the vapor flow rate increases, waves appear on the liquid-vapor interface, increase further will lead the liquid to climb up the tube wall and the flow is annular. At high vapor flow rate, the liquid is still on the walls but some liquid droplets are carried in the vapor flow and this flow is called an annular-mist flow. At low void fraction $\alpha < 0.5$, the continuity is broken (Slug flow); in this type of flow the slug moves faster than the liquid. At lower void fractions, the vapor is contained in the liquid in the form of elongated bubbles (Plug flow). Further decreasing the void induces the bubbly flow: in this regime the interface between liquid and vapor is not significant, bubbles and liquid flow at approximately the same speed. Hence, to sum the analysis up, there are different flow regimes for two phase flows. Each one has its own characteristics and its own geometrical configurations. A general methodology for physical modeling is thus needed.

3.1.2 3D Two-Fluid Model

In the literature, the basic modeling strategy for multi-phase flows is to consider a control volume in which liquid and vapor are separated by an interface. Through this interface mass, momentum, heat and volume exchange occurs: this is called the "Two-fluid Model". The derivation of the most general equations comes from the basic laws of physics: conservation of mass, conservation of momentum (Newton's second law), conservation of energy (1st law of thermodynamics) and the 2nd law of thermodynamics (Entropy never decreases). These models consider variations in (x, y, z, t) and non-thermodynamic equilibrium between the phases (i.e. mass, momentum, heat and volume exchange don't happen instantaneously, there is some time for the transition). At this step in modeling, only continuum assumptions are considered and all the state variables are well defined. The derivations are done in [79] and [62], among others, for the multi-phase case and we recall here the results.

Conservation of mass

$$\frac{\partial \rho_k}{\partial t} + \nabla \cdot (\rho_k v_k) = 0 \quad (3.1)$$

Conservation of momentum

$$\frac{\partial (\rho_k v_k)}{\partial t} + \nabla \cdot (\rho_k v_k \otimes v_k) = (-\nabla \cdot p_k + \nabla \cdot \tau_k + \rho_k b_k) \quad (3.2)$$

Conservation of Energy

$$\frac{\partial (\rho_k (e_k + \frac{1}{2} v_k^2))}{\partial t} + \nabla \cdot (\rho_k (e_k + \frac{1}{2} v_k^2)) = \nabla \cdot ((\tau_k - p_k I) \cdot v_k - q_k) + \rho_k (r_k + b_k \cdot v_k) \quad (3.3)$$

where $k = g$ (gas, vapor) or $k = l$ (liquid), and all the model variables are given in Table 3.1. In [62], the authors proved that energy transport is equivalent to entropy transport. These entropy relations are used by several authors to derive relaxation terms as we will see later. Equations (3.1)-(3.3) are bulk equations for the phases, but in multi-phase flow, phases interact with each other through an interface. The interface is assumed with no mass, then it has no momentum and kinetic energy but it has internal energy. By taking a control volume attached to the interface and also applying the basic laws of physics, one gets the following interface

ρ_k : density of each phase	v_k : velocity of each phase
p_k : pressure of each phase	τ_k : stress tensor on each phase
e_k : Internal energy of each phase	q_k : heat transfer between the the phases
r_k : External heat source	b_k : Body forces on each phase (gravity for example)

Table 3.1: Variables definitions of the 3D Two-Fluid Model

relations:

1- Mass relation: mass entering interface = mass leaving the interface:

$$\rho_g(v_g - v_i).n_g + \rho_l(v_l - v_i).n_l = 0 \quad (3.4)$$

2- Momentum relation: here we notice the appearance of the surface tension with its two components: the tangential one (caused by curvature of the interface) and the normal one (caused by temperature gradients). Applying the sum of forces on the interface:

$$0 = \rho_g v_g \otimes (v_g - v_i).n_g + \rho_l v_l \otimes (v_l - v_i).n_l - (\tau_g - p_g I).n_g - (\tau_l - p_l I).n_l - \nabla_s \sigma - 2\sigma H_{s,g} \quad (3.5)$$

3- Energy relation: the interface has internal energy but no kinetic energy, hence the variation of the internal energy inside the interface is given by:

$$\begin{aligned} \frac{\partial(e_s)}{\partial t} + \nabla_s.(v_i e_s) = & -\rho_g(e_g + \frac{1}{2}v_g^2)(v_g - v_i).n_g - \rho_l(e_l + \frac{1}{2}v_l^2)(v_l - v_i).n_l + (\tau_g - p_g I).v_g.n_g \\ & + (\tau_l - p_l I).v_l.n_l - q_g n_g - q_l n_l + r_s + 2\sigma H_{s,g}.n_g.v_i + v_i.\nabla_s \sigma \end{aligned} \quad (3.6)$$

where v_i is the interface velocity, n_g, n_l are the unit vectors normal to the interface in the direction outwards of phase g and l respectively, σ is the surface tension, $H_{s,g}$ is the algebraic value of the minimum curvature of the interface, e_s is the interface internal energy and r_s is the heat source.

Equations (3.1)-(3.3) and (3.4)-(3.6) are the basic equations for the multi-phase modeling. It is noticed that the dimension of the system is very large: variations in (x, y, z, t) and interface relations with a lot of unknowns. Averaging techniques are applied to reduce the complexity of the system.

3.1.3 Averaging and the 1D Two Fluid Model

There exists various types of averaging. Spatial averaging consists of averaging the physical quantities over a given domain (e.g. a cross-section of the tube as in [79]) i.e. instead of having variations in (x, y, z, t) , one can do area averaging along the cross-section of the tube to have variations in (x, t) only. Time averaging consists in looking at a given point in space and averaging the quantities over time. Ensemble averaging consists of averaging the quantities at a given time and at a given location taking into account all the possible realizations of the flow [62].

Averaging always implies a loss of information on the flow but in some applications, knowing every detail of the flow in (x, y, z, t) is not of significant importance so averaging may reduce the complexity of the equations. For 1D fluid models, area averaging is the technique that is most used in the literature. The interface relations which describe the exchange of mass, momentum, heat and volume between the liquid and gas phases are modeled by relaxation terms. So, before stating the 1D two-fluid model equations, it is useful to consider the following definitions:

- *relaxation time*: time needed by the system to go into equilibrium after being perturbed;
- *chemical potential*: form of potential energy that can be absorbed or released during a chemical reaction or phase change.

In a 1D two-fluid model, the two phases are assumed to have separate pressures p_k , temperatures T_k , chemical potentials μ_k and velocities v_k . The system can be moved towards equilibrium by employing relaxation terms. The model equations are given by:

Mass Conservation

$$\frac{\partial(\alpha_g \rho_g)}{\partial t} + \frac{\partial(\alpha_g \rho_g v_g)}{\partial x} = K(\mu_l - \mu_g) \quad (3.7)$$

$$\frac{\partial(\alpha_l \rho_l)}{\partial t} + \frac{\partial(\alpha_l \rho_l v_l)}{\partial x} = K(\mu_g - \mu_l) \quad (3.8)$$

Momentum Conservation

$$\frac{\partial(\rho_g \alpha_g v_g)}{\partial t} + \frac{\partial(\rho_g \alpha_g v_g^2)}{\partial x} + \alpha_g \frac{\partial P_g}{\partial x} + \Delta P_{ig} \frac{\partial \alpha_g}{\partial x} + F(v_g - v_l) = \rho_g \alpha_g g_x + f_{w,g} + v_i K(\mu_l - \mu_g) \quad (3.9)$$

$$\frac{\partial(\rho_l \alpha_l v_l)}{\partial t} + \frac{\partial(\rho_l \alpha_l v_l^2)}{\partial x} + \alpha_l \frac{\partial P_l}{\partial x} + \Delta P_{il} \frac{\partial \alpha_l}{\partial x} - F(v_g - v_l) = \rho_l \alpha_l g_x + f_{w,l} - v_i K(\mu_l - \mu_g) \quad (3.10)$$

Energy Conservation

$$\begin{aligned} \frac{\partial(\rho_g \alpha_g H_g - \alpha_g P_g)}{\partial t} + \frac{\partial(\rho_g \alpha_g v_g H_g)}{\partial x} + P_i v_i \frac{\partial \alpha_g}{\partial x} &= \rho_g \alpha_g v_g g_x + Q_{w,g} - H(T_g - T_l) \\ &- P_i J(P_g - P_l) + v_i F(v_l - v_g) + E_{g,i} K(\mu_l - \mu_g) \end{aligned} \quad (3.11)$$

$$\begin{aligned} \frac{\partial(\rho_l \alpha_l H_l - \alpha_l P_l)}{\partial t} + \frac{\partial(\rho_l \alpha_l v_l H_l)}{\partial x} + P_i v_i \frac{\partial \alpha_l}{\partial x} &= \rho_l \alpha_l v_l g_x + Q_{w,l} + H(T_g - T_l) \\ &+ P_i J(P_g - P_l) - v_i F(v_l - v_g) - E_{g,i} K(\mu_l - \mu_g) \end{aligned} \quad (3.12)$$

Pressure Relaxation

$$\frac{\partial \alpha_g}{\partial t} + v_i \frac{\partial \alpha_g}{\partial x} = J(P_g - P_l) \quad (3.13)$$

where $k=g$ (gas, vapor) or $k=l$ (liquid). H_k is the total enthalpy ($H_k = h_k + \frac{1}{2}v_k^2$ with h_k the specific enthalpy), $Q_{w,k}$ is the heat transfer from the wall to the phase k , α_k is the void fraction of the phase k , $f_{w,k}$ is the friction done by the wall, g_x is the projection of the gravitational

acceleration on the tube axis, (H, J, F, K) are relaxation constants, P_i is the interface pressure and $\Delta P_{ik} = P_k - P_i$, $E_{g,i} = \mu^* + \frac{1}{2}v_i^2$ and μ^* is the effective interface chemical potential. The velocity of the interface v_i can be taken as the average value of the two phase velocities:

$$v_i = \alpha_g v_g + \alpha_l v_l \quad (3.14)$$

Also, note that $\Delta P_{ik} = P_k - P_i$ in the momentum equations is a correction pressure term. It plays an important role in the model hyperbolicity, because in the absence of this term the model becomes non-hyperbolic. This leads to a lack of existence of a stable mathematical model as well as a loss of the stability of numerical methods [64]. This hyperbolicity condition is satisfied (neglecting pressure relaxation) if [64]:

$$\Delta P = 0.2 \frac{\alpha_g \alpha_l \rho_g \rho_l}{\rho_g \alpha_g + \rho_l \alpha_l} (v_g - v_l)^2 \quad (3.15)$$

In addition, it is necessary for the second law of thermodynamics to be satisfied. If the velocity relaxation is neglected ($F = 0$), it is proved by the authors in [42] that the second law of thermodynamics is obeyed if: $H \geq 0$, $J \geq 0$, $K \geq 0$, $\min(P_g, P_l) \leq P_i \leq \max(P_g, P_l)$ and $\min(\mu_g, \mu_l) \leq \mu^* \leq \max(\mu_g, \mu_l)$.

The general 1D two-fluid model presented in equations (3.7)-(3.15) describe the evolution of a two phase flow in a horizontal tube. It is also studied by many authors with slight differences on the modeling assumptions. For example, [60] studies the effect of all relaxation terms neglecting the velocity, [63] provides a numerical study considering pressure and velocity relaxations. The authors in [24] model CO₂ depressurization pipelines and also [73] uses this model in studying the transition in metastable liquids. In addition, [15] presents this general model to describe CO₂ transportation along pipelines.

3.1.4 Homogenous Equilibrium Model (HEM)

The HEM model is a simplified form of the above 1D two fluid model. The two phases are assumed to travel together at the same velocity and behave as single phase with properties that are defined as a weighted average of the properties of the individual phases. For instance, the bubbly flow shown on Fig. 3.1 is an example of a flow regime that can be modeled by the HEM model. To obtain the HEM model equations, the following assumptions on the two phase flow should be taken:

1. no relative motion between the phases ($v = v_g = v_l$);
2. phase change, transfer of volume, heat transfer between the phases happen instantaneously (i.e the thermodynamic equilibrium is attained instantaneously ($P = P_g = P_l$, $T = T_g = T_l$, $\mu = \mu_g = \mu_l$));
3. body forces are neglected (gravity).

Applying assumptions (1)-(3) to the 1D two fluid model in equations (3.7)-(3.15) leads to the following dynamics of the HEM model:

Mass Conservation

$$\frac{\partial \rho}{\partial t} + \frac{\partial(\rho v)}{\partial x} = 0 \quad (3.16)$$

Momentum Conservation

$$\frac{\partial(\rho v)}{\partial t} + \frac{\partial(\rho v^2 + P)}{\partial x} = f_w \quad (3.17)$$

Energy Conservation

$$\frac{\partial(\rho H - P)}{\partial t} + \frac{\partial(\rho v H)}{\partial x} = Q_{ext} \quad (3.18)$$

where ρ is the average density of the mixture ($\rho = \alpha_g \rho_g + \alpha_l \rho_l$), v is the two phase fluid velocity, P is the pressure of the flow, H is the total enthalpy, Q_{ext} is the external heat source and f_w is the friction of the wall.

3.2 Modeling of the CO₂ two phase heat exchanger

In the previous section, we have presented various classes of models that can describe a two phase flow moving inside a horizontal tube. The models can be very complex as in the case of 3D fluid models, where all 3D variations are considered, or less complicated as in the 1D two-fluid models, where the phases are separated and conservation equations are written for each phase in 1D.

The heat exchanger studied in Problem 2 has two concentric lines (see Fig. 3.1): a cold CO₂ two phase line and a hot CO₂ single phase line. Energy is passing from the hot flow to cold one. If we consider the two phase line, the goal is to choose a model from those presented in Section 3.1 that can sufficiently describe the two phase flows. The authors in [67] show that for CO₂ the ratio of the liquid density to vapor density (ρ_l/ρ_v) is small. This results in a more homogeneous two phase flows for CO₂. Hence, it is reasonable to assume that liquid and vapor phases are mixed and propagate at the same velocity: this will allow us to consider the HEM model to describe the dynamics of the two phase line in the CO₂ exchanger. On the other hand, in Problem 1, we have modeled the single phase flows by linear transport equations for temperatures. The same equations can be used here. However in Problem 2 we intend to take into account possible pressure drops along the length of the exchanger. This necessitates to insert the dynamics of the momentum into the model of the single phase line. Therefore, also a HEM model can be also associated to the liquid line. As a result, we derive the mathematical model of the CO₂ two phase exchanger based on the following assumptions:

- the flow is 1-D unidirectional (the hot fluid flows in the positive x direction);
- the two phase flow is homogeneous i.e. liquid and gas flow at the same velocity and they are in thermodynamic equilibrium;
- the kinetic and potential energies of the flows entering and leaving the tubes are neglected;
- the wall thickness is neglected (no wall dynamics) and the heat transfer and friction coefficients are constant and uniform;
- the heat exchanger is perfectly isolated and does not exchange heat with its surrounding environment.

Based on the above assumptions, the heat exchanger dynamics can be described by a set of first order hyperbolic partial differential equations of balance laws (mass, momentum and energy conservation) as follows, $\forall x \in [0, 1]$ (normalized space):

- **cold flow (two-phase):**

$$A_C \frac{\partial \rho_C(x, t)}{\partial t} - \frac{1}{L} \frac{\partial \dot{m}_C(x, t)}{\partial x} = 0 \quad (3.19)$$

$$\frac{\partial \dot{m}_C(x, t)}{\partial t} - \frac{1}{L} \frac{\partial}{\partial x} \left(\frac{\dot{m}_C^2(x, t)}{\rho_C(x, t) A_C} \right) - \frac{A_C}{L} \frac{\partial P_C(x, t)}{\partial x} + \frac{f_C \dot{m}_C(x, t) |\dot{m}_C(x, t)|}{2D_H \rho_C(x, t) A_C} = 0 \quad (3.20)$$

$$A_C \frac{\partial (\rho_C(x, t) H_C(x, t) - P_C(x, t))}{\partial t} - \frac{1}{L} \frac{\partial (\dot{m}_C(x, t) H_C(x, t))}{\partial x} = \pi D_1 h (T_H(x, t) - T_C(x, t)) \quad (3.21)$$

- **hot flow (single phase):**

$$A_H \frac{\partial \rho_H(x, t)}{\partial t} + \frac{1}{L} \frac{\partial \dot{m}_H(x, t)}{\partial x} = 0 \quad (3.22)$$

$$\frac{\partial \dot{m}_H(x, t)}{\partial t} + \frac{\partial}{\partial x} \left(\frac{\dot{m}_H^2(x, t)}{\rho_H(x, t) A_H} \right) + \frac{A_H}{L} \frac{\partial P_H(x, t)}{\partial x} + \frac{f_H \dot{m}_H(x, t) |\dot{m}_H(x, t)|}{2D_1 \rho_H(x, t) A_H} = 0 \quad (3.23)$$

$$A_H \frac{\partial (\rho_H(x, t) H_H(x, t) - P_H(x, t))}{\partial t} + \frac{1}{L} \frac{\partial (\dot{m}_H(x, t) H_H(x, t))}{\partial x} = -\pi D_1 h (T_H(x, t) - T_C(x, t)) \quad (3.24)$$

where ρ_k (Kg/m³) is the density, P_k (Pa) is the pressure, H_k (J/Kg) is the enthalpy, \dot{m}_k (Kg/s) is the mass flow rate, T_k (K) is the temperature, h (W/m² · K) is the overall heat transfer coefficient, A_k (m²) is the tube cross-sectional area, L (m) is the heat exchanger length, f_k is the wall friction coefficient and D_1, D_H (m) are the inner and hydraulic tube diameters, respectively.

The model for the hot and cold lines in equations (3.19)-(3.24) is the HEM model in (3.16)-(3.18) written in the mass flow rate variable $\dot{m} = \rho v$ instead of the velocity v . It consists of three conservation equations for each line and involves the heat exchange term ($\pi D_1 h (T_H(x, t) - T_C(x, t))$) that models the flow of energy from the hot fluid to the cold one. The system (3.19)-(3.24) has boundary conditions of the following form:

$$\begin{aligned} \dot{m}_H(1, t) &= \dot{m}_H^{out}(t), & \dot{m}_C(0, t) &= \dot{m}_C^{out}(t) \\ P_H(0, t) &= P_H^{in}(t), & P_C(1, t) &= P_C^{in}(t) \\ H_H(0, t) &= H_H^{in}(t), & H_C(1, t) &= H_C^{in}(t) \end{aligned} \quad (3.25)$$

The boundary conditions in (3.25) are of Dirichlet type and they constrain the input pressures and enthalpies as well as the output mass flow rates to some known control signals. Although equations (3.19)-(3.21) of the two-phase flow are similar to equations (3.22)-(3.24) of the liquid flow due to the homogeneous flow assumption, they are thermodynamically different. In fact,

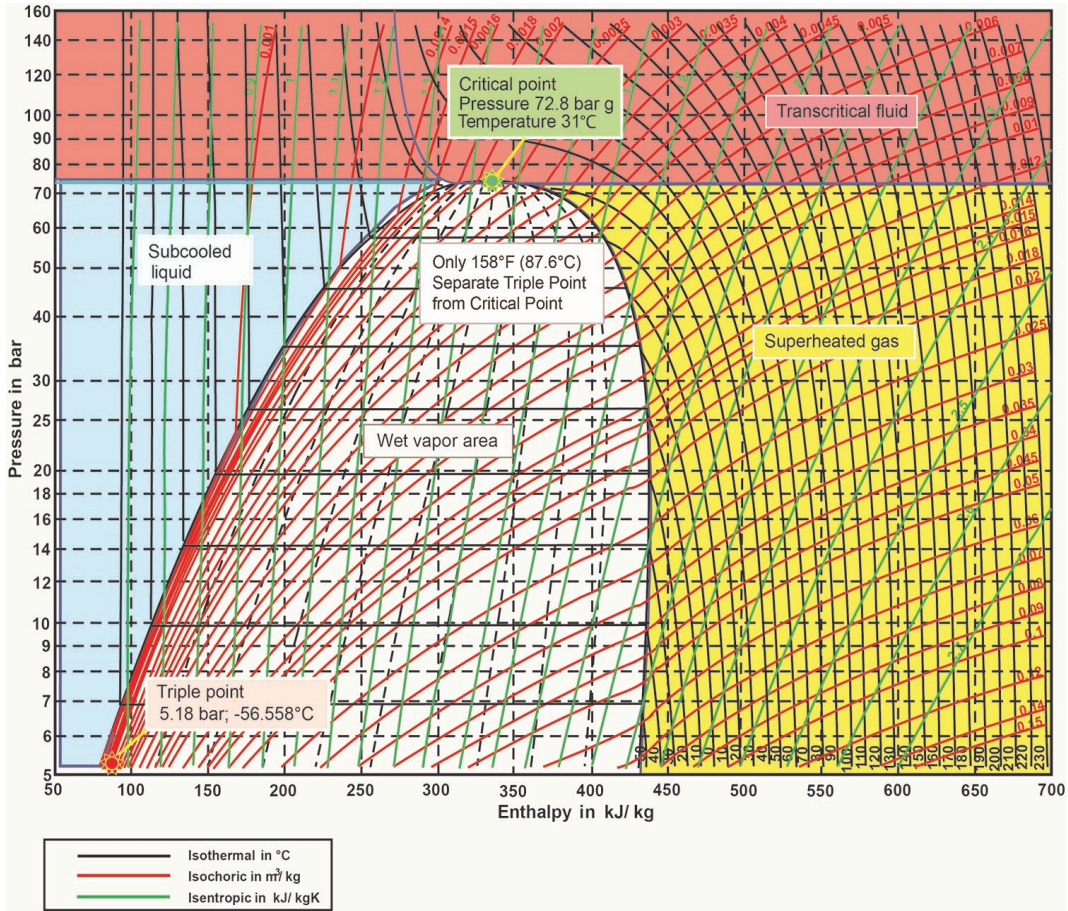


Figure 3.3: CO₂ Pressure-Enthalpy Diagram.

most refrigeration cycles are studied on a Pressure-Enthalpy diagram (P-H diagram); i.e. by knowing the pressure and enthalpy of a fluid at time t , all the other thermodynamic variables (temperature, density, etc..) can be calculated by an equation called the Equation of State (EoS). For instance, the model in (3.19)-(3.25) is completed by four static equations that relates temperature and density to pressure and enthalpy as follows:

$$T_k = f_k(P_k, H_k), \quad \rho_k = g_k(P_k, H_k) \quad (3.26)$$

with $k=H$ or C and f and g are the equations of state. For the hot flow, f_H and g_H are calculated in the liquid region while f_C and g_C are calculated in the two phase region of the P-H diagram, as we will illustrate in the next section.

3.2.1 Equation of State (CO₂)

Consider the P-H diagram of CO₂ on Fig. 3.3. The diagram is composed of three main parts: Liquid region (blue), two phase region (white) and vapor region (yellow). Given the states of

a fluid (P, H) at a certain time t , one can localize the point on the graph and determine the physical state of CO₂. The three regions are separated by the saturation curve (parabolic shape line on the diagram). Any point on this curve is either saturated liquid or saturated vapor depending on its position with respect to the critical point. The points on the black lines are of the same temperature whereas on the red ones have constant density and on the green ones have constant entropy. If we consider the range of pressure [20 bar, 30 bar] (CERN application), the objective is to approximate the equations of states: $T_H = f_H(P, H)$ and $\rho_H = g_H(P, H)$ in the liquid region and $T_C = f_C(P, H)$ and $\rho_C = g_C(P, H)$ in the two phase region.

Liquid region

If we look carefully on the black and the red lines in the blue region on Fig. 3.3, one can notice that the temperature and the density almost do not depend on pressure. Then taking a point on the saturation curve in the interval [20 bar, 30 bar] and making a 1st order Taylor expansion along constant enthalpy lines is thus a good approximation of the equation of states. Hence, we consider the following temperature and density approximations:

$$T_H(P_H, H_H) = T_{sat}(H_H) + \frac{dT_{sat}}{dp}(P_H - P_{sat}(H_H)) \quad (3.27)$$

$$\rho_H(P_H, H_H) = \rho_{sat}(H_H) + \frac{d\rho_{sat}}{dp}(P_H - P_{sat}(H_H)) \quad (3.28)$$

where $P_{sat}(H_H)$, $T_{sat}(H_H)$ and $\rho_{sat}(H_H)$ are the saturations pressure, temperature and density respectively. $\frac{dT_{sat}}{dp}$ and $\frac{d\rho_{sat}}{dp}$ are the variations of the saturation temperatures and densities to pressure. All the saturation variables are calculated using polynomial fitting of the look-up thermodynamic tables of CO₂ provided by Coolprop library [19] as follows:

$$P_{sat}(H_H) = -9.59 \times 10^{-21} H_H^5 + 6 \times 10^{-15} H_H^4 - 1.47 \times 10^{-9} H_H^3 + 0.00003 H_H^2 - 18.583 H_H + 664747.14 \quad (3.29)$$

$$T_{sat}(H_H) = -3.97 \times 10^{-26} H_H^5 + 2.93 \times 10^{-20} H_H^4 - 1.015 \times 10^{-14} H_H^3 + 1.49 \times 10^{-9} H_H^2 + 0.0004 H_H + 178.322 \quad (3.30)$$

$$\rho_{sat}(H_H) = -3.02 \times 10^{-25} H_H^5 + 2.21 \times 10^{-19} H_H^4 - 7.15 \times 10^{-14} H_H^3 + 9.81 \times 10^{-9} H_H^2 - 0.0024 H_H + 1340.91 \quad (3.31)$$

$$\frac{dT_{sat}}{dp}(H_H) = 2.44 \times 10^{-32} H_H^5 - 1.85 \times 10^{-26} H_H^4 + 5.8 \times 10^{-21} H_H^3 - 8.83 \times 10^{-16} H_H^2 + 6.75 \times 10^{-11} H_H - 2.2 \times 10^{-6} \quad (3.32)$$

$$\frac{d\rho_{sat}}{dp}(H_H) = 4.47 \times 10^{-31} H_H^5 - 3.74 \times 10^{-25} H_H^4 + 1.24 \times 10^{-19} H_H^3 - 2.02 \times 10^{-14} H_H^2 + 1.61 \times 10^{-9} H_H - 4.74 \times 10^{-5} \quad (3.33)$$

The necessary partial derivatives of T_H or ρ_H with respect to pressure and enthalpy are derived directly from equations (3.27)-(3.28).

Two phase region

The white region on Fig. 3.3 corresponds to the two phase state. One can notice that the black lines are constant all over the region. This means that the temperature in that region do not depend on enthalpy but only on pressure, and it is always equal to the saturation temperature. Hence, we can directly deduce the equation of state of $T_C(P_C, H_C)$:

$$T_C(P_C, H_C) = T_{sat}(P_C) \quad (3.34)$$

where $T_{sat}(P_C)$ is calculated using polynomial fitting from the values of the Coolprop library as follows:

$$\begin{aligned} T_{sat}(P_C) = & 6.06 \times 10^{-32} P_C^5 - 9.39 \times 10^{-25} P_C^4 + 6.04 \times 10^{-18} P_C^3 - 2.15 \times 10^{-11} P_C^2 \\ & + 5.51 \times 10^{-5} P_C + 194.26 \end{aligned} \quad (3.35)$$

Unlike temperature, density (represented by the red lines in the white region of Fig. 3.3) do change with respect to pressure and enthalpy. This is intuitive, since the fluid is changing phase and undergoing evaporation or condensation, so its density is increasing or decreasing depending whether heat is added or removed from the system. The density is approximated using the average of both the saturated liquid and vapor densities, as in the HEM model:

$$\rho_C(P_C, H_C) = \alpha \rho_{sat}^v + (1 - \alpha) \rho_{sat}^l \quad (3.36)$$

where α is the void fraction defined by: $\alpha = \frac{1}{1 - \frac{(H_C - h_{sat}^v) \rho_{sat}^v}{(H_C - h_{sat}^l) \rho_{sat}^l}}$ and $(\rho_v^{sat}, \rho_l^{sat}, h_l^{sat}, h_v^{sat})$ are the saturation enthalpies and densities for liquid and vapor. These saturation variables are calculated by polynomial fitting using the Coolprop library as follows:

$$\begin{aligned} \rho_v^{sat}(P_C) = & 7.75 \times 10^{-33} P_C^5 - 7.58 \times 10^{-26} P_C^4 + 5.2 \times 10^{-19} P_C^3 - 5.03 \times 10^{-13} P_C^2 \\ & + 2.52 \times 10^{-5} P_C + 0.76 \end{aligned} \quad (3.37)$$

$$\begin{aligned} \rho_l^{sat}(P_C) = & -1.96 \times 10^{-31} P_C^5 + 3 \times 10^{-24} P_C^4 - 1.93 \times 10^{-17} P_C^3 + 6.72 \times 10^{-11} P_C^2 \\ & - 0.00019 P_C + 1259.02 \end{aligned} \quad (3.38)$$

$$\begin{aligned} h_l^{sat}(P_C) = & 1.15 \times 10^{-28} P_C^5 - 1.78 \times 10^{-21} P_C^4 + 1.14 \times 10^{-14} P_C^3 - 4.03 \times 10^{-8} P_C^2 \\ & 0.1 P_C + 36436.2 \end{aligned} \quad (3.39)$$

$$\begin{aligned} h_v^{sat}(P_C) = & 3.57 \times 10^{-29} P_C^5 - 5.67 \times 10^{-22} P_C^4 + 3.62 \times 10^{-15} P_C^3 - 1.31 \times 10^{-8} P_C^2 \\ & + 0.02 P_C + 422294.8 \end{aligned} \quad (3.40)$$

It is also useful to define the quality q as follows:

$$q = \frac{H_C - h_l^{sat}}{h_v^{sat} - h_l^{sat}} \quad (3.41)$$

q is always between 0 and 1 and it is the percentage of vapor present in a two phase mixture. For instance, if $q = 0$ then the two phase mixture contains only saturated liquid, otherwise, if $q = 1$, only saturated vapor is present. We recall that one of the objectives of Problem 2 is to estimate q inside the domain of the two phase flow using boundary sensing.

3.3 Model Implementation

The heat exchanger model in equations (3.19)-(3.25) and (3.34)-(3.36) is a nonlinear-hyperbolic model of balance laws. It is implemented using the Finite Volume Method (FVM). This method consists in dividing the space into a set of control volumes of equal or different sizes and then integrating the conservation equations on each control volume [66]. FVM is an efficient method when dealing with the conservation laws because it ensures that every conserved quantity (mass, momentum, energy) is conserved in each control volume. Yet some problems may occur when implementing the momentum equations since it involves a pressure gradient ($A \frac{\partial P}{\partial x}$) that drives the flow. The authors in [66] argued that implementing the velocity field on the same grid as the pressure field may lead to a nonphysical solution in which we may have certain oscillations, called the "Chequerboard Oscillations". The suggested solution is to implement the momentum equations on a staggered grid; mainly for the velocity to be calculated from the difference of pressures between two adjacent cells. The numerical grid is shown on Fig. 3.4.

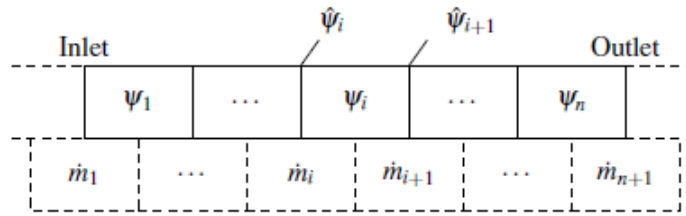


Figure 3.4: Finite volume staggered grid

It consists of two grids: the upper grid is for mass and energy equations and the staggered grid is for the momentum equations. ψ_i is the average thermodynamic property of enthalpy or pressure in the control volume i and $\hat{\psi}_i$ is the interface value, approximated using an upwind scheme as follows:

$$\hat{\psi}_i = (1 - \delta_i)\psi_{i-1} + \delta_i\psi_i \quad \text{and} \quad \delta_i = \begin{cases} 1 & \text{if } \dot{m}_i \leq 0 \\ 0 & \text{if } \dot{m}_i > 0 \end{cases} \quad (3.42)$$

The model is simulated in Matlab on a toy heat exchanger model. The exchanger is 18 meters long ($L = 18$ m) with inner diameter $D_1 = 12$ mm and outer diameter $D_2 = 33.4$ mm. The exchanger parameters are: $h = 100$ W/m² · K, $f_1 = 10$ and $f_2 = 15$. The system is simulated using constant boundary conditions:

$$\begin{aligned} \dot{m}_H(1, t) &= 0.02 \text{ Kg/s}, & \dot{m}_C(0, t) &= 0.02 \text{ Kg/s} \\ P_H(0, t) &= 3 \text{ MPa}, & P_C(1, t) &= 2.2 \text{ MPa} \\ H_H(0, t) &= 180 \text{ KJ/Kg}, & H_C(1, t) &= 200 \text{ KJ/Kg} \end{aligned}$$

and Ode15s in Matlab is used to approximate the time derivatives. Fig. 3.5 shows the steady state results for different thermodynamic profiles. On the hot side: both enthalpy and temperature decrease with the tube length. The reason is that the hot fluid is losing energy to the cold

fluid, this appears in the steady state plots where the hot inlet temperature was ($T_{Hin} = -8.577$ °C) and the outlet ($T_{Hout} = -14.5$ °C). On the cold side, the cold fluid is gaining energy, so its enthalpy should increase in the negative x-axis direction (cold fluid is flowing from $x = 1$ to $x = 0$). Since the cold flow is changing phase, we expect its temperature to remain constant and equal to the saturation temperature at constant pressure. This is verified as the cold fluid enters at (-16.22 °C) and leaves at (-16.67 °C), which are approximately the same temperatures. The small drop in the cold temperature is due to the small drop in cold pressure along the direction of the flows as shown on the pressure plots on Fig. 3.5. The energy gained by the cold fluid increases its enthalpy and as a consequence increases its quality. Hence, the cold fluid undergoes evaporation and the percent of generated vapor must be increasing along the length of the tube. This is what we see in the steady state plot of the quality.

Fig. 3.6 shows the transient behavior of the mass flow rates, pressure and temperatures. The input mass flow rates stabilizes at 0.02 Kg/s, which is the value of the boundary output mass flow rates. This result verifies the mass conservation law, since at steady state we expect the entering mass flow rate to be equal to the output mass flow rate. By comparing the output pressure plots to the output temperature and quality plots, we can observe that pressure stabilizes in a very short amount of time, of order that is not appearing on the plots. Again, this is physically understandable since energy waves propagate much slower than pressure waves.

To conclude on the model simulation results, we can say that the proposed exchanger model shows a good behavior in simulation while conserving the laws of thermodynamics. Since we have used fictitious values for the heat transfer and the friction coefficients, the pressure drop values might not reflect the experimental pressure drops. However, these coefficients can be approximated using physical correlations for single and two phase flows and inserted back into the model. This requires careful knowledge of the experimental pressure and temperature ranges as well as the real speed of the flow.

3.4 Boundary Observer Design

The transport phenomena and the exchange of heat on both hot and cold sides is modeled using 1D Navier-Stokes equations. The exchanger model (3.19)-(3.26) falls into the category of nonlinear hyperbolic systems of balance laws of the following form:

$$A(W(x, t))\partial_t W(x, t) + B(W(x, t))\partial_x W(x, t) + C(W(x, t)) = 0 \quad (3.43)$$

$$\text{B.C. } D(W(0, t), W(1, t), t) = 0 \quad (3.44)$$

where $W(x, t) = [\dot{m}_H(x, t), P_H(x, t), H_H(x, t), \dot{m}_C(x, t), P_C(x, t), H_C(x, t)]^T$ is the vector of states. $A(W)$, $B(W)$, $C(W)$ and $D(W)$ are the system matrices of appropriate dimensions. $W(x, t)$ represents the full thermodynamic profile of both flows. The objective is to estimate $W(x, t)$ from boundary measurements of the form:

$$y_1(t) = W(0, t), \quad y_2(t) = W(1, t) \quad (3.45)$$

In other words, if the input/output data ($y_1(t)$, $y_2(t)$) are measured, the problem is to estimate $W(x, t)$ inside the domain. We recall that the quality ratio is given in (3.41), and hence it is

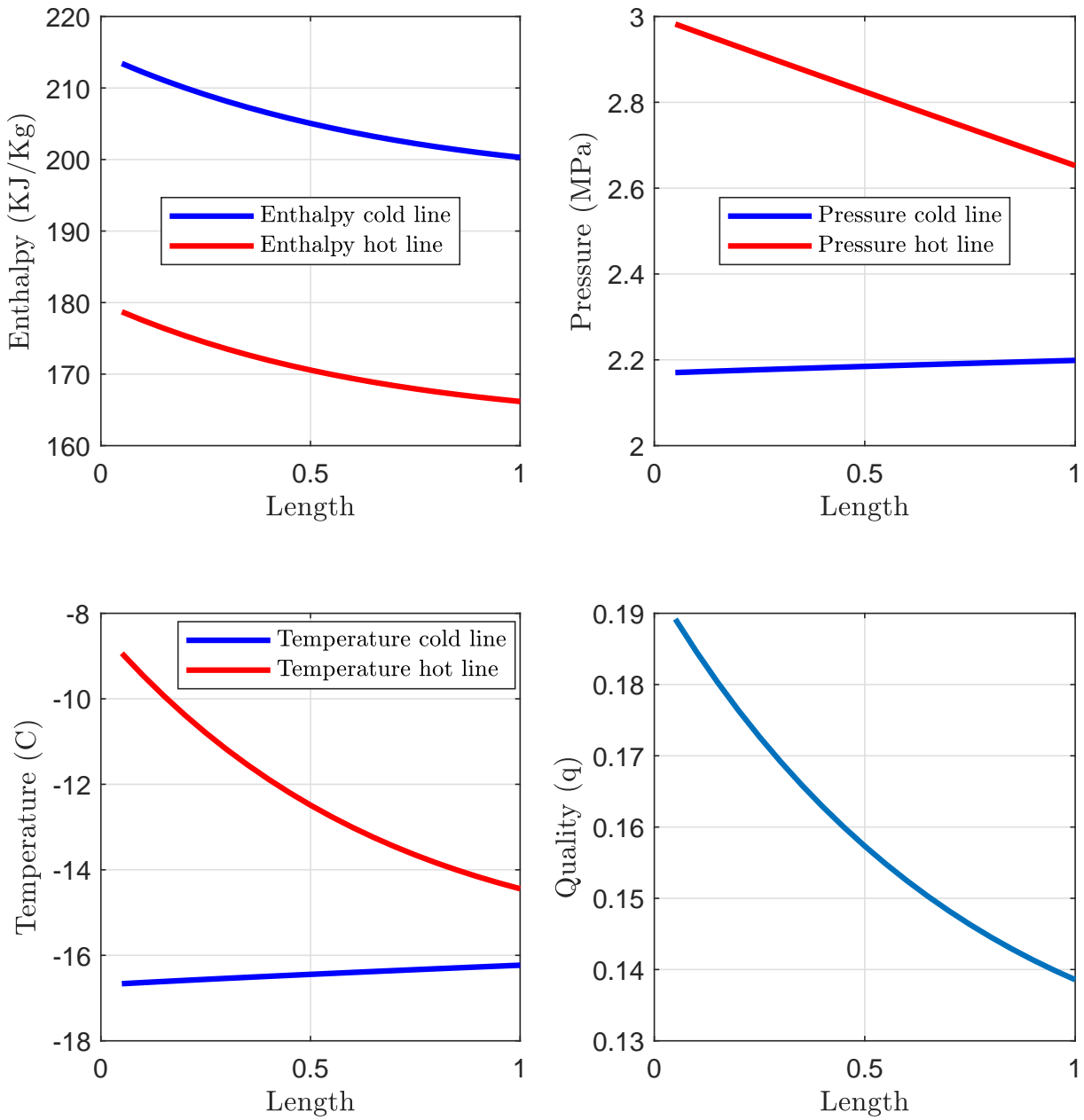


Figure 3.5: Steady state distributions of different thermodynamic variables.

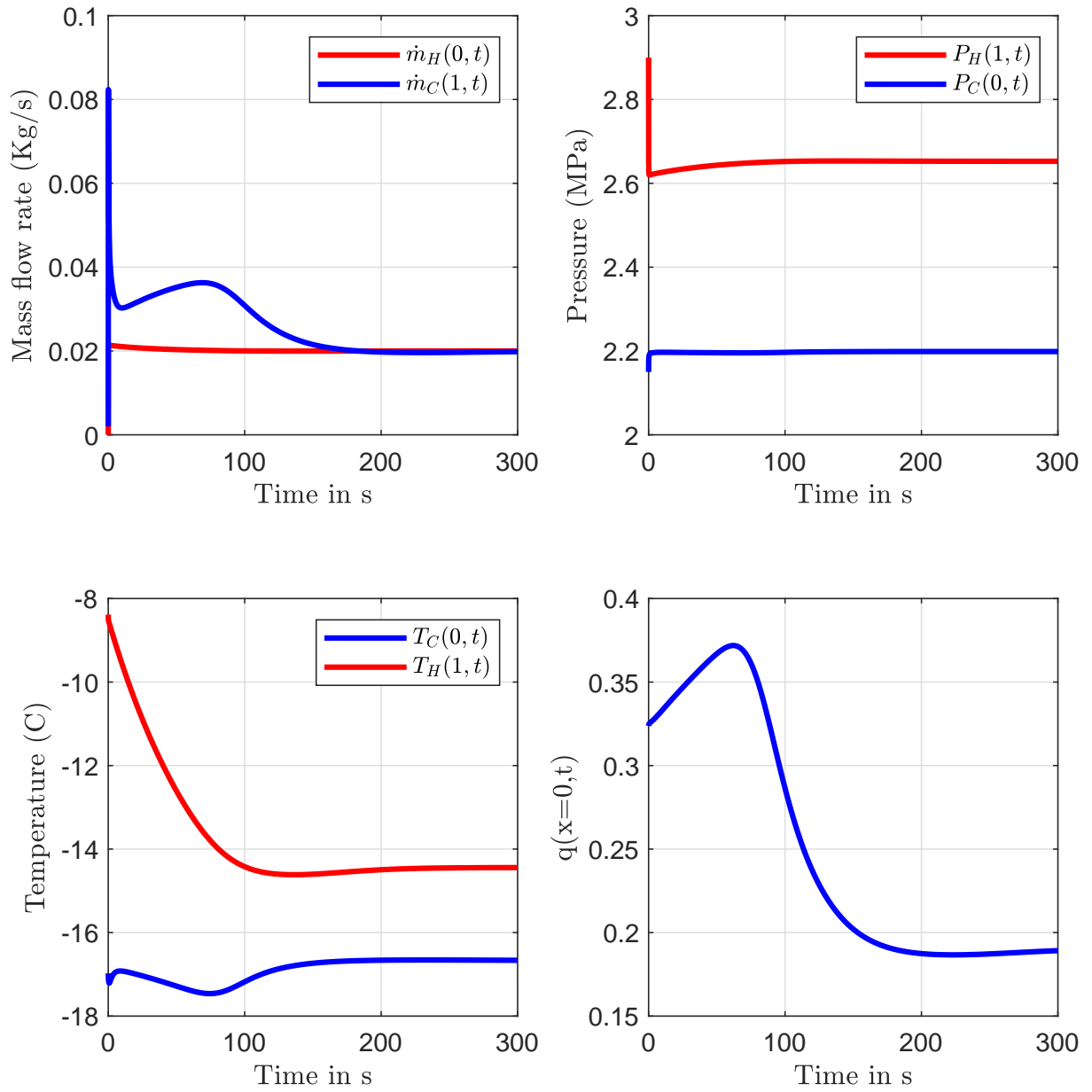


Figure 3.6: The transient behavior of the output mass flow rates, pressures, temperatures and quality.

directly estimated as a result of the estimation of $W(x, t)$.

The model in (3.43)-(3.44) is similar to the Euler equations for gas dynamics applied to two counter current flows. The authors in [17] in Chapter 1 shows that the Euler equations cannot be transformed into a characteristic form by defining a set of so-called Riemann coordinates. The characteristic form of a hyperbolic system is a diagonalized set of equations in which each wave is propagating at a certain speed depending on its Eigen value. To the best of our knowledge, most of the results on the control and estimation for hyperbolic systems are conditioned to the fact that these systems can be written in the characteristic form. Therefore, our first step in solving the problem is to linearize the system around a steady state profile. The linearized version is then written in the characteristics form and the boundary observer is built on the linearized dynamics. We have listed the various results on boundary observers for hyperbolic systems in Chapter 1. In this framework, our contribution is a complete boundary state estimation of the thermodynamic profile (pressure, enthalpy, mass flow rate) along the length of a CO₂ heat exchanger built using concentric tubes that contain two-phase flows. We get the inspiration from [85], extended to the case of three rightward and three leftward transport PDEs. Sufficient conditions for the exponential convergence of the observer are derived in form of a linear matrix inequality (LMI) and a bilinear one by using a Lyapunov functional similar to the one used in [58].

The work of this chapter is summarized and published in:

M.Ghousein, E.Witrant. “A Boundary Observer for Two Phase Heat Exchangers”. In: *18th European Control Conference (ECC)*. IEEE (2019), pp. 2332– 2337.

To begin, we start by the linearization step.

3.4.1 Linearization

We first consider the linearization of (3.19)-(3.26) around the steady state $W_S(x)$, such that:

$$W(x, t) \approx W_S(x) + \Delta W(x, t) \quad (3.46)$$

Using a Taylor expansion of order 1, the dynamics of the small perturbation $\Delta W(x, t)$ becomes:

$$A_1^S(x) \partial_t \Delta W(x, t) + B_1^S(x) \partial_x \Delta W(x, t) + C_1^S(x) \Delta W(x, t) = 0 \quad (3.47)$$

where $A_1^S(x)$, $B_1^S(x)$ and $C_1^S(x)$ are the steady state matrices computed as follows:

- $A_1^S(x)$ is $\mathcal{M}_{6,6}(\mathbb{R})$ with all zeros except the entities:
 $a_{12} = A_H(\frac{\partial \rho}{\partial P}|_h)_H$, $a_{13} = A_H(\frac{\partial \rho}{\partial h}|_P)_H$, $a_{32} = -A_H$, $a_{21} = 1$, $a_{33} = A_H \rho_H$, $a_{45} = A_C(\frac{\partial \rho}{\partial P}|_h)_C$, $a_{46} = A_C(\frac{\partial \rho}{\partial h}|_P)_C$, $a_{54} = 1$, $a_{65} = -A_C$, $a_{66} = A_C \rho_C$.
- $B_1^S(x)$ is $\mathcal{M}_{6,6}(\mathbb{R})$ with all zeros except the entities:
 $b_{11} = \frac{1}{L}$, $b_{21} = \frac{2\dot{m}_H}{L A_H \rho_H}$, $b_{22} = \frac{A_H}{L} - \frac{\dot{m}_H^2 (\frac{\partial \rho}{\partial P}|_h)_H}{L A_H \rho_H^2}$, $b_{23} = -\frac{\dot{m}_H^2 (\frac{\partial \rho}{\partial h}|_P)_H}{L A_H \rho_H^2}$, $b_{33} = \frac{\dot{m}_H}{L}$, $b_{54} = -\frac{1}{L}$,
 $b_{54} = -\frac{2\dot{m}_C}{L A_C \rho_C}$, $b_{55} = -\frac{A_C}{L} + \frac{\dot{m}_C^2 (\frac{\partial \rho}{\partial P}|_h)_C}{L A_C \rho_C^2}$, $b_{56} = \frac{\dot{m}_C^2 (\frac{\partial \rho}{\partial h}|_P)_C}{L A_C \rho_C^2}$, $b_{66} = -\frac{\dot{m}_C}{L}$.

- $C_1^S(x)$ is $\mathcal{M}_{6,6}(\mathbb{R})$ with all zeros except the entities:

$$c_{21} = f_H \frac{\dot{m}_H}{A_H \rho_H} - 2 \frac{\dot{m}_H \rho_H x}{A_H \rho_H^2}$$

$$c_{22} = -f_H \frac{\dot{m}_H^2 (\frac{\partial \rho}{\partial P}|_h)_H}{2 A_H \rho_H^2} - \frac{\dot{m}_H^2 (\frac{\partial \rho}{\partial P}|_h)_{Hx}}{A_H \rho_H^2} + 2 \rho_{Hx} \dot{m}_H^2 \frac{(\frac{\partial \rho}{\partial P}|_h)_H}{A_H \rho_H^3}$$

$$c_{23} = -f_H \frac{\dot{m}_H^2 (\frac{\partial \rho}{\partial h}|_P)_H}{2 A_H \rho_H^2} - \frac{\dot{m}_H^2 (\frac{\partial \rho}{\partial h}|_P)_{Hx}}{A_H \rho_H^2} + 2 \rho_{Hx} \dot{m}_H^2 \frac{(\frac{\partial \rho}{\partial h}|_P)_H}{A_H \rho_H^3}$$

$$c_{31} = (\frac{dH}{dx})_H$$

$$c_{32} = h \pi D_1 (\frac{\partial T}{\partial P}|_h)_H = -c_{63}$$

$$c_{33} = h \pi D_1 (\frac{\partial T}{\partial h}|_P)_H = -c_{64}$$

$$c_{35} = -h \pi D_1 (\frac{\partial T}{\partial P}|_h)_C = -c_{65}$$

$$c_{36} = -h \pi D_1 (\frac{\partial T}{\partial h}|_P)_C = -c_{66}$$

$$c_{54} = f_C \frac{\dot{m}_C}{A_C \rho_C} + 2 \frac{\dot{m}_C \rho_C x}{A_C \rho_C^2}$$

$$c_{55} = -f_C \frac{\dot{m}_C^2 (\frac{\partial \rho}{\partial P}|_h)_C}{2 A_C \rho_C^2} + \frac{\dot{m}_C^2 (\frac{\partial \rho}{\partial P}|_h)_{Cx}}{A_C \rho_C^2} - 2 \rho_{Cx} \dot{m}_C^2 \frac{(\frac{\partial \rho}{\partial P}|_h)_C}{A_C \rho_C^3}$$

$$c_{56} = -f_C \frac{\dot{m}_C^2 (\frac{\partial \rho}{\partial h}|_P)_C}{2 A_C \rho_C^2} + \frac{\dot{m}_C^2 (\frac{\partial \rho}{\partial h}|_P)_{Cx}}{A_C \rho_C^2} - 2 \rho_{Cx} \dot{m}_C^2 \frac{(\frac{\partial \rho}{\partial h}|_P)_C}{A_C \rho_C^3}$$

$$c_{62} = -(\frac{dH}{dx})_C$$

$(\frac{\partial \rho}{\partial P}|_h)_H$ is the partial derivative of density with respect to pressure at constant enthalpy for the hot flow. All other partial derivatives are interpreted in the same sense.

Furthermore, one can notice that the matrix $A_1^S(x)$ is always invertible for the flows where the density is changing either with pressure or with enthalpy. Hence, we can compute the matrices $A^S(x) = (A_1^S(x))^{-1} B_1^S(x)$ and $B^S(x) = -(A_1^S(x))^{-1} C_1^S(x)$ to obtain a simplified dynamics of $\Delta W(x, t)$:

$$\partial_t \Delta W(x, t) + A^S(x) \partial_x \Delta W(x, t) = B^S(x) \Delta W(x, t) \quad (3.48)$$

with the following boundary conditions:

$$\begin{aligned} \Delta W_1(1, t) &= \Delta \dot{m}_H^{out}(t), & \Delta W_4(0, t) &= \Delta \dot{m}_C^{out}(t) \\ \Delta W_2(0, t) &= \Delta P_H^{in}(t), & \Delta W_5(1, t) &= \Delta P_C^{in}(t) \\ \Delta W_3(0, t) &= \Delta H_H^{in}(t), & \Delta W_6(1, t) &= \Delta H_C^{in}(t) \end{aligned} \quad (3.49)$$

The system has the following perturbed input/ output measurements:

$$\Delta y_1(t) = \Delta W(0, t), \quad \Delta y_2(t) = \Delta W(1, t) \quad (3.50)$$

The observer is constructed on the linearized dynamics $\Delta W(x, t)$ and the state estimation of $W(x, t)$ is approximated using the first order Taylor expansion in (3.46).

3.4.2 Characteristic Form and Diagonalization

We know from the physics of the system that the matrix $A^S(x)$ is diagonalizable and it has 6 eigen-values (3 positive and 3 negative), since for each fluid mass and energy flow in one direction and momentum in the reverse direction (see e.g. [22]). So, we transform the system (3.48)-(3.49) into the characteristic form using a linear transformation $T(x)$ such that:

$$\Delta W(x, t) = T(x) \Delta Z(x, t) \quad (3.51)$$

Equation (3.48) can then be written as:

$$\partial_t \Delta Z(x, t) + \Lambda(x) \partial_x \Delta Z(x, t) = \Sigma(x) \Delta Z(x, t) \quad (3.52)$$

where $\Lambda(x) = T^{-1}(x) A^S(x) T(x) = \text{diag}\{\lambda_1(x) \dots \lambda_6(x)\}$ with $(\lambda_1(x) > 0, \lambda_3(x) > 0, \lambda_5(x) > 0)$ and $(\lambda_2(x) < 0, \lambda_4(x) < 0, \lambda_6(x) < 0)$ for all $x \in [0, 1]$. $\Sigma(x) = T^{-1}(x) B^S(x) T(x) - T^{-1}(x) A^S(x) T'(x)$. Let us introduce the following notation:

$$\Delta Z(x, t) = (\Delta Z^+(x, t), \Delta Z^-(x, t))$$

where $\Delta Z^+(x, t) = (\Delta Z_1(x, t), \Delta Z_3(x, t), \Delta Z_5(x, t))$ and $\Delta Z^-(x, t) = (\Delta Z_2(x, t), \Delta Z_4(x, t), \Delta Z_6(x, t))$. $\Delta Z^+(x, t)$ represents the waves that are propagating in the positive x-axis direction while $\Delta Z^-(x, t)$ are the waves that are propagating in the negative x-axis direction. The boundary conditions in (3.49) are transformed by (3.51) to the following form:

$$\Delta Z^+(0, t) = M_1 \Delta Z^-(0, t) + N_1 F_1(t) \quad (3.53)$$

$$\Delta Z^-(1, t) = M_2 \Delta Z^+(1, t) + N_2 F_2(t) \quad (3.54)$$

where M_1, M_2, N_1, N_2 are $\mathcal{M}_{3,3}(\mathbb{R})$ calculated using the transformation $T(x)$ and $F_1(t) = (\Delta P_H^{in}(t), \Delta H_H^{in}(t), \Delta \dot{m}_C^{out}(t))^T$ and $F_2(t) = (\Delta P_C^{in}(t), \Delta H_C^{in}(t), \Delta \dot{m}_H^{out}(t))^T$ are the vectors of inputs. System (3.52)-(3.54) is a hyperbolic system written in the characteristic form where at each boundary point the incoming information is determined by the outgoing information. Our aim is to build the observer on the transformed dynamics $\Delta Z(x, t)$ and then afterwards use the transformation $T(x)$ to construct the estimated state for $\Delta W(x, t)$.

3.4.3 Observer Architecture

Denote by $\Delta \hat{Z}(x, t)$ the estimated state of $\Delta Z(x, t)$. Considering that only boundary measurements are available, i.e. $\Delta z_1(t) = \Delta Z^-(0, t)$ and $\Delta z_2(t) = \Delta Z^+(1, t)$ computed using (3.50)-(3.51), a natural choice for the observer design is to set the dynamics of the estimator as, $\forall x \in [0, 1]$:

$$\partial_t \Delta \hat{Z}(x, t) + \Lambda(x) \partial_x \Delta \hat{Z}(x, t) = \Sigma(x) \Delta \hat{Z}(x, t) \quad (3.55)$$

with boundary conditions:

$$\Delta \hat{Z}^+(0, t) = M_1 \Delta Z^-(0, t) + N_1 F_1(t) - 1_{3 \times 3} L^- (\Delta \hat{Z}^-(0, t) - \Delta z_1(t)) \quad (3.56)$$

$$\Delta \hat{Z}^-(1, t) = M_2 \Delta Z^+(1, t) + N_2 F_2(t) - 1_{3 \times 3} L^+ (\Delta \hat{Z}^+(1, t) - \Delta z_2(t)) \quad (3.57)$$

The observer architecture is depicted on Fig. 3.7. The inflow boundary conditions are thus corrected by the error of the outflows boundaries, and the same is done for the outflow observer boundaries, which are corrected by the errors of the inflow boundaries. This type of boundary conditions is called dissipative, and the authors in [17] dedicated an entire volume to explain the stabilization of hyperbolic systems using such kind of boundary conditions. All the errors are weighted by the observer gains $L^+ = \text{diag}\{L_1, L_3, L_5\}$ and $L^- = \text{diag}\{L_2, L_4, L_6\}$. $1_{3 \times 3}$ is the

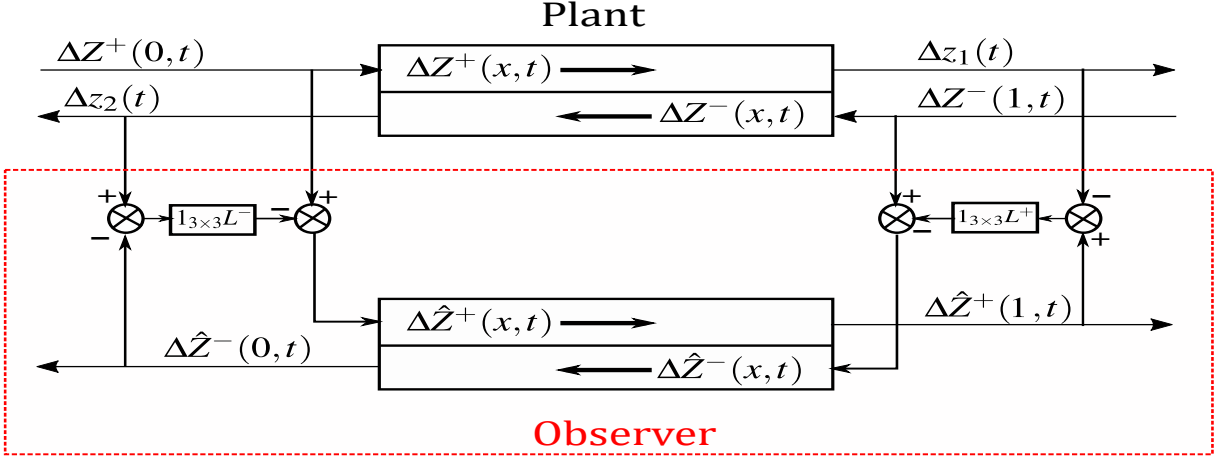


Figure 3.7: Boundary observer architecture.

3 by 3 ones matrix. The observer in (3.55)-(3.57) is a Lunbeberger-type observer with boundary corrections. The objective is to determine the proper gains L^+ and L^- that can drive the system to zero exponentially.

Now, we prove the global exponential convergence of the observer (3.55) with boundary conditions (3.56). This is done by proving the exponential convergence of the estimated error $\varepsilon(x, t) = \Delta Z(x, t) - \Delta \hat{Z}(x, t)$ towards zero. Let us start by considering the error dynamics:

$$\partial_t \varepsilon(x, t) + \Lambda(x) \partial_x \varepsilon(x, t) = \Sigma(x) \varepsilon(x, t) \quad (3.58)$$

with the following boundary conditions:

$$\begin{aligned} \varepsilon^+(0, t) &= -1_{3 \times 3} L^- \varepsilon^-(0, t) \\ \varepsilon^-(L, t) &= -1_{3 \times 3} L^+ \varepsilon^+(L, t) \end{aligned} \quad (3.59)$$

System (3.58)-(3.59) is said to be *Globally Exponentially Stable (GES)* in the L^2 norm if there exist $\gamma > 0$ and $C > 0$ such that for every initial condition $\varepsilon^0(x) \in L^2((0, 1); \mathbb{R}^6)$ and for all $t \geq 0$, the solution of the system (3.58)-(3.59) satisfies:

$$\|\varepsilon(t, \cdot)\|_{L^2([0,1]; \mathbb{R}^6)} \leq C e^{-\gamma t} \|\varepsilon^0\|_{L^2([0,1]; \mathbb{R}^6)} \quad (3.60)$$

The GES of (3.58)-(3.59) can be inferred from the following theorem.

Theorem 3.4.1. *Consider the system of PDEs (3.58) with boundary conditions (3.59). Suppose that there exist $\gamma > 0$, $\mu \in \mathbb{R}$, a positive definite matrix $Q(x) > 0$ and observer gains L^+ and L^- such that for all $x \in [0, 1]$ we have:*

$$\Sigma^T(x) |\Lambda(x)|^{-1} Q(x) + |\Lambda(x)|^{-1} Q(x) \Sigma(x) - 2\mu Q(x) \leq -2\gamma |\Lambda(x)|^{-1} Q(x) \quad (3.61)$$

$$\begin{pmatrix} -q_2^0 + \alpha L_2^2 & \alpha L_2 L_4 & \alpha L_2 L_6 & 0 & 0 & 0 \\ * & -q_4^0 + \alpha L_4^2 & \alpha L_4 L_6 & 0 & 0 & 0 \\ * & * & -q_6^0 + \alpha L_6^2 & 0 & 0 & 0 \\ 0 & 0 & 0 & -q_1^1 + \beta L_1^2 & \beta L_1 L_3 & \beta L_1 L_5 \\ 0 & 0 & 0 & * & -q_3^1 + \beta L_3^2 & \beta L_3 L_5 \\ 0 & 0 & 0 & * & * & -q_5^1 + \beta L_5^2 \end{pmatrix} \leq 0 \quad (3.62)$$

where q_i^0 and q_i^1 for $i \in \{1, \dots, 6\}$ are the diagonal entries of $Q(0)$ and $Q(1)$, respectively, $\alpha = q_1^0 + q_3^0 + q_5^0$ and $\beta = q_2^1 + q_4^1 + q_6^1$. Then system (3.58) with (3.59) is (GES).

Proof. Consider the following Lyapunov candidate, similar to the one used in [58]:

$$V(t) = \int_0^1 \varepsilon^T(x, t) |\Lambda(x)|^{-1} Q(x) \varepsilon(x, t) dx \quad (3.63)$$

where $\mu > 0$, $|\Lambda(x)|^{-1} = \text{diag}\{1/|\Lambda_i(x)|\}$ and $Q(x) = \text{diag}\{q_i e^{-\text{sign}(\Lambda_i(x))2\mu x}\}$ for all $i \in \{1, \dots, 6\}$.

Taking the time derivative of (3.63) we have:

$$\begin{aligned} \dot{V}(t) &= \int_0^1 \partial_t \varepsilon^T(x, t) |\Lambda(x)|^{-1} Q(x) \varepsilon(x, t) dx + \int_0^1 \varepsilon^T(x, t) |\Lambda(x)|^{-1} Q(x) \partial_t \varepsilon(x, t) dx \\ &= \int_0^1 \left(\varepsilon^T(x, t) \Sigma^T(x) - \partial_x \varepsilon^T(x, t) \Lambda^T(x) \right) |\Lambda(x)|^{-1} Q(x) \varepsilon(x, t) dx \\ &\quad + \int_0^1 \varepsilon^T(x, t) |\Lambda(x)|^{-1} Q(x) \left(\Sigma(x) \varepsilon(x, t) - \Lambda(x) \partial_x \varepsilon(x, t) \right) dx \\ &= \int_0^1 \varepsilon^T(x, t) \Sigma^T(x) |\Lambda(x)|^{-1} Q(x) \varepsilon(x, t) dx + \int_0^1 \varepsilon^T(x, t) |\Lambda(x)|^{-1} Q(x) \Sigma(x) \varepsilon(x, t) dx \\ &\quad - \int_0^1 \partial_x \varepsilon^T(x, t) \Lambda^T(x) |\Lambda(x)|^{-1} Q(x) \varepsilon(x, t) + \varepsilon^T(x, t) |\Lambda(x)|^{-1} Q(x) \Lambda(x) \partial_x \varepsilon(x, t) dx \end{aligned}$$

Noting that $|\Lambda(x)|^{-1} Q(x) = Q(x) |\Lambda(x)|^{-1}$ and $|\Lambda(x)|^{-1} \Lambda(x) = \check{I}_6 = \text{diag}[\text{sign}(\Lambda_i(x))]$, then

$$\begin{aligned} \dot{V}(t) &= \int_0^1 \varepsilon^T(x, t) \Sigma^T(x) |\Lambda(x)|^{-1} Q(x) \varepsilon(x, t) dx + \int_0^1 \varepsilon^T(x, t) |\Lambda(x)|^{-1} Q(x) \Sigma(x) \varepsilon(x, t) dx \\ &\quad - \int_0^1 \partial_x \varepsilon^T(x, t) \check{I}_6 Q(x) \varepsilon(x, t) + \varepsilon^T(x, t) \check{I}_6 Q(x) \partial_x \varepsilon(x, t) dx \end{aligned}$$

Using the expansion:

$$\begin{aligned} \partial_x (\varepsilon^T(x, t) \check{I}_6 Q(x) \varepsilon(x, t)) &= \partial_x \varepsilon^T(x, t) \check{I}_6 Q(x) \varepsilon(x, t) + \varepsilon^T(x, t) \check{I}_6 Q(x) \partial_x \varepsilon(x, t) \\ &\quad + \varepsilon^T(x, t) \underbrace{\check{I}_6 \partial_x (Q(x))}_{-2\mu Q(x)} \varepsilon(x, t) \end{aligned}$$

implies that

$$\dot{V}(t) = \underbrace{-[\varepsilon^T \check{I}_6 Q(x) \varepsilon]_0^1}_{\leq 0} + \int_0^1 \varepsilon^T(x, t) \underbrace{(\Sigma^T(x) |\Lambda(x)|^{-1} Q(x) + |\Lambda(x)|^{-1} Q(x) \Sigma(x) - 2\mu Q(x))}_{\leq -2\gamma |\Lambda(x)|^{-1} Q(x)} \varepsilon dx \quad (3.64)$$

The constraints (3.61) and (3.62) guarantee that $\dot{V}(t) \leq -2\gamma V(t)$ for $t \geq 0$. Hence, we have that $V(\varepsilon(t, \cdot)) \leq e^{-2\gamma t} V(\varepsilon^0)$. To finalize the proof, equation (3.63) implies that:

$$\lambda_{min} \|\varepsilon\|_{L^2([0,1]; \mathbb{R}^6)}^2 \leq V(\varepsilon) \leq \lambda_{max} \|\varepsilon\|_{L^2([0,1]; \mathbb{R}^6)}^2 \quad (3.65)$$

where $(\lambda_{min}, \lambda_{max})$ are the minimum and maximum Eigen-values of the matrix $(|\Lambda(x)|^{-1} Q(x))$ for all $x \in [0, 1]$, respectively. We obtain the GES since:

$$\begin{aligned} \lambda_{min} \|\varepsilon\|_{L^2([0,1]; \mathbb{R}^6)}^2 &\leq e^{-2\gamma t} V(\varepsilon^0) \leq \lambda_{max} e^{-2\gamma t} \|\varepsilon^0\|_{L^2([0,1]; \mathbb{R}^6)}^2 \\ &\Leftrightarrow \|\varepsilon\|_{L^2([0,1]; \mathbb{R}^6)} \leq \sqrt{\frac{\lambda_{max}}{\lambda_{min}}} e^{-\gamma t} \|\varepsilon^0\|_{L^2([0,1]; \mathbb{R}^6)} \end{aligned} \quad (3.66)$$

which implies (3.60) and completes the proof. \square

Remark 3.4.1. *An interesting fact about inequality (3.61) is that it does not include the observer gains L^+ and L^- . The existence of solutions to (3.61) highly depends on the magnitude of the states couplings $\Sigma(x)$. Since the two phase exchanger is naturally stable, we expect the magnitude of $\Sigma(x)$ to be small enough so that the inequality (3.61) can be satisfied. Otherwise, the backstepping techniques explained in Chapter 2 should be used to handle the magnitude of the couplings $\Sigma(x)$. Moreover, inequality (3.61) is an infinite matrix linear inequality. It is solved to find the coefficients of the positive definite matrix $Q(x)$, and it should be satisfied for all $x \in [0, 1]$. The authors in [58] employ a polytopic approach to handle the space variations. The polytopic approach is to define a polytope in the spatial domain. Then, to solve the inequality on the extremities of that polytope. This will guarantee that a solution exist all over the space domain.*

3.5 Numerical Evaluation of the Observer

The performance of the proposed observer architecture in (3.55)-(3.57) is evaluated by comparing the output of the system's model along with the results of the observer simulation. The evaluation scenario is done in the following order:

1. The nonlinear model (3.19)-(3.25) and (3.34)-(3.36) is simulated using the finite volume method under constant boundary conditions with toy values for the exchanger dimensions, heat transfer coefficient and friction coefficients. The simulation is completely explained in Section 3.3;
2. Once the system has reached the steady state $W^S(x)$, the linearized system matrices $A^S(x)$ and $B^S(x)$ are computed as illustrated in Section 3.4.1;

3. The matrices $\Lambda(x)$ and $\Sigma(x)$ are constructed using the transformation $T(x)$ in (3.51), then (3.61) is solved using the polytopic approach proposed by [58] to find the matrix $Q(x)$. The equation is solved for $\mu = 1.05$ and $\gamma = 10^{-4} \text{ s}^{-1}$;
4. The bilinear matrix inequality (BMI) (3.62) is solved by first ensuring that the diagonal elements are negative and then adjust the gains to satisfy the BMI. The values obtained are: $L_1 = 0.0092$, $L_2 = 0.3276$, $L_3 = 0.0104$, $L_4 = 0.2141$, $L_5 = 0.0058$ and $L_6 = 0.3943$.

After calculating all the observer gains in the offline mode, we can proceed to evaluate the estimation in real time. We present here the worst case scenario, i.e. the observer is simulated with the addition of additive Gaussian noises (signal to noise ratio SNR=100) to the boundary measurements. We start the model at the steady state $W^S(x)$ then we do a step decrease of 15 KJ/Kg in the inlet hot enthalpy at $T = 1000 \text{ s}$. The observer is started at the following initial conditions:

$$\hat{W}_0(x) = W^S(x) + \Delta \hat{W}^0(x)$$

where the values of $\Delta \hat{W}^0(x)$ are: $\Delta \hat{W}_1^0(x) = 10^{-3}$, $\Delta \hat{W}_2^0(x) = 50 \text{ KJ/Kg}$, $\Delta \hat{W}_3^0(x) = 0.15 \text{ MPa}$, $\Delta \hat{W}_4^0(x) = 10^{-3} \text{ Kg/s}$, $\Delta \hat{W}_5^0(x) = 50 \text{ KJ/Kg}$ and $\Delta \hat{W}_6^0(x) = 0.15 \text{ MPa}$. Keeping in mind that the overall objective of the observer is to estimate the states inside the domain using boundary sensing. We present in Fig. 3.8 and Fig. 3.9 the estimations at two points inside the domain at $x = 0.25$ and at $x = 0.75$ (these two points are chosen arbitrarily just to show the quality of the estimation). We can see that the observer converges close enough to the model after exhibiting some oscillations in the transient periods. The effect of linearization is not showing up since the observer initial conditions are chosen not very far from the linearization point $W^S(x)$. Fig. 3.10 shows the convergence of the estimation error in the L^2 norm. We can notice that the norm of the error converges to a steady state and not to zero. The reason is obviously the addition of white Gaussian noise to the measurements. The magnitude of the error norm at steady state is proportional to the (SNR) of the measurements. If the measurements were more noisy, we expect the steady state error to increase. But in all cases, we can conclude that the observer is reasonably robust; the addition of noise does not affect the convergence of the observer. This conclusion is simulation-based, but the theoretical proof of the the robustness of the observer to measurement noises follows straightforwardly from the Lyapunov analysis done in Section 3.4. We should also mention that increasing the observer gains L^+ and L^- lead to poor robustness with respect to measurement noises, this can be easily concluded also from the Lyapunov analysis done in Section 3.4.

3.6 Conclusion

We have proposed a boundary observer for the two phase heat exchanger with CO₂ refrigerants. The analysis is started in the modeling phase, in which we have presented various physical models for fluids undergoing change in phase from liquid to gas. Then, the model equations are chosen with a careful approximation of the equations of the states of CO₂. The observer is built on the linearized dynamics of the model assuming constant heat transfer and friction coefficients. Afterwards, we have used a Lyapunov approach to derive sufficient conditions for

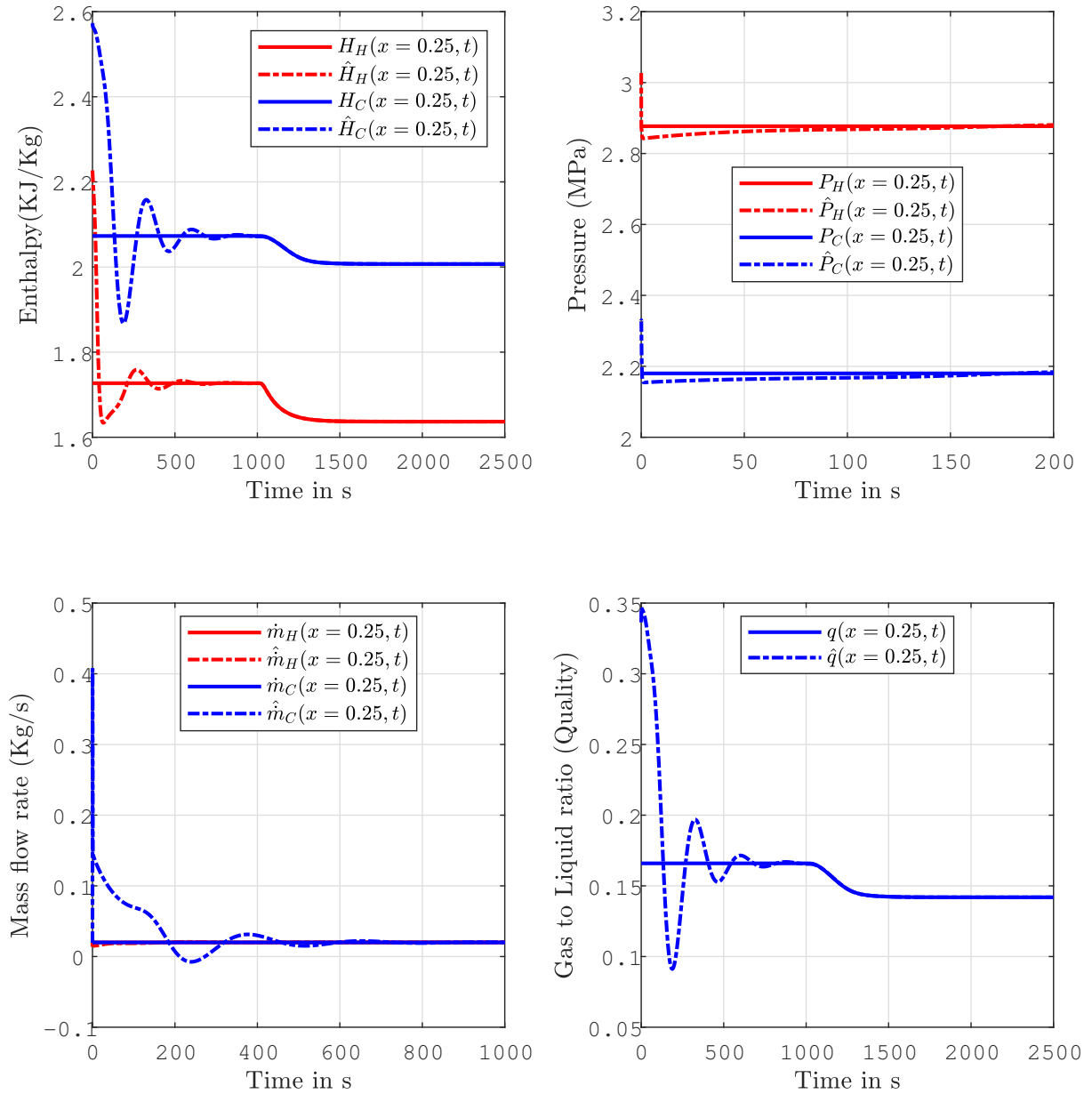


Figure 3.8: Estimation of the complete thermodynamic profile (\dot{m} , P , H) at $x = 0.25$.

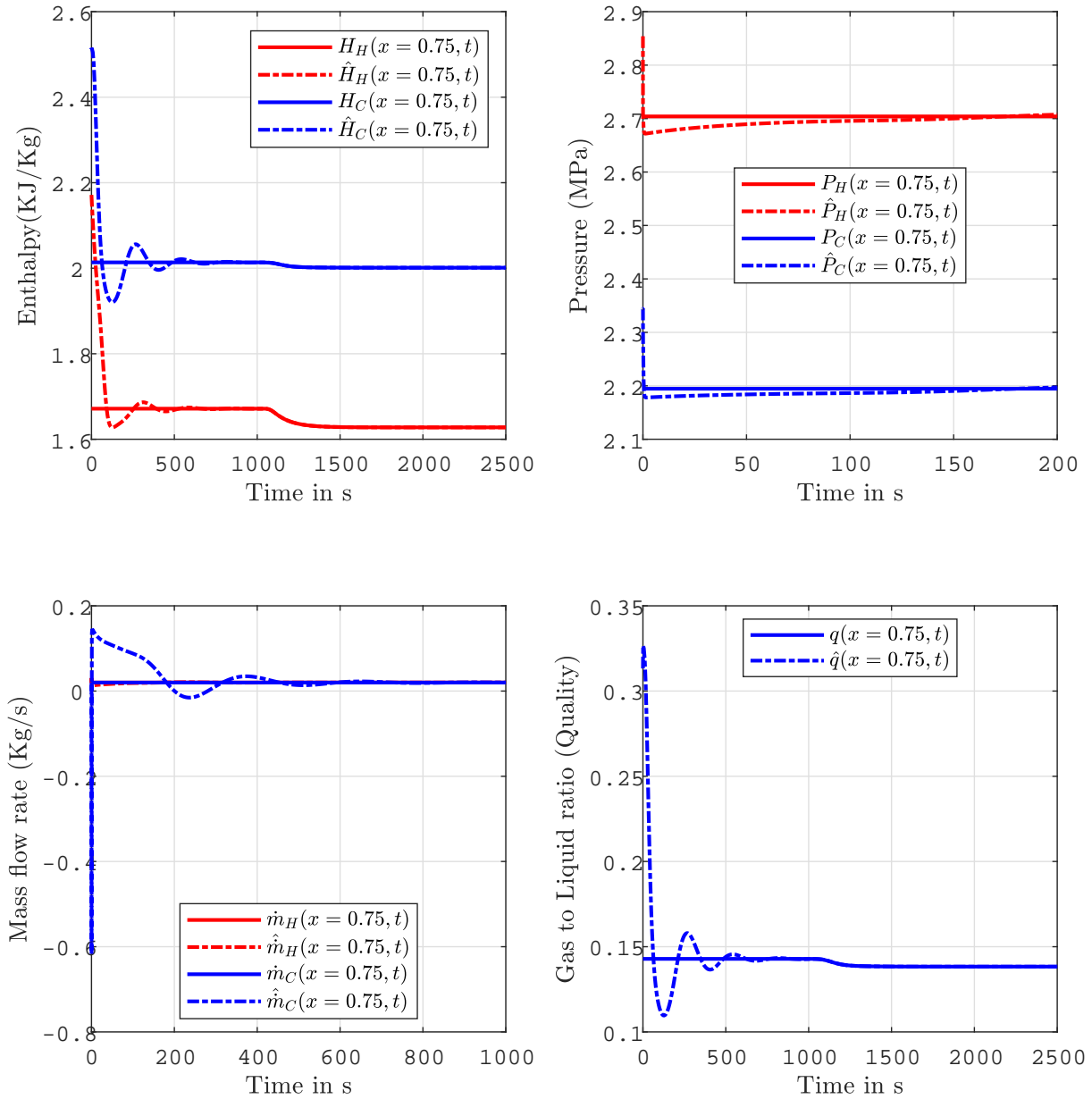


Figure 3.9: Estimation of the complete thermodynamic profile (\dot{m}, P, H) at $x = 0.75$.

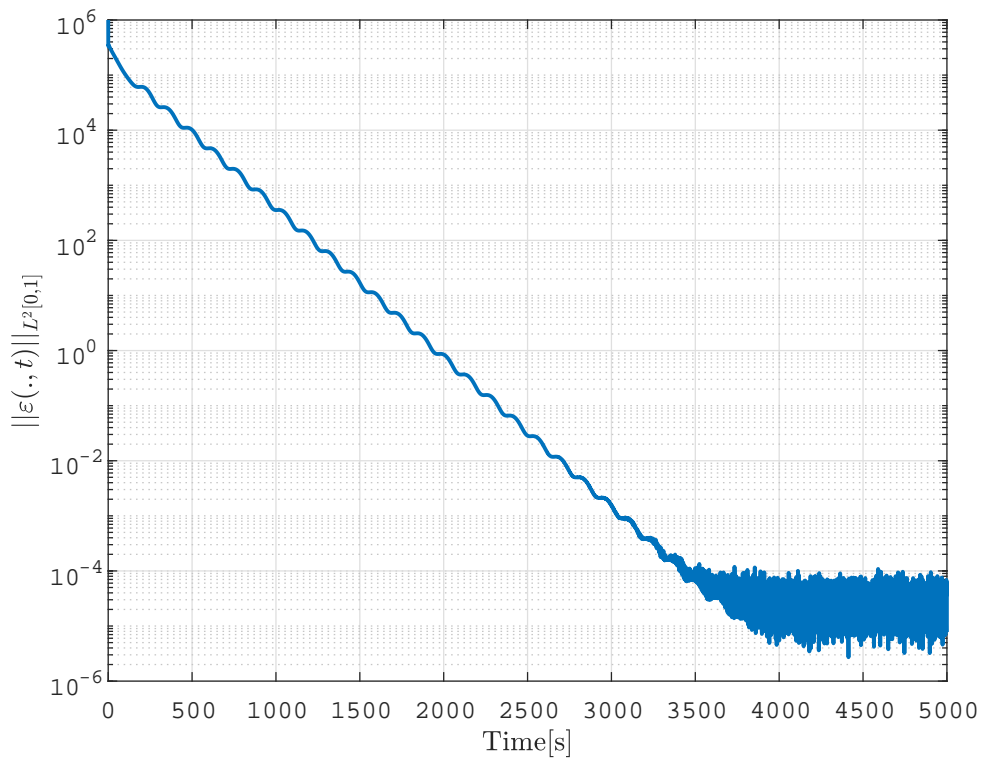


Figure 3.10: Time variation of the L^2 norm of the estimation error $\varepsilon(x, t)$.

the exponential convergence of the estimation error and to calculate the observer gains. An important future work for us is to consider state dependent heat and friction coefficients: this is more realistic specially when considering two phase flows. Also, keeping some model nonlinearities in the observer design would be an important step towards a full quasilinear observer.

Chapter 4

Backstepping control for a class of coupled hyperbolic-parabolic PDE systems

We consider the boundary stabilization of a linear diffusion equation coupled with a linear advection equation. A schematic diagram of the system is given in Fig. 4.1.

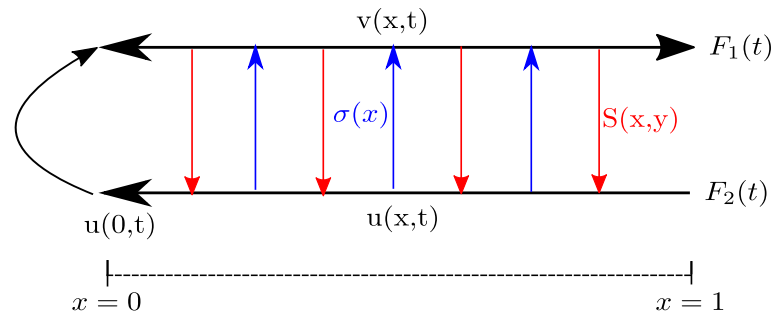


Figure 4.1: Schematic diagram of the diffusive - advective system

The diffusion state is $v(x, t)$ and the advective state is $u(x, t)$. The two equations are coupled inside the domain and at the boundary. The in-domain coupling architecture is considered from both sides i.e. an advection source term ($\sigma(x)$) driven by the advection PDE and a Volterra integral source term ($S(x, y)$) driven by the diffusion PDE. More precisely, the system

is governed by the following equations evolving in $\{(t, x) \mid t \geq 0, x \in [0, 1]\}$:

$$v_t(x, t) = v_{xx}(x, t) + \lambda(x)v(x, t) + \sigma(x)u(x, t) \quad (4.1)$$

$$u_t(x, t) = u_x(x, t) + \int_0^x S(x, y)v(y, t)dy \quad (4.2)$$

$$v_x(0, t) = u(0, t) \quad (4.3)$$

$$v(1, t) = F_1(t) \quad (4.4)$$

$$u(1, t) = F_2(t) \quad (4.5)$$

where $\lambda(x)$ is the diffusion reaction term, considered arbitrary. The system parameters $\lambda(x)$, $\sigma(x)$ and $S(x, y)$ are considered smooth enough. The outflow of the advection equation drives the diffusion equation at the boundary $x = 0$. The system is also actuated by two boundary control laws: $F_1(t)$ on the diffusion side and $F_2(t)$ on the advection side.

We recall that the overall objective to design two boundary control laws $F_1(t)$ and $F_2(t)$ so that the system (4.1)-(4.5) can achieve exponential stability in the $L^2 \times H^1$ norm.

4.1 Literature review

Coupled parabolic-hyperbolic systems naturally appear in many physical domains, such as predator-prey population models, biological chemotaxis and EUV lithography. It is important to note that many real processes that are modeled by hyperbolic equations (such as gas flow in pipelines [46], multiphase flow [35], heat exchanger networks [83], and many more) include a diffusive behavior that is neglected under specific hypotheses. As extensively illustrated in Chapter 1, a clear example regarding this property is the thermal heat exchanger tube, where heat is transferred from one fluid to another through a wall interface in which diffusion takes place. Under certain conditions related to the thermodynamic characteristics of the fluid and of the wall, the diffusion property cannot be neglected and the mathematical model involves a coupling between two different classes of PDEs, diffusion and advection.

Generally speaking, the control of partial differential equations of the same class is widely investigated in the literature. Several results exist on the boundary control of hyperbolic systems [17, 50, 26], and also of parabolic systems [57], [74], among many others. However, the boundary control of mixed hyperbolic-parabolic PDEs is less investigated by the community. The results on the existence of solutions of the initial-boundary value problems of quasilinear hyperbolic-parabolic coupled systems can be dated back to the 80s [59, 75]. Since then, few results emerges on the control design of such classes of systems. For instance, we can first mention the results of the authors in [5] on the optimal control of coupled hyperbolic-parabolic PDEs. In their work, they have considered distributed control inputs i.e. the control signals are injected inside the domain and not at the boundary. The core of the control design is based on minimizing a quadratic cost function to obtain a set of Ricatti equations similar to the ODE case. However, system stabilization by means of a boundary controller is harder than using a distributed one. The presence of an unbounded control operator at the boundary complicates the overall design. In this context, we can mention the work of the authors in [54] that investigates the stabilization of an unstable reaction-diffusion PDE with a long input delay. The delay is represented by a

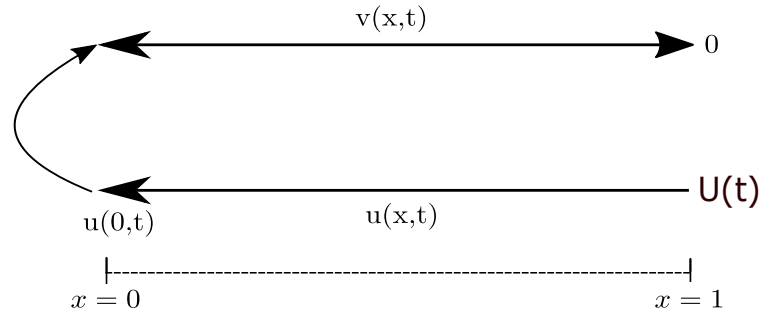


Figure 4.2: Schematic diagram of the diffusive - advective system considered in [54]

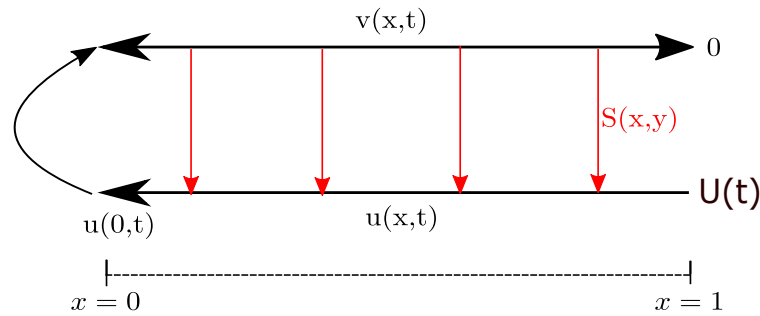


Figure 4.3: Schematic diagram of the diffusive - advective system considered in [31]

transport equation that drives the diffusion equation at the boundary as shown in Fig. 4.2. The controller $U(t)$ that stabilizes the system is obtained using the backstepping method. One can notice that, in comparison with the system we consider in Fig. 4.1, the authors in [54] consider no interior coupling between the advection equation $u(x,t)$ and the diffusion equation $v(x,t)$ i.e. $\sigma(x) = 0$ and $S(x,y) = 0$. This coupling configuration is later extended by the authors in [30] to the case of multiple diffusion equations with distinct input delays, using also the backstepping method for the controllers design. Afterwards, the authors in [31] introduced a uni-directional coupling from diffusion to advection as shown in Fig. 4.3. Hence, $S(x,y) \neq 0$ but no advection-diffusion coupling is considered. The controller design is again based on the backstepping transformations similar to the ones used by the authors in [54].

4.1.1 Contribution

To the best of our knowledge, the contributions [54, 30, 31] are the only works in the literature that address the problem of boundary stabilizing a mixed hyperbolic-parabolic system. In this framework, we consider the control of almost the same class of systems investigated in [31]. The novelty in our work is to consider a bidirectional interior coupling between the two PDEs (i.e. an advection source term $\sigma(x)$ driven by the advection PDE and a Volterra integral source term $S(x,y)$ driven by the parabolic PDE) as shown in Fig. 4.1. This additional complexity in the

model necessitates having two boundary control actuators $F_1(t)$ and $F_2(t)$ instead of only one control input $U(t)$.

The present chapter also explores the applicability of the backstepping technique on systems of distinct families. For such class of systems, it is clear that the effectiveness of the backstepping method depends on the coupling topology as certain topologies can be quite difficult to tackle in theory. The coupling structure considered in this chapter is a prime example on this difficulty.

The work done in this chapter is published in:

M.Ghousein, E.Witrant. “Backstepping control for a class of coupled hyperbolic-parabolic PDE systems”. In: *2020 American Control Conference (ACC)*, IEEE, pp. 1600-1605, Invited session.

The chapter is organized as follows. The control design is presented in Section 4.2. Section 4.3 is dedicated to the exponential stability of the closed loop system. Finally, Section 4.4 illustrates the effectiveness of the control design through simulations and some concluding remarks are given in Section 4.5.

4.2 Backstepping Control Design

The overall objective is to design two feedback control laws $F_1(t)$ and $F_2(t)$ such that the exponential stability of system (4.1)-(4.5) is achieved in closed loop. It is important to note the two reasons which can cause system (4.1)-(4.5) to be unstable in open loop: one is the reaction term $\lambda(x) > 0$ which shifts the poles of the diffusion equation to the right hand plane. The second reason is the two couplings $S(x, y)$ and $\sigma(x)$ which, depending on their magnitude, may drive the system to instability regardless of the value of $\lambda(x)$.

Our proposed idea of the control design is shown on Fig. 4.4. The diffusion equation (4.1) is first stabilized using the controller $F_1(t)$ to eliminate the instability caused by $\lambda(x)$. Hence, the plant of states $\{v(x, t), u(x, t)\}$ is transformed by a backstepping transformation (Transformation 1) into the target system 1 of states $\{z(x, t), u(x, t)\}$. At this step in the design, change only occur on the diffusion state $v(x, t)$ which is transformed into $z(x, t)$ while keeping the transport state $u(x, t)$ untouched. Afterwards, since the advection equation (4.2) can decay in finite time in case of no coupling from the diffusion equation, the idea is to decouple equation (4.2) using the controller $F_2(t)$, such that finite time decay is achieved for the advection PDE. Therefore, the advective state $u(x, t)$ in target system 1 is transformed into $w(x, t)$ in target system 2 using another backstepping transformation (Transformation 2) while keeping the diffusion states unchanged $z(x, t) = \eta(x, t)$. The resulting system, which is target system 2, will eventually be only diffusive and we give sufficient conditions that guarantees its stability in the $L^2 \times H^1$ norm (as we will show in the next sections).

To apply the previous procedure, one must know the shape the backstepping transformations and also the architecture of the target systems. We start by Transformation 1.

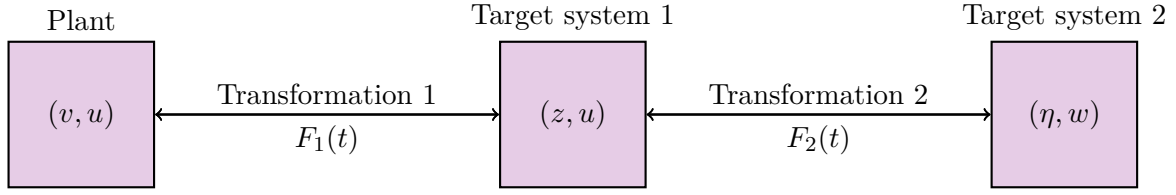


Figure 4.4: Control design strategy

4.2.1 Transformation 1: Eliminate the effect of $\lambda(x)$

The plant of states $\{v(x, t), u(x, t)\}$ is transformed into target system 1 of states $\{z(x, t), u(x, t)\}$ using the following backstepping transformation:

$$z(x, t) = v(x, t) - \int_0^x K(x, y)v(y, t)dy \quad (4.6)$$

$$v(x, t) = z(x, t) + \int_0^x L(x, y)z(y, t)dy \quad (4.7)$$

where the kernels $K(x, y)$ and $L(x, y)$ are the direct and inverse kernels, respectively, defined on the triangular domain $\Omega_1 = \{(x, y), 0 \leq y \leq x \leq 1\}$. We consider also the following dynamics for target system 1:

$$z_t(x, t) = z_{xx}(x, t) - cz(x, t) - \int_0^x T(x, y)z(y, t)dy + \sigma(x)u(x, t) + K(x, 0)u(0, t) - \int_0^x K(x, y)\sigma(y)u(y, t)dy \quad (4.8)$$

$$u_t(x, t) = u_x(x, t) + \int_0^x S_1(x, y)z(y, t)dy \quad (4.9)$$

$$z_x(0, t) = u(0, t) \quad (4.10)$$

$$z(1, t) = 0 \quad (4.11)$$

$$u(1, t) = F_2(t) \quad (4.12)$$

where $c > 0$ and $T(x, y)$ are two control design variables to be defined later, and $S_1(x, y)$ is given by:

$$S_1(x, y) = S(x, y) + \int_y^x S(x, \xi)L(\xi, y)d\xi \quad (4.13)$$

Before calculating the equations of the kernels $K(x, y)$ and $L(x, y)$, let us focus on the choice of target system 1 in equations (4.8)-(4.12). The parameter $\lambda(x)$ is substituted by c in the dynamics of $z(x, t)$ while the dynamics of $u(x, t)$ did not change. This means that if the advective state $u(x, t)$ is naturally stable, then the diffusion state $z(x, t)$ will have no problems in its stability since the effect of $\lambda(x)$ is eliminated, and this is the overall objective of transformation 1 as we mentioned earlier. The introduction of the variable $T(x, y)$ will also serve its role later on, when we give the sufficient conditions for stability of the system.

We now derive the equations of the direct transformation $K(x, y)$ only. The equations of $L(x, y)$ will follow in the same way. Differentiating (4.6) in time, substituting (4.1) and integrating by parts we have

$$\begin{aligned} z_t(x, t) &= v_{xx}(x, t) + \lambda(x)v(x, t) + \sigma(x)u(x, t) - K(x, x)v_x(x, t) + K(x, 0)v_x(0, t) \\ &\quad + K_y(x, x)v(x, t) - K_y(x, 0)v(0, t) - \int_0^x K_{yy}(x, y)v(y, t)dy \\ &\quad - \int_0^x K(x, y)\lambda(y)v(y, t)dy - \int_0^x \sigma(y)K(x, y)u(y, t)dy \end{aligned} \quad (4.14)$$

We then differentiate (4.6) twice in space and we substitute in (4.8) to get

$$\begin{aligned} z_t(x, t) &= v_{xx}(x, t) - \frac{d(K(x, x))}{dx}v(x, t) - K(x, x)v_x(x, t) - K_x(x, x)v(x, t) - cv(x, t) \\ &\quad - \int_0^x K_{xx}(x, y)v(y, t)dy + c \int_0^x K(x, y)v(y, t)dy + \sigma(x)u(x, t) + K(x, 0)u(0, t) \\ &\quad - \int_0^x T(x, y)v(y, t)dy - \int_0^x \sigma(y)K(x, y)u(y, t)dy + \int_0^x \left\{ \int_y^x T(x, \xi)K(\xi, y)d\xi \right\}v(y, t)dy \end{aligned} \quad (4.15)$$

Equalizing (4.14) and (4.15), and posing the relevant boundary condition in (4.3) leads to the following kernel equations of $K(x, y)$

$$K_{xx}(x, y) - K_{yy}(x, y) = (c + \lambda(y))K(x, y) - T(x, y) + \int_y^x T(x, \xi)K(\xi, y)d\xi \quad (4.16)$$

$$K_y(x, 0) = 0 \quad (4.17)$$

$$K(x, x) = -\frac{1}{2} \int_0^x (\lambda(s) + c)ds \quad (4.18)$$

Following exactly the same procedure, one can calculate the kernel equations for the inverse transformation $L(x, y)$ using (4.7). This gives the following set of equations:

$$L_{yy}(x, y) - L_{xx}(x, y) = (c + \lambda(x))L(x, y) + T(x, y) + \int_y^x L(x, \xi)T(\xi, y)d\xi \quad (4.19)$$

$$L_y(x, 0) = 0 \quad (4.20)$$

$$L(x, x) = -\frac{1}{2} \int_0^x (\lambda(s) + c)ds \quad (4.21)$$

The control law $F_1(t)$ is calculated to ensure that $z(1, t) = 0$ and is given by:

$$F_1(t) = \int_0^1 K(1, y)v(y, t)dy \quad (4.22)$$

It has been shown in [74] that the kernel equations (4.16)-(4.18) and (4.19)-(4.21) have a $C^2[\Omega_1]$ unique solution. The method relies on writing the kernel equations in the integral form and then to use the method of successive approximations (explained in Chapter 2/ Numerical simulations)

to prove the convergence of the iterating sequence. Interested readers are oriented to check the detailed proof in [74] in Chapter 2.

Target system 1 becomes a stable diffusion equation (with two free design variables c and $T(x, y)$) coupled with an advection equation. The objective of the controller $F_2(t)$ is then to decouple (4.9) from diffusion. By doing so, the advection equation can achieve finite time stability.

4.2.2 Transformation 2: Eliminate the effect of $\sigma(x)$ and $S(x, y)$

We consider the following backstepping transformation that maps target system 1 of states $\{z(x, t), u(x, t)\}$ to target system 2 of states $\{\eta(x, t), w(x, t)\}$:

$$\eta(x, t) = z(x, t) \quad (4.23)$$

$$w(x, t) = u(x, t) - \int_0^x P(x, y)u(y, t)dy - \int_0^1 M(x, y)z(y, t)dy \quad (4.24)$$

where the kernel $P(x, y)$ is defined on the triangular domain Ω_1 and $M(x, y)$ is defined on the rectangular domain $\Omega_2 = \{(x, y), 0 \leq x \leq 1, 0 \leq y \leq 1\}$. We also postulate the inverse of transformation 2 as:

$$z(x, t) = \eta(x, t) \quad (4.25)$$

$$u(x, t) = w(x, t) + \int_0^x Q(x, y)w(y, t)dy + \int_0^1 R(x, y)\eta(y, t)dy \quad (4.26)$$

where $Q(x, y)$ and $R(x, y)$ are the inverse kernels defined on Ω_1 and Ω_2 , respectively. Transformation 2 has a specific form i.e. if we consider (4.24), one can notice that it is a superposition of a Volterre integral in $u(x, t)$ and a Fredholm integral in $z(x, t)$. This architecture is not common in the theory of backstepping design for PDEs of the same class. However, it has been used by the authors in [54, 30, 31] on mixed classes of transport and diffusion equations in order to handle the complexity introduced by the physical fact that the advection and diffusion equations donot have the same number of spatial derivatives.

Now, we consider the following dynamics for target system 2:

$$\begin{aligned} \eta_t(x, t) &= \eta_{xx}(x, t) - c\eta(x, t) + \sigma(x)w(x, t) + K(x, 0)w(0, t) \\ &\quad + \int_0^1 C_1(x, y)\eta(y, t)dy + \int_0^x C_2(x, y)w(y, t)dy \end{aligned} \quad (4.27)$$

$$w_t(x, t) = w_x(x, t) \quad (4.28)$$

$$\eta_x(0, t) = w(0, t) \quad (4.29)$$

$$\eta(1, t) = 0 \quad (4.30)$$

$$w(1, t) = 0 \quad (4.31)$$

where $C_1(x, y)$ and $C_2(x, y)$ are two feedforward couplings defined on Ω_1 and Ω_2 respectively, and they are to be defined later. Target system 2 is composed of an advective state $w(x, t)$ that is totally decoupled from the diffusion state $\eta(x, t)$. This choice is extremely important as it ease the stability analysis and permit us to obtain sufficient conditions for exponential convergence

as we illustrate later. Now, we derive the kernel equations for transformation 2.

As we did in the derivations of transformation 1, we only derive the kernel equations for the direct transformation while the inverse transformation follow in the same order. Differentiating (4.24) in time, substituting (4.8)-(4.9) and integrating by parts we have

$$\begin{aligned}
w_t(x, t) &= u_x(x, t) + \int_0^x S_1(x, y)z(y, t)dy - P(x, x)u(x, t) + P(x, 0)u(0, t) \\
&+ \int_0^x P_y(x, y)u(y, t)dy - \int_0^x \left\{ \int_y^x P(x, \xi)S_1(\xi, y)d\xi \right\} z(y, t)dy \\
&- M(x, 1)z_x(1, t) + M(x, 0)z_x(0, t) + M_y(x, 1)z(1, t) - M_y(x, 0)z(0, t) \\
&- \int_0^1 M_{yy}(x, y)z(y, t)dy + c \int_0^1 M(x, y)z(y, t)dy \\
&- \int_0^1 \sigma(y)M(x, y)u(y, t)dy - u(0, t) \int_0^1 M(x, \xi)K(\xi, 0)d\xi \\
&+ \int_0^1 \left\{ \int_y^1 M(x, \xi)T(\xi, y)d\xi \right\} z(y, t)dy + \int_0^1 \left\{ \int_y^1 M(x, \xi)K(\xi, y)d\xi \right\} \sigma(y)u(y, t)dy
\end{aligned} \tag{4.32}$$

Differentiating (4.24) once in space gives

$$\begin{aligned}
w_t(x, t) &= w_x(x, t) \\
&= u_x(x, t) - P(x, x)u(x, t) - \int_0^x P_x(x, y)u(y, t)dy - \int_0^1 M_x(x, y)z(y, t)dy
\end{aligned} \tag{4.33}$$

By equalizing (4.32) and (4.33) and enforcing the relevant boundary conditions (4.10) and (4.11) we take:

$$\begin{aligned}
&\int_0^1 \left(M_x(x, y) - M_{yy}(x, y) + cM(x, y) + \int_y^1 M(x, \xi)T(\xi, y)d\xi \right. \\
&\left. + \mathbb{I}_{y \leq x} \left(- \int_y^x P(x, \xi)S_1(\xi, y)d\xi + S_1(x, y) \right) \right) z(y, t)dy = 0.
\end{aligned} \tag{4.34}$$

$$\int_0^1 \left(- \sigma(y)M(x, y) + \sigma(y) \int_y^1 M(x, \xi)K(\xi, y)d\xi + \mathbb{I}_{y \leq x} \left(P_y(x, y) + P_x(x, y) \right) \right) u(y, t)dy = 0. \tag{4.35}$$

$$\left(P(x, 0) + M(x, 0) - \int_0^1 M(x, \xi)K(\xi, 0)d\xi \right) u(0, t) = 0. \tag{4.36}$$

where $\mathbb{I}_{y \leq x}(x, y) = \begin{cases} 1 & \text{if } y \leq x \\ 0 & \text{if } y > x \end{cases}$ is a piecewise function defined on Ω_2 . Using (4.35) and (4.36), we get the following equations for $P(x, y)$:

$$\begin{cases} P_y(x, y) &= -P_x(x, y) + \sigma(y) \left(M(x, y) - \int_y^x M(x, \xi)K(\xi, y)d\xi \right) \\ P(x, 0) &= -M(x, 0) + \int_0^x M(x, \xi)K(\xi, 0)d\xi \end{cases} \tag{4.37}$$

Using (4.24), we have that $w(0, t) = u(0, t) - \int_0^1 M(0, y)z(y, t)dy$ with $z_x(0, t) = \eta_x(0, t) = u(0, t)$. Hence, enforcing (4.29) leads to a zero initial condition for the kernel $M(x, y)$, i.e. $M(0, y) = 0$. By imposing $M(x, 1) = 0$ and having $M(0, y) = 0$, we deduce that $M(x, y) = 0$ is a trivial solution to equations (4.34)-(4.35) for $y > x$. By imposing $M_y(x, 0) = 0$ and using (4.34)-(4.36) with $M(x, y) = 0$ for $y > x$, we directly obtain the following equations for $M(x, y)$:

$$\begin{cases} \begin{cases} M_x(x, y) = M_{yy}(x, y) - cM(x, y) - S_1(x, y) + \int_y^x P(x, \xi)S_1(\xi, y)d\xi \\ - \int_y^x M(x, \xi)T(\xi, y)d\xi \end{cases} & \text{if } y \leq x \\ M(x, y) = 0 \\ M_y(x, 0) = 0 \end{cases} \quad \text{if } y > x \quad (4.38)$$

In order to find $C_1(x, y)$ and $C_2(x, y)$, we substitute (4.23)-(4.24) in (4.27) and get

$$\begin{aligned} z_t(x, t) &= z_{xx}(x, t) - cz(x, t) + \sigma(x)u(x, t) + K(x, 0)u(0, t) \\ &+ \int_0^x \left(-\sigma(x)P(x, y) + C_2(x, y) - \int_y^x C_2(x, \xi)P(\xi, y)d\xi \right) u(y, t)dy \\ &+ \int_0^1 \left(-\sigma(x)M(x, y) + C_1(x, y) - \int_0^x C_2(x, \xi)M(\xi, y)d\xi - K(x, 0)M(0, y) \right) z(y, t)dy \end{aligned} \quad (4.39)$$

By (4.8), we also have that

$$\begin{aligned} z_t(x, t) &= z_{xx}(x, t) - cz(x, t) + \sigma(x)u(x, t) + K(x, 0)u(0, t) - \int_0^x T(x, y)z(y, t)dy \\ &- \int_0^x K(x, y)\sigma(y)u(y, t)dy \end{aligned} \quad (4.40)$$

By equalizing (4.39) and (4.40), and using (4.38) we have directly the following equations for $C_1(x, y)$ and $C_2(x, y)$:

$$C_1(x, y) = \begin{cases} \sigma(x)M(x, y) - T(x, y) + \int_y^x C_2(x, \xi)M(\xi, y)d\xi & \text{if } y \leq x \\ 0 & \text{if } y > x \end{cases} \quad (4.41)$$

$$C_2(x, y) = \sigma(x)P(x, y) - \sigma(y)K(x, y) + \int_y^x C_2(x, \xi)P(\xi, y)d\xi \quad (4.42)$$

The control law $F_2(t)$ is calculated to ensure that $w(1, t) = 0$ and is given by:

$$\begin{aligned} F_2(t) &= \int_0^1 P(1, y)u(y, t)dy + \int_0^1 M(1, y)z(y, t)dy \\ &= \int_0^1 P(1, y)u(y, t)dy + \int_0^1 M_c(1, y)v(y, t)dy \end{aligned} \quad (4.43)$$

with $M_c(1, y) = M(1, y) - \int_y^1 M(1, \xi)K(\xi, y)d\xi$. In the same way, one can calculate the kernel equations for the inverse transformation using (4.26). This gives the following set of equations:

$$\begin{cases} Q_y(x, y) &= -Q_x(x, y) + \sigma(y)R(x, y) + \int_y^x R(x, \xi)C_2(\xi, y)d\xi \\ Q(x, 0) &= -R(x, 0) + \int_0^x R(x, \xi)K(\xi, 0)d\xi \end{cases} \quad (4.44)$$

$$\begin{cases} R_x(x, y) = R_{yy}(x, y) - cR(x, y) - S_1(x, y) + \int_y^x R(x, \xi)C_1(\xi, y)d\xi & \text{if } y \leq x \\ R(x, y) = 0 & \text{if } y > x \\ R_y(x, 0) = 0 \end{cases} \quad (4.45)$$

The obtained kernel equations are of known types. For instance, the kernel equations for $P(x, y)$ is the linear transport equation solved on the triangular domain Ω_1 . Whereas, the kernel equations for $M(x, y)$ is the reaction-diffusion equation solved on the rectangular domain Ω_2 . In what follows, we discuss the wellposedness of these equations.

Well-posedness of kernel equations for transformation 2

Notice that the inverse equations (4.44)-(4.45) are similar to the direct transformation equations (4.37)-(4.38), except that $R(x, y)$ is uncoupled from $Q(x, y)$. As a result, the well-posedness of $R(x, y)$ implies the well-posedness of $Q(x, y)$, given the fact that $Q(x, y)$ is the first order transport equation. We start with the well-posedness of the direct transformation as the inverse will follow exactly in the same way. The transport equation (4.37) can be explicitly solved as a function of $M(x, y)$ using the method of characteristics:

$$\begin{aligned} P(x, y) &= -M(x - y, 0) + \int_0^y \sigma(\xi)M(x - y + \xi, \xi)d\xi + \int_0^{x-y} M(x - y, \xi)K(\xi, 0)d\xi \\ &\quad - \int_0^y \int_s^{x-y+s} \sigma(s)M(x - y + s, \xi)K(\xi, s)d\xi ds \end{aligned} \quad (4.46)$$

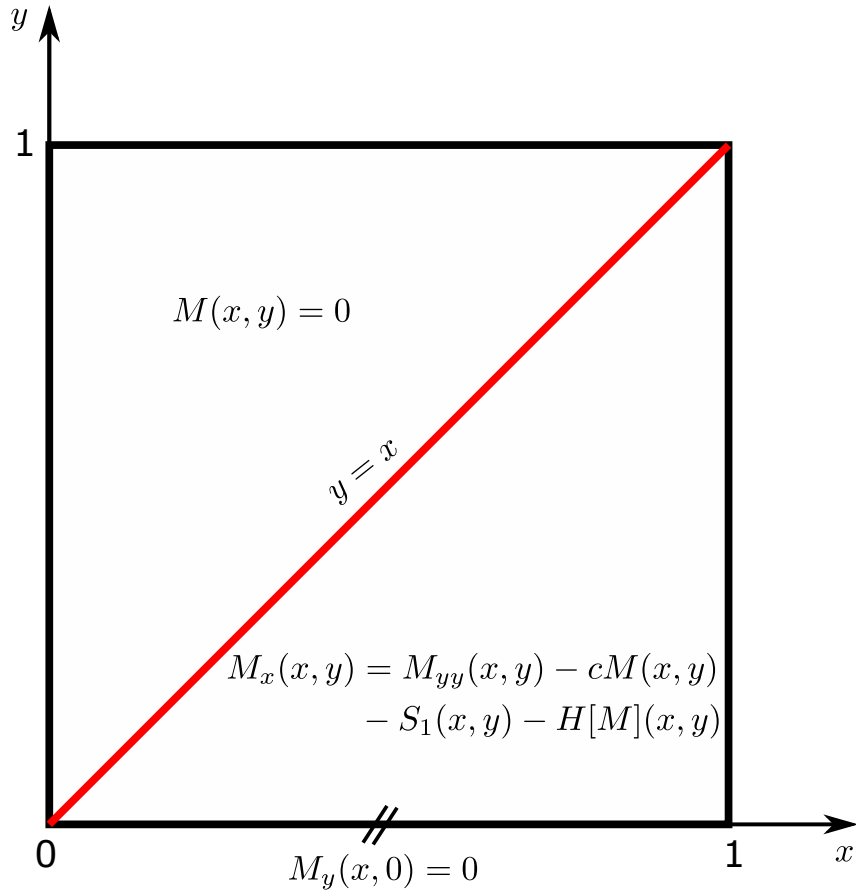
Then, the existence of $M(x, y)$ is sufficient to show that both $P(x, y)$ and $M(x, y)$ exist. Inserting (4.46) into (4.38), the $M(x, y)$ kernel equations become:

$$\begin{cases} M_x(x, y) = M_{yy}(x, y) - cM(x, y) - S_1(x, y) - H[M](x, y) & \text{if } y \leq x \\ M(x, y) = 0 & \text{if } y > x \\ M_y(x, 0) = 0 \end{cases} \quad (4.47)$$

where the linear operator $H[M](x, y)$ is given by:

$$\begin{aligned} H[M](x, y) &= \int_y^x M(x, \xi)T(\xi, y)d\xi - \int_y^x \left(-M(x - \xi, 0) - \int_0^\xi \sigma(s)M(x - \xi + s, s)ds \right. \\ &\quad \left. - \int_0^{x-\xi} M(x - \xi, s)K(s, 0)ds + \int_0^\xi \int_v^{x-\xi+v} \sigma(v)M(x - \xi + v, s)K(s, v)dsdv \right) S_1(\xi, y)d\xi \end{aligned} \quad (4.48)$$

A schematic diagram of $M(x, y)$ on Ω_2 is shown on Fig. 4.5. The domain is partitioned into

Figure 4.5: $M(x, y)$ kernel representation

two parts: the region $y > x$, where we have a diffusion equation of zero initial and boundary conditions that results in a zero trivial solution ($M(x, y) = 0$), and the second region is $y \leq x$, where we have a reaction advection diffusion equation with a source term. The $M(x, y)$ PDE kernel equations (4.47) are nearly the same as the $l(x, y)$ kernel equations obtained by the authors in [31], except that $M(x, y)$ has a zero initial condition ($M(0, y) = 0$, which gives $M(x, y) = 0$ if $y > x$, whereas in [31], $l(0, y) \neq 0$). $M(x, y)$ also contains an additional linear integral terms related to the coupling with the transport equation. To prove the existence of a weak solution, the idea is to first compute energy estimates of the solution. These estimates depend only on the initial conditions and the source terms. Afterwards, a Galerkin type argument can be used to prove the existence of solutions (see Chapter 7 in [40]). We give only partial elements of the proof as the rest is the same as in [31]. We state the energy estimates result in the following lemma:

Lemma 4.2.1. *Consider the $M(x, y)$ PDE system (4.47). There exist a function $F : \mathbb{R}^+ \rightarrow \mathbb{R}^+$ such that:*

$$\max_{s \in [0, x]} \|M(s)\|_{H^1[0,1]} + \|M\|_{L^2([0,x], H^1[0,1])} \leq F(\bar{S}) \quad (4.49)$$

where $\bar{S} = \|S_1(x, y)\|_{L^2([0,1], H^2[0,1])}$.

Proof. We define the H^1 norm of $M(x, y)$ in the y -direction as:

$$\begin{aligned} \|M(x)\|_{H^1[0,1]}^2 &= \int_0^1 M^2(x, y) dy + \int_0^1 M_y^2(x, y) dy \\ &= \|M(x)\|_{L^2[0,1]}^2 + \|M_y(x)\|_{L^2[0,1]}^2 \end{aligned} \quad (4.50)$$

Using (4.47), integration by parts, and applying Young's and Agmon's inequalities [57] we get:

$$\begin{aligned} \frac{d}{dx} \|M(x)\|_{L^2[0,1]}^2 &\leq \left(-2c + \frac{1}{2} + \bar{T} + \bar{S}_1 + \frac{1}{2}\Sigma\bar{S}_1 + \frac{1}{2}\mathbb{K}\bar{S}_1 + \Sigma\mathbb{K}\bar{S}_1 \right) \|M(x)\|_{L^2[0,1]}^2 \\ &\quad + \bar{S}_1^2 + \frac{1}{2}\bar{T} \|M(x)\|_{H^1[0,1]}^2 + \left(\bar{S}_1 + \Sigma\bar{S}_1 + \mathbb{K}\bar{S}_1 + \Sigma\mathbb{K}\bar{S}_1 \right) \max_{s \in [0, x]} \|M(s)\|_{H^1[0,1]}^2 \end{aligned} \quad (4.51)$$

where $\Sigma = \|\sigma(x)\|_{L^\infty[0,1]}$, $\bar{T} = \|T(x, y)\|_{L^2([0,1], H^2[0,1])}$ and $\mathbb{K} = \|K(x, y)\|_{L^\infty[\Omega_1]}$. In the same way, using (4.47), one can derive the following bound on the derivative of $\|M_y(x)\|_{L^2[0,1]}^2$:

$$\begin{aligned} \frac{d}{dx} \|M_y(x)\|_{L^2[0,1]}^2 &\leq \left(-2c + \frac{1}{2} + 2\bar{T} + \frac{3}{2}\Sigma\bar{S}_1 + \frac{3}{2}\mathbb{K}\bar{S}_1 + 2\Sigma\mathbb{K}\bar{S}_1 + 2\bar{S}_1 \right) \|M_y(x)\|_{L^2[0,1]}^2 \\ &\quad + \bar{S}_1^2 + \frac{1}{2}\bar{T} \|M(x)\|_{H^1[0,1]}^2 + \bar{T} \|M(x)\|_{L^2[0,1]}^2 \\ &\quad + 2 \left(\Sigma\bar{S}_1 + \mathbb{K}\bar{S}_1 + \Sigma\mathbb{K}\bar{S}_1 + \bar{S}_1 \right) \max_{s \in [0, x]} \|M(s)\|_{H^1[0,1]}^2 \end{aligned} \quad (4.52)$$

By adding (4.51) and (4.52), we get the following differential inequality in the H^1 norm of $M(x, y)$:

$$\begin{aligned} \frac{d}{dx} \|M(x)\|_{H^1[0,1]}^2 &\leq \left(-2c + \frac{1}{2} + 3\bar{T} + 2\bar{S}_1 + \frac{3}{2}\Sigma\bar{S}_1 + \frac{3}{2}\mathbb{K}\bar{S}_1 + 2\Sigma\mathbb{K}\bar{S}_1 \right) \|M(x)\|_{H^1[0,1]}^2 \\ &\quad + 2\bar{S}_1^2 + 3 \left(\Sigma\bar{S}_1 + \mathbb{K}\bar{S}_1 + \Sigma\mathbb{K}\bar{S}_1 + \bar{S}_1 \right) \max_{s \in [0,x]} \|M(s)\|_{H^1[0,1]}^2 \end{aligned} \quad (4.53)$$

We solve (4.53) by considering two separate cases: increasing and decreasing cases (the constant case is obvious). Starting with the increasing case, we have that $\max_{s \in [0,x]} \|M(s)\|_{H^1[0,1]}^2 = \|M(x)\|_{H^1[0,1]}^2$, and (4.53) becomes:

$$\frac{d}{dx} \|M(x)\|_{H^1[0,1]}^2 \leq \left(-2c + \frac{1}{2} + 3\bar{T} + 5\bar{S}_1 + \frac{9}{2}\Sigma\bar{S}_1 + \frac{9}{2}\mathbb{K}\bar{S}_1 + 5\Sigma\mathbb{K}\bar{S}_1 \right) \|M(x)\|_{H^1[0,1]}^2 + 2\bar{S}_1^2 \quad (4.54)$$

Using the comparison principle, and recalling that $M(x, y)$ has zero initial condition $M(0, y) = 0$, one can derive the following H^1 bound on $M(x, y)$:

$$\|M(x)\|_{H^1[0,1]}^2 \leq \int_0^x 2\bar{S}_1^2 \exp\left(\left(-2c + \frac{1}{2} + 3\bar{T} + 5\bar{S}_1 + \frac{9}{2}\Sigma\bar{S}_1 + \frac{9}{2}\mathbb{K}\bar{S}_1 + 5\Sigma\mathbb{K}\bar{S}_1 \right) (x-z) \right) dz \quad (4.55)$$

On the other hand, and in a quite similar way, we note in the decreasing case that $\max_{s \in [0,x]} \|M(s)\|_{H^1}^2 = \|M(0)\|_{H^1}^2 = 0$, and (4.53) becomes:

$$\frac{d}{dx} \|M(x)\|_{H^1[0,1]}^2 \leq \left(-2c + \frac{1}{2} + 3\bar{T} + 2\bar{S}_1 + \frac{3}{2}\Sigma\bar{S}_1 + \frac{3}{2}\mathbb{K}\bar{S}_1 + 2\Sigma\mathbb{K}\bar{S}_1 \right) \|M(x)\|_{H^1[0,1]}^2 + 2\bar{S}_1^2 \quad (4.56)$$

Following the same procedure, one can derive the following H^1 norm on $M(x, y)$:

$$\|M(x)\|_{H^1[0,1]}^2 \leq \int_0^x 2\bar{S}_1^2 \exp\left(\left(-2c + \frac{1}{2} + 3\bar{T} + 2\bar{S}_1 + \frac{3}{2}\Sigma\bar{S}_1 + \frac{3}{2}\mathbb{K}\bar{S}_1 + 2\Sigma\mathbb{K}\bar{S}_1 \right) (x-z) \right) dz \quad (4.57)$$

By (4.55) and (4.57), one can find a mapping F such that (4.49) is fulfilled. \square

Theorem 4.2.1. *The kernel PDE defined by (4.47) has a weak solution in $L^2([0, 1], H^1[0, 1])$.*

Proof. Using a Galerkin construction of the solution and by applying Lemma 4.2.1, a weak solution is guaranteed to exist due to the energy estimate obtained in (4.49) (see [31] for more details). \square

In order to ensure the existence of a bounded solution for $C_1(x, y)$ and $C_2(x, y)$ in equations (4.41) and (4.42), we take the following assumption on the weak solution of $M(x, y)$ proved in Theorem 4.2.1.

Assumption 4.2.1. Assume that the weak solution $M(x, y)$ of the kernel PDE defined by (4.47) is bounded for all (x, y) in Ω_2 .

The boundedness of $M(x, y)$ by assumption 1 implies the boundedness of $P(x, y)$ by (4.46). Since equation (4.42) is a Volterra equation in $C_2(x, y)$ with a bounded source $\sigma(x)P(x, y) - \sigma(y)K(x, y)$ and a bounded kernel $P(x, y)$, then by the method of successive approximations, $C_2(x, y)$ admits a bounded solution in Ω_1 . As a result, $C_1(x, y)$ also admits a bounded solution in Ω_2 using (4.41).

Remark 4.2.1. If $\sigma(x) = 0$, our results lead directly to the results obtained by the authors in [31].

4.3 Stability of the closed loop system

We start by considering the exponential stability of the system $\{\eta(x, t), w(x, t)\}$, then use transformations 1 and 2 to conclude on the exponential stability of the $\{v(x, t), u(x, t)\}$ system. The target system 2 is in a cascade form: a finite-time ($t_F = 1s$) stable transport equation $w(x, t)$ which drives a diffusion equation $\eta(x, t)$. After t_F , the stability of $\eta(x, t)$ is directly related to the magnitude of the Fredholm integral variable $C_1(x, y)$. However, the magnitude of $C_1(x, y)$ can be modified through the two design control variables c and $T(x, y)$ embedded in $C_1(x, y)$ (see equation 4.41). Moreover, the boundary connectivity of two different classes of PDEs at $x = 0$ gives rise to an unbounded input operator in the interconnection, which necessitates a high order norm in $w(x, t)$. As a result, we prove the exponential stability of $\{\eta(x, t), w(x, t)\}$ in the $L^2 \times H^1$ sense.

We start by transferring the boundary coupling between $\eta(x, t)$ and $w(x, t)$ into the spatial domain. Consider the following intermediate change of variable:

$$\xi(x, t) = \eta(x, t) - (x - 1)w(0, t) \quad (4.58)$$

Differentiating (4.58) in space and time, and substitute in (4.27) to get the following dynamics of the $\{\xi(x, t), w(x, t)\}$ system:

$$\begin{aligned} \xi_t(x, t) = & \xi_{xx}(x, t) - c\xi(x, t) + \sigma(x)w(x, t) + (1 - x)w_t(0, t) \\ & - \left(c(x - 1) - K(x, 0) - \int_0^1 C_1(x, y)(y - 1)dy \right) w(0, t) \end{aligned} \quad (4.59)$$

$$+ \int_0^x C_2(x, y)w(y, t)dy + \int_0^1 C_1(x, y)\xi(y, t)dy$$

$$w_t(x, t) = w_x(x, t) \quad (4.60)$$

$$\xi_x(0, t) = 0 \quad (4.61)$$

$$\xi(1, t) = 0 \quad (4.62)$$

$$w(1, t) = 0 \quad (4.63)$$

Hence, the transport state $w(x, t)$ drives the diffusion state $\xi(x, t)$ only from inside the domain. The following lemma states the sufficient conditions for the exponential stability of $\{\xi(x, t), w(x, t)\}$ in the $L^2 \times H^1$ sense.

Lemma 4.3.1. Consider the intermediate system $\{\xi(x, t), w(x, t)\}$ in (4.59)-(4.63) with any arbitrary initial condition $\{\xi(x, 0), w(x, 0)\}$ satisfying the compatibility conditions. If there exist $\delta_1 > 0$ and two control variables $c > 0$ and $T(x, y)$ such that

$$-\frac{\pi^2}{4} - c + \|C_1\|_{L^\infty[\Omega_2]} \leq -\delta_1 \quad (4.64)$$

then the system $\{\xi(x, t), w(x, t)\}$ is exponentially stable in the $L^2 \times H^1$ sense.

Proof. Consider the following Lyapunov function

$$V_1(t) = \frac{1}{2} \int_0^1 \xi^2(x, t) dx + \frac{1}{2} \int_0^1 p_1 e^{ax} w^2(x, t) dx + \frac{1}{2} \int_0^1 p_2 e^{bx} w_x^2(x, t) dx \quad (4.65)$$

with $p_1, p_2, a, b > 0$. $V_1(t)$ is the weighted $L^2 \times H^1$ norm of $\{\xi(x, t), w(x, t)\}$. Differentiating (4.65) in time, we have

$$\dot{V}_1(t) = \int_0^1 \xi(x, t) \xi_t(x, t) dx + \int_0^1 p_1 e^{ax} w(x, t) w_t(x, t) dx + \int_0^1 p_2 e^{bx} w_x^2(x, t) w_{tx}^2(x, t) dx \quad (4.66)$$

Substituting with (4.59)-(4.63) in (4.66), integrating by parts and applying Wirtinger inequality [57] to bound the spatial derivative of $\xi(x, t)$, one gets

$$\begin{aligned} \dot{V}_1(t) \leq & -\left(\frac{\pi^2}{4} + c\right) \|\xi\|_{L^2[0,1]}^2 + \int_0^1 \sigma(x) w(x, t) \xi(x, t) dx + w_t(0, t) \int_0^1 (1-x) \xi(x, t) dx - \frac{p_2}{2} w_x^2(0, t) \\ & + w(0, t) \int_0^1 \psi(x) \xi(x, t) dx - \frac{p_1}{2} w^2(0, t) - \frac{1}{2} \int_0^1 a p_1 e^{ax} w^2(x, t) dx - \frac{1}{2} \int_0^1 b p_2 e^{bx} w_x^2(x, t) dx \\ & + \int_0^1 \int_0^x C_2(x, y) w(y, t) \xi(x, t) dy dx + \int_0^1 \int_0^1 C_1(x, y) \xi(y, t) \xi(x, t) dy dx \end{aligned} \quad (4.67)$$

with $\psi(x) = -\left(c(x-1) - K(x, 0) - \int_0^1 C_1(x, y)(y-1) dy\right)$. Now, applying Young's and Cauchy-Schwartz inequalities [57] to the last two integral terms in (4.67) and noticing that $w_t(0, t) = w_x(0, t)$, we have:

$$\begin{aligned} \dot{V}_1(t) \leq & \left(\frac{1}{2\epsilon_3} \|\psi\|_{L^\infty[0,1]} - \frac{p_1}{2}\right) w^2(0, t) + \left(\frac{1}{2\epsilon_4} - \frac{p_2}{2}\right) w_x^2(0, t) \\ & - \int_0^1 A_1(x) \xi^2(x, t) dx - \int_0^1 A_2(x) w^2(x, t) dx - \int_0^1 A_3(x) w_x^2(x, t) dx \end{aligned} \quad (4.68)$$

where:

$$\begin{aligned} A_1(x) &= \frac{\pi^2}{4} + c - \|C_1\|_{L^\infty[\Omega_2]} - \frac{\epsilon_1}{2} \|\sigma\|_{L^\infty[0,1]} - \frac{\epsilon_2}{2} \|C_2\|_{L^\infty[\Omega_1]} - \frac{\epsilon_3}{2} \|\psi\|_{L^\infty[0,1]} - \frac{\epsilon_4}{2} \\ A_2(x) &= \frac{1}{2} p_1 a e^{ax} - \frac{1}{2\epsilon_2} \|C_2\|_{L^\infty[\Omega_1]} - \frac{1}{2\epsilon_1} \|\sigma\|_{L^\infty[0,1]} \\ A_3(x) &= \frac{1}{2} p_2 b e^{bx} \end{aligned}$$

with $\epsilon_i > 0$ for $i = 1, 2, 3, 4$ are to be chosen. Given (4.64), we can then select all the ϵ_i small enough to ensure that $A_1(x) \geq \frac{\delta_{A_1}}{2}$ for some $\delta_{A_1} > 0$. Then p_1 and p_2 are chosen such that $(\frac{1}{2\epsilon_3} \|\psi(x)\|_{L^\infty[0,1]} - \frac{p_1}{2}) < 0$ and $(\frac{1}{2\epsilon_4} - \frac{p_2}{2}) < 0$. Furthermore, we select a large enough to have $A_2(x) \geq \delta_{A_2}(\frac{1}{2}p_1 e^{ax})$ for some $\delta_{A_2} > 0$. By doing so, we can find the following bound $\dot{V}_1(t)$:

$$\dot{V}_1(t) \leq -\min\{\delta_{A_1}, \delta_{A_2}, b\}V_1(t) \quad (4.69)$$

The inequality (4.69) gives the exponential decay of $V_1(t)$ in the $L^2 \times H^1$ norm with a convergence rate $\gamma = \min\{\delta_{A_1}, \delta_{A_2}, b\}$ and concludes the proof of Lemma 4.3.1. \square

The following two lemmas are to prove the exponential stability of the system $\{\eta(x, t), w(x, t)\}$.

Lemma 4.3.2. *Consider the following positive definite functions*

$$P_1(t) = \frac{1}{2} \int_0^1 \xi^2(x, t) dx + \frac{1}{2} \int_0^1 p_2 e^{bx} w_x^2(x, t) dx \quad (4.70)$$

$$P_2(t) = \int_0^1 \eta^2(x, t) dx + \int_0^1 w_x^2(x, t) dx \quad (4.71)$$

There exist two positive constants $J_1 > 0$ and $J_2 > 0$ such that

$$J_2 P_2(t) \leq P_1(t) \leq J_1 P_2(t) \quad (4.72)$$

Proof. We start by substituting (4.58) in (4.70) to have

$$\begin{aligned} P_1(t) &= \frac{1}{2} \int_0^1 (\eta^2(x, t) - 2w(0, t)\eta(x, t)(x-1) + w^2(0, t)(x-1)^2) dx + \frac{1}{2} \int_0^1 p_2 e^{bx} w_x^2(x, t) dx \\ &\leq \frac{1}{2} \int_0^1 \eta^2(x, t) dx + |w(0, t)| \int_0^1 |x-1| |\eta(x, t)| dx + \frac{1}{6} w^2(0, t) + \frac{1}{2} \int_0^1 p_2 e^{bx} w_x^2(x, t) dx \end{aligned} \quad (4.73)$$

By using Cauchy-Schwartz inequality we get

$$\begin{aligned} P_1(t) &\leq \frac{1}{2} \int_0^1 \eta^2(x, t) dx + |w(0, t)| \left(\int_0^1 \eta^2(x, t) dx \right)^{\frac{1}{2}} \left(\int_0^1 |x-1|^2 dx \right)^{\frac{1}{2}} + \frac{1}{6} w^2(0, t) \\ &\quad + \frac{1}{2} \int_0^1 p_2 e^{bx} w_x^2(x, t) dx \\ &\leq \frac{1}{2} \int_0^1 \eta^2(x, t) dx + \frac{1}{\sqrt{3}} |w(0, t)| \left(\int_0^1 \eta^2(x, t) dx \right)^{\frac{1}{2}} + \frac{1}{6} w^2(0, t) + \frac{1}{2} \int_0^1 p_2 e^{bx} w_x^2(x, t) dx \end{aligned} \quad (4.74)$$

We have by Young's inequality that

$$\frac{1}{\sqrt{3}} |w(0, t)| \left(\int_0^1 \eta^2(x, t) dx \right)^{\frac{1}{2}} \leq \frac{1}{6} w^2(0, t) + \frac{1}{2} \int_0^1 \eta^2(x, t) dx \quad (4.75)$$

Hence, inserting (4.75) in (4.74) we get

$$P_1(t) \leq \int_0^1 \eta^2(x, t) dx + \frac{1}{3} w^2(0, t) + \frac{1}{2} \int_0^1 p_2 e^{bx} w_x^2(x, t) dx \quad (4.76)$$

By Agmon's inequality, we have that

$$\frac{1}{3} w^2(0, t) \leq \frac{4}{3} \int_0^1 w_x^2(x, t) dx \quad (4.77)$$

and (4.76) becomes

$$\begin{aligned} P_1(t) &\leq \int_0^1 \eta^2(x, t) dx + \left(\frac{4}{3} + \frac{1}{2} p_2 e^b\right) \int_0^1 w_x^2(x, t) dx \\ &\leq J_1 P_2(t) \end{aligned} \quad (4.78)$$

with $J_1 = \frac{4}{3} + \frac{1}{2} p_2 e^b$. In exactly the same way, but starting by $P_2(t)$ and substituting (4.58), one can easily find the second constant $J_2 = \frac{1}{\max(4, \frac{11}{3p_2})}$ and this concludes the proof. \square

Lemma 4.3.3. *Consider the target system 2 $\{\eta(x, t), w(x, t)\}$ with arbitrary initial conditions $\{\eta(x, 0), w(x, 0)\}$ satisfying the compatibility conditions. If there exist $\delta_1 > 0$ and two control variables $c > 0$ and $T(x, y)$ such that condition (4.64) is satisfied, then the equilibrium $\eta \equiv w \equiv 0$ is exponentially stable in the $L^2 \times H^1$ sense.*

Proof. Consider the Lyapunov function

$$\begin{aligned} V_2(t) &= \frac{1}{2} \int_0^1 \eta^2(x, t) dx + \frac{1}{2} \int_0^1 w^2(x, t) dx + \frac{1}{2} \int_0^1 w_x^2(x, t) dx \\ &= P_2(t) + \frac{1}{2} \int_0^1 w^2(x, t) dx \end{aligned} \quad (4.79)$$

Noticing that

$$\frac{d}{dt} \left(\frac{1}{2} \int_0^1 p_1 e^{ax} w^2(x, t) dx \right) = -\frac{p_1}{2} w^2(0, t) - a \left(\frac{1}{2} \int_0^1 p_1 e^{ax} w^2(x, t) dx \right) \quad (4.80)$$

which gives the exponential stability of the transport state $w(x, t)$ in the L^2 sense independently from the diffusion state $\eta(x, t)$. Then by using (4.72) and the results obtained in lemma 4.3.1, the exponential decay of $V_2(t)$ follows directly and concludes the proof. \square

Remark 4.3.1. *After the time $t_F = 1s$, the target system 2 is only diffusive and its stability depends on the magnitude of $C_1(x, y)$. It is useful to view $C_1(x, y)$ as a function of the parameters as $C_1(\lambda, \sigma, S, c, T)$. The parameter c is interpreted as a convergence rate parameter. If $c = 0$, the free variable $T(x, y)$ helps in finding δ_1 such that (4.64) is satisfied. Otherwise i.e. if $T(x, y) = 0$, the stability condition (4.64) will depend only on the magnitude of the system's parameters ($\lambda(x)$, $\sigma(x)$, $S(x, y)$). Since the dependency of $C_1(x, y)$ on c and $T(x, y)$ is extremely convoluted, we use a search algorithm to find the admissible values of c and $T(x, y)$ that satisfy (4.64) (as illustrated in Section 4.4).*

As the stability of the system $\{\eta(x, t), w(x, t)\}$ is proven, we can go in the backward direction using transformations 1 and 2 to prove stability of the initial system $\{v(x, t), u(x, t)\}$.

Theorem 4.3.1. *Consider the system (4.1)-(4.5) with arbitrary initial conditions $\{v(x, 0), u(x, 0)\}$ satisfying the compatibility conditions, with feedback control gains $F_1(t)$ and $F_2(t)$ given in (4.22) and (4.43), respectively. If there exist $\delta_1 > 0$ and two control variables $c > 0$ and $T(x, y)$ such that condition (4.64) is satisfied, the equilibrium $u \equiv v \equiv 0$ is exponentially stable in the $L^2 \times H^1$ sense.*

Proof. Consider the Lyapunov function

$$V_3(t) = \|(v(\cdot, t), u(\cdot, t))\|_{L^2 \times H^1}^2 = \frac{1}{2} \int_0^1 v^2(x, t) + u^2(x, t) + u_x^2(x, t) dx \quad (4.81)$$

Starting from the system $\{\eta(x, t), w(x, t)\}$, using the direct and inverse transformations (4.23)-(4.26) with the boundedness of their kernels, also Young's and Cauchy-Schwartz inequalities, one can find a bound that relates the target system 1 to target system 2:

$$\alpha_1 \|(z(\cdot, t), u(\cdot, t))\|_{L^2 \times H^1}^2 \leq \|(\eta(\cdot, t), w(\cdot, t))\|_{L^2 \times H^1}^2 \leq \alpha_2 \|(z(\cdot, t), u(\cdot, t))\|_{L^2 \times H^1}^2 \quad (4.82)$$

with $\alpha_1, \alpha_2 > 0$. In the same way, and using the invertibility of transformation 1 with the boundedness of the gain kernels, and applying Young's and Cauchy-Schwarz inequalities, we can derive the following bound that relates target system 1 to the plant (4.1)-(4.5)

$$\alpha_3 \|(v(\cdot, t), u(\cdot, t))\|_{L^2 \times H^1}^2 \leq \|(z(\cdot, t), u(\cdot, t))\|_{L^2 \times H^1}^2 \leq \alpha_4 \|(v(\cdot, t), u(\cdot, t))\|_{L^2 \times H^1}^2 \quad (4.83)$$

with $\alpha_3, \alpha_4 > 0$. By Lemma 4.3.3, we have that the target system 2 is exponentially decaying. Then by applying (4.82) and (4.83), there exist two real positive constants q and M such that:

$$\|(v(\cdot, t), u(\cdot, t))\|_{L^2 \times H^1} \leq M e^{-qt} \|v(x, 0), u(x, 0)\|_{L^2 \times H^1} \quad (4.84)$$

which completes the proof. \square

4.4 Numerical Simulation Results

The performance of the control architecture is evaluated on its ability to stabilize an unstable open loop system. We have performed simulations taking into consideration the two mentioned reasons for instability (see Section 4.2) i.e. we choose $\lambda = 3 > \frac{\pi^2}{4}$, $\sigma(x) = 4$, $S(x, y) = 5e^{1-y} \cos(x)$. As predicted from the chosen values of $(\lambda, \sigma(x), S(x, y))$, the plant is open loop unstable and this is confirmed by the response in Fig. 4.6. The second step is to calculate the two controllers $F_1(t)$ and $F_2(t)$ that stabilize the system. This requires solving offline the kernels $K(x, y)$, $L(x, y)$, $M(x, y)$ and $P(x, y)$ to obtain the controller gains. Two unknowns are required to solve the kernels: c and $T(x, y)$.

4.4.1 Calculation of c and $T(x, y)$

The two control variables c and $T(x, y)$ are principally calculated to ensure that inequality (4.64) is satisfied. We proceed in the following order:

- fix the variables c and δ_1 as the speed of convergence parameters;
- $T(x, y)$ is written using Legendre polynomials as follows, $\forall(x, y) \in \Omega_1$:

$$T(x, y) = \sum_{p=0}^N \sum_{q=0}^N \alpha_{p,q} P_p(x) P_q(y) \quad (4.85)$$

where $\alpha_{0,0}, \dots, \alpha_{N,N}$ are some constant coefficients, $P_q(x)$ is the q^{th} order Legendre polynomial, N is the order of the Legendre polynomials;

- we write the kernels $K(x, y)$ and $L(x, y)$ in the integral form (see [74]), these equations are approximated using the left Riemann sum approximation. Afterwards, the $M(x, y)$ kernel is discretized and calculated using a finite differences scheme. The kernels $P(x, y)$, $C_1(x, y)$ and $C_2(x, y)$ are calculated using the integral equations (4.46), (4.41) and (4.42) respectively;
- using a Monte-Carlo simulation method, we solve

$$\max_{\alpha_{p,q}} |C_1| < \frac{\pi^2}{4} + c - \delta_1 \quad (4.86)$$

to find the values of the constants $\alpha_{p,q}$. We start the search algorithm with zero degree of freedom polynomials i.e. $T(x, y) = cst$. The level of complexity can be increased to include more degrees of freedom in case of difficulties in finding solutions.

For the values of the system parameters mentioned above, inequality (4.64) was solved for $c = 1$, $\delta_1 = 0.85$ and a constant value for $T(x, y) = T = -1.67$. The controller gains are given on Fig. 4.7. Actuating the system with the two feedback control laws $F_1(t)$ and $F_2(t)$ shown in Fig. 4.8 quickly drives the system exponentially to zero after exhibiting some transient behavior due to the initial conditions, as shown by the closed loop response on Fig.4.9.

4.5 Conclusion

We have presented in this chapter a boundary control architecture for a system of coupled hyperbolic-parabolic equations. The plant under consideration has couplings in both directions, i.e. from the hyperbolic side to the parabolic side and vice versa. The control design is based on using backstepping transformations to map the initial system into an exponentially stable target system. With a clever choice of the target systems, the resulting kernel equations were very similar to the ones obtained in previous control designs [54, 30, 31] which makes the presented structure simple and familiar to implement. We have also illustrated the effectiveness of the boundary control on an unstable plant using numerical simulations.

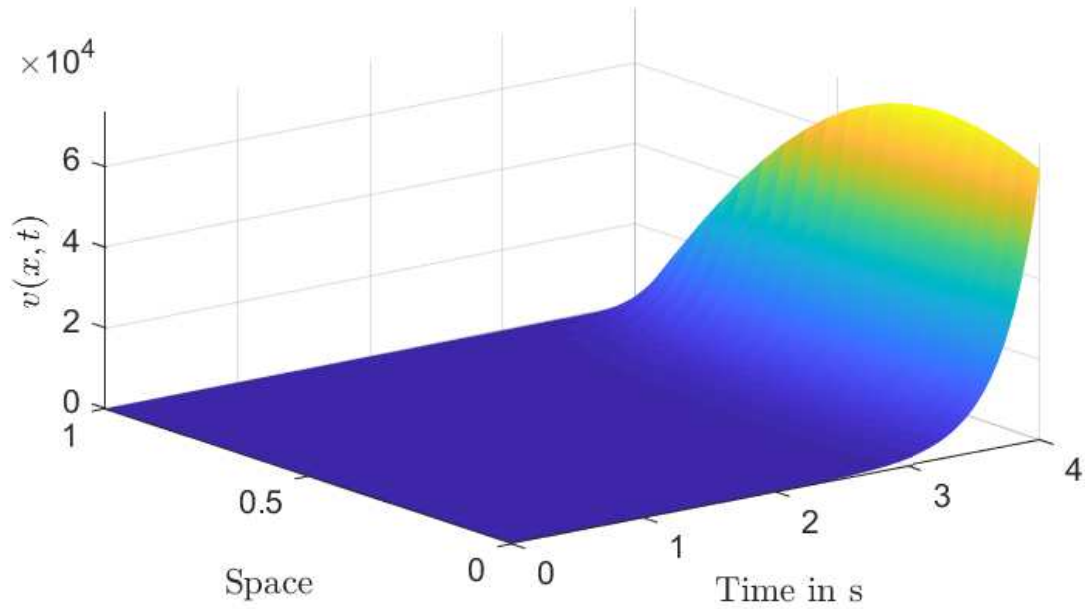
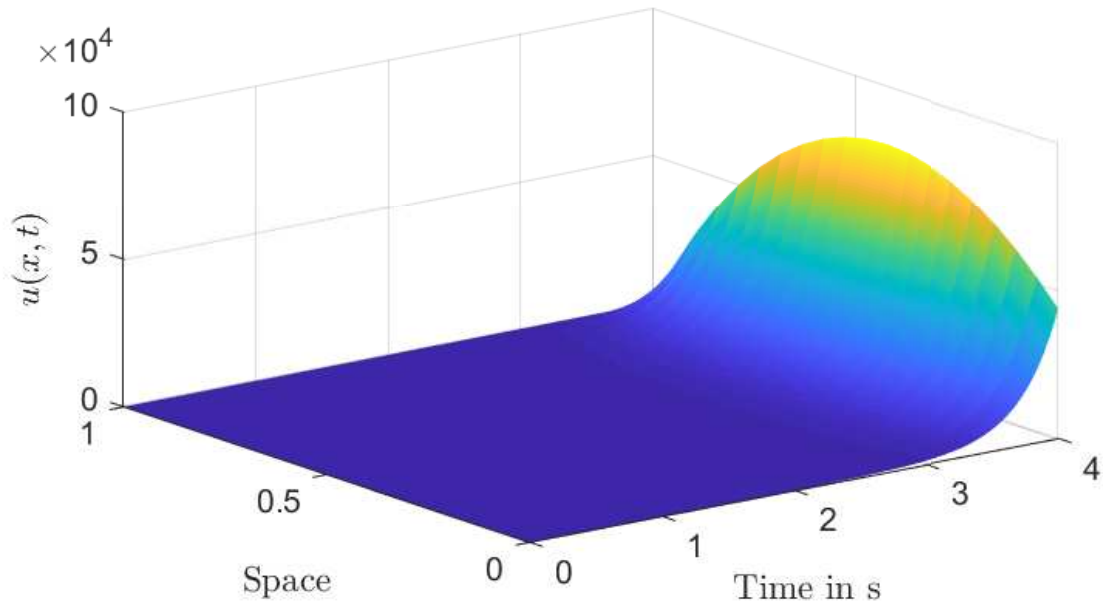


Figure 4.6: The unstable system in open loop.

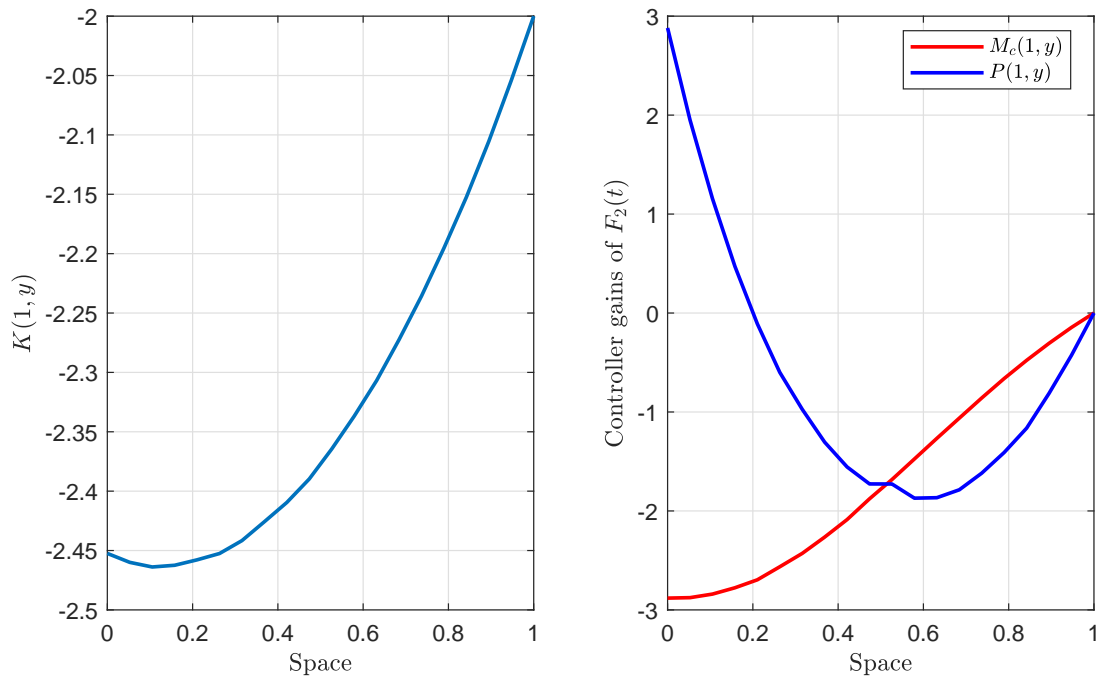


Figure 4.7: The control gain kernels.

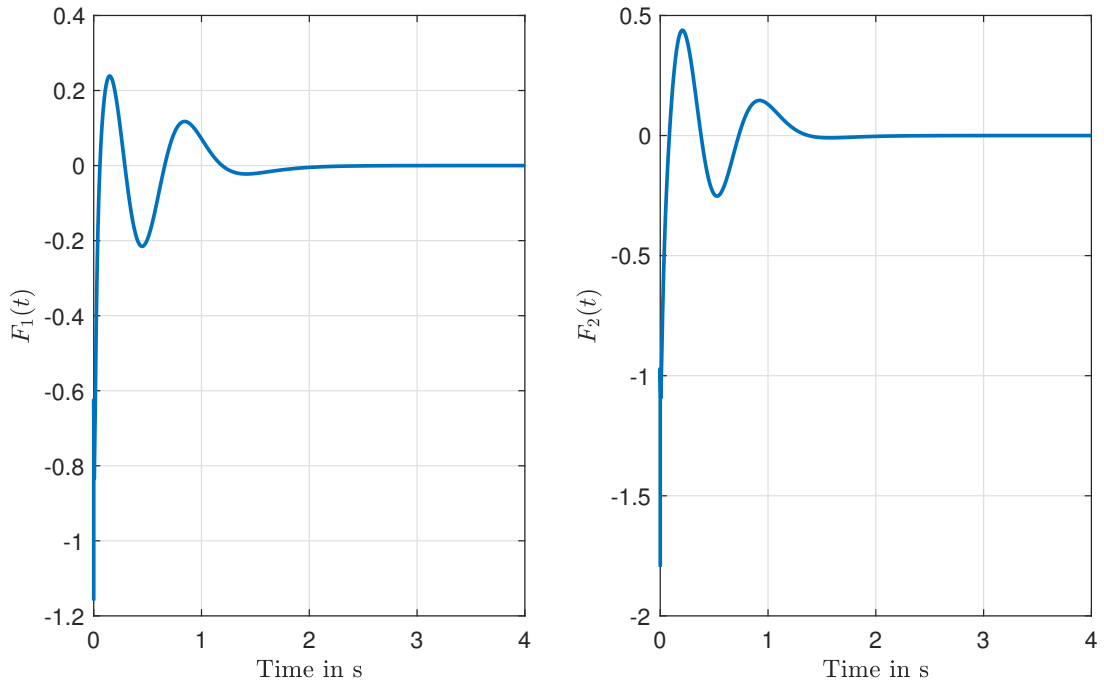


Figure 4.8: The two controllers $F_1(t)$ and $F_2(t)$.

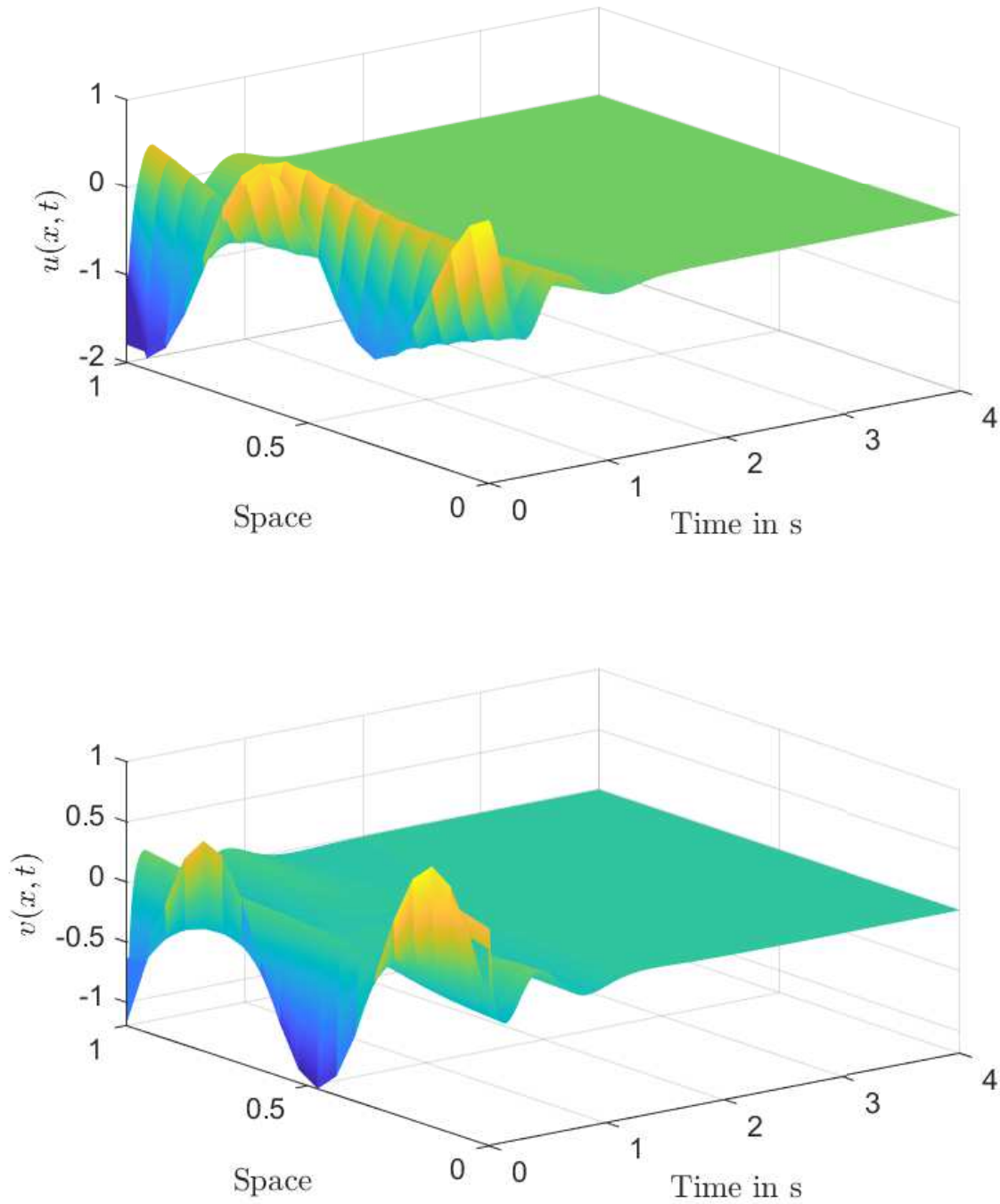


Figure 4.9: The exponentially stable closed loop system.

The primary difficulty of using backstepping design on systems of mixed-classes is the different number of space derivatives corresponding to each family in the overall plant. It is well known that the backstepping method is very powerful when dealing with coupled systems of same class, but the topic of stabilizing different classes of coupled systems is still under research.

The class of systems investigated in the paper is a step towards other interesting hyperbolic-parabolic models resulting from various physical applications, that do not have an integral term in the advective flow (just reactive coupling). Such systems appear in refrigeration cycles and specially in heat exchanger networks as we have shown in Chapter 1. This adds more importance in studying to which extent we can apply the backstepping technique on mixed classes of hyperbolic-parabolic systems.

Chapter 5

Adaptive Boundary Observer Design for coupled ODEs-Hyperbolic PDEs systems

We consider the state estimation of n_ξ hyperbolic PDEs coupled with n_X ordinary differential equations at the boundary. The hyperbolic system is linear and propagates in the positive x -axis direction. The ODE system is linear time varying (LTV) and includes a set of n_θ unknown constant parameters, which are to be estimated simultaneously with the PDE and the ODE states using boundary sensing. A schematic diagram of the system is given on Fig. 5.1.

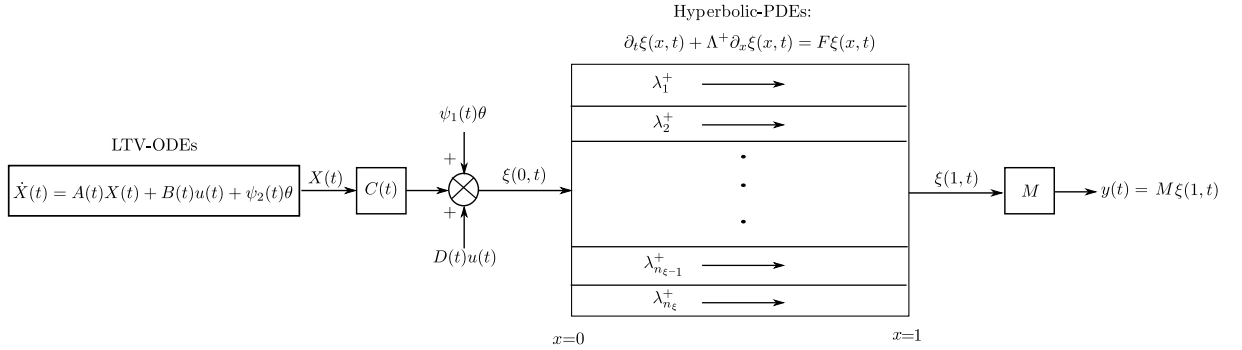


Figure 5.1: PDE - ODE network

The system is governed by the following dynamics evolving in $\Omega=[0, 1] \times [0, +\infty)$:

$$\partial_t \xi(x, t) + \Lambda^+ \partial_x \xi(x, t) = F\xi(x, t) \quad (5.1)$$

$$\xi(0, t) = C(t)X(t) + D(t)u(t) + \psi_1(t)\theta \quad (5.2)$$

$$\dot{X}(t) = A(t)X(t) + B(t)u(t) + \psi_2(t)\theta \quad (5.3)$$

where $\xi(x, t) : \Omega \mapsto \mathbb{R}^{n_\xi}$ is the PDE state vector, $X(t) : [0, +\infty) \mapsto \mathbb{R}^{n_x}$ is the ODE state vector, $\theta \in \mathbb{R}^{n_\theta}$ is the vector of the unknown parameters, $u(t) : [0, +\infty) \mapsto \mathbb{R}^{n_u}$ is a known input vector that possibly depends on $\xi(1, t)$ and $\Lambda^+ \in D_+^{n_\xi}$ is the matrix of the constant transport speeds:

$$\Lambda^+ = \begin{bmatrix} \lambda_1 & & 0 \\ & \ddots & \\ 0 & & \lambda_{n_\xi} \end{bmatrix} \quad \text{with} \quad 0 < \lambda_1 < \dots < \lambda_{n_\xi} \quad (5.4)$$

$F \in \mathbb{R}^{n_\xi \times n_\xi}$. $A(t) \in \mathbb{R}^{n_x \times n_x}$ is the ODE state matrix, $B(t) \in \mathbb{R}^{n_x \times n_u}$ is the ODE input matrix, $C(t) \in \mathbb{R}^{n_\xi \times n_x}$ is the ODE output matrix, $D(t) \in \mathbb{R}^{n_\xi \times n_u}$ is the PDE input matrix and $\psi_1(t) \in \mathbb{R}^{n_\xi \times n_\theta}$ and $\psi_2(t) \in \mathbb{R}^{n_x \times n_\theta}$ are the parameters regressor matrices on the PDE and ODE sides, respectively. We assume that all the time-dependent matrices are bounded and piece-wise continuous in time.

Recall that the goal is to estimate $\xi(x, t)$, $X(t)$ and θ assuming that the following measurements are available:

$$y(t) = M\xi(1, t) \quad (5.5)$$

where $M \in \mathbb{R}^{n_y \times n_\xi}$ is the PDE output matrix.

Remark 5.0.1. *It is obvious that the problem is not feasible if $C(t) = 0$ or $M = 0$. It is also not feasible if $\psi_1(t) = \psi_2(t) = 0$. Such conditions on system matrices will become more clear as we proceed in the analysis in the next sections.*

5.1 Literature review

In Chapter 1, we have stated the various physical systems that can be modeled by the networks of coupled PDE-ODE dynamics, and we specifically focused on the exhaust systems of diesel engines equipped with EGR loops. Practically speaking, boundary control and observation of these kinds of systems is more realistic than the distributed ones, since actuators and sensors are more frequently placed at the extremities of the domain. In addition, we may not have complete knowledge of the system's parameters on both the PDE and the ODE sides. This adds more complexity to the control and the observer designs in view of the limited amount of available measurements. In short, the idea of developing adaptive boundary controls and observers for coupled ODEs-hyperbolic PDEs systems is a necessity if we consider the significant number of physical applications.

Boundary control of ODEs coupled-hyperbolic PDEs systems is well established in the literature. Using Lyapunov design, the authors in [26] derived control laws to stabilize a system of linear hyperbolic system with dynamic boundary conditions. Sufficient conditions for the exponential convergence of the system were given by linear matrix inequalities (LMIs). In a different approach, the authors in [56] have used the theory of backstepping to stabilize an LTI system with an arbitrary input delay. The system is modeled as a transport equation coupled with an LTI system at the boundary. Moreover, the authors in [1], [9] consider 2×2 linear hyperbolic systems with boundary disturbances. In their work, they modeled the disturbance using an LTI system and they applied backstepping control to the resulting coupled ODE-PDE

system. In a recent work, the authors in [36] extended the mentioned approaches to systems of heterodirectional hyperbolic PDEs coupled with ODEs at the boundary.

Boundary observers for ODEs-coupled hyperbolic PDEs are less investigated in the literature. The authors in [25] designed a Luenberger observer for systems of linear and quasilinear hyperbolic systems with dynamic boundary conditions which are asymptotically stable. This approach was later extended by the authors in [41] to linear hyperbolic systems coupled with possibly unstable LTI systems. By keeping the same observer architecture in [25] but using a non-diagonal quadratic Lyapunov function, the authors in [41] have derived sufficient conditions for the exponential stability of the observer through bilinear matrix inequalities (BMIs). On the other hand, backstepping boundary observer designs are also investigated for coupled ODEs-hyperbolic PDEs systems. The authors in [56] synthesized an observer for LTI systems with arbitrary constant delay in the sensor measurement. The delay is interpreted as a first order transport equation and a backstepping observer design is used on the resulting coupled LTI-PDE system. This work was later extended by the authors in [48] to a 2×2 hyperbolic system coupled with a linear LTI system at the boundary.

All the results mentioned so far assume a perfect knowledge of the system. In many practical cases, some model parameters are unknown, which motivates the need for adaptive estimators. The objective of an adaptive boundary observer is to simultaneously construct the distributed PDE states, the ODE states and the unknown parameters from only boundary sensing. In fact, few results exist in the literature on the adaptive design for coupled ODEs-hyperbolic PDEs system. The authors in [10] synthesize an adaptive observer for a 2×2 hyperbolic system coupled with an uncertain LTI system. The design was done in several steps. The first step is to estimate the unknown parameters by extracting some delayed measurements from the system. The second step is to build a Luenberger state observer for the ODE states and the third step is to use swapping filters to generate estimates of the PDE states.

5.1.1 Contribution

We consider the observer design of a system of linear positive speed transport equations coupled with linear time varying ODEs at the boundary (model (5.1)-(5.3)). The system involves a set of unknown constant disturbances to be estimated. As we have explained in Chapter 1, such class of systems can be extended to model the air-path in exhaust gas systems equipped with dual-loop (EGR) for diesel car engines (see e.g. [27]). We address the estimation problem using a different methodology than the one presented in [10]. We propose an adaptive observer architecture that is built directly on the plant model, so that all states are estimated simultaneously in one step and with no necessity to require asymptotic stability of the ODE states. Inspired by the swapping design techniques (see [53] for ODEs and [74] for PDEs), we decouple the state estimation error of the infinite PDE states from the finite dimensional states of the ODEs and the parameters. Then we give sufficient conditions through differential Lyapunov inequalities (DLIs) to ensure the exponential convergence of the error system using Lyapunov analysis.

The work of this chapter is published in:

M.Ghousein, E.Witrant. “Adaptive Boundary Observer Design for coupled ODEs-Hyperbolic

PDEs systems". In: *21st IFACWorld Congress*, IFAC (2020), Invited session.

The chapter is organized as follows: the adaptive observer architecture is presented in Section 5.2. In Sections 5.3 - 5.4 we show the convergence analysis of the estimation error system. Section 5.5 is dedicated to the simulation results for a showcase example and some concluding remarks are given in Section 5.6.

Notation

The symbols S_+^n and D_+^n represent the set of real $n \times n$ symmetric positive definite matrices and the set of real $n \times n$ diagonal positive definite matrices, respectively. For a symmetric matrix A , positive and negative definiteness are denoted, respectively, by $A \succ 0$ and $A \prec 0$. In partitioned symmetric matrices, the \bullet stands for symmetric blocks. For a vector $z \in \mathbb{R}^n$, $|z|$ is the euclidean norm. Given a matrix $A \in \mathbb{R}^{n \times m}$, $\|A\|_\infty = \max |a_{ij}|$ for all $1 \leq i \leq n$ and $1 \leq j \leq m$. Let $V \subseteq \mathbb{R}^n$ and $f : [0, 1] \mapsto V$, we denote by $\|f\|_{\mathbb{L}^2([0,1]^n)} = \sqrt{\int_0^1 |f(x)|^2 dx}$ the \mathbb{L}^2 norm of f . If $f \in \mathbb{L}^2([0, 1]^n)$, then $\|f\|_{\mathbb{L}^2([0,1]^n)} < +\infty$.

5.2 Adaptive Observer Design

We introduce the following adaptive observer design:

$$\partial_t \hat{\xi}(x, t) + \Lambda^+ \partial_x \hat{\xi}(x, t) = F \hat{\xi}(x, t) + p(x, t)(y(t) - M \hat{\xi}(1, t)) + K_1(x, t) \quad (5.6)$$

$$\hat{\xi}(0, t) = C(t) \hat{X}(t) + D(t)u(t) + \psi_1(t) \hat{\theta}(t) \quad (5.7)$$

$$\dot{\hat{X}}(t) = A(t) \hat{X}(t) + B(t)u(t) + \psi_2(t) \hat{\theta}(t) + L(t)(y(t) - M \hat{\xi}(1, t)) \quad (5.8)$$

where $p(x, t): \Omega \mapsto \mathbb{R}^{n_\xi \times n_y}$ and $L(t): [0, +\infty) \mapsto \mathbb{R}^{n_x \times n_y}$ are the observer gains. $K_1(x, t): \Omega \mapsto \mathbb{R}^{n_\xi}$ is an additional feedback gain to be defined later. We denote the estimates by hat, and we define the estimation error variables $\tilde{\xi}(x, t) = \xi(x, t) - \hat{\xi}(x, t)$, $\tilde{X}(t) = X(t) - \hat{X}(t)$ and $\tilde{\theta}(t) = \theta - \hat{\theta}(t)$. By subtracting (5.6)-(5.8) from (5.1)-(5.3), we have the following error dynamics:

$$\partial_t \tilde{\xi}(x, t) + \Lambda^+ \partial_x \tilde{\xi}(x, t) = F \tilde{\xi}(x, t) - p(x, t)M \tilde{\xi}(1, t) - K_1(x, t) \quad (5.9)$$

$$\tilde{\xi}(0, t) = C(t) \tilde{X}(t) + \psi_1(t) \tilde{\theta}(t) \quad (5.10)$$

$$\dot{\tilde{X}}(t) = A(t) \tilde{X}(t) + \psi_2(t) \tilde{\theta}(t) - L(t)M \tilde{\xi}(1, t) \quad (5.11)$$

The observer designed in (5.6)-(5.8) is of Luenberger-type, which is a copy of the original system with output injections $y(t)$, and an additional feedback gain $K_1(x, t)$. Our objective is then to find the observer gains $p(x, t)$ and $L(t)$, and a proper parameter estimation law that can guarantee the exponential convergence of the estimation error in (5.9)-(5.11).

Remark 5.2.1. *The measurement corrections are introduced in the PDE interior domain and in the ODE dynamics only. The first correction which is multiplied by $p(x,t)$ is used in the PDE-ODE decoupling procedure as we will show in the next section. The second one which is multiplied by $L(t)$ is used in the ODE stabilization. Both observer gains are time varying since the ODE dynamics are as such.*

5.3 PDE-ODE Decoupling by Swapping Design

We parameterize the PDE state estimation error $\tilde{\xi}(x,t)$ in (5.9)-(5.11) using K-filters (see [53] for ODEs and [74] for PDEs) as follows:

$$\tilde{\xi}(x,t) = \tilde{\phi}(x,t) + T(x,t)\tilde{X}(t) + R(x,t)\tilde{\theta}(t) \quad (5.12)$$

The swapping filters: $T(x,t): \Omega \mapsto \mathbb{R}^{n_\xi \times n_x}$ and $R(x,t): \Omega \mapsto \mathbb{R}^{n_\xi \times n_\theta}$ will be defined later. Equation (5.12) means that the PDE estimation error $\tilde{\xi}(x,t)$ is a superposition of three errors: 1) the error due to the PDE unknown initial conditions, and is represented by $\tilde{\phi}(x,t)$, 2) the error $\tilde{X}(t)$ due to the ODE unknown initial conditions, filtered by $T(x,t)$ and 3) the error $\tilde{\theta}(t)$ due to the unknown parameters, filtered by $R(x,t)$.

Differentiating (5.12) with respect to time and space we get

$$\begin{aligned} \partial_t \tilde{\xi}(x,t) + \Lambda^+ \partial_x \tilde{\xi}(x,t) - F \tilde{\xi}(x,t) + p(x,t)M \tilde{\xi}(1,t) + K_1(x,t) &= \partial_t \tilde{\phi}(x,t) + \partial_t T(x,t)\tilde{X}(t) \\ &+ T(x,t)\dot{\tilde{X}}(t) + \partial_t R(x,t)\tilde{\theta}(t) + R(x,t)\dot{\tilde{\theta}}(t) + \Lambda^+ \partial_x \tilde{\phi}(x,t) + \Lambda^+ \partial_x T(x,t)\tilde{X}(t) \\ &+ \Lambda^+ \partial_x R(x,t)\tilde{\theta}(t) - F \tilde{\phi}(x,t) - FT(x,t)\tilde{X}(t) - FR(x,t)\tilde{\theta}(t) + p(x,t)M \tilde{\xi}(1,t) \\ &+ K_1(x,t) \end{aligned} \quad (5.13)$$

Now, substituting with (5.11) and grouping the relative terms together

$$\begin{aligned} 0 &= (\partial_t \tilde{\phi}(x,t) + \Lambda^+ \partial_x \tilde{\phi}(x,t) - F \tilde{\phi}(x,t)) + (\partial_t T(x,t) + \Lambda^+ \partial_x T(x,t) - FT(x,t) \\ &+ T(x,t)A(t))\tilde{X}(t) + (\partial_t R(x,t) + \Lambda^+ \partial_x R(x,t) - FR(x,t) + T(x,t)\psi_2(t))\tilde{\theta}(t) \\ &+ (p(x,t) - T(x,t)L(t))M \tilde{\xi}(1,t) + (K_1(x,t) + R(x,t)\dot{\tilde{\theta}}(t)) \end{aligned} \quad (5.14)$$

Equation (5.14) suggests to choose: $K_1(x,t) = -R(x,t)\dot{\tilde{\theta}}(t) = R(x,t)\dot{\tilde{\theta}}(t)$, $p(x,t) = T(x,t)L(t)$ and the following dynamics for the swapping filters

$$\partial_t T(x,t) + \Lambda^+ \partial_x T(x,t) = FT(x,t) - T(x,t)A(t) \quad (5.15)$$

$$\partial_t R(x,t) + \Lambda^+ \partial_x R(x,t) = FR(x,t) - T(x,t)\psi_2(t) \quad (5.16)$$

we also impose the following boundary conditions on the filters

$$T(0,t) = C(t), \quad R(0,t) = \psi_1(t) \quad (5.17)$$

Doing so, and using (5.14) and (5.15)-(5.17) the dynamics of $\tilde{\phi}(x, t)$ become

$$\partial_t \tilde{\phi}(x, t) + \Lambda^+ \partial_x \tilde{\phi}(x, t) = F \tilde{\phi}(x, t) \quad (5.18)$$

$$\tilde{\phi}(0, t) = 0 \quad (5.19)$$

The dynamics of $\tilde{\phi}(x, t)$ in (5.18)-(5.19) are totally decoupled from $\tilde{X}(t)$ and $\tilde{\theta}(t)$. This is to confirm the fact that the estimation of the initial conditions of $\xi(x, t)$ are not related to whether there are ODEs or parameters to be estimated.

The objective is to find an adaptation law to update $\hat{\theta}(t)$ and then to prove the convergence $\{\tilde{\xi}(x, t), \tilde{X}(t), \tilde{\theta}(t)\}$ in the L^2 sense.

5.4 Exponential convergence of $\{\tilde{\xi}(x, t), \tilde{X}(t), \tilde{\theta}(t)\}$ in the L^2 sense

The plan for the convergence analysis is as follows. Since $\xi(x, t)$ is written as a function of $\tilde{\phi}(x, t)$, $\tilde{X}(t)$ and $\tilde{\theta}(t)$ using (5.12), the idea is first to give sufficient conditions that guarantee the exponential convergence of $\{\tilde{\phi}(x, t), \tilde{X}(t), \tilde{\theta}(t)\}$ in the L^2 sense along with the boundedness of the filters $T(x, t)$ and $R(x, t)$, also in the L^2 sense. In this way, by (5.12), we can conclude directly on the exponential convergence of $\{\tilde{\xi}(x, t), \tilde{X}(t), \tilde{\theta}(t)\}$. This is what we establish in the following series of Lemmas.

Lemma 5.4.1. *Consider the system (5.18)-(5.19) with initial condition $\tilde{\phi}_0(x) \in (\mathbb{L}^2([0, 1]))^{n_\xi}$. Then for all $\gamma_\phi > 0$, there exists $C_\phi > 0$ such that:*

$$\|\tilde{\phi}(\cdot, t)\|_{(\mathbb{L}^2([0, 1]))^{n_\xi}} \leq C_\phi e^{-\gamma_\phi t} \|\tilde{\phi}_0(x)\|_{\mathbb{L}^2([0, 1])^{n_\xi}} \quad (5.20)$$

Furthermore, the equilibrium $\tilde{\phi} \equiv 0$ is reached in finite time $t_f = \frac{1}{\lambda_1}$.

Proof. Consider the following quadratic Lyapunov function

$$V_1(t) = \int_0^1 (\tilde{\phi}^T(x, t) P_1 \tilde{\phi}(x, t)) e^{-\mu x} dx \quad (5.21)$$

where $P_1 \in D_+^{n_\xi}$ and $\mu > 0$. Deriving (5.21) in time, substituting with (5.18), integrating by parts and then substituting with (5.19) yields to:

$$\dot{V}_1(t) = -\tilde{\phi}^T(1, t) \Lambda^+ P_1 e^{-\mu} \tilde{\phi}(1, t) + \int_0^1 \tilde{\phi}^T(x, t) [-\mu \Lambda^+ P_1 + F^T P_1 + P_1 F] e^{-\mu x} \tilde{\phi}(x, t) dx \quad (5.22)$$

The matrix $\Lambda^+ P_1 e^{-\mu}$ is always positive definite for any $P_1 \in D_+^{n_\xi}$. In addition, for all $\gamma_\phi > 0$ we can always choose μ large enough to have $-\mu \Lambda^+ P_1 + F^T P_1 + P_1 F \leq -\gamma_\phi P_1$. Thus, $\dot{V}_1(t) \leq -\gamma_\phi V_1(t)$, and since $V_1(t)$ is just the weighted L^2 norm of $\tilde{\phi}(x, t)$, this shows the exponential convergence of $\tilde{\phi}$ in the L^2 norm.

Given that $\Lambda^+ \in D_+^{n_\xi}$, we can change the status of t and x and rewrite (5.18) as:

$$\partial_x \tilde{\phi}(x, t) + (\Lambda^+)^{-1} \partial_t \tilde{\phi}(x, t) = (\Lambda^+)^{-1} F \tilde{\phi}(x, t) \quad (5.23)$$

and then (5.19) becomes a zero initial condition for (5.23). Then the uniqueness of solutions of (5.23)-(5.19) and the order of the transport speeds given in equation (5.4) imply that $\tilde{\phi}(x, t)$ vanishes after $t \geq \frac{1}{\lambda_1}$ (see Lemma 3.1 in [50]) and this concludes the proof. \square

Lemma 5.4.2. *Consider the filter systems $T(x, t)$ and $R(x, t)$ defined in (5.15)-(5.16) with boundary conditions (5.17). Then for all initial conditions $T_0(x) \in (L^2([0, 1]))^{n_\xi \times n_X}$ and $R_0(x) \in (L^2([0, 1]))^{n_\xi \times n_\theta}$, the PDE filters $T(x, t)$ and $R(x, t)$ are bounded in the L^2 sense.*

Proof. First, we start by $T(x, t)$. We write (5.15)-(5.17) using the index notation: for all $1 \leq i \leq n_\xi$, $1 \leq j \leq n_X$, we have

$$\partial_t T_{ij}(x, t) + \lambda_i \partial_x T_{ij}(x, t) = \sum_{k=1}^{n_\xi} F_{ik} T_{kj}(x, t) - \sum_{k=1}^{n_X} T_{ik}(x, t) a_{kj}(t) \quad (5.24)$$

$$T_{ij}(0, t) = c_{ij}(t) \quad (5.25)$$

Now, we consider the following Lyapunov function

$$V_T(t) = \sum_{i=1}^{n_\xi} \sum_{j=1}^{n_X} V_{T,ij}(t) = \frac{1}{2} \sum_{i=1}^{n_\xi} \sum_{j=1}^{n_X} \int_0^1 e^{-\mu x} T_{ij}^2(x, t) dx \quad (5.26)$$

with $\mu > 0$. $V_T(t)$ is the weighted L^2 norm of $T(x, t)$. Deriving (5.26) with respect to time, replacing by (5.24), integrating by parts and substituting by (5.25), one gets

$$\begin{aligned} \dot{V}_T(t) = & \sum_{i=1}^{n_\xi} \sum_{j=1}^{n_X} \left[-\frac{1}{2} e^{-\mu} \lambda_i T_{ij}^2(1, t) + \frac{1}{2} \lambda_i c_{ij}^2(t) - \mu \lambda_i V_{T,ij}(t) + \sum_{k=1}^{n_\xi} F_{ik} \int_0^1 e^{-\mu x} T_{kj}(x, t) T_{ij}(x, t) dx \right. \\ & \left. - \sum_{k=1}^{n_X} a_{kj}(t) \int_0^1 e^{-\mu x} T_{ik}(x, t) T_{ij}(x, t) dx \right] \end{aligned} \quad (5.27)$$

Applying Young's inequality to the last two integral terms in (5.27), we get

$$\dot{V}_T(t) \leq \sum_{i=1}^{n_\xi} \sum_{j=1}^{n_X} \left[\frac{1}{2} \lambda_i c_{ij}^2(t) + \left(-\mu \lambda_i + \sum_{k=1}^{n_\xi} (|F_{ik}| + |F_{ki}|) + \sum_{k=1}^{n_X} (|a_{kj}(t)| + |a_{jk}(t)|) \right) V_{T,ij}(t) \right] \quad (5.28)$$

Denoting by $F_{max} = \|F\|_\infty$ and $A_{max} = \max_{t \geq 0} \|A(t)\|_\infty$, we can further write (5.28) as

$$\dot{V}_T(t) \leq \sum_{i=1}^{n_\xi} \sum_{j=1}^{n_X} \left[\frac{1}{2} \lambda_i c_{ij}^2(t) + (-\mu \lambda_1 + 2n_\xi F_{max} + 2n_X A_{max}) V_{T,ij}(t) \right] \quad (5.29)$$

We can choose μ large enough to have $-\mu\lambda_1 + 2n_\xi F_{max} + 2n_X A_{max} \leq -\gamma_T$ for every $\gamma_T > 0$. Doing so, (5.29) becomes

$$\dot{V}_T(t) \leq -\gamma_T V_T(t) + \frac{\lambda_{n_\xi}}{2} \|C(t)\|_2^2 \quad (5.30)$$

with $\|C(t)\|_2^2 = \sum_{i=1}^{n_\xi} \sum_{j=1}^{n_X} c_{ij}^2(t)$. Inequality (5.30) shows that $V_T(t)$ is bounded as a direct consequence of the boundedness of the system matrices $A(t)$ and $C(t)$. Since $V_T(t)$ is the weighted L^2 norm of $T(x, t)$, then by (5.30) we can deduce that $T(x, t)$ is bounded in the L^2 sense.

The boundedness of $R(x, t)$ is done following the same methodology. Writing (5.16)-(5.17) using the index notation: for all $1 \leq i \leq n_\xi$, $1 \leq j \leq n_\theta$, we have

$$\partial_t R_{ij}(x, t) + \lambda_i \partial_x R_{ij}(x, t) = \sum_{k=1}^{n_\xi} F_{ik} R_{kj}(x, t) - \sum_{k=1}^{n_X} T_{ik}(x, t) \psi_{2,kj}(t) \quad (5.31)$$

$$R_{ij}(0, t) = \psi_{1,ij}(t) \quad (5.32)$$

Now, we consider the following Lyapunov function

$$V_R(t) = \sum_{i=1}^{n_\xi} \sum_{j=1}^{n_\theta} V_{R,ij}(t) = \frac{1}{2} \sum_{i=1}^{n_\xi} \sum_{j=1}^{n_\theta} \int_0^1 e^{-\mu x} R_{ij}^2(x, t) dx \quad (5.33)$$

Deriving (5.33) with respect to time, replacing by (5.31), integrating by parts, substituting by (5.32) and using Young's inequality, one gets

$$\begin{aligned} \dot{V}_R(t) \leq & \sum_{i=1}^{n_\xi} \sum_{j=1}^{n_\theta} \left[\frac{1}{2} \lambda_i \psi_{1,ij}^2(t) + \left(-\mu\lambda_i + \sum_{k=1}^{n_\xi} (|F_{ik}| + |F_{ki}|) + \sum_{k=1}^{n_X} |\psi_{2,kj}(t)| \right) V_{R,ij}(t) \right] \\ & + \sum_{i=1}^{n_\xi} \sum_{k=1}^{n_X} \sum_{j=1}^{n_\theta} |\psi_{2,kj}(t)| \left(\frac{1}{2} \int_0^1 T_{ik}^2(x, t) dx \right) \end{aligned} \quad (5.34)$$

Denote by $\psi_{2,max} = \max_{t \geq 0} \|\psi_2(t)\|_\infty$ and T_b the L^2 bound on $T(x, t)$, we can further write (5.34) as

$$\dot{V}_R(t) \leq \sum_{i=1}^{n_\xi} \sum_{j=1}^{n_\theta} \left[\frac{1}{2} \lambda_i \psi_{1,ij}^2(t) + \left(-\mu\lambda_i + 2n_\xi F_{max} + n_X \psi_{2,max} \right) V_{R,ij}(t) \right] + n_\theta \psi_{2,max} T_b \quad (5.35)$$

We choose μ large enough to have $-\mu\lambda_i + 2n_\xi F_{max} + n_X \psi_{2,max} \leq -\gamma_R$ for every $\gamma_R > 0$. Then, (5.35) becomes

$$\dot{V}_R(t) \leq -\gamma_R \dot{V}_R(t) + \frac{\lambda_{n_\xi}}{2} \|\psi_1(t)\|_2^2 + n_\theta \psi_{2,max} T_b \quad (5.36)$$

with $\|\psi_1(t)\|_2^2 = \sum_{i=1}^{n_X} \sum_{j=1}^{n_\theta} \psi_{1,ij}^2(t)$. By (5.36), $V_R(t)$ is bounded by the boundedness of $\psi_1(t)$ and $\psi_2(t)$ and so is $R(x, t)$ in the L^2 sense, which concludes the proof. \square

ODE error dynamics and the parameter adaptation law

The ODE dynamics are investigated as follows. We evaluate (5.12) at $x=1$, multiply by M on both sides, and then substitute in (5.11) to have

$$\dot{\tilde{X}}(t) = A_d(t)\tilde{X}(t) + (\psi_2(t) - L(t)MR(1, t))\tilde{\theta}(t) - L(t)M\tilde{\phi}(1, t) \quad (5.37)$$

with $A_d(t)=A(t)-L(t)MT(1, t)$. We introduce the piece-wise continuous shift operator

$$s(t) = \begin{cases} 1 & \text{if } t \geq t_f \\ 0 & \text{else} \end{cases} \quad (5.38)$$

in the observer gain $L(t)$ computation, i.e. we write $L(t) = s(t)l(t)$. The main reason is to remove the effect of the initial conditions of the filters $T(x, t)$ and $R(x, t)$ on the overall adaptive design. Doing so, (5.37) becomes

$$\dot{\tilde{X}}(t) = (A(t) - s(t)l(t)MT(1, t))\tilde{X}(t) + (\psi_2(t) - s(t)l(t)MR(1, t))\tilde{\theta}(t) - s(t)l(t)M\tilde{\phi}(1, t) \quad (5.39)$$

Equation (5.12) at $x=1$ also suggests the following normalized adaptation law:

$$\dot{\hat{\theta}}(t) = -\dot{\tilde{\theta}}(t) = \frac{s(t)P_\theta(t)\Phi^T(t)}{1 + \|\Phi^T(t)\Phi(t)\|^2} M\tilde{\xi}(1, t) \quad (5.40)$$

$$\dot{P}_\theta(t) = s(t) \left[\beta P_\theta(t) - \frac{P_\theta(t)\Phi^T(t)\Phi(t)P_\theta(t)}{1 + \|\Phi^T(t)\Phi(t)\|^2} \right] \quad (5.41)$$

where the regressor $\Phi(t)$ is given by $\Phi(t)=MR(1, t)$. $P_\theta(t): [0, +\infty) \mapsto \mathbb{R}^{n_\theta \times n_\theta}$ and $\beta > 0$ is the forgetting factor. The initial conditions $\hat{\theta}(0) = \hat{\theta}_0$ and $P_\theta(0)=P_{\theta,0}=P_{\theta,0}^T$ are chosen arbitrary. It is useful to illustrate that the adaptation law (5.40)-(5.41) is derived using the superposition principle, i.e. we fix $\tilde{\phi}(1, t)$ and $\tilde{X}(t)$ to zero in order to get the linear regressor equation

$$\tilde{y}(t) = M\tilde{\xi}(1, t) = MR(1, t)\tilde{\theta} \quad (5.42)$$

Then using (5.42), we choose the adaptation law (5.40)-(5.41) to estimate θ . The adaptive law (5.40)-(5.41) is called continuous time recursive least square estimator with a forgetting factor (see [51] for various linear regression estimation techniques). Using (5.40) and (5.12), we now compute the dynamics of $\tilde{\theta}(t)$ as follows

$$\dot{\tilde{\theta}}(t) = -\frac{s(t)P_\theta(t)}{1 + \|\Phi^T(t)\Phi(t)\|^2} \left[\Phi^T(t)\Phi(t)\tilde{\theta}(t) + \Phi^T(t)MT(1, t)\tilde{X}(t) + \Phi^T(t)M\tilde{\phi}(1, t) \right]. \quad (5.43)$$

Remark 5.4.1. *The formulation of (5.39) and (5.43) as a function of $s(t)$ implies that the ODE error stabilization and the parameter adaptation start functioning when the maximum delay time due to transport in space ($t_f = \frac{1}{\lambda_1}$) is passed. One can notice that the stabilization of the error due to unknown PDE initial conditions $\tilde{\phi}(x, t)$ is obtained in finite time t_f , this property is intrinsic to transport equations. In order to obtain finite-time convergence for the ODEs, one should introduce the specific architecture of finite-time observers for ODEs in the adaptive observer design (5.6)-(5.8).*

We combine the ODE error dynamics and the parameter error dynamics in one vector $\tilde{X}_c(t) = \begin{pmatrix} \tilde{X}(t) \\ \tilde{\theta}(t) \end{pmatrix}$ written in the following state-space representation:

$$\dot{\tilde{X}}_c(t) = A_c(t)\tilde{X}_c(t) + B_c(t)\tilde{\phi}(1, t) \quad (5.44)$$

where:

$$A_c(t) = \begin{bmatrix} A(t) - s(t)l(t)MT(1, t) & \psi_2(t) - s(t)l(t)\Phi(t) \\ -\frac{s(t)P_\theta(t)\Phi^T(t)MT(1, t)}{1 + \|\Phi^T(t)\Phi(t)\|^2} & -\frac{s(t)P_\theta(t)\Phi^T(t)\Phi(t)}{1 + \|\Phi^T(t)\Phi(t)\|^2} \end{bmatrix},$$

$$B_c(t) = \begin{bmatrix} -s(t)l(t)M \\ -\frac{s(t)P_\theta(t)\Phi^T(t)M}{1 + \|\Phi^T(t)\Phi(t)\|^2} \end{bmatrix}$$

Hence, the dynamics of the error system written in terms of $\{\tilde{\phi}(x, t), \tilde{X}(t), \tilde{\theta}(t)\}$ is a set of time-varying ODEs $\tilde{X}_c(t)$ driven by the output of an exponentially stable PDE given by $\tilde{\phi}(1, t)$. We are now at a point where we can state the stability result of the $\{\tilde{\phi}(x, t), \tilde{X}(t), \tilde{\theta}(t)\}$ system.

Lemma 5.4.3. *Consider the system (5.18)-(5.19) and (5.39)-(5.43) with initial conditions $(\tilde{\phi}_0(x) \in (L^2([0, 1]))^{n_\xi}, \tilde{X}_0 \in \mathbb{R}^{n_x}, \tilde{\theta}_0 \in \mathbb{R}^{n_\theta})$. If $\Phi(t)$ and $\tilde{\Phi}(t)$ are bounded and persistently exciting (PE), i.e. for all $t \geq t_f$ there exist positive constants T_0, c_0 and c_1 so that:*

$$c_0 I \leq \int_t^{t+T_0} \Phi^T(\tau)\Phi(\tau)d\tau \leq c_1 I \quad (5.45)$$

In addition, if there exist an observer gain $L(t) \in \mathbb{R}^{n_x \times n_y}$ and a bounded matrix $P_X(t) \in S_+^{n_x \times n_x}$ such that, for all $t \geq t_f$:

$$Z(t) \leq -Q(t) \quad (5.46)$$

where $Z(t)$ is given by

$$Z(t) = \begin{bmatrix} \dot{P}_X(t) + A_d^T(t)P_X(t) + P_X(t)A_d(t) & P_X(t)(\psi_2(t) - l(t)MR(1, t)) - \frac{T^T(1, t)M^T\Phi(t)}{1 + \|\Phi^T(t)\Phi(t)\|^2} \\ \bullet & -\beta P_\theta^{-1}(t) - \frac{\Phi^T(t)\Phi(t)}{1 + \|\Phi^T(t)\Phi(t)\|^2} \end{bmatrix} \quad (5.47)$$

and $Q(t)$ is a predefined bounded positive definite matrix. Then for all $t \geq t_f$, the system (5.18)-(5.19) and (5.39)-(5.43) is exponentially stable in the $|\tilde{X}|^2 + |\tilde{\theta}|^2 + \|\tilde{\phi}(\cdot, t)\|_{(L^2([0, 1]))^{n_\xi}}^2$ norm.

Proof. Using (5.41), we compute the dynamics of $P_\theta^{-1}(t)$ (the inverse of $P_\theta(t)$) as:

$$\frac{d}{dt}P_\theta^{-1}(t) = s(t) \left[-\beta P_\theta^{-1}(t) + \frac{\Phi^T(t)\Phi(t)}{1 + \|\Phi^T(t)\Phi(t)\|^2} \right] \quad (5.48)$$

It can be shown (see [51]) that if (5.45) is satisfied, then $P_\theta(t)$ and $P_\theta^{-1}(t)$ are both bounded and positive definite for all $t \geq 0$. Now, let us consider the following Lyapunov function:

$$V_2(t) = \tilde{X}_c^T(t)P_c(t)\tilde{X}_c(t) + \int_0^1 (\tilde{\phi}^T(x, t)P_1\tilde{\phi}(x, t))e^{-\mu x} dx \quad (5.49)$$

where $P_c(t) = \begin{pmatrix} P_X(t) & 0 \\ 0 & P_\theta^{-1}(t) \end{pmatrix}$. $V_2(t)$ is the L^2 norm of $\{\tilde{X}_c(t), \tilde{\phi}(x, t)\}$ weighted by $P_c(t)$ for the ODE dynamics of $\tilde{X}_c(t)$ and by P_1 for PDE dynamics of $\tilde{\phi}(x, t)$. $P_X(t)$ corresponds to the weight on $\tilde{X}(t)$ while $P_\theta^{-1}(t)$ correspond to the weight on $\tilde{\theta}(t)$. Deriving (5.49) with respect to time, we have

$$\dot{V}_2(t) = \dot{\tilde{X}}_c^T(t)P_c(t)\tilde{X}_c(t) + \tilde{X}_c^T(t)\dot{P}_c(t)\tilde{X}_c(t) + \tilde{X}_c^T(t)P_c(t)\dot{\tilde{X}}_c(t) + \dot{V}_1(t) \quad (5.50)$$

Replacing (5.44) in (5.50) leads to:

$$\begin{aligned} \dot{V}_2(t) &= \tilde{X}_c^T(t) \left(\dot{P}_c(t) + A_c^T(t)P_c(t) + P_c(t)A_c(t) \right) \tilde{X}_c(t) + \tilde{\phi}^T(1, t)B_c^T(t)P_c(t)\tilde{X}_c(t) \\ &+ \tilde{X}_c^T(t)P_c(t)B_c(t)\tilde{\phi}(1, t) + \dot{V}_1(t) \end{aligned} \quad (5.51)$$

If $t < t_f$, equation (5.51) becomes

$$\begin{aligned} \dot{V}_2(t) &= \tilde{X}^T(t) \left(\dot{P}_X(t) + A^T(t)P_X(t) + P_X(t)A(t) \right) \tilde{X}(t) + \tilde{\theta}^T(t)\psi_2^T(t)P_X(t)\tilde{X}(t) \\ &+ \tilde{X}^T(t)P_X(t)\psi_2(t)\tilde{\theta}(t) + \dot{V}_1(t) \end{aligned} \quad (5.52)$$

By Lemma 5.4.1, $V_1(t)$ is exponentially stable for all times. Then if $A(t)$ is uniformly exponentially stable (UES) we can guarantee that there exists $P_X(t)$ such that $\dot{P}_X(t) + A^T(t)P_X(t) + P_X(t)A(t) < 0$ (see Theorem 7.4 in [70]) and as a result, the Lyapunov function $V_3(t)$ is upper bounded by the magnitude of $\psi_2(t)$ for all $t < t_f$. Otherwise, i.e. if $A(t)$ is not UES, we choose $P_X(t) = P_X \in S_+^{n_X \times n_X}$ arbitrary, and $V_2(t)$ can be growing for all $t < t_f$.

However, the interesting part of the analysis is when the maximum delay time due to transport in space is passed i.e. when $t \geq t_f$. Using (5.48) it is easy to verify that

$$Z(t) = \dot{P}_c(t) + A_c^T(t)P_c(t) + P_c(t)A_c(t) \quad (5.53)$$

for $t \geq t_f$. Furthermore, using Lemma 5.4.1, $\tilde{\phi}(x, t)$ is L^2 stable and $\tilde{\phi}(1, t) \equiv 0$ is reached in finite time $t_f = \frac{1}{\lambda_1}$. Hence, if (5.46) is satisfied, using (5.51) one gets

$$\dot{V}_2(t) \leq -\tilde{X}_c^T(t)Q(t)\tilde{X}_c(t) - \gamma_\phi V_1(t) \quad (5.54)$$

for all $t \geq t_f$. Thus, by the boundedness of $Q(t)$ there exists a positive constant $\gamma_{tot} > 0$ such that $\dot{V}_2(t) \leq -\gamma_{tot}V_2(t)$, which shows the exponential stability of (5.18)-(5.19) and (5.39)-(5.43) in the $|\tilde{X}|^2 + |\tilde{\theta}|^2 + \|\tilde{\phi}(\cdot, t)\|_{L^2([0,1])}^2$ norm for $t \geq t_f$ and completes the proof. \square

Remark 5.4.2. *The existence of the Lyapunov function (5.49) on the interval $[t_f, +\infty)$ for our observer architecture depends on two intrinsic properties of the system. One is the detectability given by the existence of $P_X(t)$. The other is the persistency of parameter excitation given by the existence of $P_\theta^{-1}(t)$. To illustrate the point, let us reconsider inequality (5.46). A necessary condition for (5.46) to have solutions is that the diagonal elements in $Z(t)$ must be negative definite. If we start by $Z_{11}(t)$, we must have*

$$\dot{P}_X(t) + A_d^T(t)P_X(t) + P_X(t)A_d(t) < 0 \quad (5.55)$$

which is the differential Lyapunov equation in $A_d(t)$. It is well known that (5.55) has a unique solution $P_X(t)$ if $A_d(t)$ is UES. Any time-varying state matrix which is 1) continuously differentiable, 2) bounded, 3) slowly varying and 4) the real part of its Eigen-values is negative for all times, is UES (see e.g. Theorem 8.7 in [70]). For instance if we assume that the first three conditions of Theorem 8.7 in [70] are satisfied for $A_d(t)$ in the interval of time $[t_f, +\infty)$, we still require the real part of its eigen-values to be negative. Let us recall that for $t \geq t_f$, $A_d(t) = A(t) - l(t)MT(1, t)$. We can always choose $l(t)$ such that $A_d(t)$ is Hurwitz if the pair $\{A(t), MT(1, t)\}$ is detectable. If we look into the $T(x, t)$ filter (5.15)-(5.17), we can observe that $T(1, t)$ is a delayed version of $C(t)$ with a change in magnitude due to the coupling F and $A(t)$. Hence, finding $P_X(t)$ is directly related to the detectability of the system $\{A(t), M, C(t)\}$ through the pair $\{A(t), MT(1, t)\}$. On the other hand, $Z_{22}(t)$ is always negative-definite, since $P_\theta^{-1}(t)$ is positive definite and bounded based on the (PE) assumption (5.45). It is important to mention that the condition (5.45) is directly related to the values of $\psi_1(t)$ and $\psi_2(t)$ through $R(1, t)$. For instance, if $\psi_1 \equiv \psi_2 \equiv 0$ then by (5.16)-(5.17), after t_f , $R(1, t) \equiv 0$ which gives $\Phi \equiv 0$ then (5.45) cannot be satisfied. This completely coincides with the logic that we cannot estimate θ if ψ_1 and ψ_2 are zero (see equations (5.2) and (5.3)).

We can now state the stability result of the original error system $\{\tilde{\xi}(x, t), \tilde{X}(t), \tilde{\theta}(t)\}$.

Theorem 5.4.1. Consider the error system (5.6)-(5.8) with initial conditions $\{\tilde{\xi}_0(x) \in (L^2([0, 1]))^{n_\xi}, \tilde{X}_0 \in \mathbb{R}^{n_x}, \tilde{\theta}_0 \in \mathbb{R}^{n_\theta}\}$. Under Lemma 5.4.1, Lemma 5.4.2 and if the conditions of Lemma 5.4.3 are satisfied, then the error system $\{\tilde{\xi}(x, t), \tilde{X}(t), \tilde{\theta}(t)\}$ is exponentially stable in the $|\tilde{X}|^2 + |\tilde{\theta}|^2 + \|\tilde{\xi}(\cdot, t)\|_{(L^2([0, 1]))^{n_\xi}}^2$ norm for all $t \geq t_f$.

Proof. Consider the following Lyapunov function

$$V(t) = \tilde{X}_c^T(t)P_c(t)\tilde{X}_c(t) + \int_0^1 (\tilde{\xi}^T(x, t)P\tilde{\xi}(x, t))e^{-\mu x} dx \quad (5.56)$$

In view of (5.12), the result falls directly from Lemma 5.4.3 with the L^2 boundedness of the filters $T(x, t)$ and $R(x, t)$ proved in Lemma 5.4.2. \square

5.5 Numerical evaluation of the observer

We implement the adaptive observer in MATLAB 2018 for the scalar case $n_\xi = n_X = 1$ and $n_\theta = 1$. The system is given by:

$$\partial_t \xi(x, t) + 2\partial_x \xi(x, t) = 0.02\xi(x, t) \quad (5.57)$$

$$\xi(0, t) = X(t) + \frac{\sqrt{3}}{2}\theta \quad (5.58)$$

$$\dot{X}(t) = \sin(t)X(t) + \cos(t)u(t) + \frac{1}{2}\theta \quad (5.59)$$

The control input is constant $u(t) = 2$ and the parameter to be estimated is $\theta = 1$. The system initial conditions are

$$\xi_0(x) = 10x \quad \text{and} \quad X_0 = 5. \quad (5.60)$$

The states $\xi(x, t)$, $X(t)$ and the parameter $\theta = 1$ are to be estimated using the following available measurement:

$$y(t) = \xi(1, t) \quad (5.61)$$

The system (5.57)-(5.59) corresponds to a transport equation with first order time-varying boundary conditions. It is clear that the plant is open loop - unstable looking into the ODE dynamics $A(t) = \sin(t)$.

The adaptive observer is given by:

$$\partial_t \hat{\xi}(x, t) + 2\partial_x \hat{\xi}(x, t) = 0.02\hat{\xi}(x, t) + T(x, t)L(t)(y(t) - \hat{\xi}(1, t)) + R(x, t)\dot{\hat{\theta}}(t) \quad (5.62)$$

$$\hat{\xi}(0, t) = \hat{X}(t) + \frac{\sqrt{3}}{2}\hat{\theta}(t) \quad (5.63)$$

$$\dot{\hat{X}}(t) = \sin(t)\hat{X}(t) + \cos(t)u(t) + \frac{1}{2}\dot{\hat{\theta}}(t) + L(t)(y(t) - \hat{\xi}(1, t)) \quad (5.64)$$

We start the observer from the following initial conditions

$$\hat{\xi}_0(x) = 9(x + 1) \quad \text{and} \quad \hat{X}_0 = 10 \quad (5.65)$$

The filter matrices $T(x, t)$ and $R(x, t)$ are computed using (5.15)-(5.17) with zero initial conditions. $\hat{\theta}(t)$ is updated using the adaptation law (5.40)-(5.41). Two variables are still to be set: $L(t)$ and β . The forgetting factor β sets the speed of convergence of the parameters, it is fixed to $\beta = 0.1$ in this evaluation. The dynamic observer gain $L(t)$ is calculated at each time step to ensure that $Z(t)$ is negative definite for $t \geq t_f$. This is done in the following order:

1. use a pole placement method to calculate $L(t)$ that guarantees the existence of $P_X(t)$ that satisfies (5.55);
2. verify that (5.46) is satisfied for a predefined value of $Q(t)$.

Condition (5.46) was satisfied for all $t \geq t_f$ for a constant value of $P_X(t) = P_X = 0.5$ and for $Q(t) = 0.0125P_c(t)$ where $L(t)$ is calculated by locating the poles of $A_d(t)$ at -1 for all $t \geq t_f$. The values corresponding to $L(t)$ are plotted on Fig. 5.2. The placement starts after $t_f = 0.5$ s and $L(t)$ exhibits an oscillatory behavior due to the dynamics of $A(t)$.

A finite difference (FD) scheme in space and time is implemented to approximate both the infinite dimensional states $\{\xi(x, t), \hat{\xi}(x, t)\}$ and the finite dimensional states $\{X(t), \hat{X}(t), \hat{\theta}(t)\}$. The exponential convergence of the estimation error on both the ODE and the PDE sides is shown on Fig. 5.3. After $t_f = 0.5$ s, the estimation errors converge to zero after exhibiting some oscillatory transients. Furthermore, as predicted by the theory, the Lyapunov function $V(t)$ shown on Fig. 5.4 increases on the interval of time $[0, 0.5$ s] due to the unstable dynamics of $A(t)$ and the presence of no observer gain $L(t) = 0$, but afterwards it starts its exponential decay towards zero when measurement corrections are introduced for $t \geq t_f$. Finally, we show the estimation of the parameter θ starting from an initial condition $\hat{\theta}_0 = 6$ on Fig. 5.5. The adaptation starts after $t_f = 0.5$ s and $\hat{\theta}(t)$ converges to θ in approximately 50 s.

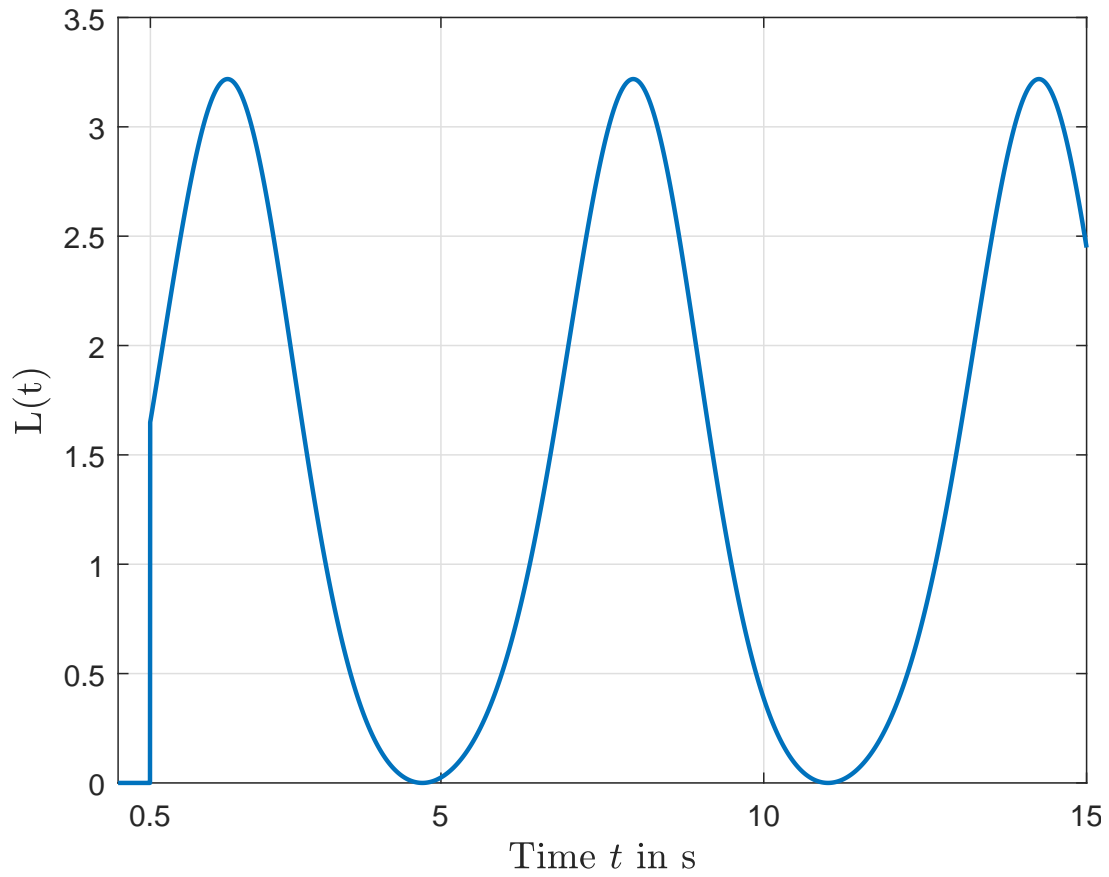


Figure 5.2: Calculated observer gain $L(t)$.

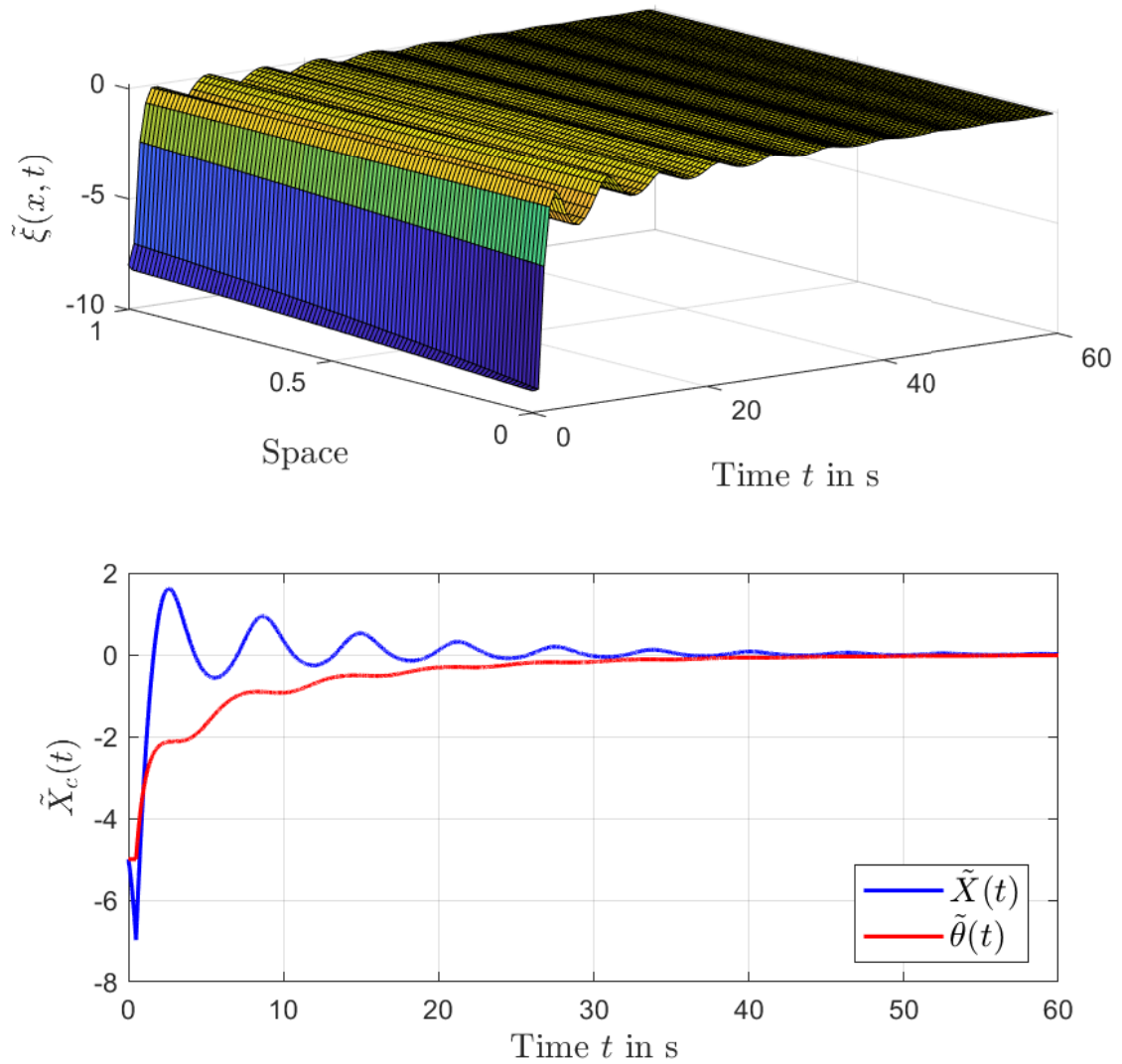
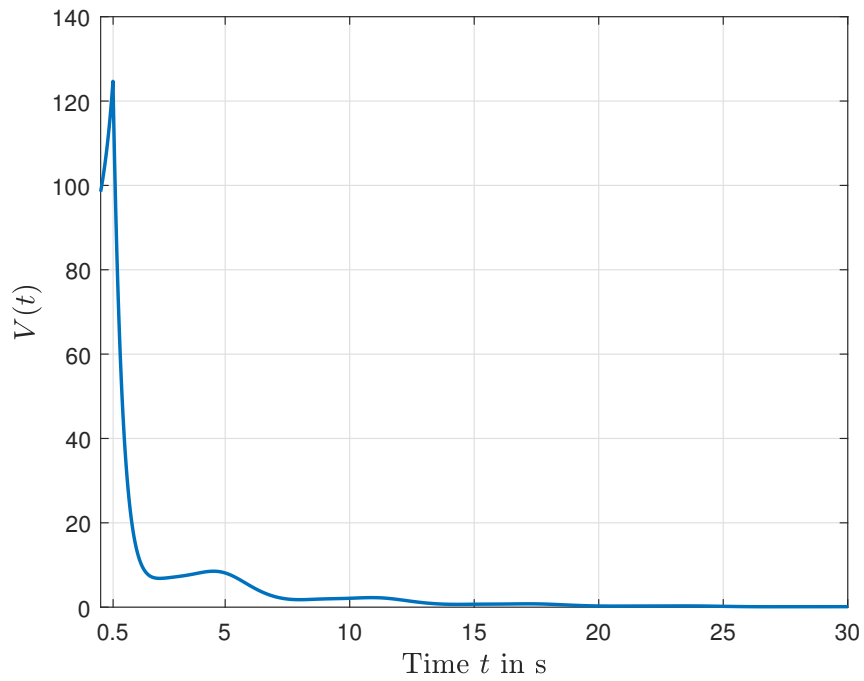
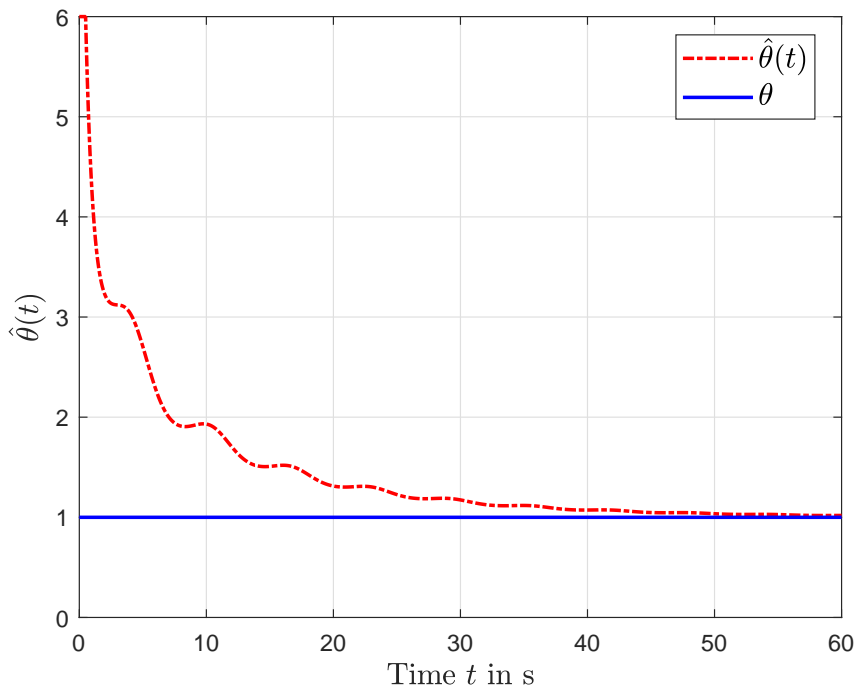


Figure 5.3: Estimation error of the PDE state $\tilde{\xi}(x, t)$ and the ODE states $\tilde{X}(t)$ and $\tilde{\theta}(t)$.

Figure 5.4: Lyapunov function $V(t)$.Figure 5.5: Estimation of the parameter state $\hat{\theta}(t)$.

5.6 Conclusion

We have proposed an adaptive observer for a system of linear transport PDEs coupled with time-varying ODEs at the boundary. The system involves constant parameters that are to be estimated together with the PDE-ODE states using boundary sensing only. We have used swapping design to decouple the estimation error of the infinite states (PDEs) from the finite states (ODEs). We thus proved boundedness of regressors filters and obtained sufficient conditions for the exponential stability of the estimation error using DLIs. For future works, it would be interesting to consider the heterodirectional case i.e. consider wave propagations not only in the positive direction but also in both positive and negative directions, while keeping the time-varying ODE connections at the boundary. It is also important to investigate the possibility of having parameter unknowns not only as input disturbances but also in the system matrices, e.g. $A(\theta, t)$.

Chapter 6

Conclusion and Perspectives

The thesis investigates the boundary estimation and control of PDEs and PDEs-ODEs networks. The PDEs are hyperbolic (transport) and parabolic (diffusion), and the ODEs are linear time varying. In total, we have solved four problems: three boundary estimation problems and a boundary control one. Problems 1, 2 and 4 are estimation problems and involve coupled hyperbolic PDEs and coupled hyperbolic PDEs-ODEs networks, while Problem 3 investigates the boundary control of a mixed class of hyperbolic-parabolic PDEs. The control applications are in the area of system cryogenics (CO₂ cooling technology at CERN) and exhaust systems in Diesel car engines (Renault).

Theoretically, in all the problems, we have tackled challenges in ensuring system stability (or error system stability in the case of estimation problems) using boundary controllers and boundary measurements and also to derive stable adaptation laws for parameters estimations. The coupling of PDEs of the same class or of different classes can always trigger stability problems. We have used Lyapunov methods to handle stability. It is well known that using Lyapunov analysis, controllers and observer gains are designed to restrict the time derivatives of an energy function (in a specific norm) to be strictly less than zero, and then, stability is achieved. Because of the complexity of the couplings architectures, it may become difficult to find a suitable Lyapunov function. An intermediate step that facilitates the Lyapunov analysis is the Backstepping method. The difficult part is to find an adequate target system and to show that the transformation is well posed on the domain of definition and that is invertible. Two types of backstepping transformations are famous in the literature: 1) the Volterra integral transformation, which is solved on the triangular domain and it is always invertible and 2) the Fredholm integral transformation, which is solved on the rectangular domain and may require proof of invertibility. Regarding the parameters estimations, we have used swapping design to decouple the PDE estimation errors from the parameter adaptation errors. This helps in finding the proper linear regressor equations to estimate the parameters directly using the standard online methods. In what follows, we summarize the four problems solved in this thesis and we give for each problem our conclusions and perspectives.

Problem 1 solves the boundary estimation of the distributed states, boundary unknowns and in-domain parameters of a 2-by-2 hyperbolic system of PDEs using boundary sensing. The basic

motivation is to estimate the temperatures and the heat transfer coefficient of a heat exchanger pipe running CO₂ as its working refrigerant. We have designed a Luneberger-adaptive observer to solve the problem, and obtained its exponential stability using the backstepping-Lyapunov method. The estimation of the parameters is done through the swapping design method. We can conclude that the backstepping method is necessary to solve the stabilization/adaptation problem. Unlike using only dissipative boundary conditions, the stabilization of the PDE error system $Z(x, t)$ by injecting distributed observer gains ($p_1(x)$ and $p_2(x)$) in the domain, then using the backstepping method, is extremely important in canceling the effect of the coupling ($\sigma_1(x)$, $\sigma_2(x)$) and in ensuring finite-time convergence. This means that the boundary estimation errors of the PDEs vanish in finite-time allowing directly to start the parameter estimation algorithm. On the experimental part, the observer shows a good response in enhancing the temperature estimations by 1K. The improvement was appreciated by the researchers at CERN working in highly accurate temperature ranges.

Our future work will be centered in estimating the heat transfer coefficient and the temperature directly without passing through the linearization step. Also we are planning to introduce unknown uncertainties in the transport speeds. We are convinced that such kind of model complexities will contribute to new theories in the field of parameter estimation for hetero-directional transport PDEs using measurements sensed at the boundary.

In Problem 2, we have solved the problem of estimating the distributed thermodynamic profiles (pressures, enthalpies, mass flow rates) of a two-phase CO₂ heat exchanger. Only input/output boundary measurements are available. We recalled the various models that can describe the behavior of a two-phase flows. Then we concluded the modeling phase by choosing the homogeneous equilibrium model. The observer design is done in two steps: 1) the linearization around a steady state point and diagonalization and 2) to synthesize a Luneberger observer with dissipative boundary corrections. The exponential stability of the observer is analyzed using a quadratic Lyapunov candidate where we give sufficient conditions that guarantee stability in the form of matrix inequalities. We can conclude that Problem 2 can become more complex when some input measurements are not available. For instance, the input enthalpy at the hot and cold sides is very hard to measure practically. Also measuring the two-phase mass flow rate is also difficult. Hence, our main interest in the future is to investigate the unknown input observers for hyperbolic systems. Furthermore, adding some model nonlinearities to the observer is also a good step in approaching the real dynamics far from steady states. We are also interested in estimating the two-phase heat transfer and friction coefficients from measurements. This can replace complex and inaccurate thermodynamical correlations.

Problem 3 studies the boundary stabilization of a mixed class of coupled hyperbolic-parabolic PDEs. The motivation is the diffusion phenomena in heat exchangers. The system involves a diffusion equation coupled with a transport equation in the domain as well as at the boundary. Using the backstepping method and then Lyapunov analysis, we have designed two boundary control laws and we give sufficient conditions that guarantee the exponential stability of the system. However, we are still searching how the condition of stability (4.64) in Chapter 4 varies as a function of the two control free variables $T(x, y)$ and c . We predict that finding a bound

on the growth rate of the kernel $M(x, y)$ will be the first step in finding the solution. The backstepping method applied to coupled systems of different classes of PDEs is still under research. For now, we can prove the wellposedness of the kernel equations only in the weak sense. The difficulty due to the different number of space derivatives present intrinsically in the system. Our first task in the future is to widely study the existence of solutions of coupled diffusion-transport equations on 2D domains. We will also try different type of coupling topologies between advection and diffusion. Note that in Problem 3, the coupling topology was a Volterra integral coupling from diffusion to advection and a linear advective one from advection to diffusion. In fact, we are interested in the linear advection coupling in both directions as it appears directly in heat exchangers networks. Also, it would be interesting if we can decrease the number of controllers in Problem 3 from two to only one controller that can stabilize the system.

In Problem 4, we design a boundary adaptive observer for a system of coupled hyperbolic PDEs-ODEs. The system is a set of linear transport PDEs propagating in the positive x-axis direction and driven by a set of linear time varying ODEs at the boundary. The system has also unknown parameters at the boundary and in the ODE dynamics. As stated in Chapter 1, the objective behind considering this type of systems is the estimation of the EGR mass flow rates in exhaust car system. The designed observer is of Lunberger type where boundary measurement corrections are inserted in the PDEs space domain and in the ODEs dynamics multiplied by time varying observer gains. The idea was to decouple the PDEs state estimation errors from the ODEs estimation errors, achieved by using the swapping design method. Then we give sufficient conditions that guarantee the exponential stability of the errors in the form of differential Lyapunov matrix inequalities while respecting the persistence of excitation conditions. We can draw the following conclusion: although the PDEs and the ODEs errors are decoupled, the swapping design method give rise to a direct and intrinsic coupling between the errors on the ODEs $\tilde{X}(t)$ and the parameter estimation errors $\tilde{\theta}(t)$. This is obvious in the off diagonal entities of the matrix $Z(t)$ in (5.47). We are investigating to what extent we can find solutions to the stability condition (5.46) apart from the detectability and the persistence of excitation constraints already discussed in Remark 5.4.2. For future works, it would be interesting to consider the heterodirectional case i.e. consider wave propagations not only in the positive direction but also in both positive and negative directions, while keeping the time-varying ODE connections at the boundary. It is also important to investigate the possibility of having unknown parameters not only as input disturbances but also in the system matrices e.g. $A(\theta, t)$.

Finally, the topic on boundary control and estimation of partial differential equations is gaining significant attention. A lot can be still done in this area of research. The introduction of system nonlinearities is one of the promising perspectives in this domain. The nonlinearity may represent more accurately the physical state of the system. It can be through the coupling between the PDEs or the coupling with nonlinear ODEs. This also can be accompanied with the presence of unknown parameters in the system. Synthesizing adaptive boundary observers and controllers for nonlinear PDE networks is a huge achievement considering the enormous amount of physical applications.

Bibliography

- [1] Ole Morten Aamo. “Disturbance rejection in 2 x 2 linear hyperbolic systems”. In: *IEEE Transactions on Automatic Control* 58.5 (2012), pp. 1095–1106.
- [2] Ole Morten Aamo. “Disturbance rejection in 2 x 2 linear hyperbolic systems”. In: *IEEE Transactions on Automatic Control* 58.5 (2013), pp. 1095–1106.
- [3] Ole Morten Aamo. “Leak detection, size estimation and localization in pipe flows”. In: *IEEE Transactions on Automatic Control* 61.1 (2016), pp. 246–251.
- [4] Kazuhiro Akihama, Yoshiki Takatori, Kazuhisa Inagaki, Shizuo Sasaki, et al. “Mechanism of the smokeless rich diesel combustion by reducing temperature”. In: *SAE Transactions* (2001), pp. 648–662.
- [5] Ilyasse Aksikas, A Alizadeh Moghadam, and J Fraser Forbes. “Optimal linear–quadratic control of coupled parabolic–hyperbolic PDEs”. In: *International Journal of Control*, vol.90 (2017), pp. 2152–2164.
- [6] Malin Alriksson and Ingemar Denbratt. *Low temperature combustion in a heavy duty diesel engine using high levels of EGR*. Tech. rep. SAE Technical Paper, 2006.
- [7] Markus Ammann, Nicholas Patrick Fekete, Lino Guzzella, and Adolf Hermann Glattfelder. “Model-based control of the VGT and EGR in a turbocharged common-rail Diesel engine: theory and passenger car implementation”. In: *SAE transactions* (2003), pp. 527–538.
- [8] Henrik Anfinsen and Ole Morten Aamo. “Adaptive output-feedback stabilization of linear 2×2 hyperbolic systems using anti-collocated sensing and control”. In: *Systems and Control Letters* 104 (2017), pp. 86–94.
- [9] Henrik Anfinsen and Ole Morten Aamo. “Disturbance Rejection in the Interior Domain of Linear 2 x 2 Hyperbolic Systems”. In: *IEEE Transactions on Automatic Control* 60.1 (2014), pp. 186–191.
- [10] Henrik Anfinsen and Ole Morten Aamo. “State estimation in hyperbolic PDEs coupled with an uncertain LTI system”. In: *2017 American Control Conference (ACC)*. IEEE, 2017, pp. 3821–3827.
- [11] Henrik Anfinsen, Florent Di Meglio, and Ole Morten Aamo. “Estimating the left boundary condition of coupled 1-D linear hyperbolic PDEs from right boundary sensing”. In: *IEEE European Control Conference (ECC)*. 2016, pp. 2179–2184.

- [12] Henrik Anfinssen, Mamadou Diagne, Ole Morten Aamo, and Miroslav Krstic. “An adaptive observer design for $n + 1$ coupled linear hyperbolic PDEs based on swapping”. In: *IEEE Transactions on Automatic Control* 61.12 (2016), pp. 3979–3990.
- [13] Henrik Anfinssen, Mamadou Diagne, Ole Morten Aamo, and Miroslav Krstic. “Estimation of boundary parameters in general heterodirectional linear hyperbolic systems”. In: *Automatica* 79 (2017), pp. 185–197.
- [14] Jean Auriol and Florent Di Meglio. “Two-sided boundary stabilization of heterodirectional linear coupled hyperbolic PDEs”. In: *IEEE Transactions on Automatic Control* 63.8 (2017), pp. 2421–2436.
- [15] Peder Aursand, Morten Hammer, Svend Tollak Munkejord, and Øivind Wilhelmsen. “Pipeline transport of CO₂ mixtures: Models for transient simulation”. In: *International Journal of Greenhouse Gas Control* 15 (2013), pp. 174–185.
- [16] AATM Aw and Michel Rasclé. “Resurrection of “second order” models of traffic flow”. In: *SIAM journal on applied mathematics* 60.3 (2000), pp. 916–938.
- [17] Georges Bastin and Jean-Michel Coron. *Stability and boundary stabilization of 1-d hyperbolic systems*. Vol. 88. Springer, 2016.
- [18] Ian H Bell, Jorrit Wronski, Sylvain Quoilin, and Vincent Lemort. “Pure and pseudo-pure fluid thermophysical property evaluation and the open-source thermophysical property library CoolProp”. In: *Industrial & engineering chemistry research* 53.6 (2014), pp. 2498–2508.
- [19] Ian H. Bell, Jorrit Wronski, Sylvain Quoilin, and Vincent Lemort. “Pure and Pseudo-pure Fluid Thermophysical Property Evaluation and the Open-Source Thermophysical Property Library CoolProp”. In: *Industrial & Engineering Chemistry Research* 53.6 (2014), pp. 2498–2508. DOI: [10.1021/ie4033999](https://doi.org/10.1021/ie4033999). eprint: <http://pubs.acs.org/doi/pdf/10.1021/ie4033999>. URL: <http://pubs.acs.org/doi/abs/10.1021/ie4033999>.
- [20] Pauline Bernard and Miroslav Krstic. “Adaptive output-feedback stabilization of non-local hyperbolic PDEs”. In: *Automatica* 50.10 (2014), pp. 2692–2699.
- [21] Michelangelo Bin and Florent Di Meglio. “Boundary estimation of boundary parameters for linear hyperbolic PDEs”. In: *IEEE Transactions on Automatic Control* 62.8 (2017), pp. 3890–3904.
- [22] Benjamin Bradu, Philippe Gayet, Silviu-Iulian Niculescu, and Emmanuel Witrant. “Modeling of the very low pressure helium flow in the LHC Cryogenic Distribution Line after a quench”. In: *Cryogenics* 50.2 (2010), pp. 71–77.
- [23] Delphine Bresch-Pietri, Thomas Leroy, Jonathan Chauvin, and Nicolas Petit. “Prediction-based trajectory tracking of external gas recirculation for turbocharged SI engines”. In: *2012 American Control Conference (ACC)*. IEEE. 2012, pp. 5718–5724.
- [24] S. Brown, S. Martynov, H. Mahgerefteh, S. Chen, et al. “Modelling the non-equilibrium two-phase flow during depressurisation of CO₂ pipelines”. In: *International Journal of Greenhouse Gas Control* 30 (2014), pp. 9–18.

- [25] Felipe Castillo, Emmanuel Witrant, Christophe Prieur, and Luc Dugard. “Boundary observers for linear and quasi-linear hyperbolic systems with application to flow control”. In: *Automatica* 49.11 (2013), pp. 3180–3188.
- [26] Felipe Castillo, Emmanuel Witrant, Christophe Prieur, and Luc Dugard. “Dynamic boundary stabilization of linear and quasi-linear hyperbolic systems”. In: *51st Annual Conference on Decision and Control (CDC)*. IEEE. 2012, pp. 2952–2957.
- [27] Felipe Castillo, Emmanuel Witrant, Christophe Prieur, Vincent Talon, et al. “Fresh air fraction control in engines using dynamic boundary stabilization of LPV hyperbolic systems”. In: *IEEE Transactions on Control Systems Technology* 23.3 (2014), pp. 963–974.
- [28] Felipe Castillo Buenaventura. “Modeling and Control of the Air-Path of Diesel Engines for the EURO 7”. Thesis. Université de Grenoble, Oct. 2013. URL: <https://tel.archives-ouvertes.fr/tel-00951387>.
- [29] Jonathan Chauvin, Gilles Corde, Nicolas Petit, and Pierre Rouchon. “Motion planning for experimental airpath control of a diesel homogeneous charge-compression ignition engine”. In: *Control Engineering Practice* 16.9 (2008), pp. 1081–1091.
- [30] Stephen Chen, Miroslav Krstic, and Rafael Vazquez. “Backstepping Boundary Control of a 1-D 2×2 Unstable Diffusion-Reaction PDE System with Distinct Input Delays”. In: *2019 American Control Conference (ACC)*. IEEE. 2019, pp. 2564–2569.
- [31] Stephen Chen, Rafael Vazquez, and Miroslav Krstic. “Backstepping control design for a coupled hyperbolic-parabolic mixed class PDE system”. In: *2017 IEEE 56th Annual Conference on Decision and Control (CDC)*. IEEE. 2017, pp. 664–669.
- [32] Jean-Michel Coron, Brigitte d’Andrea Novel, and G Bastin. “A Lyapunov approach to control irrigation canals modeled by Saint-Venant equations”. In: *IEEE European Control Conference (ECC)*. 1999, pp. 3178–3183.
- [33] Jean-Michel Coron, Brigitte d’Andrea Novel, and Georges Bastin. “A strict Lyapunov function for boundary control of hyperbolic systems of conservation laws”. In: *IEEE Transactions on Automatic control* 52.1 (2007), pp. 2–11.
- [34] C. Curro, D. Fusco, and N. Manganaro. “A reduction procedure for generalized Riemann problems with application to nonlinear transmission lines”. In: *Journal of Physics A: Mathematical and Theoretical* 44.33 (2011), pp. 33–52.
- [35] Florent Di Meglio. “Dynamics and control of slugging in oil production”. PhD thesis. École Nationale Supérieure des Mines de Paris, 2011.
- [36] Florent Di Meglio, Federico Bribiesca Argomedo, Long Hu, and Miroslav Krstic. “Stabilization of coupled linear heterodirectional hyperbolic PDE–ODE systems”. In: *Automatica* 87 (2018), pp. 281–289.
- [37] Florent Di Meglio, Delphine Bresch-Pietri, and Ulf Jakob F Aarsnes. “An adaptive observer for hyperbolic systems with application to underbalanced drilling”. In: *IFAC Proceedings Volumes* 47.3 (2014), pp. 11391–11397.
- [38] M. K. Dobson. “Heat Transfer and Flow Regimes During Condensation in Horizontal Tubes”. In: *PhD Thesis, University of Illinois* (1994).

- [39] Valérie Dos Santos and Christophe Prieur. “Boundary control of open channels with numerical and experimental validations”. In: *IEEE transactions on Control systems technology* 16.6 (2008), pp. 1252–1264.
- [40] L.C. Evans. “Partial differential equations: Graduate studies in Mathematics”. In: *American Mathematical Society, 2nd edition* (2010).
- [41] Francesco Ferrante and Andrea Cristofaro. “Boundary Observer Design for Coupled ODEs–Hyperbolic PDEs Systems”. In: *2019 18th European Control Conference (ECC)*. 2019, pp. 2418–2423.
- [42] Tore Flatten and Halvor Lund. “Relaxation two-phase flow models and the subcharacteristic condition”. In: *Mathematical Models and Methods in Applied Sciences* 21.12 (2011), pp. 2379–2407.
- [43] Volker Gnielinski. “New equations for heat and mass transfer in turbulent pipe and channel flow”. In: *International Chemical Engineering* 16.2 (1976), pp. 359–368.
- [44] Paola Goatin. “The Aw–Rascle vehicular traffic flow model with phase transitions”. In: *Mathematical and computer modelling* 44.3-4 (2006), pp. 287–303.
- [45] Olivier Grondin, Philippe Moulin, and Jonathan Chauvin. “Control of a turbocharged diesel engine fitted with high pressure and low pressure exhaust gas recirculation systems”. In: *Proceedings of the 48th IEEE Conference on Decision and Control (CDC) held jointly with 2009 28th Chinese Control Conference*. IEEE. 2009, pp. 6582–6589.
- [46] Martin Gugat and Markus Dick. “Time-delayed boundary feedback stabilization of the isothermal Euler equations with friction”. In: *Mathematical Control and Related Fields* 1.4 (2011), pp. 469–491.
- [47] Falk M Hante, Günter Leugering, and Thomas I Seidman. “Modeling and analysis of modal switching in networked transport systems”. In: *Applied Mathematics and Optimization* 59.2 (2009), pp. 275–292.
- [48] Agus Hasan, Ole Morten Aamo, and Miroslav Krstic. “Boundary observer design for hyperbolic PDE–ODE cascade systems”. In: *Automatica* 68 (2016), pp. 75–86.
- [49] Ales Hribernik. “The potential of the high and low-pressure exhaust gas recirculation”. In: *Proceeding of the SAE Conference, Paper 04*. Vol. 29. 2002.
- [50] Long Hu, Florent Di Meglio, Rafael Vazquez, and Miroslav Krstic. “Control of homodirectional and general heterodirectional linear coupled hyperbolic PDEs”. In: *IEEE Transactions on Automatic Control* 61.11 (2016), pp. 3301–3314.
- [51] Petros A Ioannou and Jing Sun. *Robust adaptive control*. Vol. 1. PTR Prentice-Hall Upper Saddle River, NJ, 1996.
- [52] Sadik Kakac, Hongtan Liu, and Anchasa Pramuanjaroenkij. *Heat exchangers: selection, rating, and thermal design*. CRC press, 2020.
- [53] Gerhard Kreisselmeier. “Adaptive observers with exponential rate of convergence”. In: *IEEE transactions on automatic control* 22.1 (1977), pp. 2–8.

- [54] Miroslav Krstic. “Control of an unstable reaction–diffusion PDE with long input delay”. In: *Systems and Control Letters* 58.10-11 (2009), pp. 773–782.
- [55] Miroslav Krstic, Ioannis Kanellakopoulos, and V.Petar. *Nonlinear and adaptive control design*. Wiley New York, 1995.
- [56] Miroslav Krstic and Andrey Smyshlyaev. “Backstepping boundary control for first-order hyperbolic PDEs and application to systems with actuator and sensor delays”. In: *Systems and Control Letters* 57.9 (2008), pp. 750–758.
- [57] Miroslav Krstic and Andrey Smyshlyaev. *Boundary control of PDEs: A course on backstepping designs*. Vol. 16. SIAM, 2008.
- [58] Pierre-Olivier Lamare, Antoine Girard, and Christophe Prieur. “An optimisation approach for stability analysis and controller synthesis of linear hyperbolic systems”. In: *ESAIM: Control, Optimisation and Calculus of Variations* 22.4 (2016), pp. 1236–1263.
- [59] Dq. Li, Dt. Lee, Wt. Yu, Wx. Shen, et al. “2nd Initial- Boundary value-problems for quasi-linear hyperbolic-parabolic coupled systems”. In: *Chinese annals of mathematics series B* 2.1 (1981), pp. 65–90.
- [60] Halvor Lund. “A hierarchy of relaxation models for two-phase flow”. In: *SIAM Journal on Applied Mathematics* 72.6 (2012), pp. 1713–1741.
- [61] Guillaume Martin. “Modélisation 0D-1D de la chaîne d’air des moteurs à combustion interne dédiée au contrôle”. PhD thesis. 2010.
- [62] Morin-Norwegian. “Mathematical modelling and numerical simulation of two phase multi-component flows of CO2 mixtures in pipes”. In: *Thesis for the degree of Philosophiae Doctor, Trondheim. University of Science and Technology* (Oct. 2012).
- [63] Svend Tollak Munkejord. “A numerical study of two-fluid models with pressure and velocity relaxation”. In: *Advances in Applied Mathematics* 2 (2010), pp. 131–159.
- [64] Michaël Ndjinga. “Influence of interfacial pressure on the hyperbolicity of the two-fluid model”. In: *Comptes Rendus Mathématique* 344.6 (2007), pp. 407–412.
- [65] Tropea Paola, Paolo Petagna, Steven Pavis, Jan Godlewski, et al. “Design, construction and commissioning of a 15 kW CO2 evaporative cooling system for particle physics detectors: lessons learnt and perspectives for further development”. In: *Proceedings of Science (PoS)*. 2014, p. 213.
- [66] Suhas Patankar. *Numerical heat transfer and fluid flow*. CRC press, 1980.
- [67] GP Peterson. “An introduction to Heat pipes: Modeling”. In: *Testing and Applications* (1994).
- [68] Jeffrey Rauch, Michael Taylor, and Ralph Phillips. “Exponential decay of solutions to hyperbolic equations in bounded domains”. In: *Indiana university Mathematics journal* 24.1 (1974), pp. 79–86.
- [69] David Fernando Novella Rodriguez, Emmanuel Witrant, and Olivier Sename. “Control-oriented modeling of fluid networks: A time-delay approach”. In: *Recent Results on Non-linear Delay Control Systems*. Springer, 2016, pp. 275–289.

- [70] Wilson Rugh. *Linear system theory*. Vol. 2. Prentice hall Upper Saddle River, NJ, 1996.
- [71] David L Russell. “Controllability and stabilizability theory for linear partial differential equations: recent progress and open questions”. In: *SIAM Review* 20.4 (1978), pp. 639–739.
- [72] Thomas W Ryan III and Andrew C Matheaus. “Fuel requirements for HCCI engine operation”. In: *SAE transactions* (2003), pp. 1143–1152.
- [73] Richard Saurel, Fabien Petitpas, and Rémi Abgrall. “Modelling phase transition in metastable liquids: application to cavitating and flashing flows”. In: *Journal of Fluid Mechanics* 607 (2008), pp. 313–350.
- [74] Andrey Smyshlyaev and Miroslav Krstic. *Adaptive control of parabolic PDEs*. Princeton University Press, 2010.
- [75] Zheng Songmu. “Initial boundary value problems for quasilinear hyperbolic-parabolic coupled systems in higher dimensional spaces”. In: *Chinese Annals of Mathematics* 4 (1983), pp. 1–3.
- [76] Rafael Vazquez, Miroslav Krstic, and Jean-Michel Coron. “Backstepping boundary stabilization and state estimation of a 2×2 linear hyperbolic system”. In: *50th IEEE Conference on Decision and Control and European Control Conference (CDC-ECC)*. 2011, pp. 4937–4942.
- [77] B. Verlaat, M. Van Beuzekom, and A. Van Lysebetten. “CO₂ cooling for HEP experiments”. In: *Topical Workshop on Electronics for Particle Physics (TWEPP-2008), Naxos, Greece*. 2008, pp. 328–336.
- [78] B. Verlaat, A. Van Lysebetten, and M. Van Beuzekom. “CO₂ Cooling for the LHCb-VELO Experiment at CERN”. In: *8th IIF/IIR Gustav Lorentzen Conference on Natural Working Fluids*. 2008.
- [79] Atul Kumar Vij and WE Dunn. *Modeling of two-phase flows in horizontal tubes*. Tech. rep. Air Conditioning and Refrigeration Center. College of Engineering. University of Illinois at Urbana-Champaign., 1996.
- [80] Christian Wagner and Noreen Harned. “Lithography gets extreme”. In: *Nature Photonics* 4.1 (2010), pp. 24–26.
- [81] Junmin Wang. “Hybrid robust air-path control for diesel engines operating conventional and low temperature combustion modes”. In: *IEEE Transactions on Control Systems Technology* 16.6 (2008), pp. 1138–1151.
- [82] Martin Weiss, Pierre Bonnel, Rudolf Hummel, Urbano Manfredi, et al. “Analyzing on-road emissions of light-duty vehicles with Portable Emission Measurement Systems (PEMS)”. In: *European Commission* (2017).
- [83] Cheng-Zhong Xu and Gauthier Sallet. “Exponential stability and transfer functions of processes governed by symmetric hyperbolic systems”. In: *ESAIM: Control, Optimisation and Calculus of Variations* 7 (2002), pp. 421–442.
- [84] Fengjun Yan and Junmin Wang. “Control of dual loop EGR air-path systems for advanced combustion diesel engines by a singular perturbation methodology”. In: *Proceedings of the 2011 American Control Conference*. IEEE. 2011, pp. 1561–1566.

- [85] Fairouz Zobiri, Emmanuel Witrant, and François Bonne. “PDE observer design for counter-current heat flows in a heat-exchanger”. In: *IFAC-PapersOnLine* 50.1 (2017), pp. 7127–7132.
- [86] Lukasz Zwalinski, Florian Corbaz, Paolo Petagna, Sylvain Nichilo, et al. “CO2 cooling system for Insertable B Layer detector into the ATLAS experiment”. In: *PoS* (2015), p. 224.